The Manchester School of Engineering
Division of Mechanical Engineering
University of Manchester

EXPERIMENTAL STUDY OF THE DEVELOPMENT OF A TURBULENT FREE JET, WITH AND WITHOUT AERODYNAMIC EXCITATION

by

Ahmed H. S. AL-Sudane, B.Sc., M.Sc.

A thesis submitted to the University of Manchester in support of an application for the degree of Doctor of Philosophy in the Faculty of Science

1997

TABLE OF CONTENTS

LIST OF FIGURES

LIST OF TABLES

ABSTRACT

A detailed experimental programme has been carried out to study the behaviour of an axisymmetric turbulent free jet of air, with and without excitation. Preliminary measurement using single channel constant temperature hot film anemometry has been used mainly to check the symmetry of the jet under consideration and to develop the experimental apparatus. Subsequently, a very detailed programme of measurement has been carried out using a two-component LDA system. Both techniques have required the application of high speed computer based data acquisition and analysis methods.

Measurements of the time mean velocity profiles, two components of the turbulent fluctuating velocity levels, and the turbulence shear stress profiles, have been made at nine axial stations downstream of the nozzle exit plane using the LDA system. The BURstware software package supplied by Dantec has been used to collect the data in combination with two Burst Spectrum Analyzers (BSAs), one for each velocity component in the axial and radial directions.

A principle objective has been to examine how the development of a free jet can be controlled by the use of aerodynamic excitation. In the present study, this excitation was introduced by pulsing a thin annular jet (the secondary jet) which surrounds and is co-axial with the main central jet (the primary jet). This has been achieved by interrupting the secondary jet with a rotating valve assembly in the manifold supply line. A range of excitation frequencies from 5Hz to 198Hz has been used, corresponding to Strouhal numbers based on the nozzle diameter ranging from $St_D = 0.2$ to $St_D = 0.8$. Preliminarily checks showed that volumetric flow rates

of the secondary jet up to 5% of that of the primary jet have the optimum (i.e. largest) effect on the turbulence levels at the centre-line. Based upon these experiments, a fixed value of 2% ($Q_s = 0.02Q_o$) was subsequently chosen for the remaining series of experiments. Three Reynolds numbers were chosen for the investigation (namely $1.5x10^4$, $7.0x10^4$ and $1.7x10^5$). These values are considered to be representative of many industrial applications.

The experimental data has been processed in two ways. Firstly, the aim has been to show how the excitation influences the time mean quantities and integral flow parameters, such as the time mean velocity distributions and the entrainment rate, which describe the jet development. In this part of the calculations, the case of the natural free jet (without excitation) has been used as the datum against which the influence of the different excitation levels can be judged. Excitation at Strouhal numbers of $St_D = 0.2$ and $St_D = 0.6$ has been shown to exhibit the strongest effect on the behaviour of the jet flow.

In a further analysis of the instantaneous velocity information yielded by the LDA system, an attempt has been made to determine the intermittent turbulent flow characteristics of the excited jet. Here, the novel method proposed by a previous worker - Jeung (1993) - has been utilised. Some progress in applying the method has been achieved but the experimental results so obtained are still less then satisfactory.

A parallel flow visualisation study has been carried out to reveal the presence of the toroidal vortices which are formed by pulsation of the secondary annular jet. These toroidal vortices, which essentially consist of a regular form of "large scale

coherent structures", appear to have a very strong influence on the development of the jet. This flow visualisation has been achieved by injecting smoke from a smoke generator in the supply line of the secondary jet, then illuminating the flow by a laser light sheet. A video camera was used to capture the movement of the jet on film, from which selected frames could be digitised and presented in photographic form. These results have led to an improved understanding of the behaviour of the excited jet.

DECLARATION

No portion of the work referred to in this thesis has been submitted in support of any application for another degree or qualification of this or any other university or other institution of learning.

ACKNOWLEDGMENT

The author is grateful to his supervisor, Dr. J. T. Turner for his guidance and kind encouragement throughout the duration of the project and for the time spent reading the draft of this thesis.

The author wishes to express his thanks to Dr. D. I. Robinson for his role in the setting up of the LDA system and for many useful discussions during the course of this work.

Many thanks are also offered to Mr. J. Kindon, Mr. D. Golding, and Mr. P. Reid, for their practical assistance in the manufacture and assembly of the various components of the experimental rig. Here, it is noted that the major parts of the traversing unit were manufactured in the Central Workshop of the School of Engineering. The stepper motor drive box was built in the Departmental Instrumentation workshop. Thanks are due to all those persons who participated in the making of these components.

Thanks are also due to Mr. V. Chan, Dr. A. Szajner (Gdansk Technical University, Poland), and Dr. R. Slezas (Lithuanian Energy Institute) for their stimulating discussions and useful ideas. Thanks are also extended to the author's friends in Amara town (Iraq) and in particular, Mr. Abbas. K. Authmann, for their encouragement and invaluable support.

The author wishes to thank Ms Diana J. Cookson, for the continual encouragement and moral support. Her meticulous perusal and critical review of the thesis manuscript deserves the highest appreciation.

Finally, but by no means least, the author offers sincere thanks to his family in Iraq for their unlimited support and patience during the whole period of this project, especially to his mother who suffered most during his long period of absence. May God bless her.

DEDICATION

To my parents, sisters , brothers, and my nephews Ahmed and Noor Al-Dean.

NOMENCLATURE AND ABBREVIATIONS

Symbol	Meaning
A	area
B_o	width of rectangular slot in case of plane jet
B	empirical constant of the CTA calibration
C	constant in equation 7.4
c_o	constant in equation 2.1
c_1	constant in equation 2.4
D	diameter in the nozzle
E	bridge output voltage for constant temperature anemometer
E_o	no-flow bridge voltage for constant temperature anemometer
F_u , F_v	flatness factor of u, v respectively
f	frequency
f_D	Doppler frequency
f_d	detected Doppler frequency
f_s	optical frequency shift
G	constant in equation 7.4
I(r,t)	intermittency function
K	constant in equation 7.4
k_1	constant in equation 2.4
L	length of the nozzle
N	total number of samples
n	empirical constant in the CTA calibration
Q_o	mass flow rate at the nozzle outlet

Q_s	mass flow rate of the secondary jet
Q_s/Q_o	ratio of secondary to primary jet flow rate
Q_x	mass flow rate at given axial position
Q(r)	time mean average of a typical flow variable at position r
Q(r,t)	value of a typical variable at time t and position r
R	radial distance
R_o	nozzle radius
$R_{1/2}$	lateral dimension of jet based on radius at which axial velocity component falls to half velocity level at jet centre-line
$R/R_{1/2}$	non-dimensional radial position
Re	Reynolds number based on jet velocity at nozzle exit plane (U_j) and the nozzle diameter (D), $Re = U_j \times D/\nu$
S(f)	spectral energy at frequency f
St_D	Strouhal number based on nozzle diameter and pulsation frequency, $St_D = f \times D/U_j$
St_θ	Strouhal number based on momentum thickness of free shear layer at the nozzle outlet, $St_\theta = f \times \theta/U_j$
S_u , S_v	skewness factor of u and v respectively
t_p	time period of the pulsation
t	time
U	time mean velocity component in streamwise direction
U_{cl}	time mean velocity at the centre-line
U_{cln}	time mean velocity at the centre-line of the natural jet
U_j	time mean velocity at the centre-line of the nozzle exit plane
U_s	time mean velocity level of secondary jet in nozzle exit plane

V	time mean velocity component in transverse direction
u',v'	fluctuating velocity components in streamwise and radial directions, respectively
u_{rms}	root mean square value of u
v_{rms}	root mean square value of v
u'v'	instantaneous product of u' and v'
x,y,z	coordinate directions (defined in figure 3.1)
x_o	axial coordinate of the virtual origin of the jet
x/D	non-dimensional axial position
λ	wavelength of the laser light
η	non-dimensional radial coordinate ($\eta=R/(x-x_o)$)
γ	intermittency factor
ν	kinematic viscosity

Suffices

e	excited
G	Global
non	non-turbulent
n	natural occurring
tur	turbulent
p	pulsation

CHAPTER 1

INTRODUCTION

CHAPTER ONE
INTRODUCTION

1.1 The Turbulent Free Jet

Turbulent jet flow occurs when a fluid is discharged from a nozzle into a medium at rest, provided that the Reynolds number is sufficiently high. It can then be shown that there is no direct effect of any fixed boundary on the development of the turbulent flow and, moreover, that the jet becomes completely turbulent at a short distance from the point of discharge. Due to the difference between the velocity levels in the jet and the surrounding fluid, turbulent eddies are created in the region of highest shear at the free boundary of the jet. This immediately results in a lateral mixing process which progresses in both the radially inward and outward directions and is a function of distance from the nozzle. During this mixing process, the kinetic energy of the fluid jet is dissipated by entrainment of the surrounding fluid and is converted into potential energy and heat. As a direct result of this conversion process, the centre-line velocity of the fluid decreases steadily in the axial direction, whereas both the total volumetric flow in the jet and the overall width of the jet steadily increase in magnitude with distance from the exit plane of the nozzle.

The importance of turbulent fluid jets, to engineers and scientists alike, has led to extensive research into the subject. This type of flow system plays an important practical role in fluid mechanics, being central to the flow behaviour in jet pumps and ejectors, jet mixing in combustion systems, the discharge of effluent

into rivers, and many other important technological applications.

In the last two decades, the subject of jet flow has again been revived. It is, on the one hand, a logical extension of the research into coherent structures and, on the other hand, driven by the need for improved technical processes wherever a turbulent flow is involved. There is also the necessity for reduced consumption of energy, which has both economical and ecological implications.

1.2 Characteristics of the Turbulent Free Jet

The term "free" implies that the jet flow is at a sufficient distance from any fixed boundary condition (e.g. solid walls), and that there is no constraint on the development of the jet (i.e. on the entrainment process). In this situation, the jet flow develops first into a mixing region (principally due to the presence of free shear layers formed by the boundary layers created by the nozzle wall). After the eventual merging of the mixing layers, the true jet flow develops into its final state where self-similarity is achieved. Based upon this simplified model, a flow of this kind can be divided into three reasonably discrete regions which are known as:-

(i) the potential core.

(ii) the transitional region.

(iii) the fully developed region.

Each of these regions shows a characteristic flow pattern as will now be explained.

1.2.1 Initial Region

In this part of the free jet flow, a thin and initially laminar shear layer is established in the immediate vicinity of the nozzle exit. This layer surrounds the

axisymmetric jet where the central region has a uniform axial velocity level and is referred to as the "potential core". As the fluid moves downstream, the thickness of the shear layer increases and the radius of the potential core reduces. Simultaneously, the turbulence level close to the centre of the jet increases and the whole of the flow cross-section can be classed as fully turbulent. These continual changes of the flow condition arise because of the "entrainment" of non-turbulent ambient fluid across the free boundary and into the main flow.

This initial region of the free jet extends from the nozzle exit section to the point where the inner boundary of the annular shear layer meets the axis of the jet. Experiments show that the length of the potential core depends greatly on the turbulence level at the nozzle exit and the Reynolds number, based upon the mean velocity of the flow in the nozzle exit plane and the nozzle diameter. One of the most important features of this region is that the axial velocity U_j is constant across the whole potential core region.

The initial region also contains the mixing zone which lies between the potential core and the surrounding medium as shown in figure 1.1. Since the velocity gradient across this mixing zone is relatively high, the turbulence levels are also high and the flow may exhibit intermittent behaviour in which the flow switches randomly from turbulent to non-turbulent.

The characteristics of this developing zone of the jet flow were previously investigated by many workers, including Tollmien (1926), Corrsin (1943), Corrsin and Uberoi (1950), Corrsin and Kistler (1954), Townsend (1956), Wygnanski and Fiedler (1969), Schlichting (1968), Bradshaw (1971), Capp (1983), Fiedler and

Fernholz (1990) and Hussein et al (1994). As a results, it is now generally accepted that the potential core extends for a distance of approximately 4 to 7 diameters from the nozzle outlet plane exit.

1.2.2 Transitional Region

In an axisymmetric jet flow, this region extends downstream from the end of the potential core region, where the mixing shear layer has penetrated to the centre-line of the jet. Here, the centre-line velocity begins to reduce steadily with axial distance, and the cross-sectional area of the flow increases to maintain the total momentum flux of the free jet, Schlichting (1968). This region has received little attention from most researchers, since measurements in a free jet flow shows that the mean velocity profiles exhibit self-similarity immediately after the potential core although the turbulence itself is not yet fully developed. In this case, the cross section in which the main and the initial areas come together is termed the transitional cross section of the jet. For this reason, the length of the transitional region is often assumed to be zero (see Abramovich (1963)).

1.2.3 Main Similarity Region

Beyond the transitional region, the cross-sectional area of the jet continues to increase due to the entrainment process and the time mean level of the axial velocity component is everywhere less than the nozzle exit velocity U_j.

This is the zone of fully established flow in which the entire central part of the jet has become fully turbulent and the non-dimensional profiles of the time mean velocity components and the turbulent intensities in each direction collapse upon one another when plotted in terms of the appropriate scaling parameters. To achieve this

"similarity condition", the mean velocity components and the turbulent intensities must be non-dimensionalised in terms of characteristic jet properties as will be explained in Chapter Six.

Deceleration of the fluid in the jet occurs through simultaneous capture (or entrainment) and then acceleration of the surrounding (ambient) fluid, so that the total rate of mass flow through successive planes orthogonal to the jet axis increases with increasing distance from the exit plane. The essential feature of this region is that the distributions of the time mean velocity components and the turbulence intensity profiles reach a similarity form in which one function (of axial position and radius) can be used to describe the behaviour of the axisymmetric jet.

This region of the jet has been studied in great detail by many experimentalists: see, for example, Wygnanski and Fiedler (1969) Capp (1983), Panchapakesan and Lumley (1993) and Hussein et al (1994). For an introduction to the associated computational work which has been reported, the reader is referred to Abramovich (1963), Rajaratnam (1976), Taulbee et al (1987), Abid (1994) and Sharpe (1994).

1.3 Background to the Project

The experimental programmes described in this thesis have been carried out to investigate how the mean velocity and turbulence structure of an axisymmetric air jet can be varied by means of excitation to produce large scale turbulence structures.

A preliminary study into the influence of aerodynamic excitation on the

behaviour of a turbulent free jet was carried out previously by Szajner and Turner (1987). Here, excitation of the main jet is introduced by pulsing a thin annular jet which surrounds and is co-axial with the main central jet. A single constant temperature hot film anemometer was used to explore the potential flow region of the jet. The measurements showed how the spread of the jet could be altered drastically by the excitation, leading to entrainment rates up to twice those of the natural free jet.

Subsequently, Jeung (1993) employed laser Doppler anemometry to study the intermittency characteristics of the same turbulent free jet. First he experimented on a free jet of air using a single component constant temperature hot film anemometer. However, the results obtained from the hot film anemometer were unsatisfactory since it proved impossible to find reliable turbulence detector functions on the basis of single component measurements. The available literature, see for example Morrison and Bradshaw (1989), also suggested that such turbulence detector functions could only be obtained by using two-channel instrumentation capable of yielding more representative quantities such as the Reynolds stress terms. Due to the known difficulties in operation of two channel constant temperature anemometry - see for example Turner (1971) - and the availability of advanced laser Doppler anemometry equipment, it was then decided that two component laser Doppler anemometry should be employed. However, the need for the presence of the appropriate seeding particles and for both the jet and the surrounding fluid to be seeded was recognised. After considering these difficulties, Jeung decided to study the intermittent nature of the flow in a free jet using a water flow system.

In the present investigation, which has concentrated on the behaviour of an

excited jet, the author has overcome the problems of seeding encountered by Jeung and has thereby been able to make measurements in an air jet system. This improvement has been achieved by enclosing the space occupied by the free air jet inside a large containment made of timber and polythene and with dimensions of 5.5m×5.0m×5.0m. This modification will be explained in more detail in Chapter Five, see also Al-Sudane and Turner (1994). Having made this change, it became possible to use the laser Doppler anemometer to investigate the behaviour of the air jet subjected to aerodynamic excitation. Detailed experimental data have therefore been collected over the range of axial positions defined by x/D = 1.0 to x/D = 15.0. The objective of this study has been to achieve a better understanding of the jet excitation phenomena and to produce a detailed data base of the time mean and turbulence properties for the stated range of axial positions and over the full radial extent of the jet.

1.4 Objectives of the Present Study

Most engineering flows are turbulent and the study of turbulent flow behaviour is one of the most important branches of fluid mechanics for engineers and scientists. Theoretical approaches to the prediction of turbulent flow behaviour have been inadequate in the past and have usually been unable to deliver a physical understanding of the phenomena. Since an analytical approach inevitably requires assumptions, the role of experimentation has always been important. This is in marked contrast to most other branches of applied physics, where experimentation is normally used to prove or disprove theories rather than to explore the physical situation. Even today, in turbulence research, it is commonly accepted that experiment is needed for 'inspiration' - see, for example, Kovasznay (1959). Thus,

the present research investigation has been aimed at gaining an improved understanding of the fundamental characteristics of the turbulent free jet when subjected to aerodynamic excitation. The relationship between the excitation conditions and the distribution of the time mean velocity and turbulent fluctuation levels have been of particular concern. The opportunity has also been taken to explore the intermittent (turbulent/non-turbulent) nature of the flow in the free jet, with and without excitation.

1.5 Layout of the Thesis

The main body of this thesis consists of nine chapters, of which this Introduction forms the first. Chapter Two covers the literature review and discusses the previous related work. Chapter Three describes the experimental flow apparatus.

In Chapter Four, the first part of the research programme is described, including a discussion of the use of the constant temperature hot film anemometer and the experimental results so obtained. Chapter Five deals with the laser Doppler anemometer (LDA) technique and includes a brief treatment of the basic principles and the methods by which the performance of the LDA equipment can be optimised.

Chapter Six contains information about the computer software which has been used for data acquisition and processing during the investigation. The experimental results are discussed in Chapter Seven, leading to preliminary conclusions about the influence of the excitation on the time mean velocity distributions and the turbulence fluctuation levels in the free air jet. Chapter Seven also presents and discusses the intermittency results of the flow in the free turbulent jet, with and without excitation.

In Chapter Eight, the qualitative observations derived from the flow visualisation study using the laser light sheet are presented and discussed in relation to the quantitative results found using the hot film and laser Doppler anemometry techniques. Finally, Chapter Nine summarises the influence of the excitation on the jet behaviour and makes recommendations for future work.

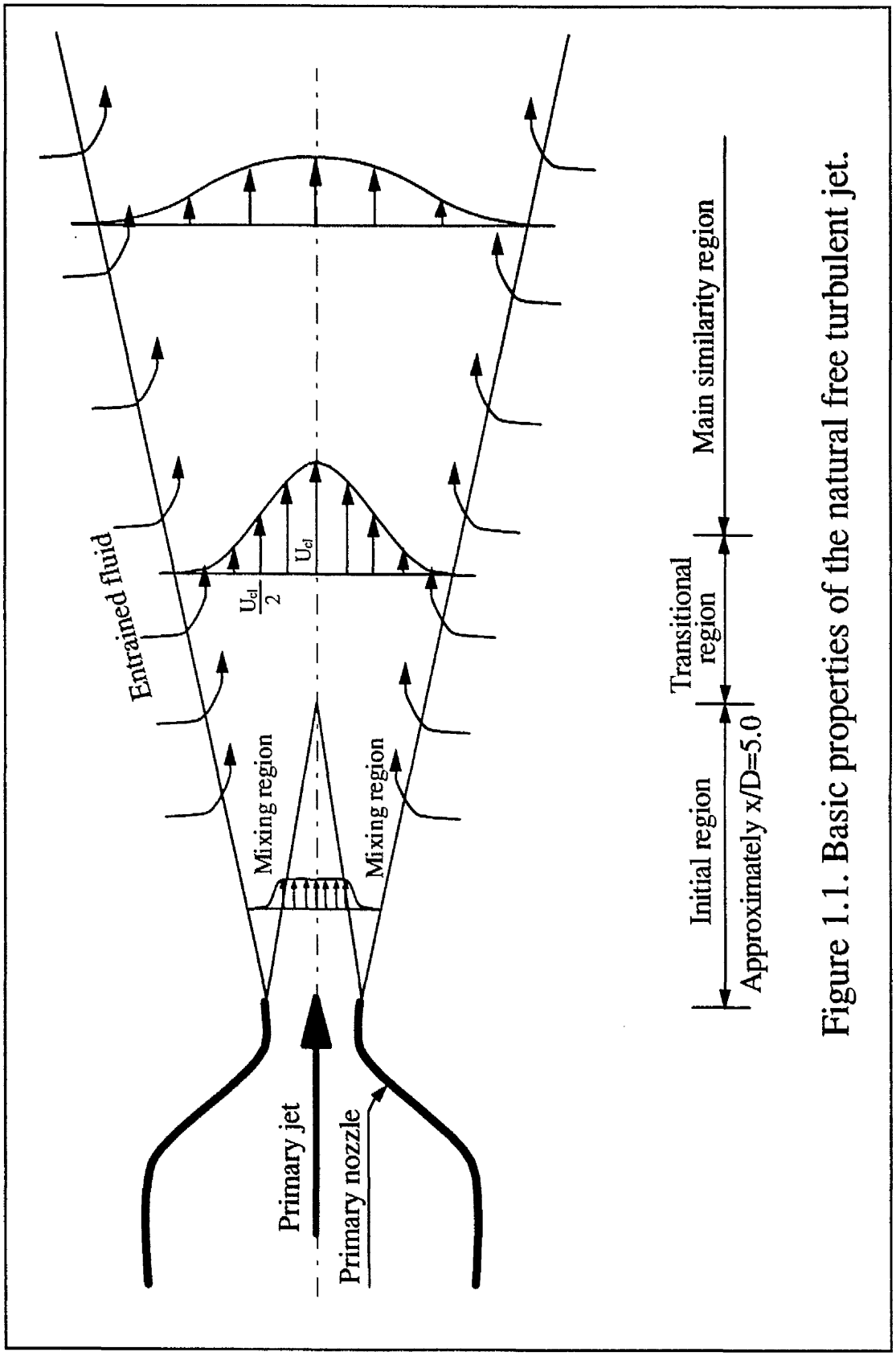

Figure 1.1. Basic properties of the natural free turbulent jet.

CHAPTER 2

LITERATURE REVIEW

CHAPTER TWO
LITERATURE REVIEW

2.1 Introduction to Free Jet Flows

The type of flow seen in a turbulent free jet can be produced readily in a laboratory and occurs in many branches of engineering. As mentioned in section 1.2, this flow first develops in the initial region, immediately after the source of discharge or nozzle (see figure 1.1), and eventually reaches a state of self-similarity further downstream, extending from x/D = 70.0 in an axisymmetric jet and approximately x/D = 120.0 for a plane jet in stagnant surroundings. The reported differences between the turbulent round jet and the plane jet are attributed to the differences in the structure of the shear layers. In the case of an axisymmetric jet, toroidal vortex rings are formed which interact around the circumference, whereas the weaker vortices formed by a plane jet are less predictable and may act symmetrically, antisymmetrically, or may fluctuate between the two modes in antiphase for opposite sides of the jet.

Jet flows are traditionally classified according to their geometrical characteristics and are typically referred to as axisymmetric, plane, radial, co-axial or confined. One of the special characteristics of a turbulent free jet is the absence of any solid boundaries in contact with the flow and, consequently, the absence of a laminar sub-layer such as appears in a turbulent boundary layer. These facts led theoreticians to assume that the equations of motion of such flows can be simplified. An example of this simplification process is that the pressure distribution will be

assumed uniform throughout the main body of the jet, and swirl will be ignored. In the absence of swirl, the azimuthal mean and turbulent fluctuation components can be dropped from the equations of motion. Albertson et al (1948) concluded, on the basis of experimental evidence, that it may safely be assumed that the static pressure distribution is essentially hydrostatic throughout the zone of motion. This means that the sole force producing the deceleration of the fluid in the jet and acceleration of the surrounding fluid is derived from the tangential shear stress in the mixing region.

Most of the earlier experimental investigations on the axisymmetric free jet have been summarised by Schlichting (1968), including the works of Reichardt (1941), Corrsin (1943), and Corrsin and Kistler (1955). These results have shown that the turbulence intensities in the three orthogonal directions fail to attain the self-preservation - at least up to x/D = 70.0. Subsequently, the work of Wygnanski and Fiedler (1969), using a linearised constant temperature hot wire anemometer became the standard reference on which to base a quantitative description for profiles of the mean velocities and the turbulent stresses.

Rodi (1975) developed a new method for analysing the signals derived from a constant temperature hot wire, measuring the jet characteristics in the self-preserving region ($x/D \geq 75.0$). The results of these analysis were believed to be more reliable than those of Wygnanki and Fiedler (1969). Capp (1983) used the LDA technique to investigate a turbulent axisymmetric air jet at axial stations given by x/D = 67.0 and 97.0. More recently, Panchapakesan and Lumley (1993) have investigated a free air jet using a constant temperature flying hot wire system. It was found that the measured profiles of the time mean velocity and turbulence intensities

of these studies did not agree particularly well with those presented by Wygnanski and Fiedler (1969). In a more recent study on the axisymmetric air jet, the three techniques of the stationary hot wire, the flying hot wire and LDA have been examined by Hussein et al (1994). The latter analysed the experimental data together with the governing equations and boundary conditions which apply to the axisymmetric jet. These authors concluded that the flying hot wire and the LDA results satisfy these equations, and they stated "the results derived from stationary hot wire reported here and presented in many of the experiments performed earlier are not representative of an axisymmetric jet".

2.2 Measurement in Axisymmetric Free Jet

2.2.1 Review of the Behaviour of the Measured Parameters

2.2.1.1 Mean Velocity Field

The distributions of the time mean axial velocity have been measured in most previous investigations of the free jet. As a result, it has been concluded that the velocity varies as a "top-hat" profile in the potential core of the jet, where the velocity maintains a value equal to that in the exit plane of the nozzle, provided that the nozzle contracts smoothly and has a large contraction ratio (say 20:1). Far downstream, at approximately 20 diameters from the nozzle, the profiles tend to follow a Gaussian form and show evidence of self-similarity. Thus, when plotted in a non-dimensional form, they show a reasonable fit to the expression:-

$$\frac{U}{U_{cl}} = e^{-c_o(R/R_{1/2})^2} \qquad 2.1$$

where c_o is an empirical constant. In practice, the value of c_o varies from 0.688 as

given by Donaldson et al (1971) to the value of 0.832 reported by Thomas (1991). These differences in the value of c_0 are believed to be related to the nozzle geometry and the actual measuring technique which was used.

The constant temperature hot wire anemometer technique has been widely used in flow investigations - see, for example, Maczynski (1962), Smith and Hughes (1977), and Biringen (1986). However, Since the output of a hot wire anemometer does not vary linearly with the instantaneous velocity, some measurement difficulties have been reported at the edges of the jet where the mean velocity is lowest and the turbulent fluctuation levels are particularly high. These problems arise because, generally, all jet flows show large gradients in the time mean axial component of the velocity across the plane which is perpendicular to the main flow direction.

Donaldson et al (1971) measured the distribution of the axial velocity component of a free air jet issuing from a 13.0mm diameter nozzle using the Pitot tube and hot film anemometer techniques. Excellent agreement was found between the two sets of data in the central region of the jet. This is seen most clearly when the axial decay of the centre-line velocity of the axial component profiles are examined. However, the axial velocity distributions obtained by the Pitot tube method show lower velocity levels away from the centre than those formed by the hot film method. This difference is almost certainly a reflection of the different types of error which are inherent in the two methods.

Taulbee et al (1987) obtained measurement of the distribution of the time mean axial velocity component using both constant temperature hot wire

anemometry and LDA in the range of $x/D \geq 70.0$. They found that the velocity levels obtained by hot wire measurement are slightly higher than those from LDA for radial positions in the range $0.2 < R/R_{1/2} < 1.5$. These differences were ascribed to cross flow errors which modify the response of the hot wire anemometer system.

Wygnanski and Fiedler (1969) measured the distributions for the time mean axial velocity component of a free jet in the self-preserving region. They discovered that their experimental data did not agree very well with the theoretical prediction reported by Tollmien (1926) which was based on Prandtl's mixing length hypothesis. Tollmien's solution of Prandtl's mixing length hypothesis agrees moderately well with Wygnanski and Fiedler's measurements in the outer part of the jet, while the solution by Schlichting using Prandtl's eddy viscosity model, based on the assumption that the eddy viscosity is constant over the cross section of the jet, is in better agreement with their measurements near the centre - see figure 2.1.

Capp (1983) attempted to fit experimental data for the mean axial velocity distributions, obtained using LDA, into both polynomial and Gaussian forms. A comparison of these two assumed profiles at $x/D = 67.0$ shows that polynomial fit is best near the centre of the jet, but diverges from the experimental data with increasing radius. In contrast, the Gaussian curve is slightly high near the centre, but gives better agreement at the edges of the jet. A good discussion relating the velocity distribution functions to other bulk parameters, such as the entrainment function and the momentum flux can be found in Capp (1983). He concluded that the Gaussian profile provides the best basis for estimating the volume flux in the jet since this showed the best agreement with the experimental data for $R/R_{1/2} \leq 2.5$.

Hussein et al (1994) carried out experiments on the jet using the constant temperature flying hot wire technique and LDA on the same jet facilities as were originally used by Capp (1983). The distribution of the time mean axial velocity component obtained using these techniques was least squares fitted to yield the expression:-

$$\frac{U}{U_{cl}} = [1 + 1.212\times10^{1}\eta^{2} + 2.815\times10^{3}\eta^{4}]\, e^{-111\eta^{2}} \qquad 2.2$$

where $\eta = R/(x - x_o)$, and x_o is the virtual origin[1] of the free jet which is approximately four nozzle diameters upstream of the exit plane of the nozzle. It can be seen that equation 2.2 combines both the polynomial and exponential expressions which were reported by Hussein et al (1994).

2.2.1.2 Decay of the Centre-Line Velocity

The axial decay of the centre-line velocity level has been determined in most investigations in this area of research. In the case of a self-preserving free jet, the entrainment process coupled with the principle of conservation of axial momentum shows that the centre-line velocity must decrease with increasing axial distance. This is verified by all the experimental data which is available. Moreover, it is commonly assumed, for a fully developed free turbulent jet far downstream from the nozzle, the flow becomes independent of the initial conditions at the origin. However, the distance necessary to establish this independence is influenced by the initial conditions. As previously stated in section 1.2.1, the time mean axial velocity

[1]The imaginary point where the lines representing the approximate jet boundaries intersect the jet centre- line is known as the virtual origin.

level at the centre of the jet begins to decrease from the output nozzle value beyond the downstream limit of the potential core. Albertson et al (1948) observed that the centre-line velocity starts to decrease beyond x/D = 6.2 where the jet issued from a sharp edged circular orifice. However, when the jet issued from a rectangular slot of width B_o , the decay was observed to start after an axial distance of $5.2B_o$. The data could then be represented by the following relationship:-

$$\frac{U_j}{U_{cl}} = 0.438 \sqrt{\frac{x}{B_o}} \qquad 2.3$$

George and Hussein (1989) also investigated the flow distributions within an axisymmetric air jet using a flying hot wire anemometer. Their measurements for the decay of the centre-line velocity agree with those of Capp (1983) who used LDA and Wygnanski and Fiedler (1969) whose results were obtained using a stationary hot wire. This agreement between data obtained by the three techniques could perhaps have been anticipated since the minimal turbulent intensity at the centre-line will generally lead to low experimental errors. However, when the distributions of the time mean axial velocity component across the radius obtained by the three different methods were compared, the results yielded by the flying hot wire and the LDA techniques were found to agree closely but were slightly lower than those obtained with the stationary hot wire anemometer.

2.2.1.3 Influence of the Nozzle

Obot et al (1984) and Trabold et al (1987) investigated the effect of the nozzle design features on the behaviour of the jet. Their results for the mean velocity profiles appear to suggest that the length of the nozzle should be one to five

times its outlet diameter to suppress any inlet disturbances. However, the decay of the centre-line axial velocity component (i.e. the end of the potential core) for a short nozzle starts at x/D = 5.0, at a rate shown in table 2.1, while the decay of the long nozzle (L/D = 12.0)[2] starts at x/D = 8.0 and is less gradual. This agrees with the measurements of Corrsin, Corrsin and Uberoi, and Hinze and van der Hegge Zijnen which were reported by Townsend (1976). These results concluded that the length of the potential core region is eight diameters, measured from the nozzle exit plane, but disagree with the results obtained by Forstall and Shapiro (1950) who reported that the decay starts beyond x/D = 4.0. Hill (1971) attributed these discrepancies to the nozzle shape, and its influence on the initial distribution of the axial velocity component. The experiments of Hussain and Clark (1977) supported that finding by showing how the initial conditions influence the decay of the centre-line velocity. In the fully developed region, when U_{cl}^2/U_j^2 is plotted against x/B_o, the measurements can be expressed by the equation:-

$$\frac{U_j^2}{U_{cl}^2} = k_1\left(\frac{x}{B_o} - c_1\right) \qquad 2.4$$

where k_1 and c_1 are empirical constants, dependent on the geometry of the nozzle used and the thickness of the initial shear layer. Quinn and Militzer (1989) investigated the effect of non-parallel diverging flow in the nozzle exit plane on an axisymmetric turbulent free jet, for two nozzle types having the same exit area. The distributions of the mean streamwise velocity component at the centre-line of the jet revealed that the flow accelerated within the initial region (x/D > 3.0) before

[2] Where L is the length of the nozzle, and D is the diameter.

decelerating. This acceleration was thought to be related directly to the magnitude of the mean radial velocity component. They concluded that the radial velocity component in the exit plane of a sharp-edged nozzle is significantly larger than that for the jet from a contoured nozzle - see figure 2.2.

Reference	$d(U_j/U_{cl})/d(x/D)$	Nozzle configuration
Albertson et al (1948)	0.161	convergent
Wygnanski & Fiedler (1969)	0.196	convergent
Boguslawski & Popiel(1971)	0.169	L/D=50.0
Rodi (1975)	0.166	convergent
Capp (1983)	0.172	
Obot et al (1984)	0.170 0.190	L/D=12.0 L/D=1.0
Taulbee et al (1987)	0.169 hot wire 0.172 LDA	convergent
George & Hussein (1989)	0.169	convergent
Thomas (1991)	0.196	convergent
Panchapakesan &Lumley (1993)	0.165	convergent

Table 2.1. Decay rate of the axial velocity component at the centre-line.

2.2.1.4 Turbulence Intensity

The velocity shear is zero at the centre-line of the jet in the region of the potential core ($x/D \leq 5.0$) and high in the sub-mixing region - see figure 1.1. It is not surprising, therefore, that the turbulence intensity should be low in the region close to the centre-line and higher at the edges of the jet.

One of the first attempts to determine the variation of the turbulence intensity was made by Kuethe (1935) who developed a simple type of constant current hot wire anemometer. However, this device was not sophisticated enough to respond to the rapid velocity fluctuations in the jet flow so that erroneous readings were certainly obtained for the turbulence properties.

In comparing experimental data for free jets, it is always necessary to consider the method used. Caution is especially needed when hot wire anemometer has been employed. Thus, it is worth mentioning that the method of analysing the signals produced by a constant temperature hot wire anemometer introduced by Rodi (1975) gives marginally lower values for the longitudinal fluctuation $(\overline{u^2})^{1/2}/U_{cl}$ near the centre-line of the jet, in comparison with the results calculated using the conventional analytical methods which have been reported by Wygnanski and Fiedler (1969). Surprisingly, in the outer region of the jet, the longitudinal fluctuation data from the two experiments is in close agreement.

The dependence of the root mean square velocity fluctuation $(\overline{u^2})^{1/2}$ on the initial conditions upstream of the nozzle exit plane can be seen in the results obtained by Hussain and Clark (1977). The authors' results show that the initial growth rate of the intensity $(\overline{u^2})^{1/2}/U_j$ is higher for the jet issuing from a rectangular channel in comparison to the jet discharged from a nozzle.

Boguslawski and Popiel (1979) suggested that from x/D = 4.0 to x/D = 9.0, there is a rapid increase in the turbulent intensity. This increase is thought to be due to interaction of the two merging free shear layers, which also produced a higher gradient of the axial velocity component in the radial direction.

Beyond an axial position of x/D = 9.0, they found the turbulence intensity continued to increase but more slowly than in the initial region.

Obot et al (1984) and Trabold et al (1987) noticed that the turbulent velocity components and the shear stress levels rise more slowly in the initial region of the free jet, when produced by a long nozzle (L/D = 12.0), because the mixing process is less intense than in a jet arising from a short nozzle (L/D = 1.0). In practice, the decay of the centre-line velocity was found to be about 20% higher than for the long nozzle.

Quinn and Militzer (1989) investigated the effect of the nozzle geometry on the behaviour of a free air jet. The radial profiles of the axial turbulent fluctuation $((\overline{u^2})^{1/2}/U)$ were found to agree closely at x/D = 1.12, for both a sharp-edged slot and a contoured nozzle. However, the distributions of the radial turbulence fluctuation $((\overline{v^2})^{1/2}/U)$ in the jet from the contoured nozzle were 17% higher than those in the jet from the sharp-edged slot.

Panchapakesan and Lumley (1993) used the flying hot wire anemometer technique to obtain values for the turbulent fluctuation terms $(\overline{u^2})^{1/2}/U_{cl}$, $(\overline{v^2})^{1/2}/U_{cl}$ and $(\overline{w^2})^{1/2}/U_{cl}$. They found that the radial distributions of the turbulent fluctuation in the fully developed flow region are lower at the centre of the jet and higher at the edges in comparison with the data given by Wygnanski and Fiedler (1969) and Rodi (1975). Both these investigations used the stationary constant temperature hot wire anemometer technique to obtain their results. It is also relevant to observe that Capp (1983) obtained data for the turbulence intensity variations using LDA which agree qualitatively with those of Panchapakesan and Lumley (1993).

2.2.1.5 Shear Stress

Measurement of the flow properties in two dimensions was difficult before the development of the crossed hot wire probe. Subsequently, the emergence of the LDA technique has enabled the generation of more accurate data. Both techniques provide simultaneous information about the turbulent fluctuations in two directions as well as the degree of flow turbulence. In recent studies, these techniques have been used to detect the turbulent shear stress levels in the developing jet flow.

Wygnanski and Fiedler (1969) found good agreement between the measured turbulent shear stress parameter $\overline{uv}$ and the calculated shear stress term $\overline{uv}$, obtained from the time mean velocity profiles after neglecting the normal stress term in the momentum equation. Similarly, Rodi (1975) calculated the turbulent shear stress $\overline{uv}$ from the complete momentum equation and found close agreement with the measured values. The latter result is believed to be more reliable than those of Wygnanski and Fiedler(1969) due to the new method of analysing the hot wire signals - see Rodi (1975). Measurements of the radial distributions of the turbulent shear stress made by Capp (1983) using LDA and other data obtained using a flying hot wire anemometer by Panchapakesan and Lumley (1993) show distributions across the radius which are wider and contain higher values than those found by Rodi and Wygnanski and Fiedler (1969). These changes are thought to be attributable to the better resolution of flow reversals achieved by the flying wire and the LDA, thereby eliminating the rectification and cross flow errors which are inevitably present with a stationary hot wire anemometer at the high levels encountered at the edges of a turbulent free jet - see figure 2.3.

The comprehensive study by Hussein et al (1994) on an axisymmetric air jet showed that the distributions of the shear stress obtained using the stationary hot wire, the flying hot wire and LDA all attained self-preservation at the two considered axial locations i.e. x/D = 70.0 and 100.0. The experimental results of the shear stress ($\overline{uv}$) using the stationary hot wire did not agree with the values calculated from the equation of motion. Calculation of these values was based upon the time mean axial velocity term only, and produced results which are higher than the experimental data in the region of $R/R_{1/2} < 1.5$ and lower in the region of $R/R_{1/2} > 1.5$. Hussein et al (1994) also calculated $\overline{uv}$ from the equation of motion by including approximation to the Reynolds stresses up to second-order. The shear stress profiles follow the same trend as that calculated from the mean velocity distributions only, but with a higher peak value. In fact, the alternative peak values of the non-dimensional shear stress term $\overline{uv}/U^2_{cl}$ are approximately 0.0185, 0.0217 and 0.0235 respectively, for stationary hot wire results, the calculations based on the time mean velocity only, and calculations made with inclusion of the Reynolds stresses. The experimental data obtained using the flying hot wire and the LDA systems were also reported by Hussein et al (1994). The experimental shear stress data obtained with both these techniques are consistent with the prediction of the equation of motion particularly when the Reynolds stresses are included.

2.2.1.6 Rate of Spreading

The rate of spreading of a free jet is most commonly expressed as the variation of the jet half-width $R_{1/2}$ with longitudinal distance x. The half-width $R_{1/2}$ corresponds to the radial position at which the velocity has fallen to half of the centre-line velocity (U_{cl}) at any particular axial position of the jet. This definition

is preferred because the radial position at which the velocity of the jet reaches zero would involve far more difficulties than finding the point where the velocity reaches half of its maximum value. It is known that the centre-line velocity (U_{cl}) decreases linearly with distance x to fulfill the need for conservation of momentum flux in the case of the natural free jet. As a direct result of this variation in the centre-line, the width of the jet represented by the dimension $R_{1/2}$ should increase linearly with distance along the axis of the jet. It is therefore possible to determine the rate of spreading from the distribution of the time mean axial velocity. This rate of spreading is commonly expressed in terms of the derivative $d(R_{1/2})/d(x)$.

Wygnanski and Fiedler (1969) used constant temperature hot wire anemometry to obtain the distribution of the time mean axial velocity profiles, and derived a value for the rate of spread of the jet $[d(R_{1/2})/d(x)] = 0.086$. This result has been confirmed by Rodi (1975). However, Donaldson et al (1971) reported a difference of 5% between time mean measurements of the streamwise velocity distributions made using a constant temperature hot film anemometer and a Pitot tube at $x/D = 20.0$, although the best fit for both data sets yielded the same rate of spread $d(R_{1/2})/d(x) = 0.091$. Here it should be noted that both the flying hot wire and LDA produced slightly different but probably more reliable data for the mean velocity field than the conventional constant temperature hot wire anemometer. Thus, different values of the rate of spreading may be expected due to the intimate relationship between the jet parameters. The spreading rate $dR_{1/2}/dx$ measured by Capp (1983) with LDA is 0.094 which is in good agreement with the results of Hussein and George (1989) who used a flying hot wire.

Hussain and Clark (1977) found that the width of a free jet which is

initially laminar increases at a greater rate than a jet which is turbulent from the start. Gutmark and Ho (1983) studied this same problem and observed the strong affect of the laminar instability waves on the rate of spreading. These laminar instability waves develop in the shear layer originating from the nozzle lip and then roll-up into strong coherent structures. The same authors also noticed that modification of the initial conditions could affect the frequency of the initial instability and, consequently, the preferred modes and spreading rates in the downstream flow. Subsequently, Obot et al (1984) found that the initially laminar jet spreads more rapidly from a short nozzle of one diameter in length than for a longer nozzle of 12.0 diameters in length - see also section 2.2.1.3. In other terms, the jet from the short nozzle was found to entrain as much as three times more fluid than the jet generated by the long nozzle. Obot et al (1984) reported values for the spreading rate of 0.08 and 0.078 respectively. These values are quite close to that given by Boguslawski and Popiel (1978) (i.e. 0.079 for a long nozzle with L/D = 50). The reason given for these differences is that the short nozzle is susceptible to changes in the up-stream flow properties, whereas such entrance effects are almost damped out for the longer nozzle. Close to the nozzle (at x/D = 0.0), turbulence intensity for the short nozzle increases from 1.7% at the centre to a maximum value at the edge of the jet of approximately 36%. In contrast, the intensity only rises to 9% for the long nozzle at the edge of the same downstream station, - Obot et al (1984).

Since the turbulence level across the radius of the jet determines the degree of flow mixing, it is understandable that the local entrainment rates will vary between nozzles of different dimension characteristics. This understanding was

tested by Trabold et al (1987), who examined the performance of three different lengths of sharp-edged inlet nozzle with diameter ratios L/D = 1.0, 5.0 and 12.0. The data for the spreading rate for the nozzle with L/D = 1.0 and 5.0 are close and fall almost on a straight line with a slope of 0.097, while the rate of spreading decreases to 0.077 for the nozzle with L/D = 12.0.

Quinn and Militzer (1989) also reported that a jet from a contoured nozzle spreads faster than that from a sharp edged orifice in the initial region. Additionally their data for the variation of the half-jet width became perfectly linear with increasing axial distance after x/D = 7.5. This is due to the pronounced effect of the vena contracta in directing the stream lines of the flow downstream of the nozzle exit plane and is consistent with their observation of the linear decay of the centre-line velocity.

2.2.1.7 Entrainment Rate

Entrainment and growth in the cross-sectional area are characteristics of all unconfined turbulent free jet flows. The entrainment rate has traditionally been defined in terms of a volume or mass balance, based solely on the time mean velocity distributions of the jet flow. When a shear layer which is initially laminar becomes unstable, velocity variations arise which increase in amplitude with downstream distance, resulting in "vortex roll-up" and the creation of a train of spanwise rectilinear vortex elements. Any slight lack of equality in the vortex spacing, or in the strengths of two or three adjacent vortices, will induce them to roll around one another (i.e. to pair-up) so as to form a single large vortex. In this pairing process, some ambient fluid becomes trapped between the pairing vortices and, due to this mixing process, a phenomenon known as entrainment occurs.

Recognition of the importance of this entrainment process represented a step forward in understanding the behaviour of an axisymmetric jet and enabled the mixing process to be explained. Entrainment determines the relationship between the width and shape of the mean velocity distributions and is a key parameter in calculating the rate at which ambient fluid is entrained into the jet. The entrainment rate of a free jet is also practically important, since it controls the flow patterns in such devices as combustion chambers and furnaces. Additionally, many systems in the chemical industry rely on entrainment to achieve a high level of mixing.

The entrainment rate can be measured directly or indirectly. Direct measurements were carried out by Ricou and Spalding (1961) by injecting a free jet into a partially closed cylinder with porous walls. In these experiments, the amount of fluid which flowed radially through the porous walls was adjusted to make the pressure inside the chamber equal to the surrounding ambient pressure. The amount of this flow was measured and could be assumed to be equal to the naturally entrained surrounding fluid in the absence of the chamber -see Hill (1971) and Ricou and Spalding (1961) for more details. The last authors presented their data in a mathematical form which was recently verified by Panchapakesan and Lumley (1993).

Indirectly, a convenient practical way of calculating the entrainment rate is to measure the distribution of the time mean axial velocity component at different axial locations. These distributions can then be integrated across the jet cross-section to determine the mass flow at each station. Hence, the rate of increase of the mass flow rate (the entrainment) can be calculated. However, there are some difficulties in the technique and errors arise because of complications in obtaining

accurate measurements of the low velocity levels near the edge of the jet. This is especially true far downstream from the nozzle so that, in practice, this method is limited to an axial length of about x/D = 60.0.

Since the initial conditions at the exit plane of the nozzle have such a profound effect on the decay of the mean velocity level and the rate of spreading, some differences in the rates of entrainment for different configurations can be anticipated. The initial distribution in the jet for a given nozzle configuration, or initial boundary layer distribution, often shows a non-linear entrainment rate or two different rates of entrainment. The first rate will apply over the length of potential core, while the second rate corresponds to conditions in the fully developed region. The rate of fluid entrainment is normally higher within the potential core region.

Albertson et al (1948) developed empirical formulae which enable prediction of the entrainment rate, in both the near (up to x/D = 4.0) and far field regions, for plane and circular section jets at moderate ($Re = 5.0x10^4$) and high Reynolds numbers ($Re = 8.8x10^5$). Hussain and Clark (1977) found that the entrainment rate of a jet discharged from an axisymmetric nozzle was 25% higher than for a jet which issued from a rectangular channel up to a distance of $x/B_o = 4.0$. Beyond this, the rate is, approximately 10% higher than for the case of the channel. By way of comparison, Szajner and Turner (1987) found that the rate of entrainment for an aerodynamically excited jet increases by 50% in the initial region and remains higher by at least 20% beyond 5 diameters from an axisymmetric nozzle, when compared with an axisymmetric natural jet.

Trabold et al (1987) reported that axisymmetric jets issuing from a long

nozzle have lower rates of entrainment than those produced by a relatively short nozzle - see also section 2.2 1.3. Boguslawski and Popiel (1978), measured the entrainment rate for the jet issuing from a long pipe (L/D = 50.0) and produced results which are close to those of Trabold et al for L/D = 12.0 - see figure 2.4.

Obot et al (1984) noticed that there were differences in the mean flow development when a free jet was produced by a flanged or an unflanged nozzle. For the latter, the rate of entrainment is linear in the initial as well as the fully developed regions of the jet. However, with a flanged nozzle, a non-linear variation of the entrainment rate is established in the near region (x/D < 15.0). This is believed to be due to the reduction in entrainment rate in the initial region due to the restriction imposed by the flange.

2.2.1.8 Similarity and Self-Preservation

Far downstream from the nozzle exit plane, the time mean and turbulence properties of the free jet are known to approach a similarity condition - Schlichting (1968). This condition of dynamic similarity in the similarity region of the free jet requires that the angle between the jet boundaries and the axis must be constant at all axial positions. For example, the distribution of the time mean velocity components at different positions downstream can each be collapsed onto a single unique curve, by a process of normalisation using local length or velocity scales. In this situation, the non-dimensional parameters describe the flow behaviour and the free jet can be said to exhibit "self-similarity". If the time mean velocity field and the Reynolds stress distributions are all self-similar then the whole flow can be considered to be "self-preserving". Hussain and Zedan (1978) defined self-preservation in two different ways based on their study into the effects of the initial

conditions on the development of an axisymmetric turbulent free shear layer. The first definition, where self-similarity of the time averaged properties may be reached in a short distance from the exit plane of the nozzle, was called "mean or near-field" self-preservation. The second type of flow is called "structure self-preservation" in which the higher order turbulent fluctuation terms can achieve a unique state of self-similarity. They found that this second state can only be achieved far downstream of the nozzle.

The literature is confusing with regard to the attainment of self-similarity. Thus, Forstall and Shapiro (1950) reported that similarity of time mean velocity distributions are reached at approximately x/D = 6.0. A similar observation was made by Smith (1975) who suggested that all data points for the time mean axial velocity component should collapse fairly well onto one curve beyond the distance x/D = 6.55. In contrast, Wygnanski and Fiedler (1969) observed that the time mean velocity distributions become self-similar at about 20.0 nozzle diameters from the exit. Then, Boguslawski and Popiel (1978) reported that self-similarity of the velocity distributions was attained at x/D = 8.0. The discrepancies between these different studies in achieving self-similarity are probably explained by the different levels of disturbance which are input to the flow at the nozzle exit plane. These disturbances influence the nature of the large scale structures in the initial regions of the jet and, in turn, control the dynamic behaviour of the free shear layers.

The cross-stream distributions of the turbulence intensity require a much longer distance from the nozzle, in contrast to the time mean velocity components, to become self-preserving. Based upon the findings of Wygnanski and Fiddler (1969), the mean square value of the longitudinal turbulent velocity fluctuation

component becomes self-preserving approximately 40.0 diameters from the nozzle and reaches an asymptotic value of approximately $(\overline{u^2})^{1/2}/U_{cl} = 0.28$. In contrast, the radial tangential fluctuations require a distance of x/D = 70.0. Measurements of the axial turbulence intensity taken by Panchapakesan and Lumley (1993), using a flying hot wire anemometer system, showed self-similarity at x/D = 70.0 with an asymptotic value of approximately 0.23. However, the radial intensity continued to increase steadily beyond x/D = 70.0.

On the other hand, for the case of a jet immersed in a free stream, a higher asymptotic value of the turbulence intensity was reported by Antonia and Bilger (1973), and Biringen (1975). Subsequently, Biringen (1986) pointed out that the distributions of the normal Reynolds stresses tend to become self-similar at around x/D > 115.0 for U_j/U_s = 10.0 and 5.0, with asymptotic values of 0.29 and 0.32 respectively. Observe that both these values are higher than of 0.28 which had been reported by Wygnanski and Fiedler (1969) for the case of a turbulent free jet. Self-similarity of the turbulence intensities was not observed within the axial range (x/D < 200.0) of Biringen's (1986) experiments, for the case of U_j/U_s = 3.3. However, the turbulence intensity $[(\overline{u^2})^{1/2}/U_j]$ reached a highest value of approximately 0.4.

This gradual approach to self-similar behaviour is to be expected, since energy is transferred directly from the mean flow field to the streamwise velocity fluctuations while the mean velocity gradients are required to transfer the energy to other components of the turbulent motion. Rodi (1972) experimented on a free air jet with a nozzle of 12.9mm outlet diameter and found that the self-preserving region started at a distance x/D = 62.0. He suggested that, at this distance, the achievement

of self-preserving conditions behaviour should depend on the local value of the time mean axial velocity component and less strongly on the initial conditions of the jet at the nozzle exit plane.

2.3 Measurement in Jets with co-Flowing Stream

The introduction of a secondary free stream, coaxial with the main axisymmetric free jet, strongly influences the characteristics of the jet. Although the changes in the time mean velocity component are less obvious than for the turbulent fluctuating components. However, it is often proposed that such jet flows have a universality in the shape of the axial mean velocity distributions, even when conditions of exact self-preservation are not possible. Based upon the literature, it appears that the (inner) jet can be assumed to have a uniform axial velocity distribution over its cross-section at the nozzle exit plane. Mixing with outer stream occurs at the edge of the jet and a velocity deficit zone may be generated at the nozzle lip. This region of wake flow is still noticeable as far as x/D = 25.0, which makes this type of the flow more complicated to model than the standard free jet - see Al-Sudane (1990) and Abid (1994).

Smith and Hughes (1977) investigated the behaviour of a free turbulent jet surrounded by a co-flowing stream. Their non-dimensional velocity distributions were found to reach similarity at approximately x/D = 7.41, for the two velocity ratios $U_j/U_s = 1.75$ and $U_j/U_s = 3.5$[3]. This information is in conflict with that given by Biringen (1989) who observed that the profiles of the time mean axial velocity component reach self-similarity "as early as x/D = 20.0", for all velocity ratios

[3] U_j is the jet velocity at the exit plane of the nozzle. U_s velocity of the secondary stream.

(U_j/U_s) considered in the investigation. Similarly, Yule and Damou (1993) reported that the normalised values of the time mean axial velocity distributions collapse upon one another and the similarity of the distributions is attained within the range of $13.3 \leq x/D \geq 32.2$ for different combinations of the velocity ratios within the range $6 \leq U_j/U_s \geq 30$.

Curtet and Ricou (1964) found that the decay of the axial velocity component along the centre-line of the jet is faster as the velocity ratio U_j/U_s is increased. In other words, when the velocity of the secondary flow is increased the decay of the centre-line velocity becomes slower and the spreading rate of the jet is reduced. Abid (1994) also reported a slight increase in the length of the potential core when the velocity of the secondary flow (U_s) was increased. Smith and Hughes (1977) compared their results for the spreading rate of the jet with those of other investigators including Antonia and Bilger (1973), Biringen (1975), and Wygnanski and Fiedler (1969). They showed that the various spreading rates followed similar trends, but that the gradients were different and did not correlate fully with the velocity ratio. The studies of the present author - Al-Sudane (1990) - and Abid (1994) may help to explain the lack of agreement between the results of the above investigators, which presumably arises because of differences in the initial conditions in the various investigations.

The presence of the secondary stream has a very strong influence on the development of the turbulence. Smith and Hughes (1977) pointed out that the local values of the radial and circumferential normal stresses $(\overline{v^2})$ and $(\overline{w^2})$ are not affected by the introduction of the free stream to the same extent as the decay of the longitudinal component $(\overline{u^2})$. Curtet and Ricou (1964) observed that the turbulence

intensity $\overline{(u^2)}^{1/2}/U_{cl}$ along the centre-line of the jet reaches its maximum value of approximately 0.24 at x/D = 40.0 in the case of free jet whereas, with a secondary stream, the intensity increases monotonically up to x/D = 60.0. Antonia and Bilger (1973) pointed out that, for the velocity ratio $U_j/U_s = 3.5$, the longitudinal turbulence intensity is slightly larger than that reported by Wygnanski and Fiedler (1969) for the free jet. The centre-line intensity reaches approximately 0.3 for x/D = 75.0. However, for a velocity ratio $U_j/U_s = 2.0$, a centre-line value of 0.5 is reached at x/D = 150. A similar observation was reported by Biringen (1986) who investigated a turbulent round jet in a co-flowing stream using the three velocity ratios of $U_j/U_s = 10.0$, 5.0, and 3.3. The axial profiles of the turbulence intensity showed gradually increasing levels as the velocity ratio of the primary jet to the secondary flow (U_j/U_s) was increased. The levels were also higher than those for the free jet within the range of axial positions investigated ($x/D \leq 200.0$).

Durao and Whitelaw (1973) considered the influence of an annular secondary jet surrounding the primary jet for three velocity ratios[4] $U_j/U_s = 0.0$, 0.23 and 0.62. Similarity of the time mean axial velocity distributions was reached at approximately x/D = 12.0, 13.0, and 8.0 for velocity ratios $U_j/U_s = 0.0$, 0.23 and 0.62, respectively. In contrast, Wygnanski and Fiedler (1969) reported that similarity of the time mean axial velocity distributions was attained at x/D = 20.0 in the case of the natural free jet in isolation. The reason for this different behaviour is thought to be related to the initial condition at the exit plane of the nozzle. Durao and Whitelaw (1973) also observed that the decay of the centre-line velocity was higher than the case of the natural free jet - see table 2.1. These rates of decay were

[4] In this case, U_s represents the maximum velocity of the secondary jet at x/D=0.0.

$[d(U_j/U_{cl})/d(x/D)] = 0.24$, 0.26 and 0.2 for velocity ratio $U_j/U_s = 0.0$, 0.23 and 0.62 respectively. Additionally the calculated spreading rate from the radial distributions of the axial mean velocity at x/D = 10.36 was $[d(R_{1/2})/d(x)] = 0.088$, which lies within the range of values reported in section 2.2.1.6 for the case of the free jet. Durao and Whitelaw (1973) also reported that the longitudinal turbulent velocity fluctuations did not attain the self-preserving state within the axial range of their investigation ($0.0 \leq x/D \geq 16.0$). The turbulent intensity $\overline{(u^2)}^{1/2}/U_{cl}$ along the centre-line of the jet reached its maximum values of approximately 0.256, 0.24 and 0.23 for the three velocity ratios respectively. Ribeiro and Whitelaw (1980) carried out experiments on the same experimental arrangement used by Durao and Whitelaw (1973) and observed that the secondary jet does not influence the mean velocity levels along the centre-line close to the nozzle (up to an axial distance of three nozzle diameters). However, other parameters were seen to be slightly affected. For example, the Reynolds normal stresses $\overline{v^2}$ and $\overline{u^2}$ were found to be particularly high, when the velocity of the secondary jet was 1.5 times that of the primary jet (i.e. $U_j/U_s = 0.65$).

The shear stress distribution is also effected by the presence of the co-flowing stream, with the maximum value generally occurring further downstream and being higher in magnitude, than for the free jet. For example, Antonia and Bilger (1973) reported that the maximum value of the term $\overline{uv}/U_j^2$ was attained in the similarity region at a distance of x/D = 246.0. Values of 0.039 and 0.064 were measured for velocity ratios $U_j/U_s = 3.0$ and 4.0 respectively. In contrast, the maximum values of the shear stress reported by Biringen (1986) were 0.025 at x/D = 200.0 for velocity ratio $U_j/U_s = 10.0$, 0.029 at x/D = 178.0 for $U_j/U_s = 5.0$,

and 0.033 at x/D = 182 for $U_j/U_s = 3.0$. Previously, Smith and Hughes (1977) had reported a maximum value of 0.028 for the shear stress, which was reached at x/D = 40.0. The one common feature of all these values of the shear stress is that they are significantly higher than the value of 0.017 given by Wygnanski and Fiedler (1969) for the single free jet. This suggests that a jet immersed in a co-flowing stream will show greater levels of mixing and contain more organised turbulent structures than that found in the case of the single free jet.

2.4 Influence of Excitation on Jet Behaviour

The small disturbances in the initially laminar shear layer in the exit plane of the nozzle have a tendency to become periodic further downstream. Controlled excitation from an acoustic source or any other source of energy (see the succeeding section) can cause the shear layers to oscillate close to the exit plane of the nozzle. Such oscillation can result in the shear layers roll up into discrete vortices. These will have a major influence on the overall behaviour of the jet and will change its mixing and entrainment rates.

As previously stated in section 2.1, the movement of the jet into stagnant air has been widely studied. However, comparatively little attention has been focused on the behaviour of jets which are excited and still less is known about the characteristics of the aerodynamically excited jet. The behaviour of turbulent jet flows subjected to excitation is important in the study of combustion chambers and burners, and has a direct bearing on the generation of noise by the jet flow, since there is a strong connection between the excitation and the large turbulence scale structures which this creates.

Many investigators, for example Crow and Champagne (1971) and Husian and Hussain (1983), have utilised acoustic devices (see section 2.4.1) in studies of the behaviour and mixing characteristics of a free jet. Another form of excitation, referred to as aerodynamic excitation, was introduced by Szajner and Turner (1987), using an earlier version of the apparatus employed by the present author. This aerodynamic excitation, produced by the action of a pulsed annular jet surrounding the main jet (see section 3.3), is the method which has been adapted in the present investigation. The efficiency of this approach and the results will be dealt with in more detail throughout this thesis as they arise.

An early report by Crow and Champagne (1971) on acoustic excitation revealed that introducing the excitation with a Strouhal number of 0.3, based on the exit plane velocity (U_j) and the nozzle diameter (D), produced the highest turbulence intensity value in the centre-line on the jet at $x/D \approx 3.75$. Crow and Champagne (1971) also noticed that the decay of the centre-line velocity starts earlier than for the jet without excitation, and the potential core is shortened by approximately two nozzle diameters to $x/D \approx 3.0$. Baltas and Morris (1984) subsequently reported that the fluctuation levels at the centre-line can be doubled in an acoustically excited jet at a distance from the nozzle of $x/D = 3.0$ and 4.0 but reach saturation at the end of the potential core, presumably because the coherent motions reach maximum amplification by that position. This is in agreement with the observation of Hussain and Zaman (1981) who found that acoustic excitation modifies the turbulence structure and has the greatest effect within the first 5.0 diameters from the nozzle exit plane. Furthermore, for $x/D > 8.0$, there appears to be no significant difference between the root mean square fluctuations of the axial component (u_{rms}) in the

excited and natural jets. Hussain and Zaman (1981) also produced the contours of the time mean axial velocity component, which illustrated the relative widening of the excited shear layer, the more rapid spread of the jet and the shorter the potential core compared with the natural jet.

Collins et al (1984) carried out measurements on an excited plane jet using two component LDA technique. The jet was excited by means of a vane located in the potential core of the jet, and driven by a vibrator. These authors observed that the plane (two-dimensional) jet responds in similar fashion to the axisymmetric jet and that the decay of the centre-line velocity and the growth of the jet half-width are both more rapid than for the corresponding steady jet (without excitation). The scaled value of the axial turbulence intensity $[(\overline{u^2})^{1/2}/U_{cl}]$, based on the centre-line time mean velocity levels rather than the local values, increased by approximately 80% in the core region and the radial turbulence intensity $[(\overline{v^2})^{1/2}/U_{cl}]$ also increased throughout the jet. The entrainment rate was strongly influenced by the excitation and was approximately 1.5 times higher than in the natural free jet.

Wicker and Eaton (1994) investigated the influence of excitation by producing timewise variations of the mean axial velocity in the co-flowing jet. These authors reported that excitation of the core flow did not produce a significant change in the behaviour of the external co-flowing. However, excitation of the annular co-flowing jet produced large scale outer layer structures similar to those observed in the single jet: these structures were observed to provide strong coupling between the outer and inner layers.

Raman and David (1994) employed the fluidic excitation technique in

two modes, referred to as the sinuous and varicose modes - see the following section. These authors used several radial directed secondary jets which were caused to pulse by means of a fluidic oscillator. Their results show that there are dramatic differences between these two modes with regard to the decay of the centre-line velocity level and the entrainment rate. These authors also noticed large changes between the performance of the two excited jets and the natural free jet. In particular, the length of the potential core of the two excited jets was reduced to about 80% of that for the natural jet and the entrainment rate was approximately 1.6 times that for the natural jet.

Obot et al (1984) and Trabold et al (1987) measured the variation of the centre-line turbulence intensity for a jet produced by square-edged entrance nozzle and produced results which were in close agreement with those of Crow and Champagne (1971), for a free air jet under excitation condition of $St_D = 0.6$, based on the nozzle diameter. This similarity was explained by noting that both the square-edged entry and the more conventional convergent nozzle with excitation produce a jet whose frequency of oscillation is considerably larger than that produced by a conventional convergent nozzle alone. These experiments are in close agreement with the present author's findings for a conventional convergent nozzle, both with and without excitation. This agreement will be discussed further in Chapter Seven.

Lai and Simmon (1984) used a form of mechanical excitation with an oscillating vane located in the potential core. Their measurements of the mean velocity distributions show significant increases in the rate of spreading and entrainment compared with the turbulent jet without excitation.

Bremhorst and Hollis (1990) studied the influence of the aerodynamic excitation on the behaviour of the jet. They excited the main jet by means of pulsation which was produced by two rollers (one at each side of the jet) synchronized by gears. These rollers acted as a valve geometry resulting in an on-to-off rate of 1:2. Bremhorst and Hollis (1990) observed that excitation of this kind influenced the general behaviour of the jet. In particular, the volumetric flow and entrainment rates were much larger than the steady unexcited jet.

Finally, Vandsburger and Ding (1995) examined the influence of excitation on two streams separated by a splitter plate. Each jet emerged from a rectangular nozzle 63.0mm high and 102.0mm with different velocities to create a low-speed side and a high-speed side. The planar shear layer between these two sides was excited by a length of piano wire strung across the flow test section. An increase of 35% in the entrainment rate was found compared to the case without excitation.

Overall, on the basis of the previous discussion, it can be concluded that different types of excitation can be used to generate a highly ordered series of coherent structures which result in greater mixing and thereby enhance entrainment of the surrounding fluid.

2.4.1 Methods of Excitation

Excitation of the free jet can be introduced artificially by a periodic input of some form of energy. There are different ways to introduce such periodic perturbations into the flow, but the method which has been most commonly used is known as the acoustic technique. The advantages of acoustic "drivers" are that they

are convenient and easy to use. Unfortunately, experience shows that they are not suitable for controlling flows of practical interest, due to their enormous weight, power and maintenance requirements. The literature contains details of a wider range of excitation methods which can be summarised as follows:-

(i) Acoustic excitation in the form of sound waves generated by loudspeakers connected to a variable frequency power supply placed up-stream of the settling chamber of the flow facility arrangement - see for example Freymuth (1965), Crow and Champagne (1971), Zaman and Hussain (1980). In an extension of this method, Kusek et al (1990) employed excitation in the initial region of an axisymmetric jet. The excitation was produced by an azimuthal array of miniature speakers placed in close proximity to the lip of the exit face of the nozzle.

(ii) Mechanically driven exciters such as vanes and oscillating obstructions. For example, Collins et al (1984) used an oscillating vane which was located symmetrically in the potential core near the nozzle exit plane. Similarly, Lai and Simmons (1981) used a small vane located in the middle of the potential core and driven by a vibrator.

(iii) Aerodynamic excitation, where the main jet can be pulsed, Bremhorst and Hollis (1990) or can be surrounded by a secondary annular jet which is pulsed. This latter technique was first introduced by Szajner and Turner (1987), and is the method which has been adopted in the present investigation.

(iv) Fluidic excitation, where the jet is forced by miniature exciter jets which

are inclined to the axis of the main jet. See, for example, Raman and David (1994).

(v) Self-excitation in which, for example, a length of Piano wire is strung across the flow in the zone near the trailing edge of a splitter plate. The impinging wake flow causes the wire to oscillate and therefore no external energy is required - see Vandsburger and Ding (1995).

2.4.2 The Preferred Mode

The preferred mode for a jet flow is the particular type of flow oscillation (frequency, amplitude and phase distribution) for which the centre-line turbulent intensity attains its maximum levels. The frequency associated with this mode is usually based on one-dimensional spectral measurements made in the potential core - see, for example, Crow and Champagne (1971).

Sato (1959) observed that the fundamental frequency is approximately proportional with $(U_j)^{3/2}$ for a two-dimensional jet of rectangular cross-section issuing from a slit of 40mm width. A similar relation between the fundamental frequency and the jet velocity was found by Gutmark and Ho (1983) for a circular jet.

Crow and Champagne (1971) reported that the largest amplification of the turbulence intensity (u_{rms}/U_{cl}) measured along the centre-line of the jet occurred at a frequency corresponding to a Strouhal number $St_D = 0.3$. This value has been confirmed by Hussain and Zaman (1981), who also observed two peaks in the variation of the root mean square fluctuation level u' with the axial distance. They determined that the first peak is related to the roll-up of the turbulent shear layer into

the preferred mode structure while the second peak can be attributed to the breakdown of the initial toroidal vortex structures at the end of the potential core. The roll-up and breakdown processes which occur within the initial region of the jet can be seen clearly in the results of the flow visualisation studies by Freymuth (1965). He concluded that the breakdown is associated with interaction between the toroidal vortices.

Zaman and Hussain (1980) redefined the preferred mode in a different way to that specified reported by Crow and Champagne (1971). They determined that the root mean square of the axial fluctuation component (u_{rms}) on the centre-line of the potential core received maximum amplification at a frequency corresponding to a Strouhal number $St_D = 0.8$. In contrast, the fundamental root mean square amplitude ($(u_{rms})_f$) along the centre-line of the potential core reached its maximum at a frequency corresponding to $St_D = 0.3$. Husain and Hussain's (1983) results for the controlled excitation of elliptical jets are slightly different from Zaman and Hussain (1980). The peak of $(u_{rms})_f$ occurs at a frequency corresponding to a Strouhal number[5] $St_{De} = 0.4$, whereas the peak for u_{rms} occurs at a Strouhal number $St_{De} = 0.85$.

In the case of the round jet, the preferred mode is commonly based on the nozzle diameter as a characteristic length, and may conceivably be independent of the (laminar) shear layer characteristics in the nozzle exit plane. This idea was supported by Zaman and Hussain (1980) who stated that the preferred mode was the same, and appeared to be independent of whether the nozzle boundary layer was

[5] This Strouhal number (St_{De}) is based on the mean velocity of the jet at the nozzle exit plane (U_j), and the equivalent diameter of the elliptical nozzle (D_e).

laminar or turbulent.

Szajner and Turner (1987) pointed out that several modes can be excited in a free jet flow : they referred to the "potential core mode" and the "shear layer mode". The situation was more complicated than this however, since two regions of strong jet response were observed when the jet was excited with the potential core mode. The first of these occurred at low frequencies, corresponding to a Strouhal number (St_D) between 0.35 and 0.4. The second but weaker response was detected at a Strouhal number (St_D) of approximately 0.8. Another region of interest was detected by these authors when the jet was excited at higher frequencies, corresponding to $St_D = 1.0$, and St_θ lay in the range 0.005 to 0.018. In this case, the response of the jet in the shear layer mode was found to depend strongly upon the amplitude of the excitation as well as the frequency.

In view of all the experimental findings which have been reported, it is clear that the response of an excited jet, and particularly the attainment of maximum turbulence intensity levels as described by the "preferred mode" can occur over a wide range of the Strouhal number St_D extending from 0.279 to 0.85. This variation of the excitation frequency value for the preferred mode can be attributed to the experimental facilities, range of Reynolds number, excitation technique, and the basis on which the preferred mode is being evaluated.

2.5 Intermittent Flow

The continued switching of the flow from non-turbulent to turbulent motion and vice versa, has received a great deal of attention, since it was first reported by Corrsin (1943). This alternation of the fluid state is an essential feature

of all free jet flows and has fundamental importance in the study of fluid motion in general. The phenomenon is termed "intermittency" and can be influenced by many factors such as surface roughness, free stream turbulence, surface curvature, pressure gradient, temperature variation, Reynolds number, Mach number, acoustic radiation and injection or suction of boundary layer.

In spite of the effort that has been expended in studies relating to intermittency, there is still little agreement among authors as to how the changes from non-turbulent to turbulent flow conditions should be measured. In the case of intermittency measurement, schemes to isolate the turbulent flow state and selection of the turbulence detection criteria are even less standardised. The literature shows that there is a considerable degree of arbitrariness from one investigator to another and that each group has tended to employ different criteria. However, it has been usual to specify the balance between non-turbulent and turbulent flow conditions by an intermittency factor, defined as the ratio between the time in which the flow is turbulent to the total length of the time record - see Hinze (1975). In order to calculate the intermittency factor for any general fluid flow where the conditions have been recorded as a time series, there are two essential requirements. One is to define a turbulence detection threshold so that the flow is considered to be turbulent when some particular variable, or combination of variables, exceeds this predetermined threshold level. The second is to specify the time window so that the threshold criterion can be applied to a specified length of the time series to arrive at a decision on the intermittency condition.

Here, it is worth mentioning that the rest of this section concentrates upon the method used in the present work to determine the intermittency factor.

However, there is a wealth of information in the literature reported by Jeung (1993) by which to trace the development of ideas on the intermittency phenomenon from the time when it was initially identified. A full discussion of the subject, including the choice of the turbulence detector function, the threshold level, and the application of different statistical schemes has also been given by Jeung (1993).

2.5.1 Generation of the Detection Function

The intermittency function I(t), defined by I = 1 in the turbulent fluid and I = 0 in the non-turbulent fluid, needed to be set up before the zonal average could be obtained. The criterion adopted for determining I(t) and hence the intermittency factor γ was that $|u'v'(t)_G|$ had to exceed a pre-determined threshold level.

Discrimination is applied on a time record of a particular flow variable (e.g. the shear stress function u'v'(t)). Figure 2.5 summarises the method of detecting the switch from turbulent/non-turbulent states. Following Jeung (1993), a threshold value is chosen for a given variable (e.g. the shear stress). The flow is then said to be turbulent when this threshold is exceeded. Hence, the conditional or zonal averages can be calculated for each of the turbulent/non-turbulent flow states.

In describing any property of the flow, based upon time series information, it is usual to define a time mean value Q(r) in terms of the individual values in the time series such that:-

$$\overline{Q}(r) = \frac{1}{T}\int_0^T Q\,(r,t)\,dt \approx \frac{\sum_{i=1}^{N} Q\,(r,t_i)\,\Delta t_i}{\sum_{i=1}^{N} \Delta t_i} \qquad 2.5$$

In this expression, the symbol $Q(r,t_i)$ represents the value of the property at time t_i and position r, and N is the number of samples, T is the total time of the record, and Δt_i is the arrival time of individual bursts which have been collected using the LDA system. By definition, the intermittency function I(r,t) assumes a value of one when the flow is fully turbulent and is zero otherwise. Then the overall average value of the intermittency function is expressed as:-

$$\gamma = \bar{I}(r) = \frac{1}{T}\int_0^T I(r,t)\,dt \approx \frac{\sum_{i=1}^{N} I(r,t_i)_{tur}\,\Delta t_i}{T} \qquad 2.6$$

where γ is the intermittency factor. As can be seen, γ takes the time mean value of I(r,t) over the full length of the time record. This value is sometimes referred to as the turbulence fraction.

2.5.2 Zonal Average

Having defined the detection function and the threshold level, separation between the non-turbulent and turbulent flow events becomes possible - Jeung (1993), Jeung and Turner (1994). By definition, the zonal average of the non-turbulent zone of the time series can be expressed as:-

$$\overline{Q}(r)_{non} = \frac{1}{(1-\gamma)}\int_0^T [1-I(t)]Q(r,t)dt \approx \frac{\sum_{i=1}^{N}[1-I(r,t_i)]Q(r,t_i)\Delta t_i}{T\,[1-\gamma]} \qquad 2.7$$

Likewise, the turbulent zonal average can be expressed as:-

$$\overline{Q}(r)_{tur} = \frac{1}{\gamma} \int_0^T I(t)\ Q(r,t)\ dt \approx \frac{\sum_{i=1}^{N} I(r,t_i)\ Q(r,t_i)\ \Delta t_i}{T\ \gamma} \qquad 2.8$$

The quantity T[1-γ] represents the fraction of the total time for which the flow lies in the non-turbulent state and Tγ is the fraction of the total time for which the flow lies in the turbulent state. Employing these two conditional values, the overall average becomes:-

$$\overline{Q}(r) = \gamma\ \overline{Q}(r)_{tur} + [1-\gamma]\ \overline{Q}(r)_{non} \qquad 2.9$$

Treating the whole time record of the flow, the fluctuation can be expressed in terms of the total time record (the global condition) as:-

$$q(r,t)_G = Q(r,t_i)_G - \overline{Q}(r)_G \qquad 2.10$$

The instantaneous fluctuation from the non-turbulent zonal average is then:-

$$q(r,t)_{non} = Q(r,t_i)_{non} - \overline{Q}(r)_{non} \qquad 2.11$$

Similarly, the instantaneous fluctuation from the turbulent zonal average is defined as:-

$$q(r,t)_{tur} = Q(r,t_i)_{tur} - \overline{Q}(r)_{tur} \qquad 2.12$$

Then the physically meaningful mean square values in the corresponding domains are:-

$$q^2(r)_G\ ,\ q^2(r)_{tur}\ ,\ q^2(r)_{non} \qquad 2.13$$

The above relationships represent equalities between the conventional (global) and conditional (zonal) averages and can be applied to all the usual turbulence

parameters. Thus, they may be used to calculate the value for the normal stress (u'^2) which has been given most attention in this investigation. Changing the threshold level alters the relative proportions of the turbulent/non-turbulent zones in any time record and, thereby, determines the value of the intermittency factor and the related conditional averages. This offers a method for determining the appropriate threshold level for any turbulence detector function so that, when convergence has been achieved, the corresponding value of the intermittency can be calculated.

The intermittency analysis reported by Jeung (1993) was based on the above concepts (i.e. that there should be defined equalities between the global and zonal averages, and that these equalities can only be satisfied for one particular threshold level). Jeung's (1993) method has been adapted in this present investigation, since it is believed to be logically and analytically convincing. It is important to stress that the present scheme is completely different from the more conventional criteria described in the literature (Jeung (1993)) which have been based on an arbitrary definition of a turbulent detector function and the threshold level.

The mathematical analysis and the related variable which have been chosen to test and verify this approach will be dealt with in more detail in section 6.2.2.

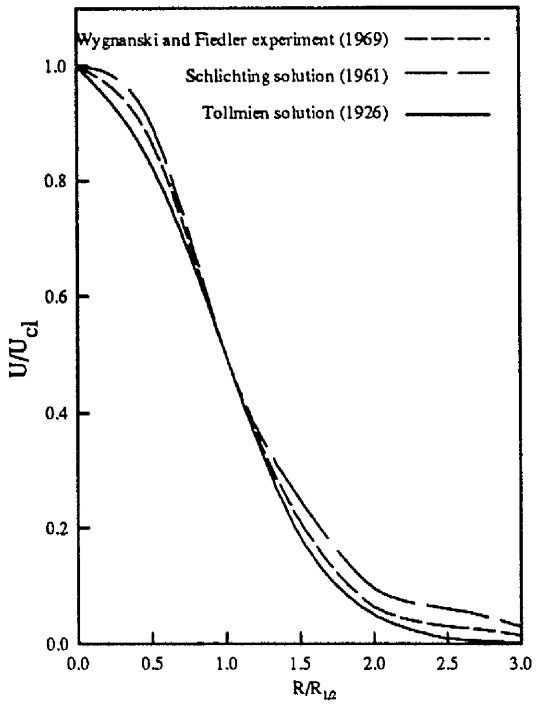

Figure 2.1. Mean velocity profiles Wygnanski and Fiedler experiment (1969).

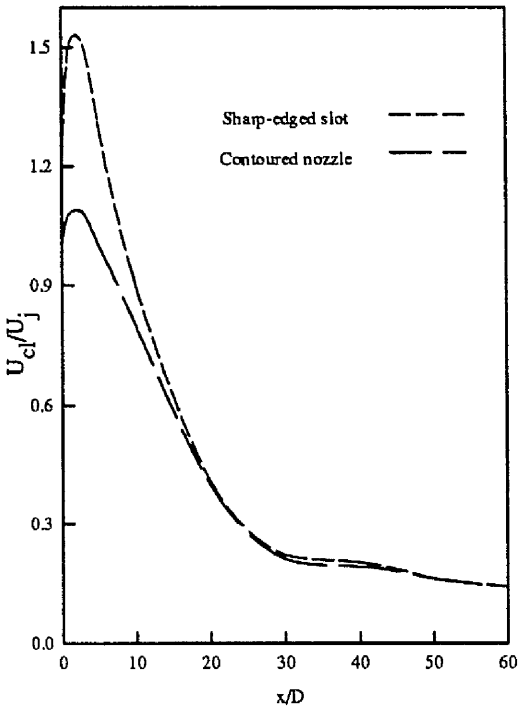

Figure 2.2. Decay of the centre-line velocity Quinn and Militzer experiment (1989).

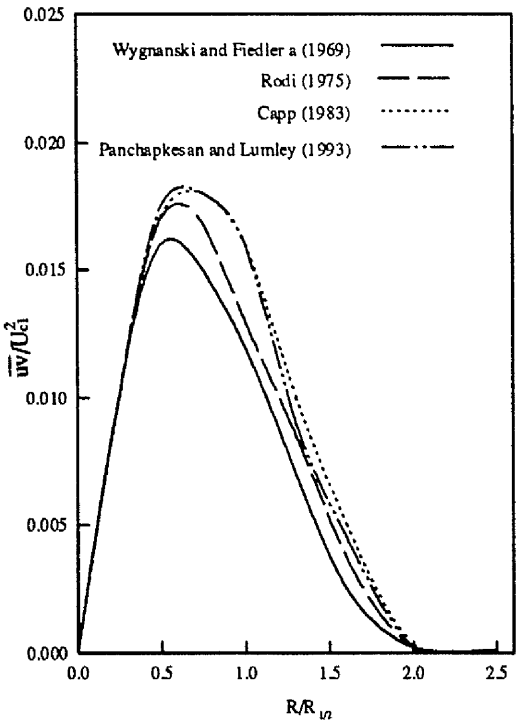

Figure 2.3. Shear stress variation across the jet.

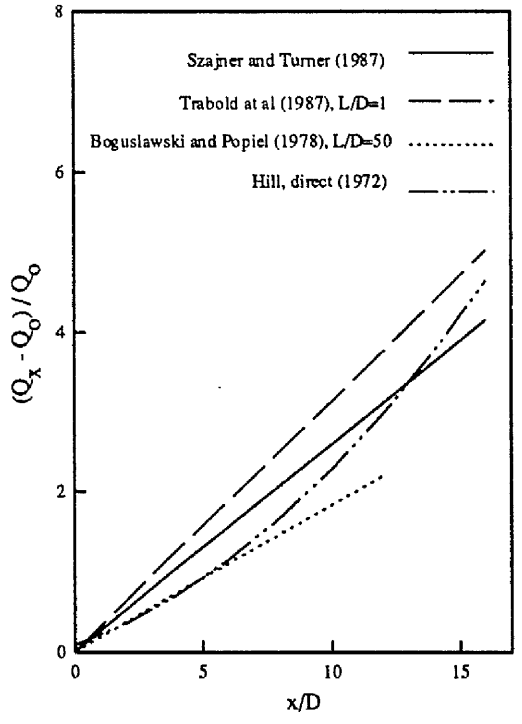

Figure 2.4. Variation of the entrainment rate.

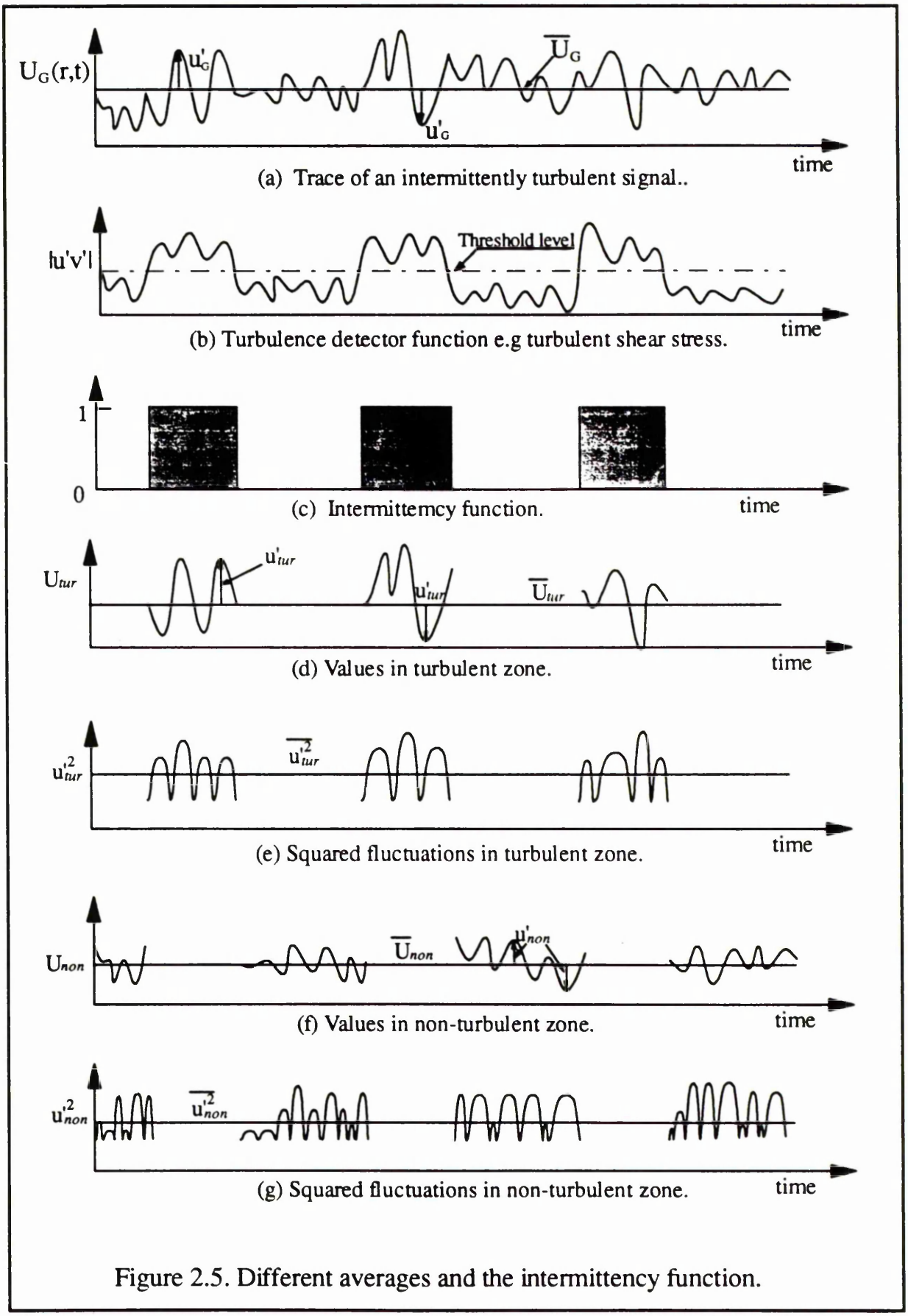

Figure 2.5. Different averages and the intermittency function.

CHAPTER 3

EXPERIMENTAL APPARATUS

CHAPTER THREE
EXPERIMENTAL APPARATUS

3.1 Turbulent Flow Rig

The jet test rig is based upon a closed return 100.0mm diameter pipe flow rig which was originally designed and constructed in 1967 in the Department of Engineering for turbulent flow studies -see Turner (1971). Since then, many modifications have been made on the rig as it has been adapted progressively to suit different aspects of turbulent flow research. The last major modification which was carried out by the author consisted of lifting the jet producing nozzle by an extra meter above the horizontal return duct work to obtain more symmetrical boundary conditions around the free jet.

In its open return form, the turbulent flow rig has nine main sections as shown in figure 3.1. These consist of:-

(i) a smooth axisymmetric contraction with a 20:1 area ratio

(ii) a series of nylon smoothing gauzes to reduce the turbulence level and increase the uniformity of the mean velocity profiles at inlet to the contraction

(iii) two square section cascade bends to turn the flow through 90 degrees

(iv) a newly fitted section (450.0mm square) which has been added to the rig to raise the nozzle by 1m

(v) a precision flap valve on a screw adjuster which is used to control the flow rate inside the rig

(vi) a circular section pipe return with a diameter of 305.0mm, approximately 11.0

metre long

(vii) a water cooled cross flow heat exchanger to maintain constant temperature air flow conditions

(viii) flexible tubing to connect the fan to the return circuit

(ix) an axial flow fan driven by a constant speed motor.

The primary flow of the jet, supplied by an axial flow fan coupled to a DC motor, yielded a maximum air speed of 29.0m/s. The air was filtered at the fan inlet using filters to remove any particles larger than 50μm since these could have damaged the hot film probe used in the first part of the investigation. Subsequently, this filter was removed during the laser Doppler anemometer measurement programme when the rig was converted to a closed circuit arrangement. The 11.0m 305mm diameter pipe after the heat exchanger ensures steady flow conditions and the removal of velocity non-uniformities before the contraction. The flow rate along the rig is controlled precisely by a butterfly screw-operated valve at the end of the pipe. A uniform mean velocity profile in the nozzle outlet plane is produced by a well-designed axisymmetric contracting nozzle of 20:1 area ratio and 102.0mm outlet diameter. The nozzle is preceded by the settling chamber represented by section 2 in figure 3.1.

A secondary nozzle surrounding the main nozzle is used to provide a pulsing annular jet which lies coaxial with the main axisymmetric jet - see section 3.3. After the modification to raise the exhaust level of the nozzle had been completed, the mean flow characteristics of the rig were measured to check the effect of the modification. Measuring the pressure drop across the contraction, based on wall static pressure tappings, against the dynamic pressure at the centre-line of the nozzle

exit plane. This produced a straight line relationship between the dynamic pressure and the pressure drop across the contraction as shown in figure 3.2. Both pressures were measured using a manometer[1]. The pressure drop across the contraction was measured by connecting the manometer to two fine holes (approximately 1.0mm in diameter) drilled through the wall of the nozzle. The first hole situated before the contraction and the second hole after the contraction - see figure 3.1. The dynamic pressure was measured using a Pitot-static tube positioned at the centre-line of the nozzle at approximately x/D = 0.1.

3.2 Traversing Unit

A sophisticated three-dimensional traversing mechanism was used to explore the behaviour of the jet over a large volume which can be considered as the working section for the investigation. This traversing unit took several months to construct and commission. Even when completed, movement of the hot film sensor, and later the LDA optics, was found to require a considerable level of skill to ensure correct alignment and accuracy of positioning in each of the three orthogonal directions x, y and z.

The traversing unit is supported on an optical laboratory table[2] which provides enhanced damping, and ensures that the table surface and the remainder of the traversing unit remain relatively free from vibrations which would otherwise be transmitted through the laboratory floor. The table has a working area of 2500.0mm x 1000.0mm and is 120.0mm thick. It sits on four free standing rigid mounts as

[1] Manufactured by Airflow Development Ltd.

[2] Manufactured by Photon Control Limited.

shown in figure 3.3.

The table was carefully aligned so that its surface lies in a plane which is parallel to the physical centre-line of the nozzle. This alignment was achieved by directing the beam from a Helium Neon laser[3] from the traversing unit back into the nozzle outlet plane. This laser, was mounted at a distance of 3.5m from the nozzle exit plane.

A rigid plastic tube, 370.0mm long and with a diameter of 101.0mm, was also used in the alignment process. The tube was fitted inside the primary nozzle and aligned with the axis. A diaphragm was inserted at each end of the tube, each diaphragm being drilled with a 1.0mm diameter hole to allow passage of the laser beam. This enabled reasonably good alignment with approximately 1.5mm error to be achieved by directing the laser beam through the two holes. This alignment error was assessed by aligning the centre point of the traversing unit i.e. the centre point of the traversing frame shown in figure 3.3 with laser beam at x/D = 1.0. The traversing frame then moved along the optical table to x/D = 15.0, where the centre point was noticed to be shifted approximately 1.5mm from the laser beam.

Horizontal and vertical movements (corresponding to the y-z plane according to the convention used in the investigation) were achieved using an existing traversing framework which permitted coverage of a 1.0m x 1.0m working area. To obtain the third direction of the movement, a specially designed trolley was positioned on the optical table, supported on four bearing wheels running along tracks parallel to the jet axis. Two pieces of straight metal bar were cut to serve as psuedo-railway tracks

[3] Hughes type 7225 model, 5mW He-Ne.

for the trolley, and the forward and backward movements were controlled by a threaded shaft running through the trolley and extending across the full length of the optical table. The threaded shaft was fixed at both ends of the optical table by two self-aligning flanged bearing boxes, as is shown in figure 3.3. A DC motor[4] was connected to the shaft at one end via a reduction gear box to provide a 10:1 speed ratio. By this means, very fine positional adjustment of the trolley position in the z-direction was achieved. It is estimated that the positional accuracy in the streamwise direction was approximately ± 0.25mm using a control box[5].

To satisfy the safety regulations applying in the University with regard to use of the LDA equipment, and at the same time to reduce the chance of flow disturbances, the traversing unit was remotely controlled from outside the box. Thus, the vertical movement was driven using a stepper motor[6], while the horizontal movement was driven using another type of stepper motor[7]. Both motors can be programmed to operate in a standard step angle mode of 1.8° or in the half-step mode giving 0.9° rotation per step. Thus, positional accuracy in the x, y directions (at a fixed axial position) is estimated to be better than ± 0.1mm.

A PC 386 computer was used to control the rotation of the stepper motors via a standard motor drive board[8]. For this purpose, a digital interface board[9] was

[4] Manufactured by ABB Limited, type MK110020-S.

[5] SSD limited control box, model 583/1.500/3/2.

[6] Manufactured by RS Limited, Model RS-344-631.

[7] Manufactured by RS Limited, Model RS-322-082.

[8] RS Limited type board, model RS-334-098.

[9] Manufactured by Keithley Metrabyte, model PIO-24.

implemented by the Instrumentation Department of the School to provide a communication link between the computer and the stepper motor drive box.

Control over direction and distance of the traverse step was then achieved using software developed previously within the Research Group - Heyes (1994) - and subsequently modified by the author. All instructions with regard to range, axis of traverse, interval between stations, and direction, were fed to the computer using additional software written by the author.

3.3 Jet Excitation

In the present investigation, an approach has been adopted in which the excitation is introduced by pulsing a thin annular jet (1.05mm in thickness - see figure 3.5) which surrounds and is co-axial with the main jet. It has been found that the secondary jet interacts with the free shear layer springing from the wall of the nozzle to create coherent structures in the form of regularly spaced toroidal vortices. These have a pronounced influence on the behaviour of the jet as will be explained in Chapter Seven.

The secondary flow was supplied from the high pressure compressed air system available within the laboratory. A pressure regulator, air filter, variable air flow and an on-off valve were installed in the supply line to provide the necessary control over the rate of secondary flow. Using the simple system which had been developed previously (Szajner and Turner (1987)), pressure pulsations are imposed on the secondary air supply by means of a rotating valve, with one rotation of the valve shaft resulting in two pressure pulses of comparable amplitude, see figure 3.4. An appropriate range of frequencies (between 5Hz and 198Hz) was achieved using

this system and the actual frequency could be determined by means of a shaft encoder and a Digital Counter[10] which were connected to the shaft driven by a variable speed DC motor[11]. A specially designed manifold, shaped to produce the secondary jet flow from an annulus which is coaxial with the axis of the main nozzle, is connected to six inlet pipes distributed circumferentially. This manifold was designed so that the cross-sectional area of the contraction varies smoothly in the flow direction as shown in figure 3.5. Previous studies have confirmed that this system produces an annular jet which is uniform around its circumference. Information on the design of this system and further performance details can be found in Szajner and Turner (1987).

3.4 Smoke Generator

Smoke particles were introduced (for the LDA measurements) into the closed circuit recirculating airflow system by injecting through the back wall of the working box into which the free jet was injected, see figure - 5.6. Other positions were tried but no real advantages for any of the injection positions could be observed, see section 7.1.

The "smoke" was produced using a commercial smoke generator[12]. The vapour is generated by passing the mineral oil[13] over an electrically heated element and then mixing the vapour with inert CO_2 gas in a specially designed mixing chamber. The smoke generated by this method is clean, dense and pure white in

[10] Appolo frequency counter and timer manufactured by Black Star Limited, model TSA 6635/M.

[11] Manufactured by Parvalux Electronic Motors Limited, type RS716-042.

[12] Manufactured by C.F.Taylor Ltd. model 3020.

[13] Shell Ondina vapourising oil.

colour and consists of droplets which are typically in the range 1μm to 5μm in diameter. Moreover, since the injection rate of the vapour is controllable, this method produced good conditions for the LDA measurements, and highly visible flow patterns during the flow visualisation stage of the project.

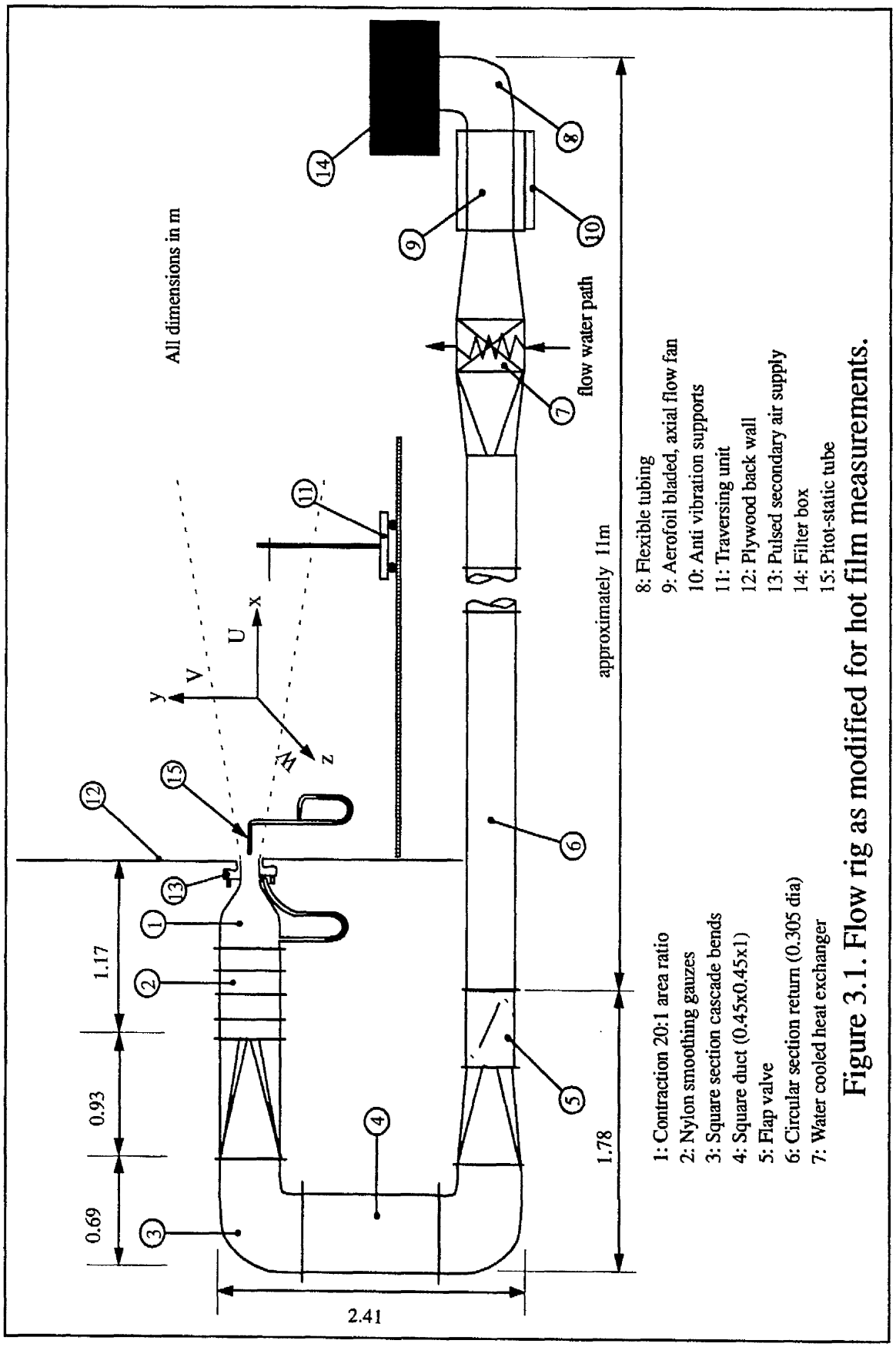

Figure 3.1. Flow rig as modified for hot film measurements.

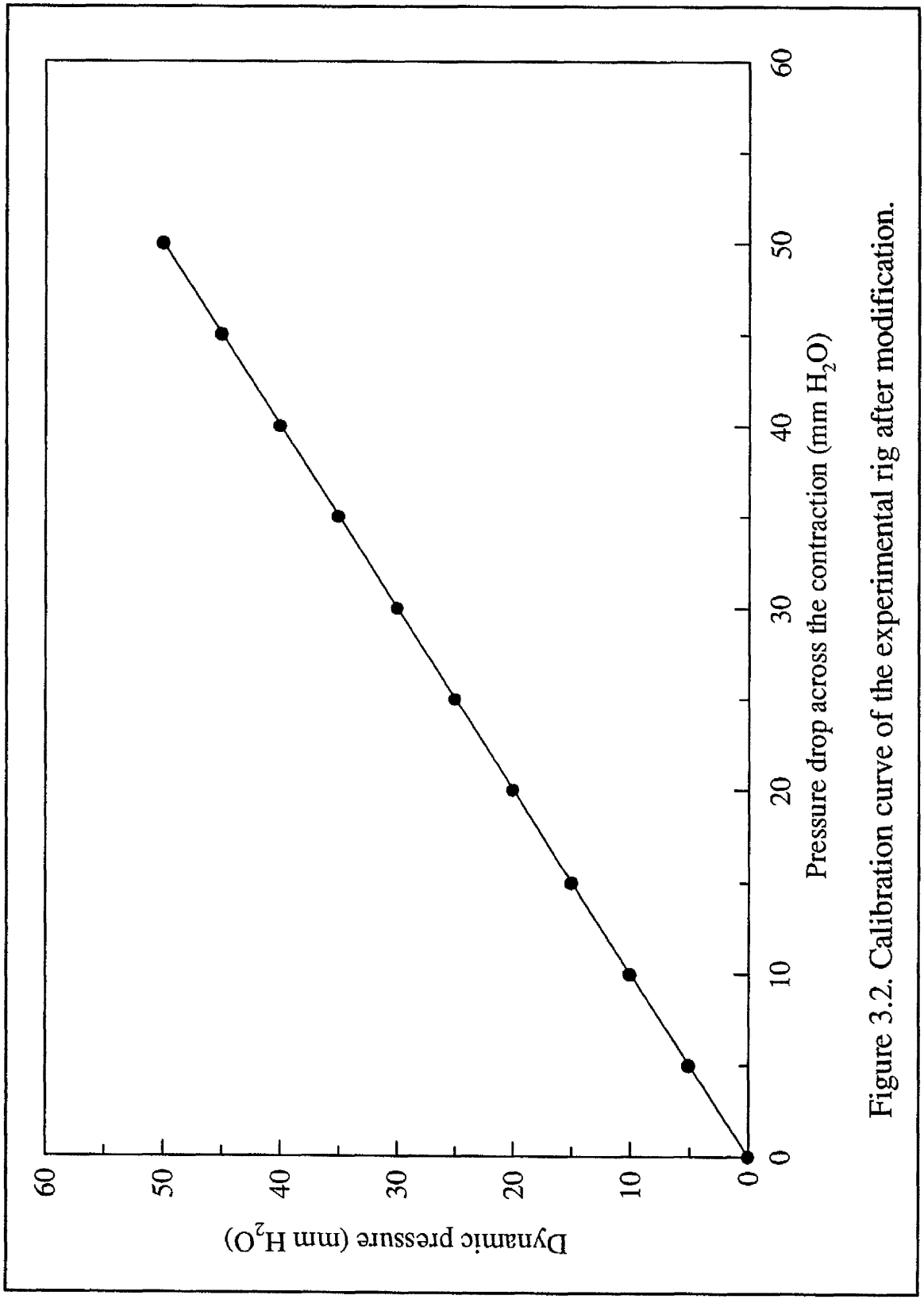

Figure 3.2. Calibration curve of the experimental rig after modification.

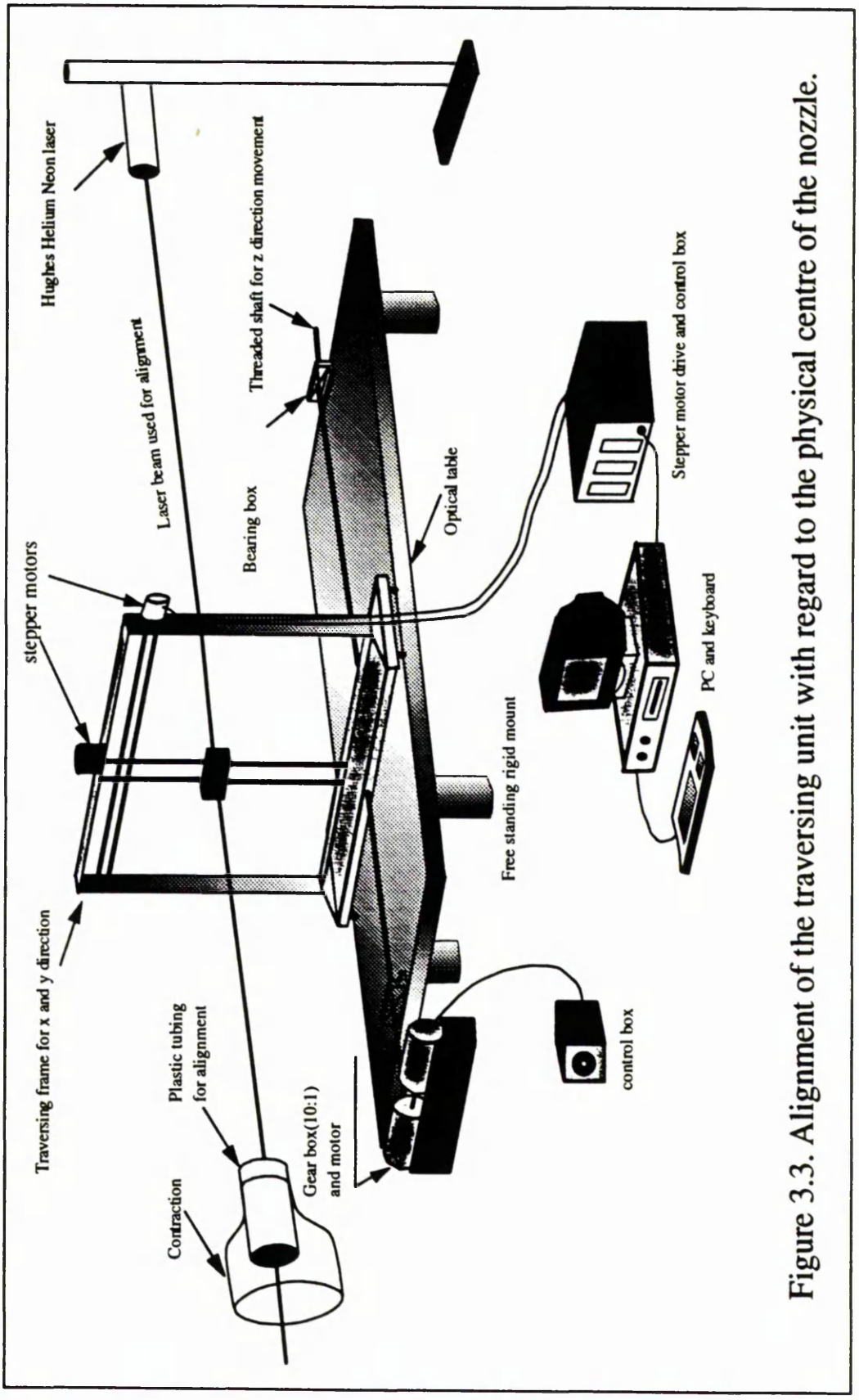

Figure 3.3. Alignment of the traversing unit with regard to the physical centre of the nozzle.

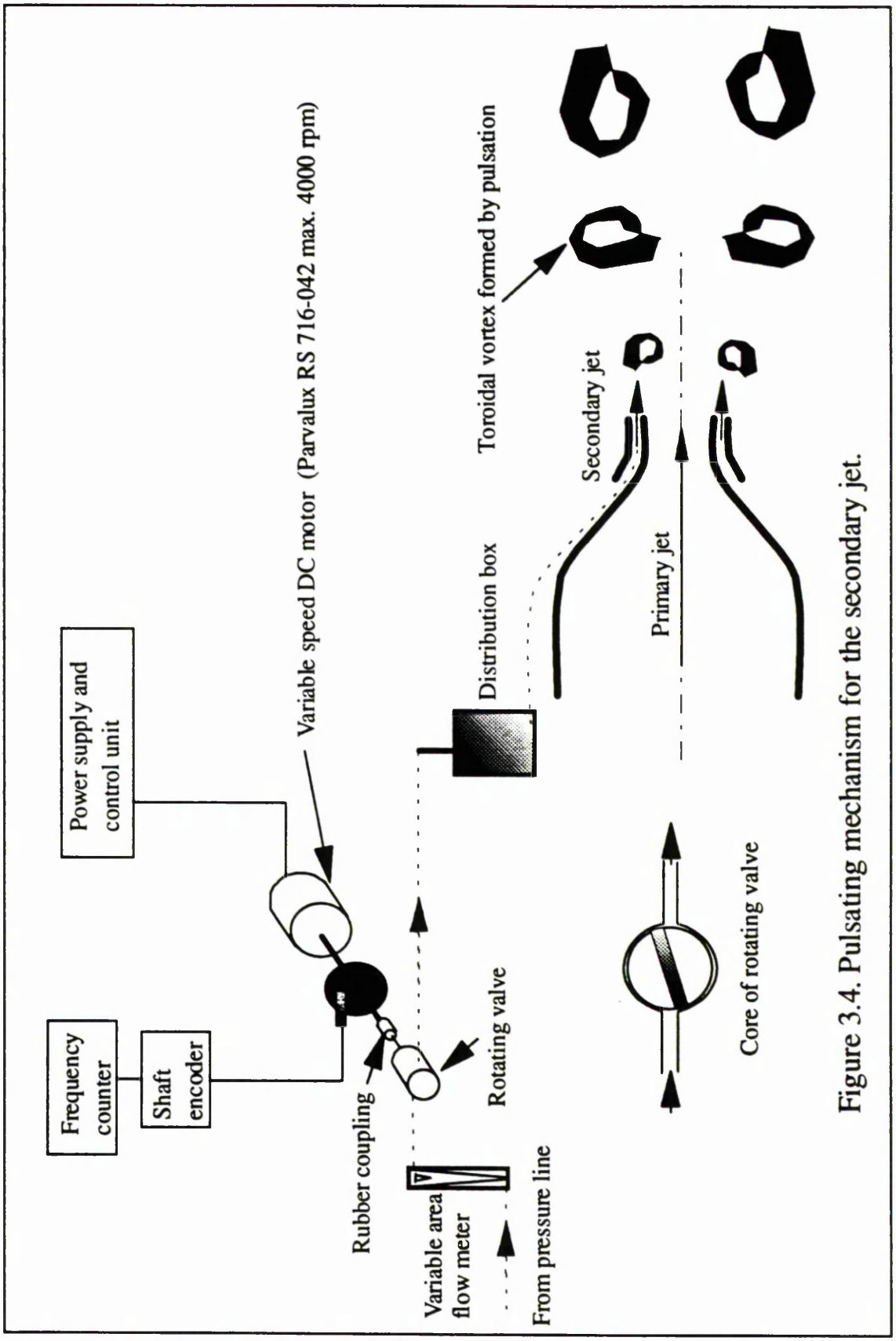

Figure 3.4. Pulsating mechanism for the secondary jet.

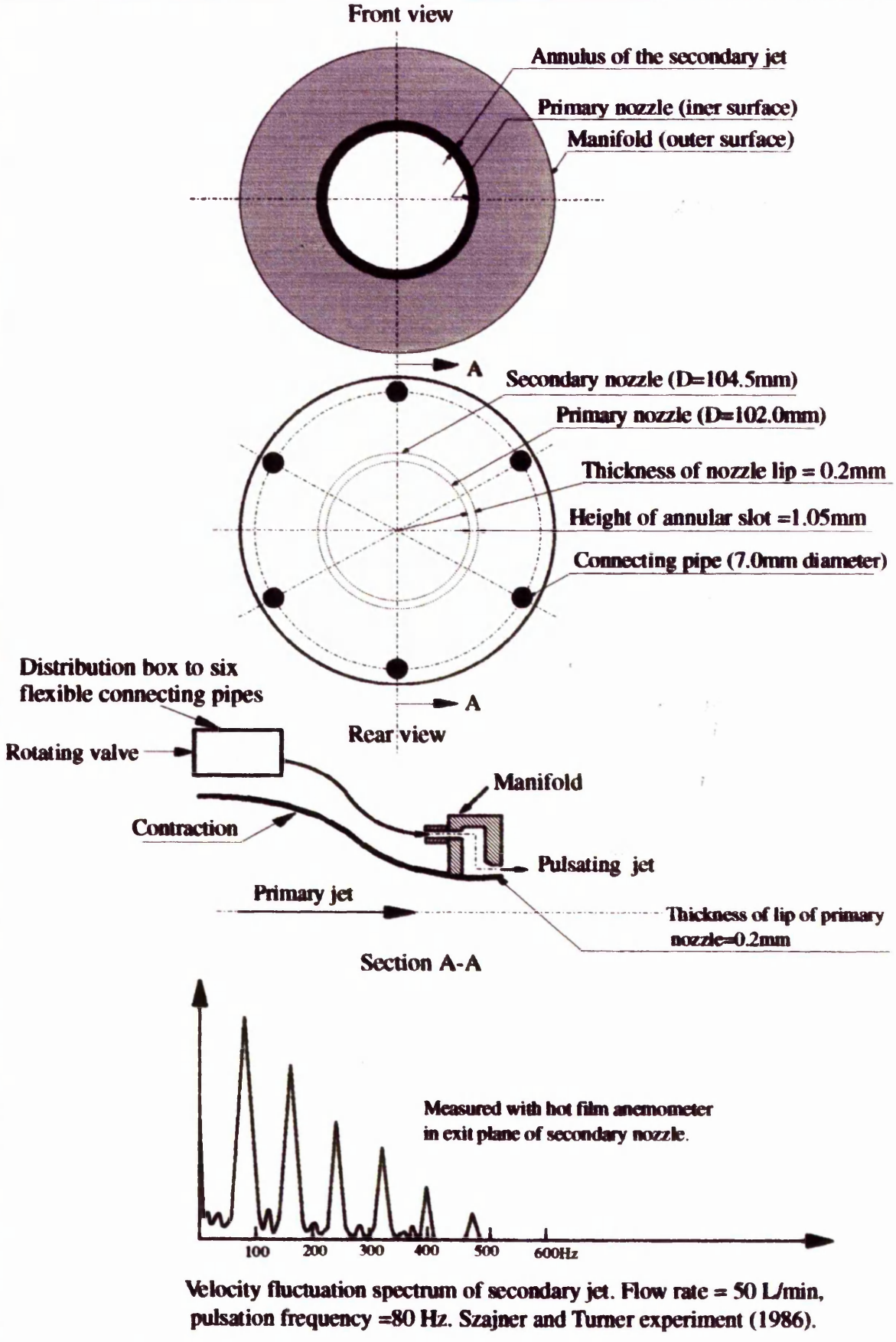

Velocity fluctuation spectrum of secondary jet. Flow rate = 50 L/min, pulsation frequency =80 Hz. Szajner and Turner experiment (1986).

Figure 3.5. Schematic of manifold used to produce the pulsating secondary jet and the spectrum of velocity wave form.

CHAPTER 4

MEASUREMENTS USING HOT FILM ANEMOMETRY

CHAPTER FOUR

MEASUREMENTS USING HOT FILM ANEMOMETRY

4.1 Introduction

A Constant Temperature Hot Film Anemometer (hereafter referred to as HFA) was used in the earlier stages of this study to familiarize the author with the nature of the excited jet flow problem. This first stage of the work also enabled development of the experimental apparatus for the final part of the project in which laser Doppler anemometry (LDA) was used.

The hot film anemometer bridge was operated in the constant temperature mode. It was interfaced to an existing high speed on-line data acquisition system which had been built in the department (Jeung (1993)) and was then further developed by the author.

The unlinearized voltage signal from the anemometer bridge is first digitized by 12 bit analogue to digital converter (ADC). These values are passed into the Zenith IBM compatible personal computer memory for further processing. Once the digitized signal from the HFA has been stored in the computer memory, it can be processed by suitable programs in order to extract relevant turbulent flow information such as the mean velocity levels and the turbulent velocity components. The general arrangement of the HFA system is shown in figure 4.1.

4.2 Hot Film Probe

The hot film probe[1] actually used was of the forward facing wedge type and consisted of an electrically conducting nickel film deposited on a wedge shaped epoxy support. The approximate dimensions of the film sensor are 0.2mm in diameter and 1.0mm in length. This sensor is protected by a quartz coating which is approximately 0.5μm in thickness and the probe is supported by a probe holder[2] of 0.8m length and 4.0mm diameter. This probe is operated as the fourth (velocity sensitive) element of a dynamic Wheatstone bridge circuit[3]. During measurement, the probe was electrically heated above the ambient temperature of the fluid by up to 150C°. Any imbalance between the preset resistance R_1 and the probe resistance R_p (see the block diagram below) produces an error voltage signal which is amplified and fed back to the bridge by a servo amplifier. This enables the temperature and

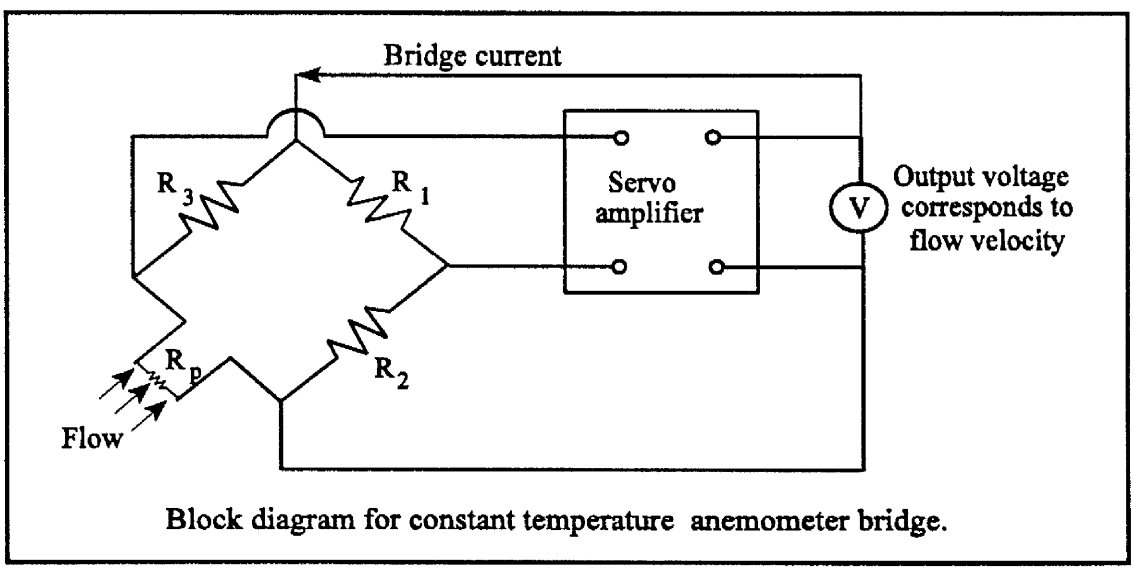

Block diagram for constant temperature anemometer bridge.

[1]Manufactured by Dantec, model 55R32.

[2]Dantec type probe holder, model 55H20.

[3]Disa 55MO1 constant temperature anemometer bridge.

hence the resistance of the sensor to be maintained at a constant resistance. Since resistance and temperature are related, this explains the term "constant temperature operation" used to describe the operation of the anemometer bridge.

4.3 Anemometer Bridge

The bridge consists of the probe, filter, square-wave generator, auxiliary protection circuits and a series of resistances which can be adjusted by the operator. The decade resistances allow measurement of the resistance of the probe and its electrical lead and make possible adjustment of the desired operating probe temperature. For the purpose of this investigation, the overheat ratio was set to 1.3, in accordance with instructions in the Disa 55M CTA Standard Bridge Instruction Manual. The bridge was connected to the probe by a Disa 5.0m cable incorporation standard BNC connector at each end.

A digital voltmeter[4] was used in combination with the bridge to display the bridge voltage which can be related to the measured velocity of the flow through the calibration equation.

During any traverse across the jet diameter, the full range of velocities encountered by the probe varied from the high velocity level at the centre of the jet in the initial region to the relatively low velocity levels at the jet edges in the far field downstream from the nozzle. Experience shows that special care must be taken to manipulate the output signal of the bridge if the probe is to operate satisfactorily over this wide range of velocities. To satisfy the above condition, a signal

[4]Disa model 55D31.

conditioner[5] was used. This consists of an adjustable offset capability, together with a signal amplifier, enabling adjustment between the levels of the anemometer output voltage and the analogue to digital convertor[6] (ADC). By this means, it became possible to subtract a known constant voltage from the input signal and then amplify the resultant signal sufficiently so that the turbulent flow fluctuations covered the maximum ±2.5V range of the ADC. Subsequently, the digitized value of the voltage was divided by the amplification and the offset value was added in the processing software to reconstruct the original anemometer output voltage - see section 4.5.2 for further details.

The ADC was attached to a computer board, which is referred to as the ADC carrier[7]. This contains a high speed, 12 bit ADC, an input multiplexer and a channel scanner which can operate with up to eight channels providing a typical conversion time of 11.25 μsec per sample (in total). The ADC has switchable ranges of ±2.5, ±5, and ±10 volts. In the present work, a range of ±2.5V was selected to suit the signal conditioner, thereby obtaining a maximum resolution of 1.22mV in the smallest turbulent fluctuations (i.e. $5.0/2^{12}$).

4.4 Hot Film Calibration

The hot film was calibrated before measurement of any of the flow characteristics (e.g. the mean velocity and turbulence quantities). The experimental rig described in section 3.1 was used to calibrate the HFA probe in order to

[5]Disa model 55D26.

[6]Burr Brown model PCI-20019M-1A.

[7]Burr Brown model PCI-20041C-3A.

minimise the measurement errors which could be produced by the temperature variation of the jet, noting that these variations in the jet temperature amounted to no more than ±1C° during each run.

The first step in the calibration procedure was to position the hot film normal to the flow direction on the centre-line of the nozzle and at an axial position defined by x/D = 0.1. Then, the anemometer bridge voltage at zero flow velocity was recorded. Secondly, the maximum voltage of the bridge was determined for the maximum velocity level of the jet. For example, if the maximum jet flow velocity to be considered was 10.0m/s, then the maximum velocity for the calibration was chosen to be around 12.0m/s so that all the calibration points could be concentrated within the velocity range of interest. This method was adopted to minimise the errors which occur during the linearization process of the calibration curve. Taking all the experimental programme, the maximum velocity ever encountered for calibration purposes was 29.0m/s, corresponding to a highest expected velocity in the jet flow of 25.5m/s.

The reason why the voltage is recorded at both the zero and maximum velocities is so that the correct gain and offset can be calculated for the signal conditioning unit, enabling the whole range of the 12 bit ADC to be utilised - see section 4.3. After calibration of the HFA, and determination of the Collis Williams (1959) constants which describe the performance - see section 4.5.1, this information was entered into the PC computer so that the mean velocity and turbulence quantities could be derived from the output signals of the anemometer bridge. The calibration procedure will be referred to in more detail in the following section.

4.5 Related Computer Programs

4.5.1 Program CalHF

This program was written by the author in FORTRAN 77 in conjunction with a subroutine written in assembly language to ensure compatibility between the software and the computer hardware. It was written to permit calibration of a single hot film probe in order that the constants A, B and n in the Collis Williams (1959) equation can be determined. Hence the calibration of the HFA is given by:

$$E^2 = A+BU^n \qquad 4.1$$

A technique used by Swaminathan et al (1983, 1984) was adopted in the first stage of the calibration process development to solve A, B, and n simultaneously. A computer program was written in FORTRAN 77 based on the mathematical treatment on equation 4.1 by Swaminathan et al (1983, 1984) - see Al-Sudane (1996). Other techniques were also tried. For example, the constant A was calculated separately, and the voltage at zero velocity E_o was multiplied by 0.8, which is the optimum value found by Bruun et al (1988) and corresponds to a minimum value of the fitting uncertainty. Finally, the constant A was directly given the value of the voltage at zero velocity (E_o). All the above techniques resulted in very small differences in the value of the constants (typically in the range 0.05-0.1%). Consequently, the latter method was adopted for convenience.

The HFA calibration program CalHF initially requires input of the ambient temperature and pressure to calculate the air density and process the calibration values. The gain and offset applied to the input signal after passing through the signal conditioner are also required so that the original bridge output voltage can be

reconstructed for each velocity level - see section 4.3. An average 15 points were taken for every calibration run. At each calibration point, the program requires input of the pressure drop across the contraction and then computes the air velocity using the relationship:-

$$\overline{U} = \sqrt{\frac{2\rho_1 gh}{\rho_2}} \qquad 4.2$$

where $\overline{U}$ is the time mean velocity of the air, ρ_1 is the density of water. It should be noted that the manometer fluid was Paraffin, but commercially calibrated to give the pressure column h in mm of water. Variable ρ_2 represents the density of the air, and g is the gravity constant.

An inclined manometer[8] was used to provide the pressure difference reading across the contraction. This had a scale length of 250.0mm, and could be inclined at four different angles to give scale factors of 0.05, 0.1, 0.2, and 1 respectively. CalHF stores the calculated velocity levels and the sampled bridge voltages which are input directly to the ADC and hence the host computer.

Having collected the corresponding velocity and voltage pairs for the required number of data points, the program calls upon subroutine CFIT. This subroutine processes the data according to equation 4.1, enabling the empirical constants A, B and n to be determined using CRAMER's rule. Then the program proceeds to compute the goodness of fit for the empirical correlation (equation 4.1) by listing the uncertainty in the velocity for each pair of data points. This is defined as:-

[8]Manufactured by Airflow Development Ltd.

$$uncertainty = \frac{measured\ velocity - calculated\ velocity}{measured\ velocity} \times 100\%$$

In this expression, the "measured velocity" represents the velocity determined from the pressure drop across the contraction and the "calculated velocity" is the velocity computed from equation 4.1, after substitution of the appropriate constants.

Whenever the uncertainty exceeded 2.5%, for the particular point, the data point was discarded and the calibration process was then repeated fully for the whole velocity range. The calibration data were then stored in a data file for subsequent use by the Umean program used to calculate the time mean velocity. The calibration data was verified at the end of each experiment to ensure that the calibration did not shift during the course of the experiment. The flow chart for this program is shown in figure 4.2.

4.5.2 Program Umean

Once the hot film is calibrated and the appropriate calibration constants have been calculated then the HFA is ready to take measurements. The program asks for the following information to be entered:- the name of the calibration data file, the gain and offset applied to input signal, the date of measurement, the axial distance in mm, jet temperature in °C, reference pressure difference (pressure drop across the contraction) in mm of water, the atmospheric pressure level in mm of mercury and the step length for the radial traverse i.e. the distance between consecutive radial stations in mm. The amount of time required to process the signals from the HFA has been reduced in this program by introducing a look-up table following the method described by Bruun (1986). This look-up procedure is employed after input

of the calibration constants, the gain of the amplifiers and the offset, and permits calculation of the 4096 velocity levels which correspond to the discrete values obtained from the 12 bit ADC. This procedure may be presented in the form:-

$$U(m) = \left(\frac{\left(\frac{J(m) \times 5}{Gain \times 4096} + E_{Offset} \right)^2 - A}{B} \right)^{\frac{1}{n}} \qquad 4.2$$

where A, B and n are the appropriate calibration constants, and m is the number of samples collected at each measurement location. Typically, 100,000 values were collected in the present investigation. The term J(m) is the ADC number corresponding to the anemometer bridge voltage after the digitisation process, and takes a value from 1 to 4096 ($1 \leq J \geq 4096$). The term U(m) represents the instantaneous flow velocity (m/s).

For any bridge output voltage E input to the ADC, the computer will select the nearest value of J which minimizes $\left([E(m) - E_{offset}] \times Gain - J\frac{5}{4096} \right)$. Therefore, the look-up table need only be calculated once at the beginning of the program and can then be stored in the memory. Subsequently, it is used to calculate the instantaneous velocity level at every discrete sampling time.

During any test run, the time interval between values was set to 100 μsec (giving a sampling rate of 10,000 samples per second) for every sample and 100,000 values were collected at each measuring point. Having obtained the velocity record (U(m)), the program carries on calculating the time mean value $\overline{U}$.

$$\overline{U} = \frac{1}{N} \sum_{m=1}^{N} U(m)$$

and the root mean square value of the turbulence level $(\overline{u^2})^{1/2}$.

$$(\overline{u^2})^{\frac{1}{2}} = \frac{1}{N} \sqrt{\sum_{m=1}^{N} [U(m) - \overline{U}]^2}$$

It was necessary to incorporate an assembly language subroutine in the main program to secure communication between the hardware of the computer[9] and the ADC carrier. The time mean value of the velocity and the root mean square of the turbulent fluctuation level, together with the radial position, are written to an output data file for further processing in order to calculate the various non-dimensional parameters which describe the development of the jet. These typically include the non-dimensional time mean value of the excited velocity U/U_{cl} and the non-dimensional radial position $R/R_{1/2}$, as well as integral parameters such as the entrainment rate $\{(Q_x - Q_o)/Q_o\}$. This program, which was modified further at a later stage of the study, will be dealt with in more detail in section 6.2. At this stage, it is sufficient to refer to the flow chart of the program which is shown in figure 4.3.

4.6 Results and Discussion

This section of the thesis presents the experimental results obtained for the turbulent axisymmetric jet flow using the hot film anemometer and discusses the main findings. Note here that checks on the axial symmetry of the jet have been

[9]The computer was an IBM PC compatible Zenith model ZDF-2327 BK.

made only by using HFA.

Figures 4.5 to 4.7 show the non-dimensional profiles of the time mean axial velocity component at axial locations of x/D = 3.0, 9.0 and 13.0. In these graphs, the vertical axis represents the time mean velocity U at each measured position across the jet, normalised with regard to the velocity at the centre-line of the jet U_{cl} for the axial station under question. The horizontal axis represents the radial location R normalised with regard to the radial location $R_{1/2}$ at which the velocity falls to half the value of the centre-line velocity. It seems that all data points for these mean velocity distributions collapse fairly well onto one single curve for the different azimuthal positions defined by the circumferential angle θ. These measurements were taken at different angles with the z axis being taken vertically upwards and corresponding to the angle θ = 0. Anti-clockwise rotation (viewed along the flow direction) was chosen for positive angle movement and the measurements were made at each axial station across the jet for eight angular positions (θ = 0°, 30°, 45° 60°, 90°, 120°, 135° and 150°). Traversing at each downstream station was accomplished in a stepwise fashion by moving in two directions across the y-z plane, as shown in figure 4.4. To achieve this systematically, a grid was generated within the y-z plane to map the probe movement. For example, movement along the diameter at a slope of 30° in equal intervals (of say 5.0mm) was accomplished by moving the probe first along the z axis at a distance equal to 5.0 cos30° and then along the y axis at a distance of 5 sin30°. This grid was generated by an auxiliary computer program (Gridxyz.FOR) and was input as an initial requirement into the software which controlled the probe traverse - see also section 3.2.

Figures 4.8 to 4.10 present the cross-section of the jet in the form of iso-velocity contours at axial positions of x/D = 3.0, 9.0 and 13.0. These figures have been obtained by resolving the velocity vector into its separate y and z components for each of the different angles. These data were stored in an ASCII data file and then input to the QFV software package for further processing and graphical presentation.

The positional relationship between the data shown in the velocity contours and the radial distributions of the axial mean velocity may be ascertained by reference to figure 4.4.

A large box needed to be built[10] to contain the flow working section, thereby complying with University Safety Regulations which are enforced with regard to the use of laser equipment. Possible contamination of the laboratory atmosphere by the LDA seeding particles was another consideration. As mentioned earlier in this chapter, the main part of this investigation has been carried out using the LDA technique and the primary object of this first series of HFA measurements was therefore to develop the apparatus to suit that purpose.

Preliminarily experiments confirmed that the presence of the boundaries making up the containment had negligible effect on the development of the jet. Figures 4.11 to 4.13 clearly illustrate this. Since there are no systematic differences between the two sets of data (with and without the box) for any of the three axial positions. All the tests of the axial symmetry of the flow were performed to ensure that the flow conditions satisfied the requirements for a natural free jet. These

[10]This will be shown clearly in the next chapter.

conditions were clearly aided by the decision to lift the return duct work and the jet producing nozzle by 1.0m, thereby eliminating the effect of the optical table.

4.7 Summarising Remarks

Throughout this chapter, only a single free jet of air without excitation has been considered. It soon became apparent that the use of the two-dimensional LDA technique would be more appropriate than the HFA to investigate the influence of excitation on the development of the jet. This conclusion was reinforced by the need to obtain both time mean and turbulence information under very difficult (pulsating) flow conditions.

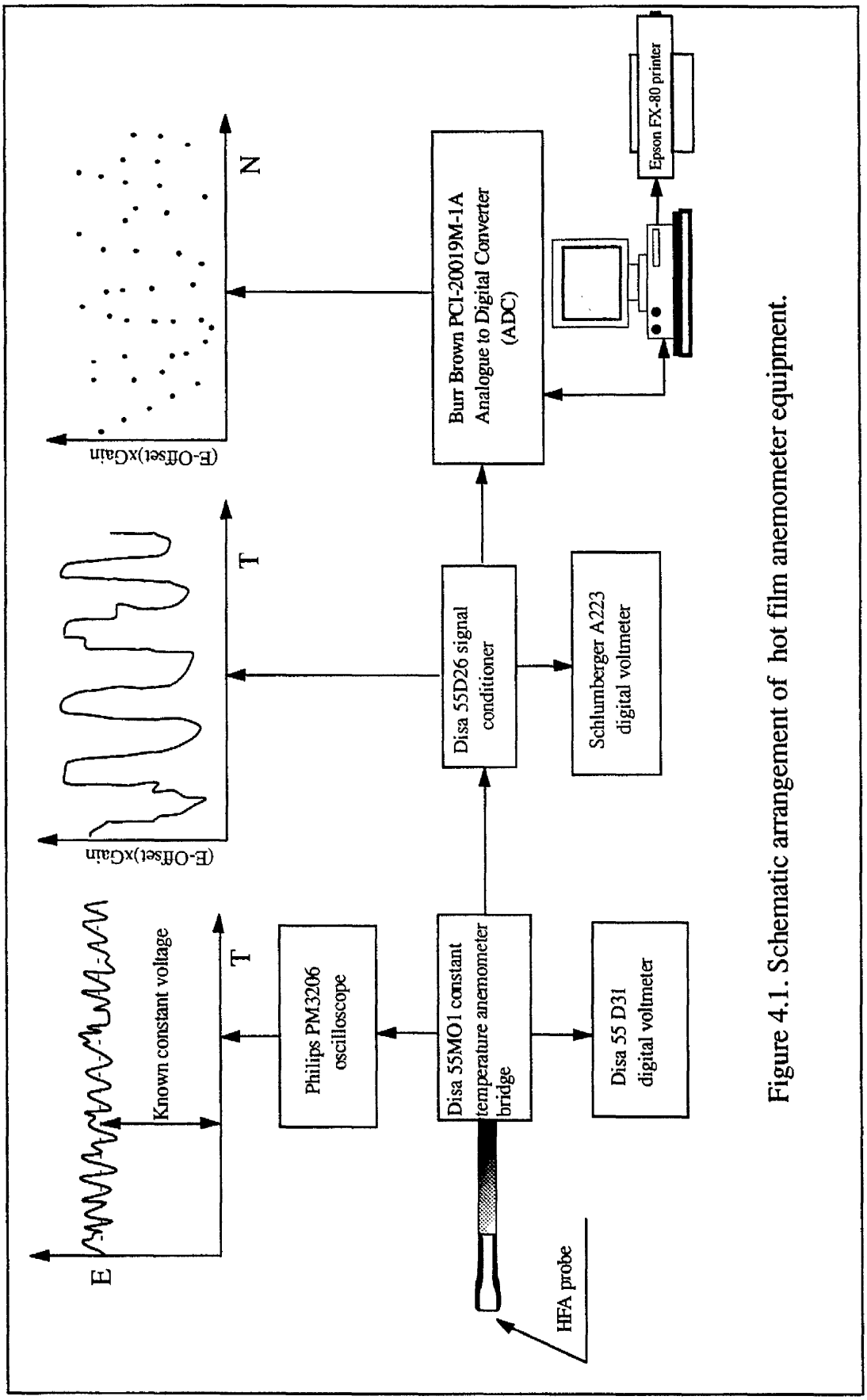

Figure 4.1. Schematic arrangement of hot film anemometer equipment.

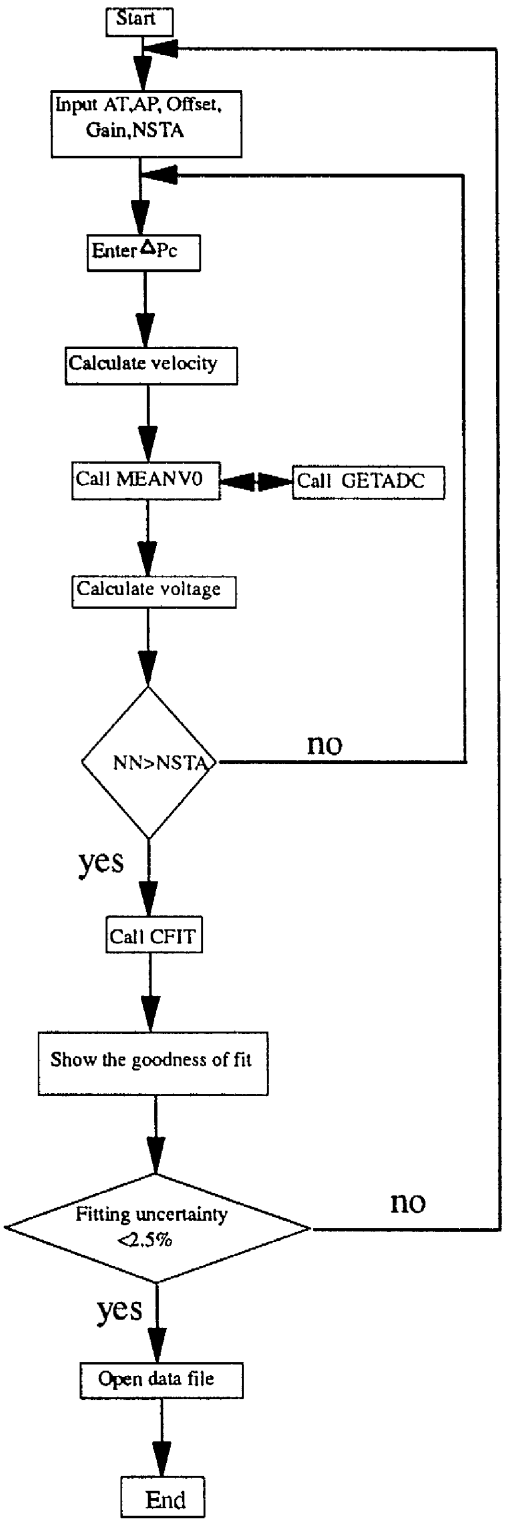

AT : ambient temperature

AP : atmospheric pressure

Offset : offset applied to input signal

Gain : gain applied to input signal

NSTA : number of data points

ΔPc : pressure drop across the contraction in mm of water column (h)

Calculate velocity : see section 4.5.1

Calculate voltage : the reconstruction of the original input voltage as is shown in the following equation:

$$E_{input} = \frac{\frac{J(m) \times 5}{4096}}{Gain} + Offset$$

where J(m) is the ADC number corresponding to input voltage after the signal conditioner

NN : the do loop number.

Figure 4.2. Flow chart for the calibration program (calHF).

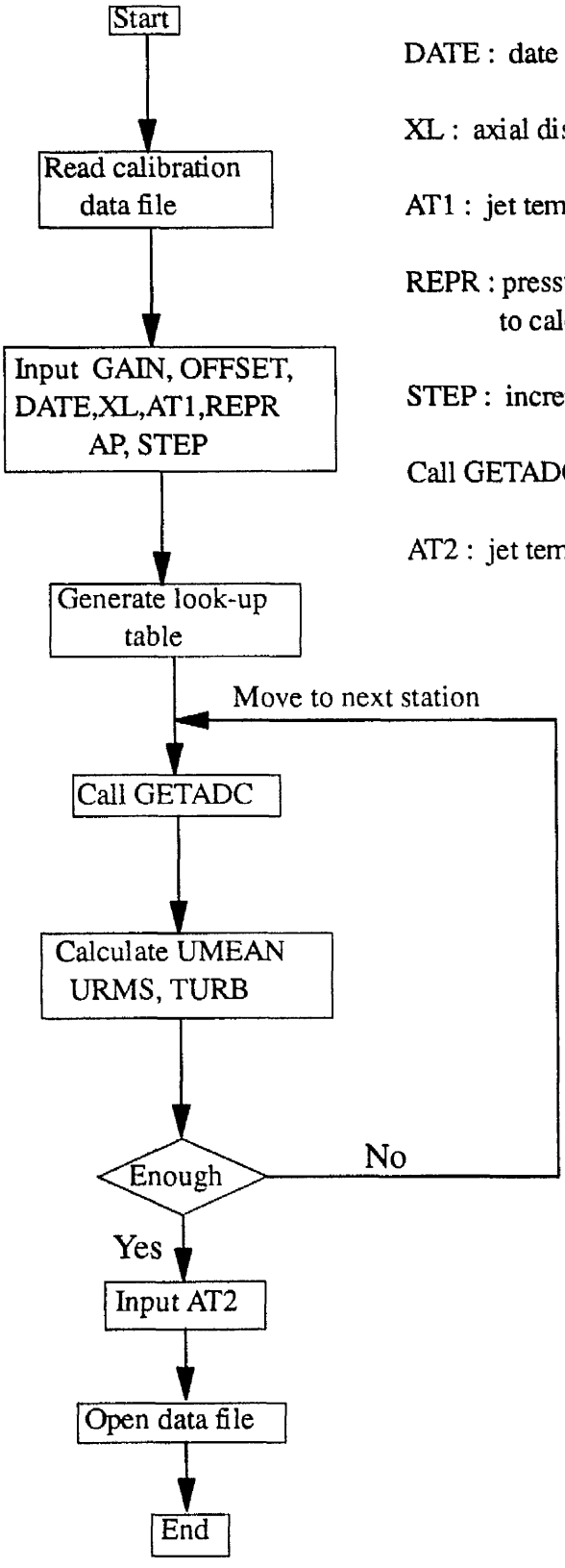

Figure 4.3. Flow chart for data collection program.

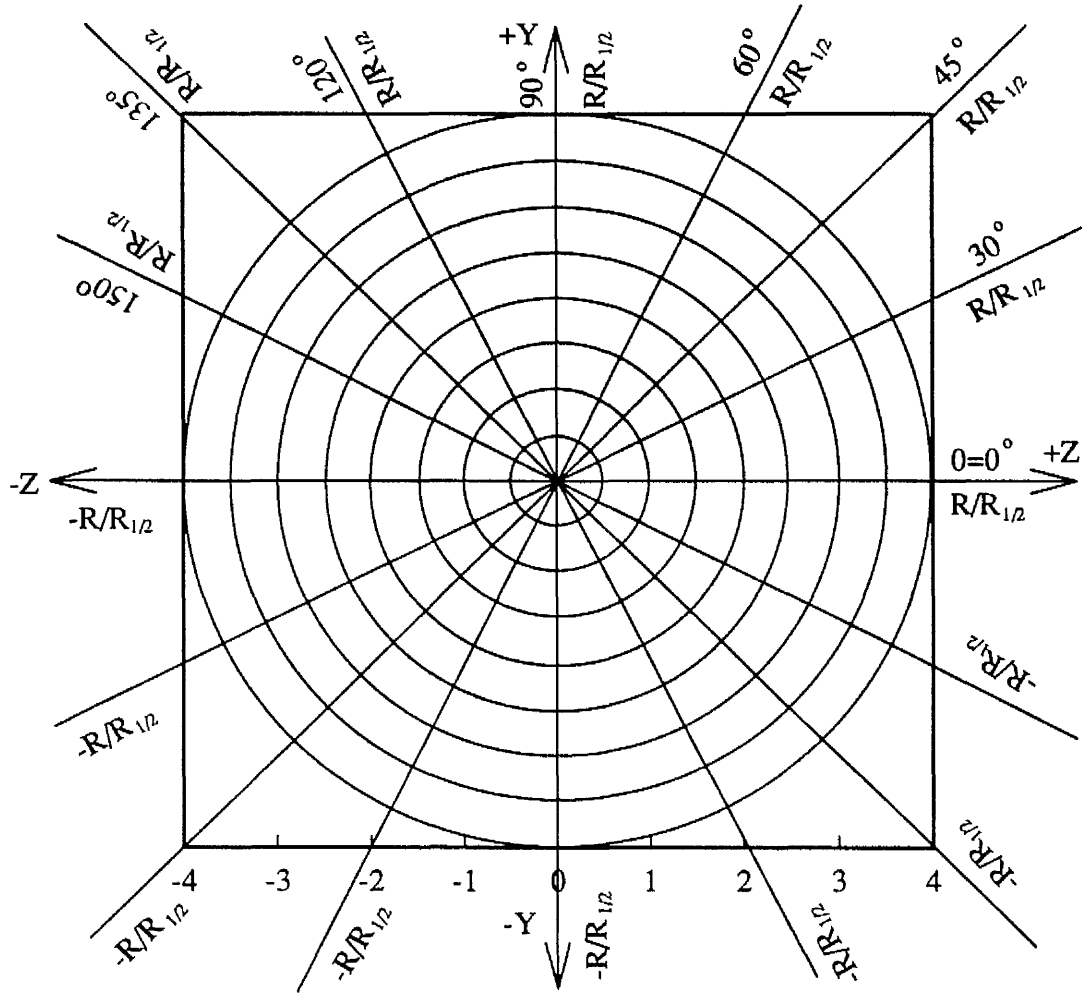

Figure 4.4. Location of the measurement points in terms of radii and azimuthal angle. Flow into paper.

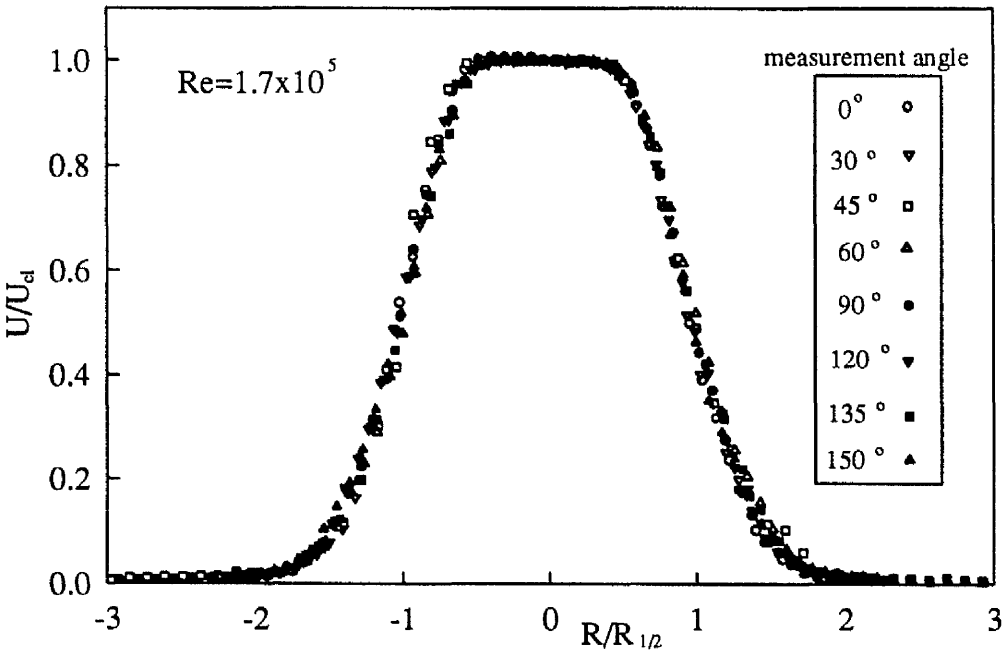

Figure 4.5. Mean velocity profiles for natural jet at x/D=3.0, for different azmuthal angles.

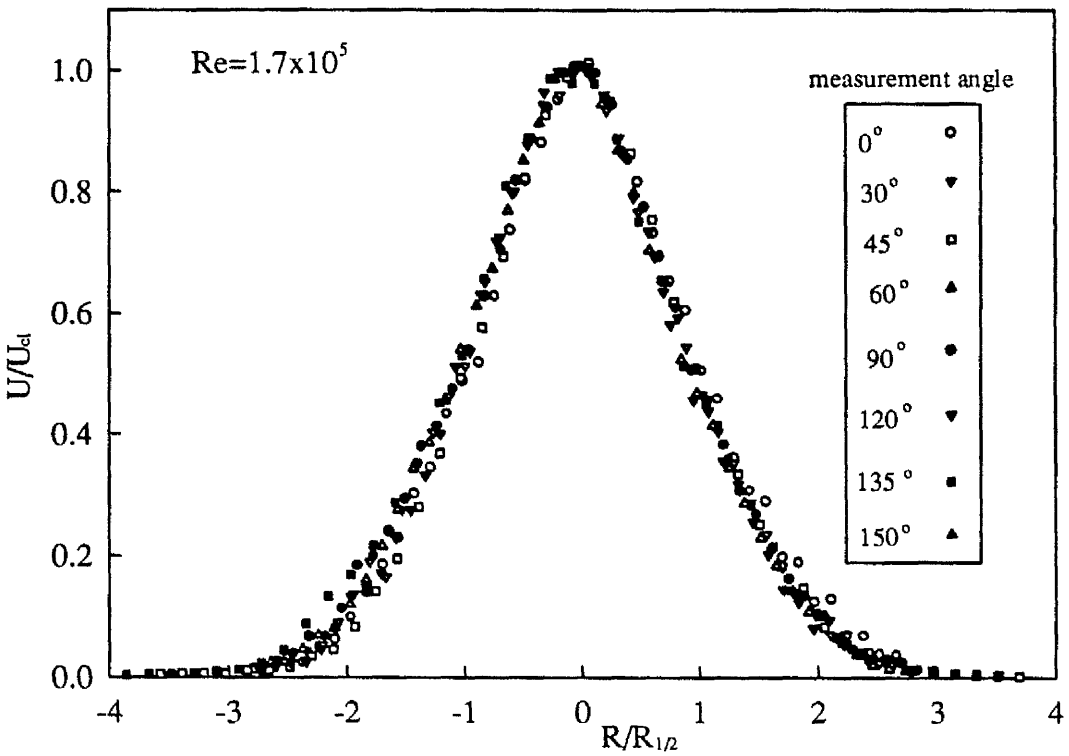

Figure 4.6. Mean velocity profiles for natural jet at x/D=9.0, for different azimuthal angles.

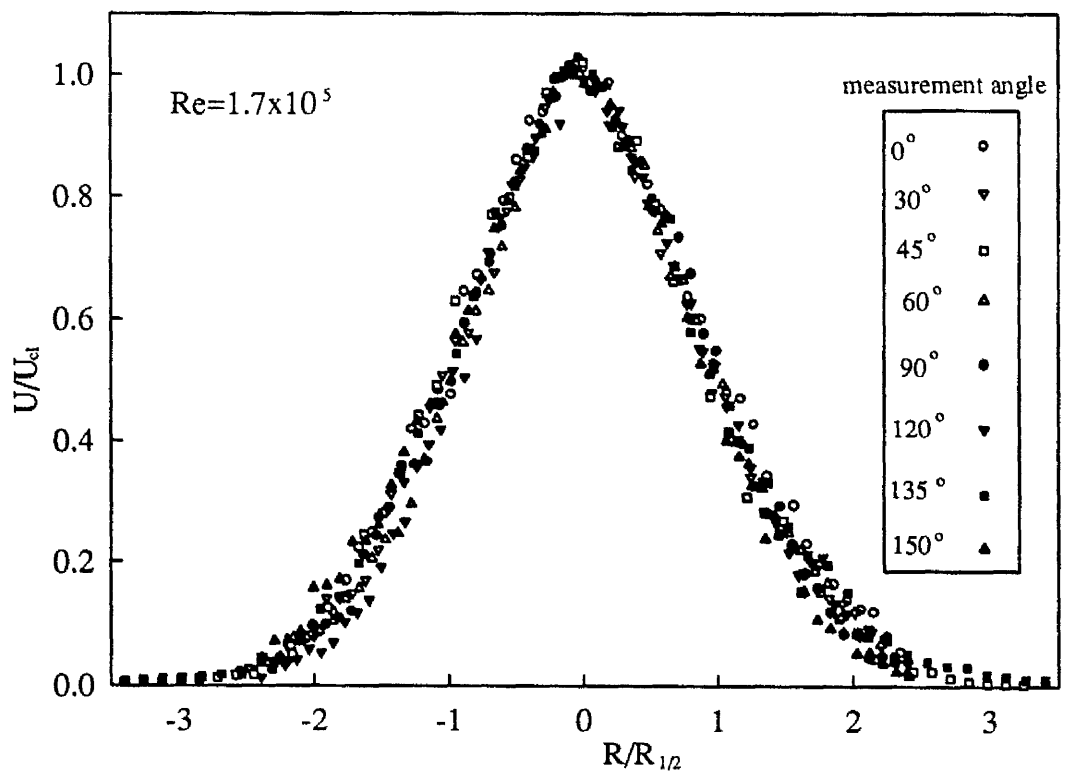

Figure 4.7. Mean velocity profiles for natural jet at x/D=13.0, for different azimuthal angles.

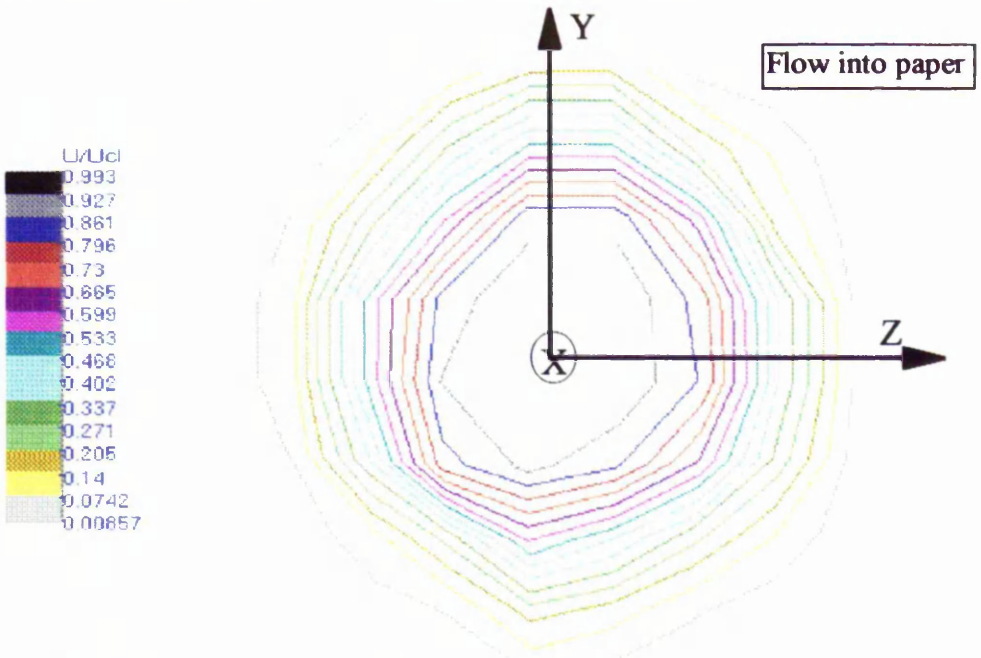

Figure 4.8. Constant velocity contours of the natural jet flow field, at x/D=3.0.

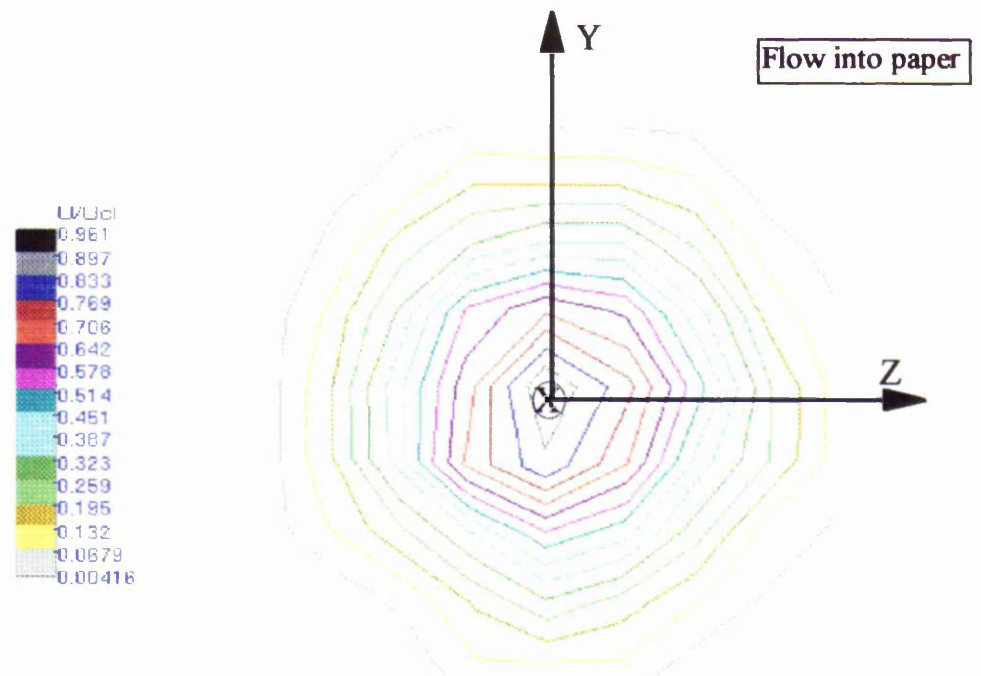

Figure 4.9. Constant velocity contours of the natural jet flow field, at x/D=9.0.

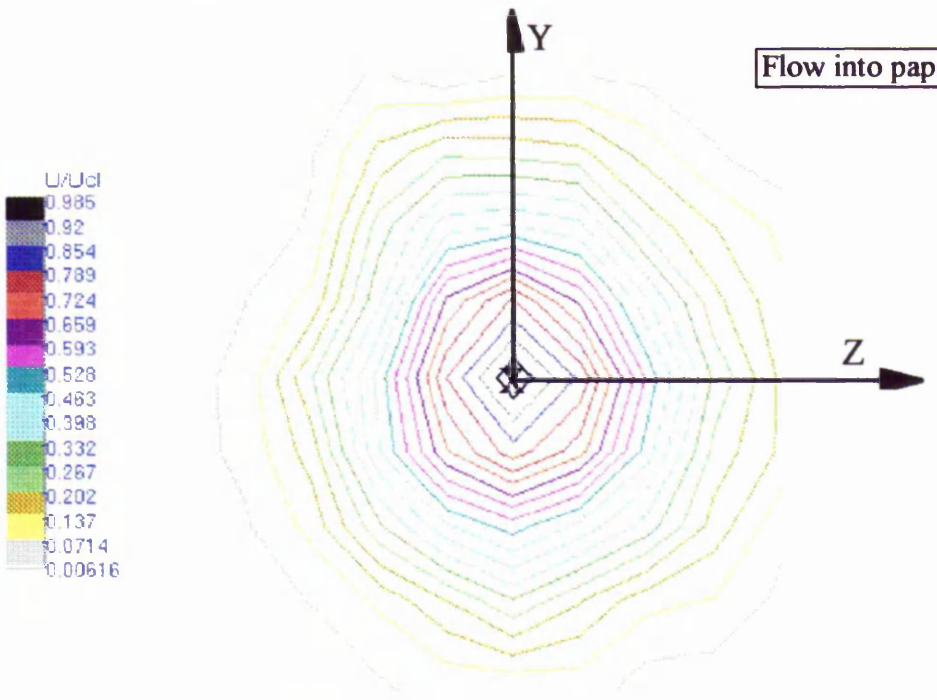

Figure 4.10. Constant velocity contours of the natural jet field, at x/D=13.0.

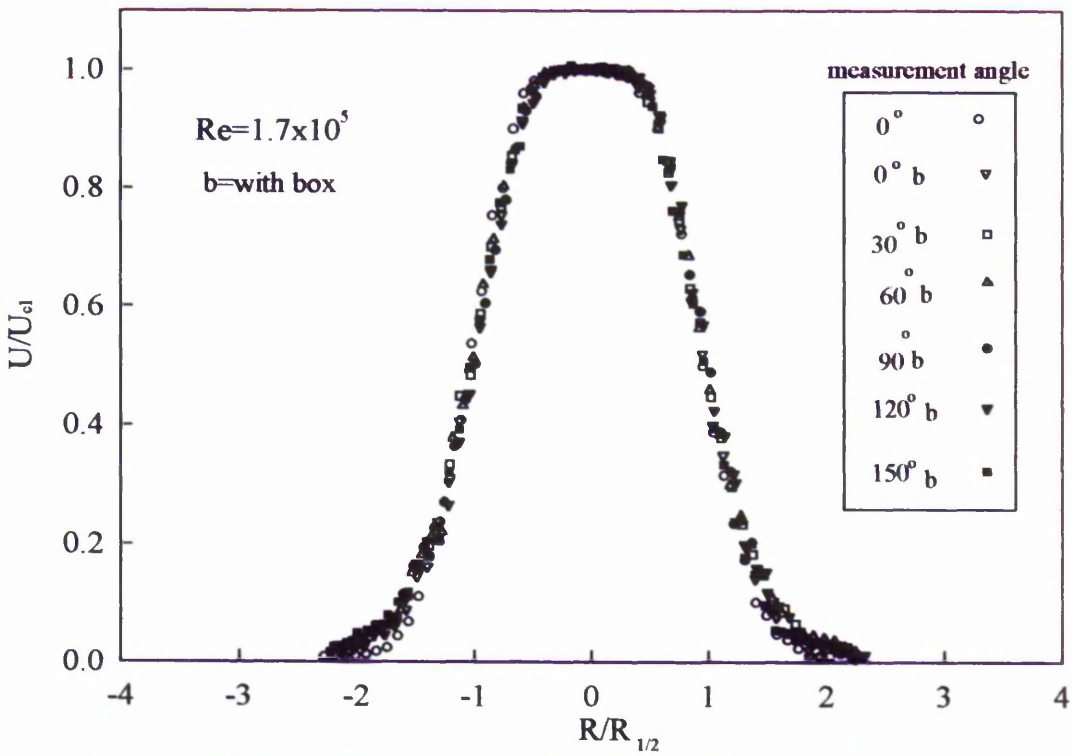

Figure 4.11. Mean velocity profiles at x/D=3.0, for different azimuthal angles to show negligible influence from the containment box.

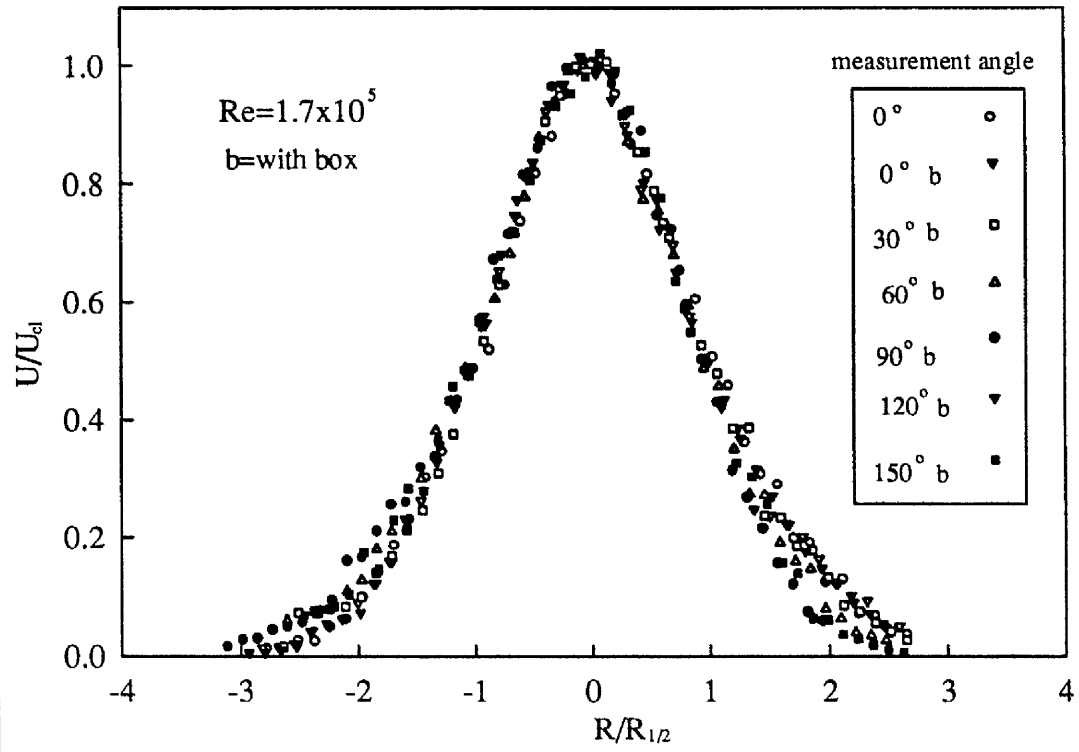

Figure 4.12. Mean velocity profiles at x/D=9.0, for different azimuthal angles to show negligible influence from the containment box.

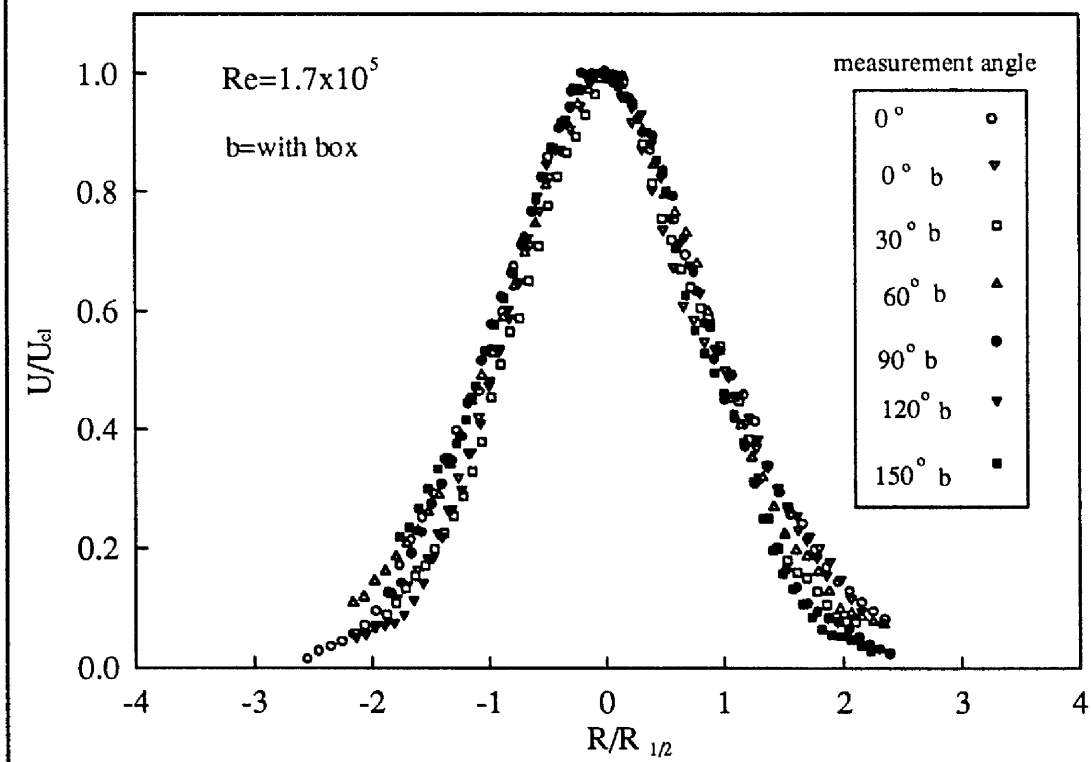

Figure 4.13. Mean velocity profiles at x/D=13.0, for different azimuthal angles to show negligible influence from the containment box.

CHAPTER 5

LASER DOPPLER ANEMOMETRY

CHAPTER FIVE
LASER DOPPLER ANEMOMETRY

5.1 Principle of Operation

Laser Doppler anemometry (LDA) is based on a physical phenomena associated with wave propagation known as the Doppler frequency shift. This phenomenon occurs when the source, the receiver, or the medium through which the wave is transmitted, are in relative motion. It can then be shown that the magnitude of the Doppler frequency shift is directly related to the vector velocity of the relative movement.

Yeh and Cummins (1964) reported on one of the first attempts to perform a simple light scattering experiment on small particles suspended in a fluid. Since then, LDA has undergone much development and intensive research and is now commonly used as a non-intrusive, general purpose, velocity measuring technique.

Any laser Doppler anemometer used in fluid flow measurement can be divided into a light transmitter, an optoelectrical receiver and a signal processor. The transmitter defines the way in which the measuring volume containing the scattering particles is illuminated. Furthermore, application of the technique may require the addition of appropriately small particles to the flow in a process known as seeding. These particles must be small enough to follow the rapid changes of the flow and yet large enough to scatter sufficient light - here, the reader is referred to section 5.2 for further discussion. The receiving system is used to collect the light scattered by each particle as it crosses the measuring volume, while the effect of

other background (or stray) light coming from outside the measurement volume is reduced by a spatial filtering process. Then, the collected light energy is converted into an electrical signal by means of some suitable photodetector. Thus, the optical components making up the transmitter and the receiver system jointly define the way in which the fluid velocity information is encoded. The most commonly used optical configuration is called the dual beam (fringe mode) system (see the typical arrangement shown in figure 5.1 - Drain (1980)). An alternative optical arrangement which is less commonly used but has certain advantages in special applications is known as the reference beam technique - see figure 5.2 (Drain (1980)).

LDA offers a linear response to the flow velocity and is capable of sensing reverse flow. Other advantages are its high spatial resolution and a very wide dynamic velocity range. Finally, perhaps the most desirable feature of LDA is the non-intrusive nature of the technique. Since no probe need to be inserted into the flow, no disturbance is caused to the flow in contrast to intrusive methods like the hot film anemometer or a pressure probe.

Due to these features, LDA has been widely used in laboratory research to measure flows in rotating machinery, and to study combustion flows, the recirculating flow within the cylinders of an internal combustion engine, and in complex two-phase flows. It finds application particularly in relation to Computational Fluid Dynamics (CFD), when measurements of the moments of the higher order turbulence terms are required in complex flow configuration, perhaps to be used for computer code validation.

LDA has also been shown to have great potential for industrial application,

especially in fluid flow and the measurement of velocity of a solid surface where access is particularly difficult. For example, velocity measurements are frequently needed on the solid surfaces which are of interest in connection with the production of paper, metal, and plastic sheets. In medicine, laser anemometry has been adopted to investigate both the human respiratory system and arterial flow, and in the development of many forms of medical flow system e.g. the artificial heart, or the nebuliser used for drug delivery (Lading et al (1994)).

Unfortunately, LDA is not without its disadvantages. It is more complicated to apply than conventional constant temperature anemometer techniques so that a high level of skill is necessary to set-up and properly align the optics and then obtain the optimum performance. Experience shows that, improper adjustment of the optics may result in a significant reduction in the signal to noise ratio of the Doppler signal.

5.2 Seeding the Flow

Artificial seeding to produce the optimum concentration of light scattering particles in the measurement volume at any one time may be necessary if the fluid medium is relatively "clean" such as will be the case for filtered air or water. This seeding can be introduced by adding seeding particles to the upstream flow in order to produce a strong scattering action at the measurement volume so that the velocity dependent optical signal can be detected by the photodetector. This seeding may disturb the flow field if care is not exercised and the size and concentration of the seeding particles are critical factors (Buchhave (1993)). Thus, the particles travelling across the measurement volume should be big enough to scatter a

sufficient level of light energy to the detector so that a high signal to noise ratio is produced. This will enable the electronic signal processor to determine the flow velocity information with sufficient accuracy. On the other hand, larger particles, possessing much greater inertia than the equivalent size of fluid element, would be insensitive to the sudden changes in direction and velocity of the turbulent flow field. For this reason, the particles should be small and light enough to follow the high frequency oscillations of the (turbulent) flow field - Irhouma (1991).

Another factor to be considered with regard to the seeding is the seeding concentration (i.e. the number of particles per unit volume of fluid). This matter must be dealt with carefully and is very much a function of the flow problem to be examined. The present author experimented following the guidance given by Buchhave (1993). In the procedure finally adopted, the concentration of the seeding particles is kept low at the beginning so that the flow field is not affected by their presence. It has been found that if the concentration of the seeding particles is slowly increased, by injecting more smoke into the containment box - see section 5.3, both the data and the validation rates will also increase. These two rates can be monitored on the front panel of the Burst Spectrum Analyzer (BSA). Initially, at low seeding levels, this will indicate that high quality burst type signals are reaching the photodetector. However, as the seeding density continues to increase, the quality of the Doppler bursts will deteriorate and a reduced number of valid bursts will be transmitted to the processor. Thus, the increased seeding density will produce a reduced data rate for the LDA system.

In the present investigation, seeding particles have been produced by evaporating Shell Ondina oil by passing it through the element of the smoke

generator described in section 3.4. Introducing this seeding through the wall of the box - see figure 5.8 - was found to be very satisfactory, providing a high data rate and good validation. Estimates of the size of the particles suggested values up to 5μm, according to the classification by Buchhave (1993) - this is in line with previous studies in the Research Group where Phase Doppler Anemometry (PDA) was used to size the particles (Irhouma (1991)). Experience showed that these particles were retained for a long time in the closed-circuit of the flow rig, so that the constant circulation of the particles around the loop resulted in uniform seeding of the jet itself, as well as the surrounding fluid volume. This uniformity is known to be desirable since it avoids the possibility of the so-called "velocity gradient" effect (Buchhave (1993)). Additional seeding was then introduced into the flow as necessary during the experiments, taking care not to allow the LDA optics to become contaminated by the deposition of seeding particles.

5.3 Basic LDA Configuration for the Present Study

The use of the experimental rig, for LDA measurements described in section 3.1 necessitated the building of a large containment box around the working area containing the free jet. Eventually, the box shown in figure 5.8 with dimension 5.0 x 5.0 x 5.5 m was constructed from timber and polythene sheeting. This was necessary to prevent contamination of the whole laboratory which was being used by other people and to contain the laser beams within the working section. Both of these requirements were needed to satisfy safety regulations. A further advantage of the containment was that disturbance to the ambient air surrounding the free jet flow could be minimised - see figure 5.3.

A dual beam optical arrangement was used in the present investigation, consisting of a laser light source, a transmitting unit, a 20.0m long fibre link, receiving optics and signal processing equipment, as shown in figure 5.4. Here, the reader should note that the discussion of LDA given in this thesis is concentrated mainly on the LDA configuration actually used in the present study. No attempt is made to give a comprehensive review of the LDA techniques. On the contrary, the aim has been to provide basic information so that the reader can develop a physical understanding of the specialised concepts which are introduced in the present investigation. Complete and rigorous treatment on the theory of LDA and its applications can be found in Durst et al (1976), Drain (1980), and Lading et al (1994).

5.4 LDA Measuring Volume

The measuring volume of a dual beam LDA system is formed when two laser beams intersect at the position of their waists. Then, a close examination of the optical interference which occurs in the measuring volume shows that the distribution of optical intensity corresponds to a set of destructive and constructive planar fringes. This phenomenon is illustrated in figures 5.5 and 5.6.

Based upon the standard physical model for optical interference, the spacing between the fringes can be calculated from the wavelength of the laser light λ, and the angle of intersection of the beams θ, as shown in equation 5.1.

Thus

$$\delta_f = \frac{\lambda}{2\sin\frac{\theta}{2}} \qquad 5.1$$

When particles cross the measurement volume, they scatter light in all directions with a frequency shift f_D from the incident laser frequency f_L which depends only on the speed of the particles and the spacing between the fringes. A detector placed at any position so as to receive a fraction of this scattered light will show a high frequency signal, superimposed upon a low frequency signal related to the Gaussian distribution of intensity across the beam intersection. The frequency shift of the detected light is called the Doppler frequency (f_D) and is proportional to the velocity component normal to the fringe planes. This can be expressed by the following equation:-

$$f_D = \frac{u_x}{\delta_f} = \frac{2u_x \sin\frac{\theta}{2}}{\lambda} \qquad 5.2$$

where $\frac{\lambda}{2\sin(\theta/2)}$ is the constant of the proportionality C. Consequently, the linear behaviour of the LDA system can be described by the expression:-

$$u_x = C f_D$$

5.5 Resolving the Sign of the Velocity

It is not possible to determine the direction of movement of the particles, from which the flow velocity is inferred, with such a simple LDA arrangement. The simple explanation given in the previous section shows that it is impossible to detect reverse flows since the measured Doppler frequency f_d will always be positive, regardless of the direction of movement of the particles through the beam intersection volume.

The remedy for this "directional ambiguity" is to introduce a frequency shift for one of the laser beams. This process alters the frequency of one of the beams relative to the other and can be achieved by means of an electroacoustical device known as a Bragg Cell. Under these conditions, the size of the measurement volume and the fringe spacing remain unchanged. However, the fringes now appear to move at a constant velocity of $u_s = \delta_f \times f_s$ through the measurement volume, where u_s is the fringe velocity, and f_s is the Bragg Cell frequency shift (typically 40MHz). The arrangement is shown in figure 5.6.

Consideration of this arrangement shows that if the particle and the fringe pattern both move in the same direction, then the detected frequency f_d will be reduced. This frequency is then given by equation 5.3 as:-

$$f_d = f_s - f_D = \frac{u_s - u_x}{\delta_f} \qquad 5.3$$

However, if the particle and the fringe pattern are moving in different directions, then the detected frequency will be increased and can be calculated from equation 5.4.

$$f_d = f_s + f_D = \frac{u_s + u_x}{\delta_f} \qquad 5.4$$

A frequency shift of 40MHz is typically used in commercial LDA systems. However, this shift frequency is rather large for many LDA applications and is above the range of some processing instruments. Hence, it is often necessary for the detected frequency f_d to be varied by electronic downmixing with an oscillator of

around 30-35 MHz. The signal is then low pass filtered within a range of typically 0-10 MHz before being input to the signal processor. An appropriate selection of the frequency shift enables accurate determination of the particle velocity even in the more complex cases, such as in reversed or highly turbulent flows. This is another important advantage of LDA over the conventional intrusive techniques such as hot wire anemometry where directional ambiguity can not be removed.

5.6 LDA Instrumentation Used in the Present Investigation

5.6.1 The Laser Source

An argon ion laser[1] was used to produce the original laser beam light. This was of the water cooled type and could operate in the all lines TEM_{oo} mode to produce 1.7W in the green wavelength at 514.5nm and 1.0W in the blue wavelength at 488.0nm. More information about the installation of this laser, and operational guide lines can be found in the manual supplied by the manufacturer.

5.6.2 Transmitting Unit

In the fibre optics LDA system used in this study, the beams are delivered to the measurement region by means of a "fibre flow" transmitting unit[2]. This consists of the beam launching unit or transmitter, mechanical manipulators to optimise the alignment of the fibre with the input beam, and the probe distribution box which has several functions to be described subsequently.

[1]4W Coherent Innova 70.

[2]Dantec 60X Fibre Flow series.

(i) Transmitter

The transmitter[3] is the most important part of a "Fibre Flow" transmitting unit, since it is here that all the manipulations on the original beam take place. As shown in figure 5.7, the colour separator splits the original (all lines) beam into two colours, namely the green (514.5nm) and the blue (488.0nm) beams. Each colour is then split again into two beams with approximately the same intensity. Two of the four beams, one from each colour, are passed through the Bragg Cell and are frequency shifted. Then all four beams are transmitted to the measurement volume (the "probe") via the optical fibre link. The optical fibre was attached to the back of the beam expander unit[4], which first expands and then focuses the four beams so that they overlap at a common focal region to form the measurement volume.

(ii) Manipulators

Four mechanical manipulators[5] have been used, one for each of the beams. Each manipulator has four adjustable screws: two of these provide lateral adjustment in two orthogonal directions and the other two allow for angular adjustment. These manipulators enable the optimum alignment between the laser beam and the optical fibre link to be obtained so that the four beams can be transmitted to the measurement volume with the minimum loss of optical power.

---

[3]Dantec 60X40 type.

[4]Dantec 60X type

[5]Dantec 60X24 type.

5.6.3 Optical Head

An integrated optical probe[6] and separate beam expander have been used to deliver the four laser beams so that the measurement volume is formed. This optical probe was 60.0mm in diameter and 250.0mm long. A front lens with 600.0mm focal length was included in the beam expander unit, leading to a probe volume 2.5mm long and 0.15mm in diameter. For the theoretical background which enables the parameters describing the measurement volume to be calculated, the reader should consult Durst et al (1976), Drain (1980), and Lading et al (1994). For the present purpose, table 5.1 in combination with figure 5.5 summarises the parameters of the optical system used in the present investigation. The laser beams were transmitted from the distribution box to the measurement volume, along the same optical fibre link[7] as was used to collect the scattered light and transmit this signal back to the box. The 20.0m length of the optical fibre link allowed the laser source to be kept in an adjacent laser safety room with only the optical head needing to be placed in the working section. This arrangement permits much safer working conditions and minimises the risk that the seeding liquid might spoil the performance of the other LDA instrumentation. Indeed, the extra advantages of flexible optical fibre links have helped to ensure that LDA becomes possibly the most versatile tool in the experimental study of fluid mechanics. The optical distribution box serves as a convenient interface between the optical probe, the transmitter, the receiver, and the measurement volume.

---

[6]Dantec 60X11 type.

[7]Dantec 60X30 model.

Diameter of beam before expansion	(d_1)	1.25 mm
Beam separation before expansion	(D_2)	72.0 mm
Beam intersection angle	(θ)	6.86°
Focal length of front lens	(f)	600.0 mm
Diameter of focused laser beam	(d_f)	0.155 mm for 514.5 nm 0.150 mm for 488.0 nm
Fringe spacing	(δ_f)	4.3 μm for 514.5 nm 4.08 μm for 488.0 nm
Calibration factor	(C)	4.30 ms^{-1}/MHz for 514.5 nm 4.08 ms^{-1}/MHz for 488.0 nm
Measurement volume diameter	(d_x)	0.15 mm
Measurement volume diameter	(d_z)	2.5 mm

Table 5.1. LDA parameters for the system used in this study.

5.6.4 Receiving Optics

The chosen approach using two-component LDA measurement called for the system to operate in the back-scatter mode in which the scattered light is collected and focused back through the optical head - see figure 5.9. The optical probe was then positioned to one side of the jet so as to minimise interference with the flow - see also figure 5.8. The fact that this arrangement was chosen underlines the importance of selecting the optical arrangement to suit each particular experimental task and emphasises the advantage of operation in the back scatter mode.

The scattered light was collected back through the optical head to the distribution box. The two measured optical components were then isolated by the

colour separator[8], and input to the two photomultipliers[9], as shown in figure 5.9.

5.6.5 Signal Processing

Some other disadvantages of the LDA technique are that it is a relatively sophisticated method which requires expensive processing equipment. The laser light scattered by the particles is converted to an electrical current by the photomultiplier which produces a signal for each particle (the Doppler burst) such as the one shown in figure 5.10. As indicated previously, a Burst Spectrum Analyzer[10] (BSA) operating in the frequency domain was used to process the Doppler signals. As mentioned in section 5.5, the signal is first low pass filtered and then digitised using an Analogy to Digital Converter (ADC). The BSA then performs a spectral analysis on the Doppler signal in order to extract the Doppler frequencies by applying the Discrete Fourier Transformer (DFT) over a number of samples. The actual number of samples can be specified by the user to have values of 8, 16, 32, or 64.

The burst is "validated" by comparing the two largest local maxima in the distribution of the power spectral density which is calculated by the DFT. If the ratio between these two power levels is greater than 4 then, according to the manufacturers, the spectrum can be considered to be of a sufficiently high quality and the burst is said to be validated (i.e. can be accepted). The BSA instrument is also used to control the drive frequency for the Bragg Cell and takes this frequency

[8]Dantec model 9055x0352.

[9]Dantec model 9055x0352.

[10]Dantec type 57N10.

shift into account when calculating the Doppler frequency. In addition, it yields other information such as the arrival and transit times for each particle crossing. A good theoretical background, including mathematical derivations to represent the signal processing which must be applied for different type of LDA configuration can be found in Lading et al (1994).

In the present study, two BSA instruments were employed, one for each of the colour separated channels. Since the green line (514.5nm) is invariably the stronger of the two, this green channel was set-up to detect the (smaller) radial velocity component of the flow and was defined to be the "master channel". The blue line (488.0nm) was set-up to detect the axial velocity component, and was defined as "the slave". During two-channel operation, the two BSAs communicate using a common clock source via a synchronous bus to test for the arrival times shown on both channels and to secure acceptance if the coincidence limit is satisfied. This interaction is called hardware coincidence filtering and is utilised automatically by choosing the master and slave modes. Then the data is passed to a PC 486 via an IEEE 488 interference board, as shown in figure 5.4. Setting-up of the BSA parameters is achieved either from the controls on the front panel of the instrument itself or remotely via the BURstware software and the keyboard on the host computer.

5.7 Experimental Programme

One of the objectives of the present study was to obtain a large sample of reliable data for the turbulent jet flow problem, with and without excitation.

Experiments have therefore been performed for a range of flow rates and

aerodynamic excitation conditions, based upon the methods described in the previous studies of Szajner and Turner (1987) and Jeung and Turner (1994). In this method of excitation, the central axisymmetric jet (the primary jet) is surrounded by an annular secondary jet which is pulsed to create the excited jet flow conditions.

For the purposes of this study, the Reynolds and Strouhal numbers have both been based on the diameter of the primary nozzle and the mean velocity U_j of the jet in the nozzle exit plane. They can be expressed as follows:-

$$Re = \frac{U_j D}{\nu} \qquad (Reynolds\ number)$$

$$St_D = \frac{f D}{U_j} \qquad (Strouhal\ number)$$

where ν is the kinematic viscosity of air and f is the excitation frequency of the secondary jet.

For the present investigation, the findings of previous workers (Szajner and Turner (1986) and Jeung (1993)) have been used to define the range of test conditions. On this basis, excitation frequencies ranging from 5Hz to 198Hz, corresponding to four Strouhal numbers ranging from 0.2, 0.4, 0.6 to 0.8, were used for each Reynolds number. These details are summarised in table 5.2. In addition, the flow rate of the secondary jet (Q_s) was fixed at a value of 2% of the primary jet flow rate (Q_o) - see section 7.2, for all the cases considered in the experimental programme.

Re	U_i (m/s)	U_s (m/s)	St_D	f (Hz)
$1.5x10^4$	2.3	1.8	0.2	4.5
			0.4	9.0
			0.6	13.5
			0.8	18.1
$7.0x10^4$	10.3	8.3	0.2	20.0
			0.4	40.0
			0.6	60.0
			0.8	80.0
$1.7x10^5$	25.3	20.4	0.2	49.0
			0.4	99.0
			0.6	148.5
			0.8	198.0

Table 5.2. Experimental conditions for jet flow measurements.

Data were collected at nine axial locations corresponding to x/D = 1.0, 2.0, 3.0, 4.0, 5.0, 7.0, 9.0, 12.0, 15.0. Noting that the radial extent of the jet increased with axial position, the number of data points measured across the jet and the interval between successive radial locations was varied to suit the axial position under consideration. For example, data was collected at 50 radial positions at x/D = 15.0 with a fixed interval of 12.0mm. In contrast, data were collected at 120 radial positions for x/D = 1.0, with an interval of 1.5mm. The full range of test conditions is summarised in table 5.3.

x/D	Step (Δy)mm	No. of radial positions for which data were collected
1	1.5	110
2	2.0	90
3	3.0	80
4	3.5	75
5	4.0	70
7	5.0	60
9	7.0	50
12	10.0	50
15	12.0	50

Table 5.3. Grid covering the experimental area to show size of data sample.

In any attempt to measure the energy content of a turbulent flow, low frequency fluctuations cause particular problems because of the need to obtain a representative time series at any particular position. The problem is compounded using LDA because of the intermittent nature of the signals which are to be analysed. For these reasons, extended time records of the velocity signals were required for this free jet problem so that suitable average conditions could be estimated. In this investigation, time records of up to 120sec, which typically correspond up to approximately 50,000 validated bursts, were recorded for each measurement point. To accomplish this, the two-channel BSA system was operated in the FIFO[11] mode. After implementing the hardware coincidence filtering process mentioned in section 5.6.5 and the software filtering - see section 6.2, the validation rate was typically 95%. Here, the software coincidence filtering, which can be

[11]FIFO stands for "First In First Out", which means that the BSA transfers data to PC in sequence of steps of 2047 bursts at a time, until 50,000 bursts have been transferred.

viewed as an enhancement to the data processing using the hardware coincidence filter, was achieved on the host PC using the BURstware software supplied by the manufacturer. In this mode of operation, the arrival times of each burst from different channels are compared with each other. If the arrival times for a given burst fit inside the pre-defined coincidence time window, here set to 1msec, then the burst is considered to be validated. Only one arrival time is saved along with this burst, being given a value which is the average of the two (or three) arrival times.

During an experiment, the data was first stored on the 50 MB hard disk of the host computer before being archived onto an optical disk for subsequent analysis. A total of approximately 10 GB of data were collected during the whole series of jet flow experiments.

5.8 Three Component LDA Measurements

Three component LDA was tried in the first stage of this investigation - Al-Sudane and Turner (1994). The LDA apparatus used in this case consisted of a Dantec 60X optical unit which launched the blue 488.0nm and green 514.5nm beams from a 4W Argon-Ion laser. A separate violet 476.5nm beam was launched by an independent Dantec 55X optical unit from another similar laser operating in the single mode. An off-axis back-scatter technique was used so that the scattered light could be collected by a second transmitting system, as shown in figure 5.11.

Considerable efforts were then expended in an attempt to obtain the optimum alignment of the system so that a suitable high data rate could be obtained from each channel.

The pin-hole meter developed by Swales et al (1993) was constructed to obtain a high level of alignment. Despite efforts extending over several months, it proved impossible to obtain overlap of the measurement volumes for all three colours. It was concluded that apparatus offering much higher precision would be necessary and that every combination of rotation, tilt and lateral adjustment would be needed to yield a successful outcome. Therefore, it was obvious to the author that such a combination of high precision was not possible with the facilities in hand. Eventually, due to severe constraints on time available for the experimental programme, attempts to make measurements with the three component LDA system were abandoned.

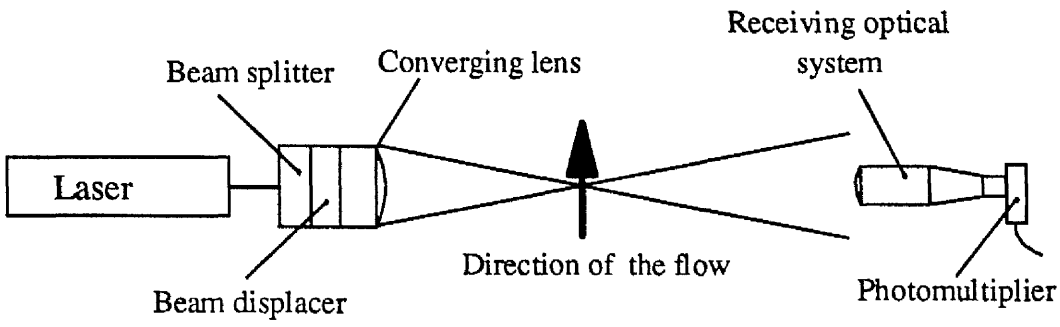

Figure 5.1. Typical dual beam (fringe mode) LDA system.

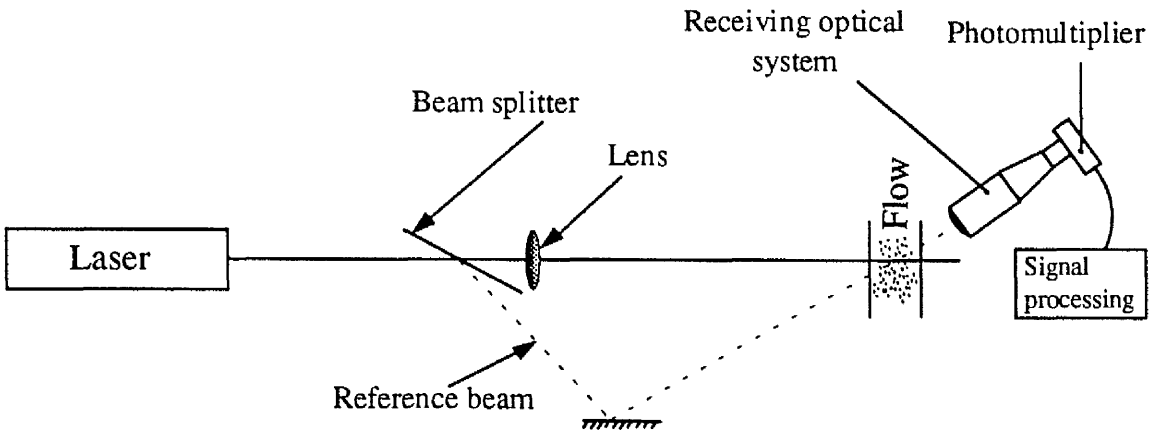

Figure 5.2. A simple laser Doppler anemometer employing the reference beam technique.

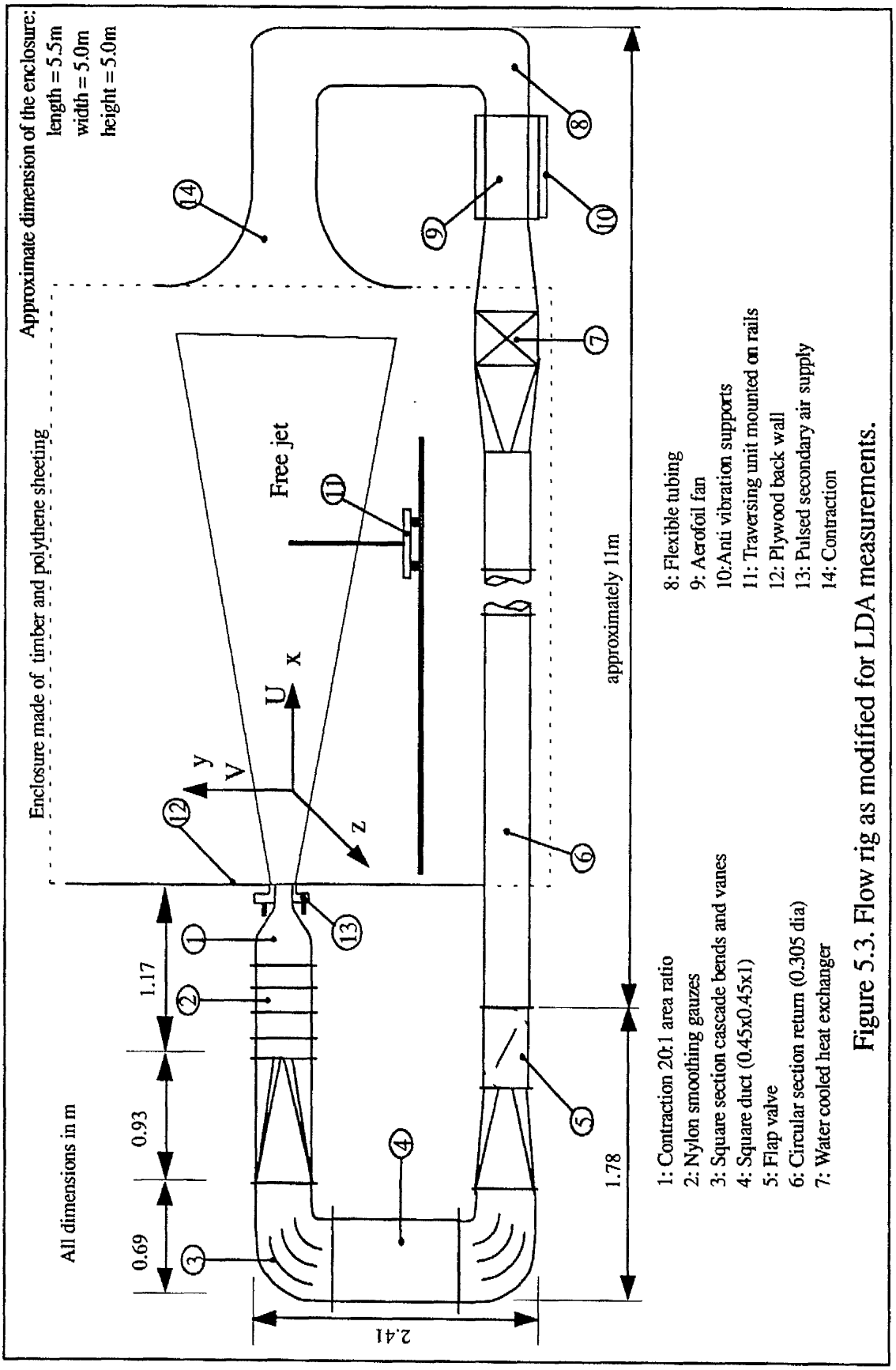

Figure 5.3. Flow rig as modified for LDA measurements.

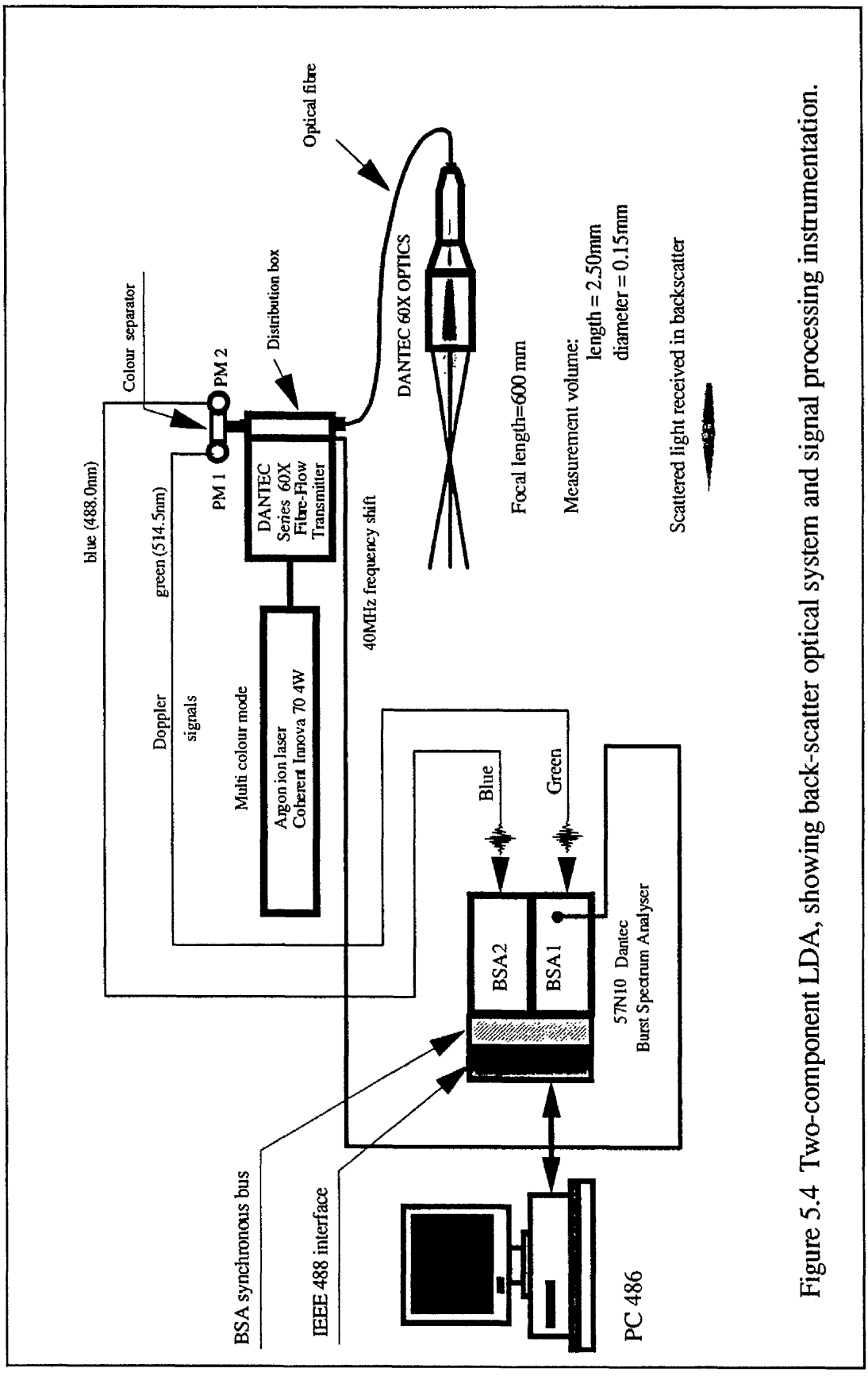

Figure 5.4 Two-component LDA, showing back-scatter optical system and signal processing instrumentation.

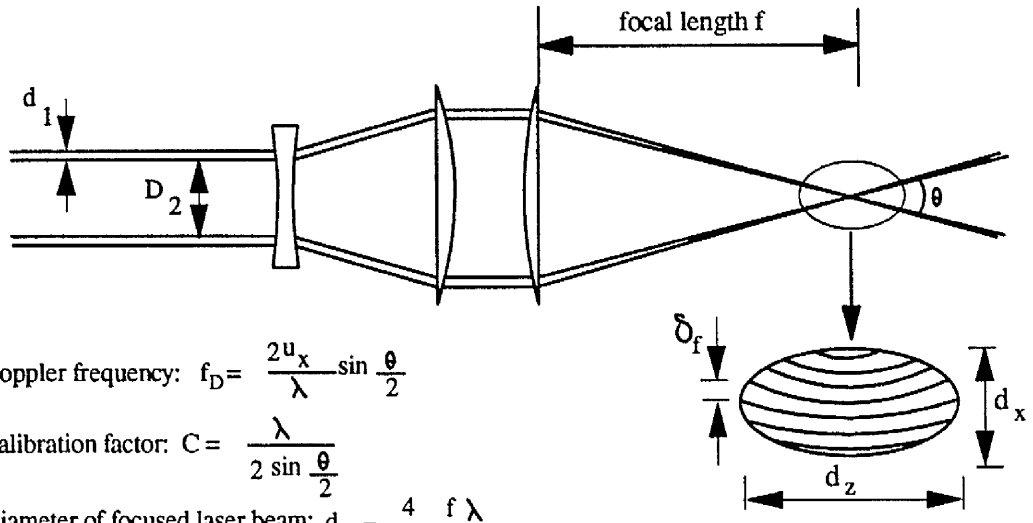

Doppler frequency: $f_D = \frac{2u_x}{\lambda} \sin\frac{\theta}{2}$

Calibration factor: $C = \frac{\lambda}{2 \sin\frac{\theta}{2}}$

Diameter of focused laser beam: $d_f = \frac{4}{\pi}\frac{f\lambda}{E\,d_1}$

Fringe separation: $\delta_f = \frac{\lambda}{2 \sin\frac{\theta}{2}}$

Fringe number : $N_f = \frac{8}{\pi}\frac{f}{E\,d_1}\tan\frac{\theta}{2} = \frac{4}{\pi}\frac{D_2}{d_1}$

Measuring volume dimensions

Length: $d_z = \frac{d_f}{\sin\frac{\theta}{2}}$

Diameter: $d_x = \frac{d_f}{\cos\frac{\theta}{2}}$

Figure 5.5. Parameters of the measurement volume.

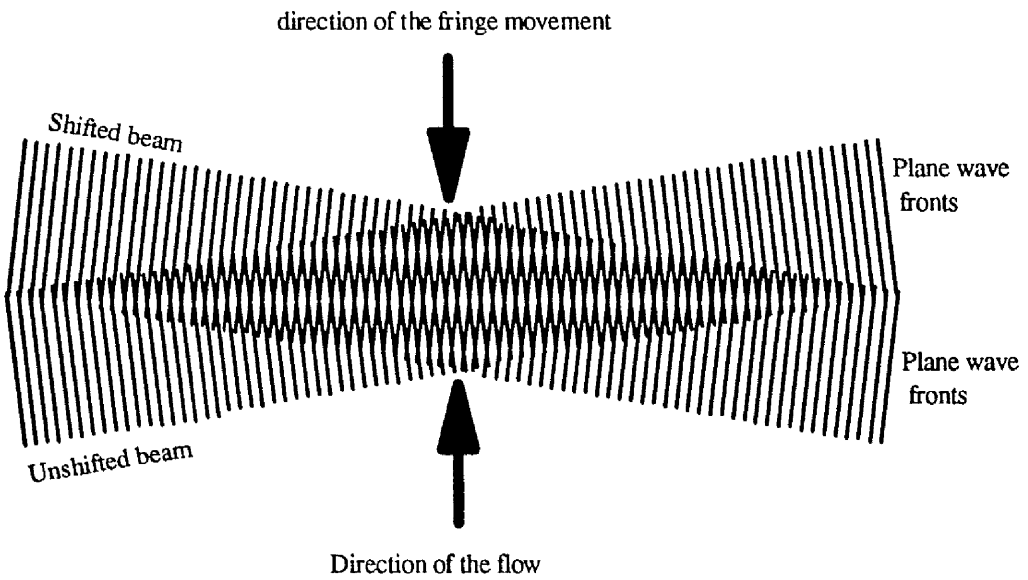

Figure 5.6. Formation of moving fringes.

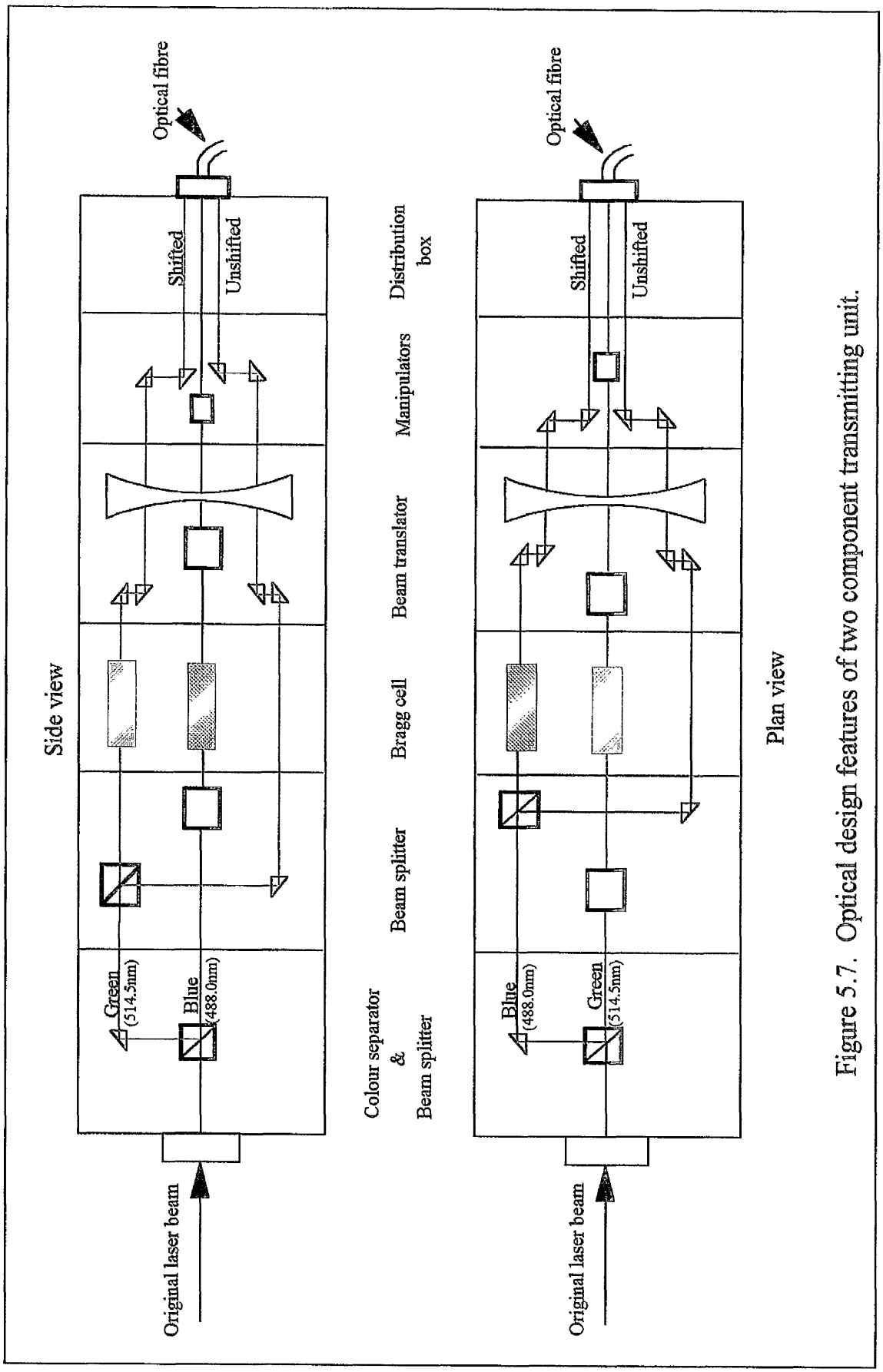

Figure 5.7. Optical design features of two component transmitting unit.

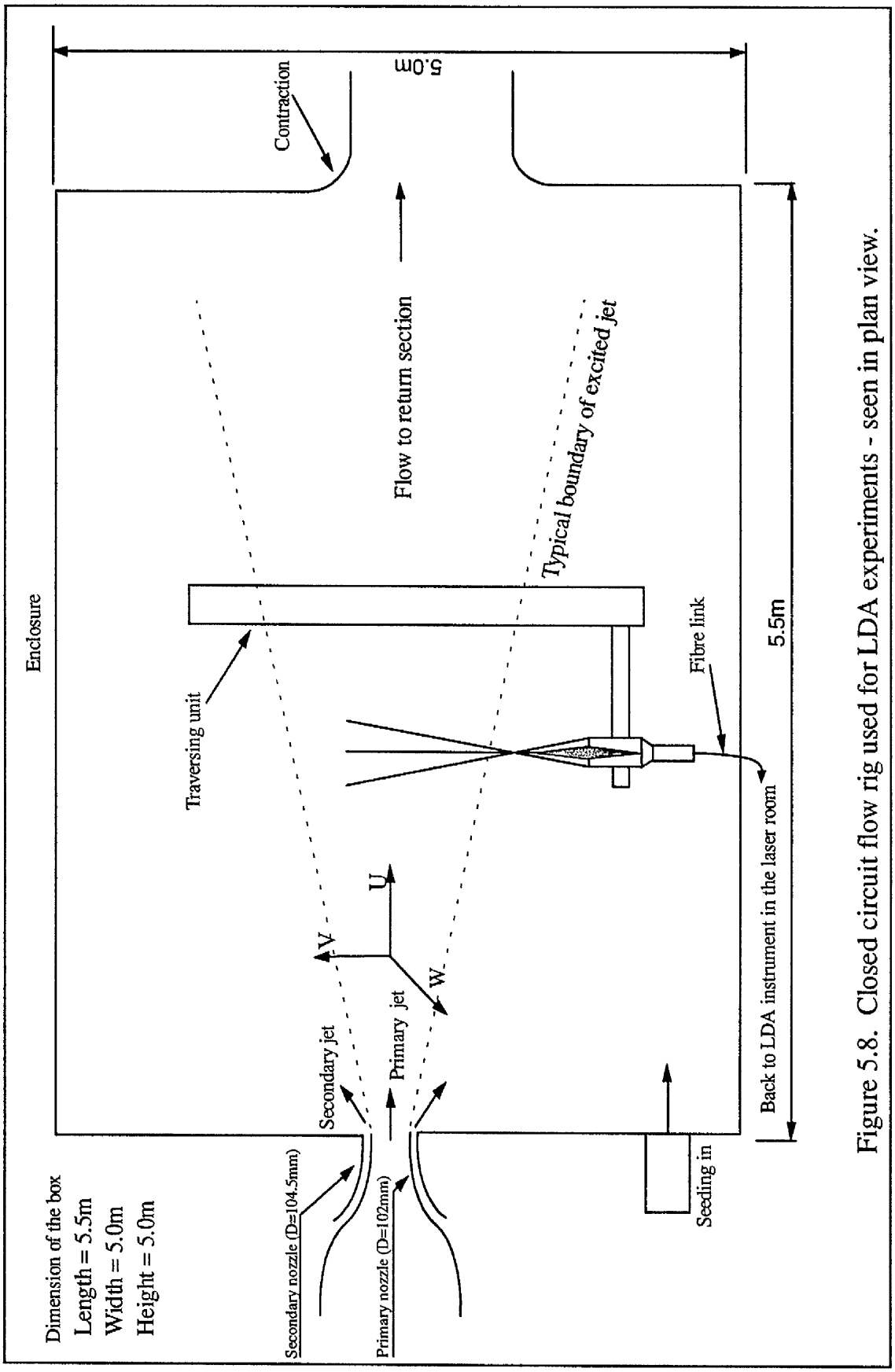

Figure 5.8. Closed circuit flow rig used for LDA experiments - seen in plan view.

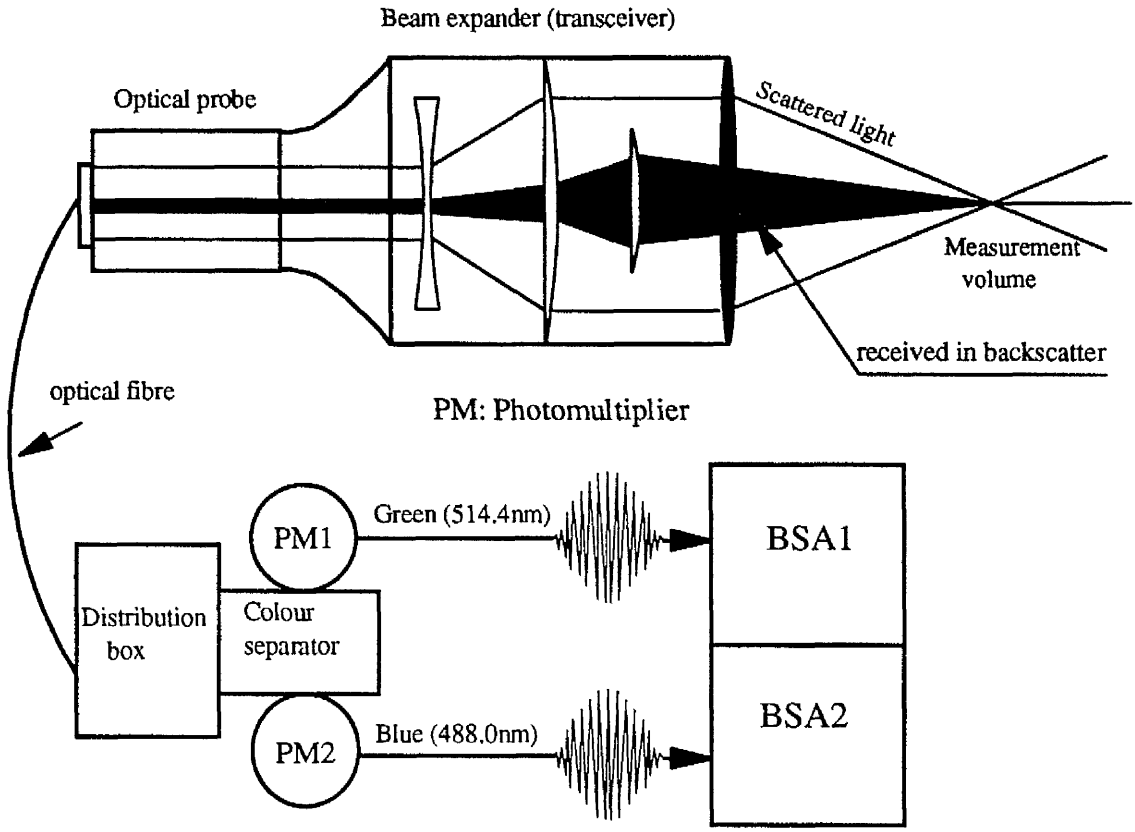

Figure 5.9. Schematics of LDA optics and processing instrumentation.

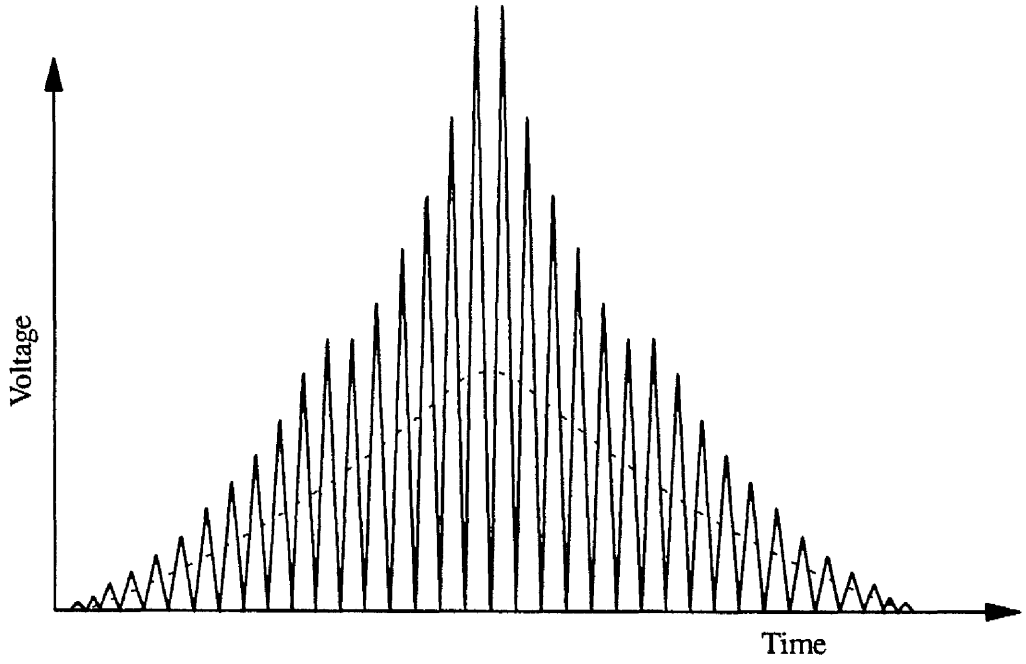

Figure 5.10. An ideal Doppler burst with pedestal.

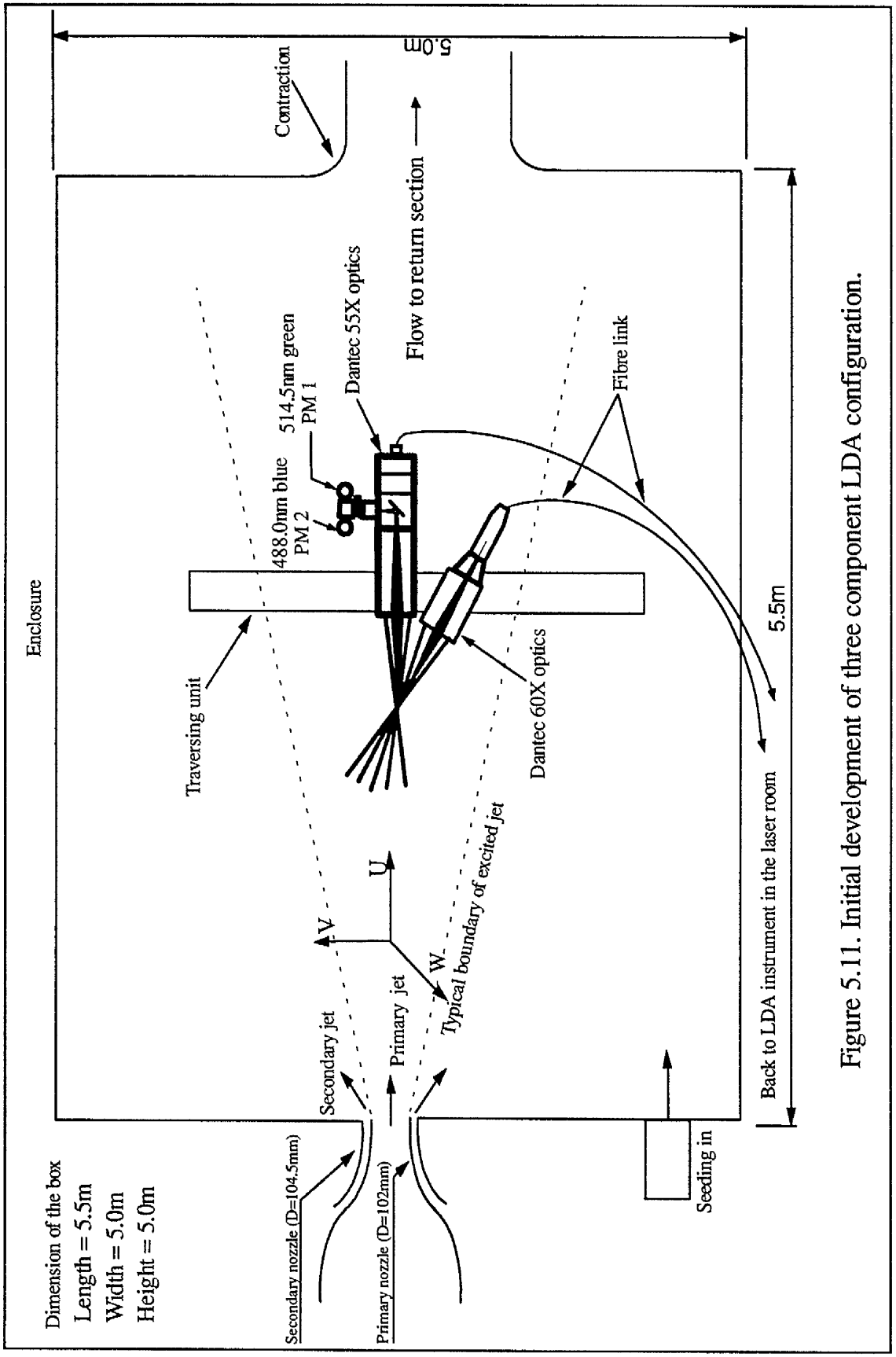

Figure 5.11. Initial development of three component LDA configuration.

CHAPTER 6

RELATED COMPUTER PROGRAMS

CHAPTER SIX
RELATED COMPUTER PROGRAMS

6.1 Data Collection

Time series data have been collected at each radial position across the jet within the range of experimental conditions described in tables 5.2 and 5.3. BURstware software was used in collecting all the experimental data sets. The BURstware was loaded and run on an IBM compatible personal computer, equipped with a 60 MB hard disk to ensure that sufficient memory was available for the data derived from at least one location in the jet. The data were then stored on an optical disk, controlled by an optical disk driver which can communicate with the PC via a SCSI card using the COREL communications software. Some preliminarily data collection and processing were performed to check the instrumentation and enable the experimental programme to be planned before any serious measurement could take place. Furthermore, before the start of each individual experiment, the airflow rig and the attached instruments (for flow, pressure etc.) were left running for approximately half an hour. This was done so that a steady temperature state could be reached and to enable uniform seeding to be achieved over the whole volume of the working section. The optimum parameters were then selected for the BSAs so as to produce the highest validation rate. A 95% validation rate was typically achieved.

Having cleared all these obstacles, data for the whole experimental programme described in section 5.7 were collected and transferred to the optical disk

unit ready for secondary processing.

6.2 Data Processing

At the start of this project, it seemed obvious to the author that use of a PC offered the most efficient way of processing the LDA data whereas, previously the University main frame or a DEC Micro Vax computer had been used in the Research Group. This change necessitated up-grading of the PC by installing a new mother board fitted with a post processor (80486 DX2) and 66 MHz CPU clock, in addition to the insertion of 500 Megabytes of hard disk.[1]

The experimental data have been processed in two parts. In the first stage, the overall time mean values of the steady velocity components and the turbulent velocity fluctuations were calculated. This enabled the distributions of these properties across the jet to be determined for each axial location. From this knowledge, the integral parameters could be calculated. In the second stage, the intermittency of the nominally fully turbulent flow was calculated for selected positions within the jet flow.

In both parts of this data reduction process, BURstware was the initial tool used to interpret the raw Doppler frequency data supplied by the LDA system and relate this to the measured flow parameters. This processing of the raw data could be separated into two stages. The first stage yielded the two components of the instantaneous fluid velocity, and the arrival and transit times for successive Doppler bursts as recorded by each channel. The second stage incorporated a pre-defined coincidence time window which was set to 1ms in the present investigation. This

[1]Caviar AC2540 model, manufactured by Western Digital Ltd.

software coincidence filter serves as a second filtering gate and ensures that the Doppler bursts can be considered absolutely valid - as defined in section 5.7. This validation is achieved by comparing the arrival times of each burst supplied by the two channels. Then, if the two bursts fit inside the prescribed coincidence time window, the bursts are assumed to be coincident and to originate from the same particle.

Now the data can be exported as an ASCII data file for further processing. This file contains the number of bursts and the arrival times, taken as the average of the two arrival times in the two-dimensional system used here. (Three arrival times are generated in the case of a three-dimensional system.) The file also contains a transit time representing the time for the particle to cross the measurement volume, and the two velocity components (radial velocity V and the axial velocity U). In addition to the headings which combine the parameter surrounding the raw data file collection, figure 6.1 shows an example of such a file. These data files have purposely been exported under incrementing file names to indicate the number of data points across the jet for each traverse. The second and third characters of the file name are incremented by one after each point. For example, the file name 'F01625vc.lst' incorporates 'F' for the natural free jet, '01' for point number 1, '6' for x/D = 12.0, '25' for U_j = 25.0 m/s. Finally, 'vc.lst' is the software convention used to indicate that the file contains coincident velocity data. This file naming system enables the programs which follow to open the data files in sequence and thereby to ensure efficient batch processing. Any reader who may be interested in running the Dantec BURstware software, or wishes to understand its special features, is referred to the BURstware manual.

6.2.1 Calculation of the Integral Parameters of the Jet Flow

BURstware is only able to process individual points, so that calculation of the mean and turbulence intensities for a sequence of points across the jet is not possible. For example, the software does not permit automatic incrementation of the filename. Nor does it provide for the direct calculation of mean and turbulent intensity values which can be exported as a data file for further processing. Finally, perhaps its most important limitation is that the output data files from the software are not in the most convenient form for further processing (for the purpose of this study). Thus, it quickly became obvious to the author that more computer programs would be required to complete the processing of the data. Subsequently, a number of main and auxiliary programs were written in the FORTRAN 77 language and were then compiled using the Salford 77 compiler. The list of the source codes for these programs can be found in an Internal Report (Al-Sudane (1996)).

6.2.1.1 Calculation of the Overall Mean Values (RD.FOR)

The first stage of the processing is carried out by a program called RD.FOR. This program reads the data files produced by BURstware, which contains information for each radial position across the jet and for every axial location. This processing is performed automatically without any interaction by the user so that it can be considered to be part of the batch processing operations to be dealt with later in this chapter. The main structure of this program RD.FOR contains two loops. The outer loop starts from one edge of the jet, where the number of the radial position equals one (i. e. NN = 1), to the other side of the jet, where the number of position equals the final point (i. e. NN = NSTA). The inner loop calculates the overall mean value of the flow parameters numerically for each individual radial

location as expressed by equation 6.1.

$$\overline{Q}(r) \quad \frac{\sum_{i=1}^{N} Q(r,t_i)}{N} \qquad 6.1$$

In this expression, Q(r,t) can be taken to represent one of the following parameters U, V, u_{rms}, v_{rms}, $\overline{u'^2}$, $\overline{u'^3}$, $\overline{u'^4}$, $\overline{uv}$, $\overline{u'^2v'}$, $\overline{v'^2}$, $\overline{v'^3}$, $\overline{v'^4}$, $\overline{v'^2u}$, fu, su, fv, and sv. N is the valid number of bursts at each point. This was typically 48,000 on average, after applying the hardware and software coincidence filters.

It should be noted that the numerical average of the flow properties calculated using equation 6.1 differs from the overall time mean, weighted by the arrival time of each individual burst, by 1 - 2% - see also Kelemenis (1993). This is due to the uniform seeding of the jet and the surrounding space resulting in a high rate of data collected by the LDA system. In view of these small differences, it was decided that the numerical average of each property could be used (programe RD.FOR) in order to reduce computational time.

Program RD.FOR must be supplied with the number of data points for a specified axial position and a dummy input file name to start with (see the list of source files). Then the program automatically increments the input data file name by incrementing the third character of the previous input data file name. This takes place within the outer loop. The results from application of this program are written to an output data file for further processing. Figure 6.2 shows the flow chart for operating this program, while figure 6.3 presents an example of the results which are output from the program.

6.2.1.2 Calculation of the Non-dimensional Parameters and their Distribution Across the Jet (UV12.FOR)

As mentioned in section 4.5.2, this program was initially developed to process the single channel data derived from the hot film anemometer, but was modified to process the data taken from two channels of the LDA. This program computes the non-dimensional parameters and their distribution across the jet for the particular axial station under consideration. It was applied to each of the five jet flow arrangements, namely to the natural jet and the four jet flows with excitation at the different Strouhal numbers (St_D = 0.2, 0.4, 0.6, and 0.8). The time meaned velocities and the turbulence components were non-dimensionalised with respect to the centre-line time mean velocity of the natural jet (U_{cln}) for each axial station. The radial positions were non-dimensionalised with regard to $R_{1/2}$, which is the radial position at which the time mean axial component has fallen to half of its centre-line value. The program initially requires the time mean axial velocity of the primary jet (U_j) at the exit plane of the nozzle (x/D = 0.0) to calculate the Reynolds number. It consists of three loops, in which the outer loop runs axially and permits determination of the flow properties for the whole area occupied by the jet from x/D = 1.0 to x/D = 15.0. In other words, the program starts with the axial location x/D = 1.0 and calculates the radial distributions of the flow parameters (i. e. the time mean values for the velocity and velocity fluctuation levels). Then the program moves on to x/D = 2.0 and so on sequentially up to x/D = 15.0. These calculations were carried out by the program for the natural jet as well as for the four jet flows with excitation.

At the start, the program asks for the axial distance, the equally divided

distance interval between the radial positions (STEP), and the input data file name to be entered. The second loop is fixed and runs radially in five iterations, to cover the natural jet and the four excited jet conditions. The third inner loop deals with each individual case in turn and runs according to the number of radial positions in each case (from NN = 1 to NN = NSTA). For convenience, the number of radial positions should be approximately the same in these different cases, to aid comparison. In the present study, the number of radial positions was 110.0 (NSTA = 110.0) at x/D = 1.0 for both natural jet and the four jet flows with excitation.

Program UV12.FOR reads all the information from the input data file, then determines the position of the central point of the velocity profile by finding the maximum velocity (U_{max}) then $0.9U_{max}$ and $0.8U_{max}$, for both the right hand, and the left hand sides of the mean velocity profiles. Then the program carries on to calculate the radial positions corresponding to the coordinates for the measured velocity values. The two output data files produced by this program are in dimensional and non-dimensional form for further processing and graphical presentation. Figure 6.4 shows the flow chart of this program, figures 6.5 (a) and (b) show typical output data files in both dimensional and non-dimensional form.

6.2.1.3 Calculation of the Entrainment Rate (ENTRA.FOR)

For the purposes of this parameter, an assumption needed to be made about the flow conditions. In fact, the flow was assumed to be axisymmetric at every plane considered.

For an elemental area A, which is rotated around a central axis, the resultant

volume traced out can be expressed by equation 6.2, where R is the distance from the centre of the area of the element to the central point of rotation. In the present situation, this point corresponds to the centre-line of the velocity profile. This basic mathematical approach (the theorem of Pappus) has been used to calculate the volumetric flow of the fluid based upon the velocity profile across a vertical plane cutting through the axis of the jet. Figure 6.6 illustrates this approach and explains the origin of the equation.

$$VFR = 2\pi RA \qquad 6.2$$

First, the velocity profile was divided into elements of width equal to the radial steps employed during the traversing. Then, the cross-sectional areas defined by two adjacent radial positions, and the effective volumes of the individual radial elements, were calculated assuming radial symmetry. Careful mathematical manipulations were applied at the edge of the velocity distribution following the methods described by Szajner (1986) and illustrated in figure 6.7. In addition, the LDA data were collected at relatively small radial steps for each axial position to minimise the errors and hence ensure that reasonable accuracy was obtained for the estimates of volumetric flow at each jet cross-section. The volumetric flow of the jet was then calculated by the summation of all the elemental volumetric flow components based upon the right and the left hand sides of the velocity distribution as explained in figure 6.7. The average value for the two sides of the jet was then taken to be the best estimate of the total volumetric flow at any given axial position. Figure 6.7 shows a flow chart for this series of calculations.

The program used to perform these calculations consists of a main loop which runs nine times in sequence, corresponding to the number of axial positions

along the length of the jet where data were obtained. The program asks for the input data file and output data file names to be entered. Then the entrainment rate $\{(Q_x - Q_o/Q_x)\}$ is determined.

6.2.2 Intermittency Calculations (RLSA.FOR)

Up-grading of the personal computer used by the author (see section 6.2), and particularly the installation of a new hard disk offering 500 MB memory enabled the intermittency calculations to be carried out on the PC.

The approach of Jeung (1993) was adopted and some of his data was re-analysed in the first stage of these calculations. For the present study, however, the software written by Jeung needed to be further developed and modified to run on the PC operating system, as opposed to the DEC Micro-Vax machine previously available. These modifications were made to avoid some of the difficulties previously experienced by Jeung, associated with system storage limitations, communication obstacles between the Micro-Vax and PC systems, and excessively long computation times. With the new PC 486 based system used here, the time taken to process a file was reduced to one-fifth of that required for the Micro-Vax. An auxiliary program was written to calculate the mean values of the axial and radial velocity components U and V. This data, plus other information such as the input data file name and the preliminary (starting) value of the threshold level, were also stored. The software is therefore suitable for batch processing by calling the information needed from within the PC. The resultant data file from this program was given the same input data file name, but with extension (*******.THR) for simplicity.

Unfortunately, after considering the results of these intermittency factor calculations made using Jeung's method, it was concluded that the derived values were illogical. It appeared to the present author that the numerical averages of the global and zonal properties were not valid in the form obtained because they were based on ensemble means and did not take account of the different arrival times of the individual bursts.

In other words, the time history of the velocity time records was being replaced by simple numerical averages of the global and zonal values. Thus, the software needed to be re-written to calculate the intermittency factor on the basis of the time averages. At this stage, only the normal stress variable (u'^2) should be considered.

The revised software written by the present author can be divided into three main subroutines. These calculate the overall averages, the zonal averages, and the intermittency values at each measurement position based on the arrival times between successive bursts. Figure 2.5 illustrates how these procedures are implemented in the software.

6.2.2.1 The Overall Average (READ1.FOR)

This subroutine is called by the main program RLSA as mentioned in the previous section. It calculates the overall time averages of the normal stress which is then used to determine the optimum threshold level and hence the appropriate intermittency factor. This can be expressed mathematically as follows - see Kovasznay et al (1970). For the normal stress, the global and the zonal time mean values satisfy the relationship:-

$$\overline{u^2}(r)_G = \gamma\overline{u^2}(r)_{tur} + (1-\gamma)\overline{u^2}(r)_{non} \qquad 6.3$$

Firstly, the overall time mean average of the normal stress described by the Left Hand Side (LHS) of equation 6.3 is calculated using the Trapezoidal Rule to approximate to the velocity variations between successive velocity realisations (or LDA bursts). This can be defined by the expression:-

$$\overline{u^2}_G = \frac{1}{T}\int_0^T [U(r,t) - \overline{U}_G]\, dt \approx \frac{\sum_{i=1}^{N} [U(r,t_i) - \overline{U}_G]\, \Delta t_i}{T} \qquad 6.4$$

6.2.2.2 Zonal Average Calculations (SL1.FOR)

The turbulence detector function chosen to be used in the present work was the instantaneous shear stress u'v'(t) based upon departure of each velocity component from its global mean value i.e. $(u'v')_G = \sum[(U-U_G)\,(V-V_G)\,\Delta t]/T$.

Initial calculations to determine the zonal average values of both the turbulent and non-turbulent quantities are based on an initial input value for the threshold level. This, typically, can be taken as half the value of the overall average of the shear stress at the beginning of the calculation. Using this assumed threshold level, the instantaneous velocity levels in the time series data can be divided into turbulent and non-turbulent zones dependent upon whether the instantaneous shear stress (u'v') is above or below the threshold. Only the time mean velocities for each of the turbulent and non-turbulent zones are calculated at this stage of the calculations using the following approximations to the full integral values :-

$$\overline{U}_{tur} = \frac{1}{T_{tur}} \int_0^{T_{tur}} U(r,t)\ dt \approx \frac{\sum_{i=1}^{N_{tur}} [U(r,t_i)\ \Delta t_i]_{tur}}{T_{tur}} \qquad 6.5$$

$$\overline{U}_{non} = \frac{1}{T_{non}} \int_0^{T_{non}} U(r,t)\ dt \approx \frac{\sum_{i=1}^{N_{non}} [U(r,t_i)\ \Delta t_i]_{non}}{T_{non}} \qquad 6.6$$

6.2.2.3 Intermittency Factor Calculations (SL2.FOR)

Having discriminated between the turbulent and non-turbulent states and calculated the time mean of the zonal velocities, calculation of the intermittency function and the zonal normal stresses become possible. By definitions, this intermittency function has a value of unity when the flow is in the turbulent state and is zero otherwise. Subsequently, the intermittency factor is defined as the average value of the intermittency function taken over the whole sample length at a particular position in the flow. The intermittency factor was calculated using the following expression:-

$$\gamma = \frac{1}{T} \int_0^T I(t)\ dt \approx \bar{I}(r) \approx \frac{\sum_{i=1}^{N} I(r,t_i)\ \Delta t_i}{T} \qquad 6.7$$

where γ is the intermittency factor and $I(r,t_i)$ is the intermittency function. The zonal averages of the normal stresses of the turbulent and non-turbulent zones are calculated using the following approximations :-

$$\overline{u^2}_{tur} = \frac{1}{T_{tur}} \int_0^{T_{tur}} [U(r,t)_{tur} - \overline{U}_{tur}]dt \approx \frac{\sum_{i=1}^{N_{tur}} [U(r,t_i)_{tur} - \overline{U}_{tur}]\Delta t_{i_{tur}}}{T_{tur}} \qquad 6.8$$

$$\overline{u^2}_{non} = \frac{1}{T_{non}} \int_0^{T_{non}} [U(r,t)_{non} - \overline{U}_{non}]dt \approx \frac{\sum_{i=1}^{N_{non}} [U(r,t_i)_{non} - \overline{U}_{non}]\Delta t_{i_{non}}}{T_{non}} \qquad 6.9$$

6.3 Determination of the Optimum Threshold

At the start of the present investigation, the procedure to determine an optimum threshold level was believed to represent the maximum novelty of Jeung's method. Jeung (1993) established an iterative method of solution to determine the optimum threshold level and hence obtained what was thought to be the unique value of the intermittency factor which corresponded to this. After calculation of the RHS and LHS of equation 6.3 for any assumed threshold, an inequality can be defined as {(LHS - RHS)/LHS}x100%. Jeung's method states that, if this difference is zero within a prescribed limit for the flow variable under consideration, then the corresponding threshold level should be at its most probable value.

Unfortunately, Jeung's method of analysis was found to be questionable towards the end of this study since it had been based on numerical averages, rather than on the full time history as described by the arrival times of the individual bursts in a particular velocity time record.

Figure 6.8 shows an example of the file list which results after processing for one assumed threshold level. This whole procedure is repeated sequentially from

section 6.2.2.1 to 6.2.2.3 as shown in figure 6.9 until the optimum threshold is found. This repetitive series of calculations is performed in the main program by updating the threshold level and restarting the calculation process so that the total range of calculations is completed. By a process of iteration, the inequality error is minimised to obtain a compatible set of turbulent flow parameters. Figure 6.10 shows the basic principles for this method of choosing the optimum threshold level.

6.4 Batch Processing

This processing is one of the features of the operating system, enabling successive operations to be carried out without interaction from the user. All the commands and sub-commands to carry out a certain task can be written in a file called the batch file which is denoted by the extension (****.bat). This batch job approach has been used in nearly every stage of data processing performed in this investigation. This approach has obvious advantages, particularly in the intermittency calculations, where processing of a single point to find the optimum threshold level can take between one to two hours on average.

By way of illustration, figure 6.11 shows an example of one of the batch files used during the course of this work.

Ascii Export from File ▸ C:\AHMED\B40225VC.000 ◂
Current Date : 05/27/95
Current Time : 13:49:33
Devices : BSA1/BSA2
Coincidence window : 1.000000 ms
Coincident Bursts : 48074
Output Data Format: Velocity/Trans Time/Arr Time

	A.T.(ms)	T.T.(ms)	U (m/s)	V (m/s)
1	0.4160	0.0027	26.8747	0.0491
2	0.5147	0.0017	26.7194	0.3437
3	0.8373	0.0023	25.7940	0.4849
4	1.8693	0.0022	23.3736	0.2578
5	2.7920	0.0015	21.3997	-0.1473
6	3.5893	0.0033	20.1054	-0.9329
7	3.7147	0.0027	20.2607	-0.9452
8	4.0107	0.0015	19.9371	-1.2705
9	4.5227	0.0040	19.8530	-1.6879
10	6.2533	0.0027	21.7880	-2.2587
11	9.1307	0.0030	30.3371	4.3025
12	9.7787	0.0017	27.7678	3.9956
13	10.0320	0.0012	28.4797	0.0737
14	10.3493	0.0030	27.7290	0.2762
15	10.3760	0.0022	27.7549	0.0614
16	12.1200	0.0038	24.1307	1.1416
17	12.9413	0.0030	21.9757	0.0000
18	14.6160	0.0035	18.2221	-2.2403
19	15.1093	0.0035	17.5232	-2.1789
20	15.7227	0.0050	18.2545	-2.3016

Figure 6.1. Example of exported ASCII result file using BURstware.

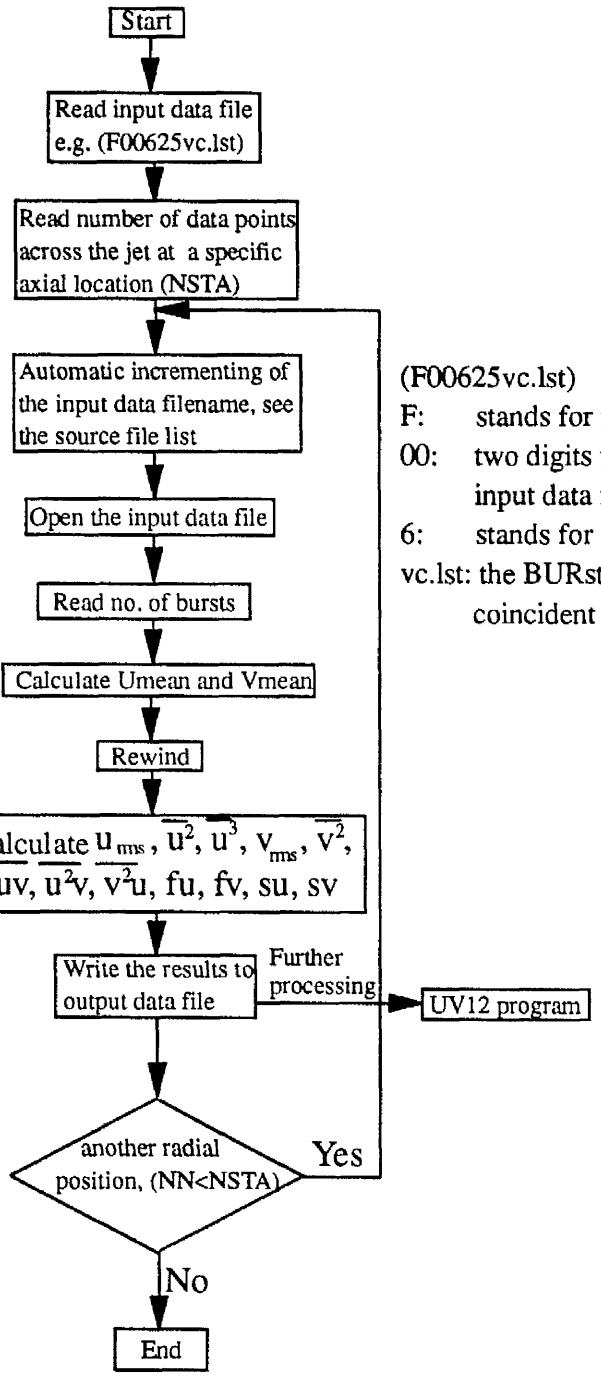

(F00625vc.lst)

F: stands for natural free jet.

00: two digits for automatic increment of the input data file name.

6: stands for x/D=12.

vc.lst: the BURstware assignment for an ASCII coincident velocity data file.

Figure 6.2. Flow chart for the program used to calculate overall mean values, (RD.FOR).

NSTA= 49

No.	U	u_{rms}	u2	u3	u4	V	v_{rms}	v2	v3	v4	uv	u2v	v2u	Fu	Fv	Su	Sv
1	1.6001	1.5126	2.2880	3.4022	18.6838	-0.0299	1.2094	1.4626	-1.9694	10.3369	-0.8172	-1.6054	1.4712	3.5696	4.8312	0.9832	-1.1132
2	1.8402	1.5459	2.3898	2.9306	21.7900	-0.1343	1.2502	1.5630	-1.3792	9.9766	-0.7476	-1.1477	0.9591	3.8154	4.0839	0.7933	-0.7058
3	1.9733	1.3824	1.9110	2.4134	13.6607	0.0365	1.1795	1.3912	-1.8792	10.6226	-0.5857	-1.0072	1.0006	3.7407	5.4890	0.9136	-1.1453
4	2.3113	1.8087	3.2714	2.8345	28.7908	-0.3485	1.3809	1.9069	-2.0582	13.5696	-0.9043	-0.7785	0.9052	2.6904	3.7314	0.4791	-0.7816
5	2.7037	1.5871	2.5189	2.2260	21.1764	-0.1769	1.3205	1.7437	-1.7306	11.1178	-0.8314	-1.0867	0.9042	3.3378	3.6567	0.5568	-0.7516
6	2.8462	1.6652	2.7729	1.7181	25.3536	-0.2829	1.3892	1.9299	-1.7716	14.9626	-0.7475	-0.5511	0.6923	3.2975	4.0172	0.3721	-0.6608
7	3.1032	1.8057	3.2606	3.6337	37.7208	-0.5655	1.5870	2.5186	-2.1322	22.6829	-0.6444	-0.5660	0.9066	3.5481	3.5761	0.6172	-0.5335
8	3.5886	1.9027	3.6203	7.2892	60.9475	-0.1589	1.5215	2.3150	-2.8082	21.3618	-1.0502	-1.6247	1.5527	4.6500	3.9857	1.0582	-0.7972
9	3.5909	2.0783	4.3193	3.6529	53.6862	-0.4030	1.6310	2.6602	-2.7631	25.1068	-1.1519	-0.4987	0.9066	2.8776	3.5480	0.4069	-0.6369

Figure 6.3 Example of RD program result file: all velocity levels in m/s.

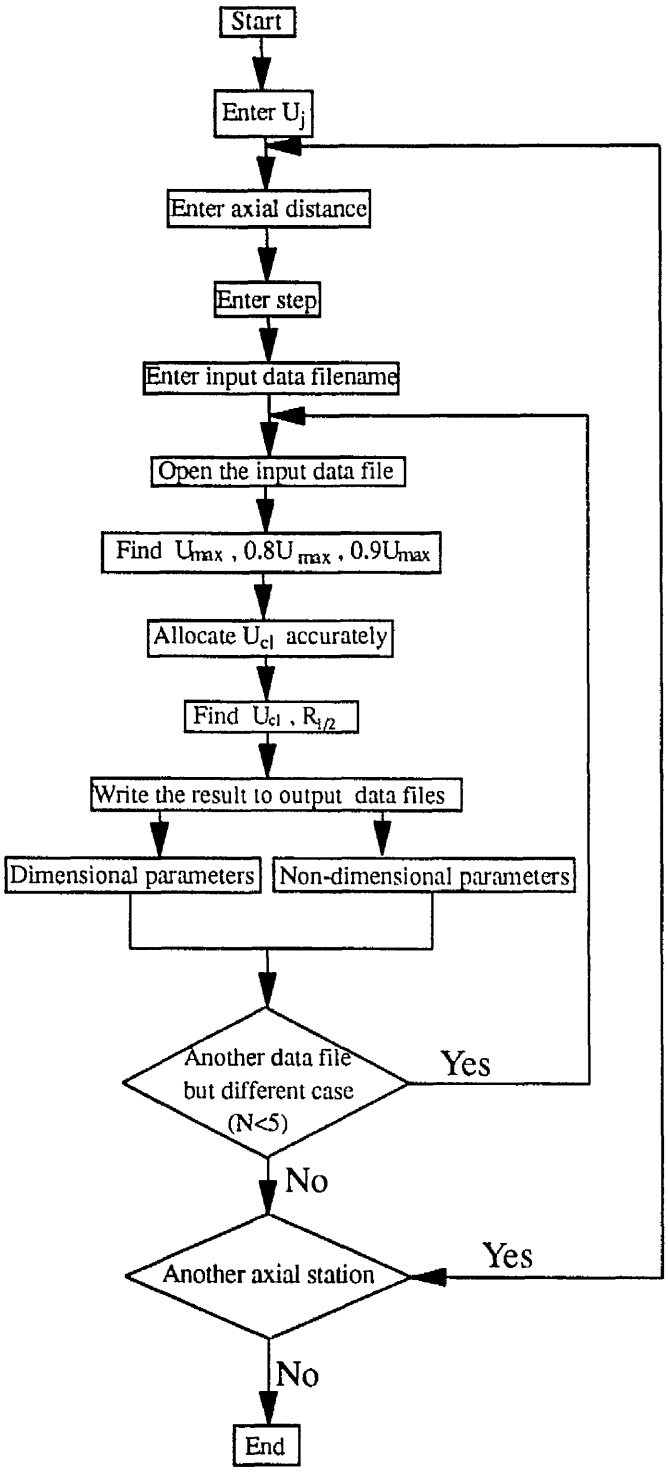

Figure 6.4. Flow chart for the program used to calculate radial distributions, (UV12.FOR).

.1720E+06 25.3000 10.3453 15.0000 12.0000 0.1958
Half-jet width(l.r.aver)= 146.217 147.196 146.706
Half-jet diverg(l.r.aver)= 0.0956 0.0962 0.0959
Half-jet angle(l.r.aver)= 5.4571 5.4934 5.4753

Y	U	u	u2	u3	u4	V	v	v2	v3	v4	uv	u2v	v2u
-302.3491	1.6001	1.5126	2.2880	3.4022	18.6838	-0.0299	1.2094	1.4626	-1.9694	10.3369	-0.8172	-1.6054	1.4712
-290.3491	1.8402	1.5459	2.3898	2.9306	21.7900	-0.1343	1.2502	1.5630	-1.3792	9.9766	-0.7476	-1.1477	0.9591
-278.3491	1.9733	1.3824	1.9110	2.4134	13.6607	0.0365	1.1795	1.3912	-1.8792	10.6226	-0.5857	-1.0072	1.0006
-266.3491	2.3113	1.8087	3.2714	2.8345	28.7908	-0.3485	1.3809	1.9069	-2.0582	13.5696	-0.9043	-0.7785	0.9052
-254.3491	2.7037	1.5871	2.5189	2.2260	21.1764	-0.1769	1.3205	1.7437	-1.7306	11.1178	-0.8314	-1.0867	0.9042
-242.3491	2.8462	1.6652	2.7729	1.7181	25.3536	-0.2829	1.3892	1.9299	-1.7716	14.9626	-0.7475	-0.5511	0.6923
-230.3491	3.1032	1.8057	3.2606	3.6337	37.7208	-0.5655	1.5870	2.5186	-2.1322	22.6829	-0.6444	-0.5660	0.9066
-218.3491	3.5886	1.9027	3.6203	7.2892	60.9475	-0.1589	1.5215	2.3150	-2.8082	21.3618	-1.0502	-1.6247	1.5527
-206.3491	3.5909	2.0783	4.3193	3.6529	53.6862	-0.4030	1.6310	2.6602	-2.7631	25.1068	-1.1519	-0.4987	0.9066

Figure 6.5(a). Example of dimensional parameters given in result file of UV12 program: all velocity levels in m/s.

49
0.1720E+06 25.3000 10.3453 15.0000 12.0000
Half-jet width(l.r.aver)= 146.217 147.196 146.706
Half-jet diverg(l.r.aver)= 0.0956 0.0962 0.0959
Half-jet angle(l.r.aver)= 5.4571 5.4934 5.4753

Y/Y05	U/UCL	u/UCL	u2/UCL2	u3/UCL2	u4/UCL3	V/UCL	v/UCL	v2/UCL2	v3/UCL3	v4/UCL4	uv/UCL2	u2v/UCL3	v2u/UCL3	FU	FV	SU	SV
-2.0609	0.1547	0.1462	0.0214	0.0031	0.0016	-0.0029	0.1169	0.0137	-0.0018	0.0009	-0.0076	-0.0014	0.0013	3.5696	4.8312	0.9832	-1.1132
-1.9791	0.1778	0.1494	0.0223	0.0026	0.0019	-0.0130	0.1208	0.0146	-0.0012	0.0009	-0.0070	-0.0010	0.0009	3.8154	4.0839	0.7933	-0.7058
-1.8973	0.1907	0.1336	0.0179	0.0022	0.0012	0.0035	0.1140	0.0130	-0.0017	0.0009	-0.0055	-0.0009	0.0009	3.7407	5.4890	0.9136	-1.1453
-1.8155	0.2234	0.1748	0.0306	0.0026	0.0025	-0.0337	0.1335	0.0178	-0.0019	0.0012	-0.0084	-0.0007	0.0008	2.6904	3.7314	0.4791	-0.7816
-1.7337	0.2613	0.1534	0.0235	0.0020	0.0018	-0.0171	0.1276	0.0163	-0.0016	0.0010	-0.0078	-0.0010	0.0008	3.3378	3.6567	0.5568	-0.7516
-1.6519	0.2751	0.1610	0.0259	0.0016	0.0022	-0.0273	0.1343	0.0180	-0.0016	0.0013	-0.0070	-0.0005	0.0006	3.2975	4.0172	0.3721	-0.6608
-1.5701	0.3000	0.1745	0.0305	0.0033	0.0033	-0.0547	0.1534	0.0235	-0.0019	0.0020	-0.0060	-0.0005	0.0008	3.5481	3.5761	0.6172	-0.5335
-1.4883	0.3469	0.1839	0.0338	0.0066	0.0053	-0.0154	0.1471	0.0216	-0.0025	0.0019	-0.0098	-0.0015	0.0014	4.6500	3.9857	1.0582	-0.7972

Figure 6.5(b). Example of non-dimensional parameters given in result file of UV12 program.

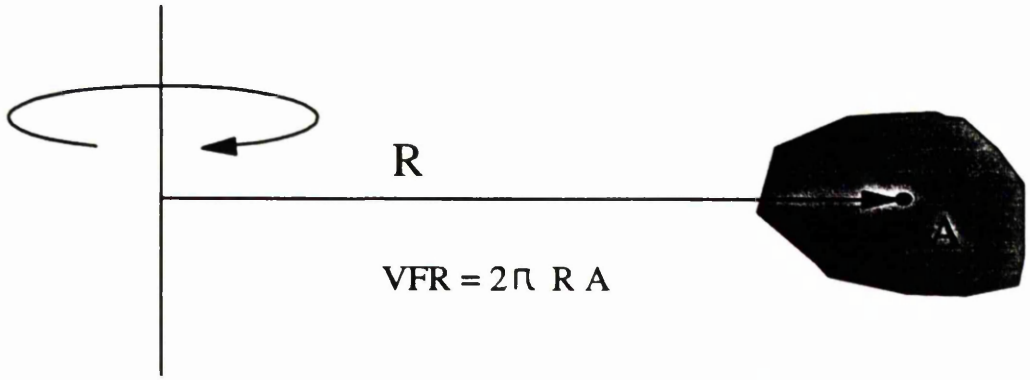

Figure 6.6. Axisymmetric flow conditions. Basic mathematical approach used to calculate the effective volume represented by area A, when rotating around the vertical axis (the theorem of Pappus).

$$Q_o = \Pi * \left(\frac{D}{2}\right)^2 * U_j$$

Entrainment rate = $(Q_x - Q_o / Q_x)$

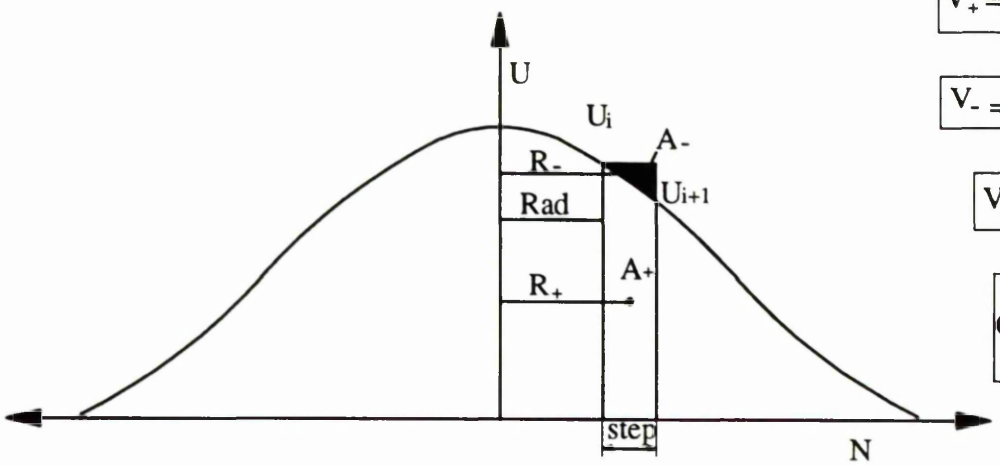

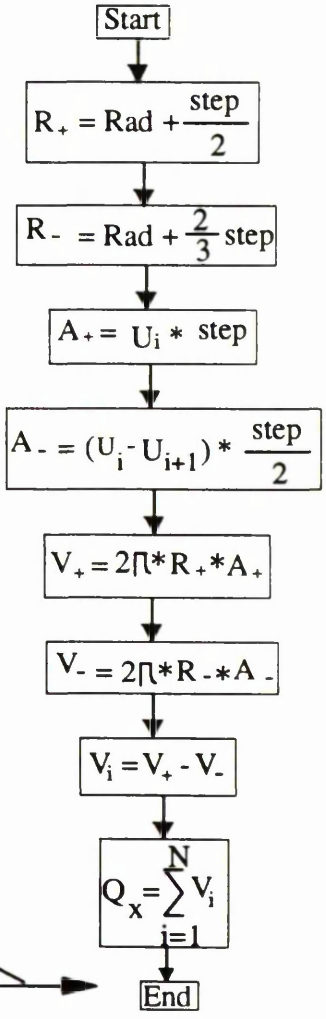

Figure 6.7. Calculations of the volumetric flow of the fluid from time mean velocity distribution.

TH	ITF	FUD	SUD	uvD	u2D	UZOT	VZOT	u2ZOT	SHZOT	UZOL	VZOL	u2ZOL	SHZOL	NF
1.34441	0.255681	-5.649638	1.739043	15.078955	9.831928	1.860723	-0.460698	4.046293	-2.412362	1.639943	-0.177291	0.942360	-0.193901	7252
0.94108	0.388506	-3.057012	-0.639887	6.607742	4.447978	1.767095	-0.358410	3.479456	-1.971474	1.668310	-0.200720	0.797493	-0.116297	8594
0.65876	0.515125	-0.226339	-0.076087	0.433124	0.301858	1.734367	-0.312819	3.083405	-1.670082	1.683533	-0.217885	0.682481	-0.066171	9406
0.46113	0.624838	1.928900	0.767142	-3.440499	-2.468757	1.720116	-0.294505	2.797645	-1.462423	1.694223	-0.225227	0.598459	-0.035522	9766
0.47910	0.613750	1.659652	0.662648	-2.980015	-2.131678	1.720822	-0.295618	2.821739	-1.479872	1.693696	-0.224961	0.606505	-0.038071	9724
0.49706	0.602849	1.491243	0.564456	-2.689018	-1.918505	1.721817	-0.296511	2.849774	-1.499692	1.692869	-0.225214	0.614420	-0.040993	9696
0.51503	0.592253	1.314372	0.502849	-2.377816	-1.697007	1.722609	-0.298096	2.879418	-1.518843	1.692370	-0.224485	0.618995	-0.044245	9674
0.53300	0.581970	1.168617	0.443467	-2.132400	-1.516329	1.724394	-0.299239	2.907120	-1.539249	1.690618	-0.224451	0.627708	-0.046844	9702
0.55096	0.571579	0.929176	0.351404	-1.705881	-1.209442	1.724695	-0.300787	2.932801	-1.558025	1.690826	-0.223785	0.634944	-0.049070	9686
0.56893	0.561753	0.705433	0.261536	-1.300846	-0.920741	1.726930	-0.303082	2.957815	-1.575584	1.688607	-0.222202	0.641717	-0.052110	9624
0.58689	0.552061	0.497811	0.176374	-0.925994	-0.653316	1.729074	-0.305084	2.981995	-1.593728	1.686650	-0.221113	0.650536	-0.055211	9568
0.60486	0.542551	0.319507	0.113454	-0.598893	-0.421349	1.729986	-0.307991	3.009019	-1.613578	1.686281	-0.219092	0.657193	-0.057244	9510
0.62283	0.533248	0.197382	0.069777	-0.373714	-0.261857	1.730786	-0.309332	3.037037	-1.635122	1.686117	-0.219086	0.665483	-0.059329	9468
0.64079	0.524209	-0.008567	-0.002995	0.016315	0.011398	1.731287	-0.310911	3.060311	-1.652814	1.686206	-0.218640	0.673837	-0.062425	9438
0.65876	0.515125	-0.226339	-0.076087	0.433124	0.301858	1.734367	-0.312819	3.083405	-1.670082	1.683533	-0.217885	0.682481	-0.066171	9406

**** END OF CONVERGING AREA ****

**** TOTAL ELAPSED TIME IS 3084.62SEC

Figure 6.8. Example of result file for intermittency calculations: all velocity levels in m/s.

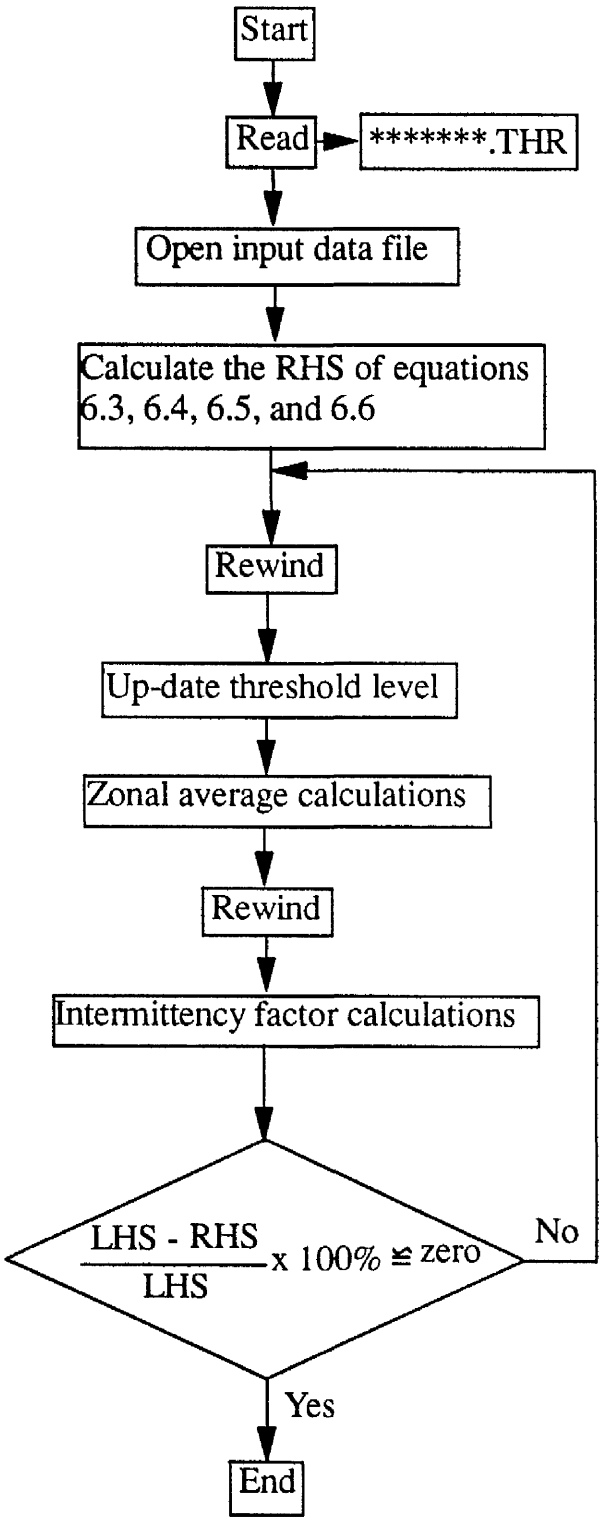

Figure 6.9. Flow chart for the intermittency calculations program.

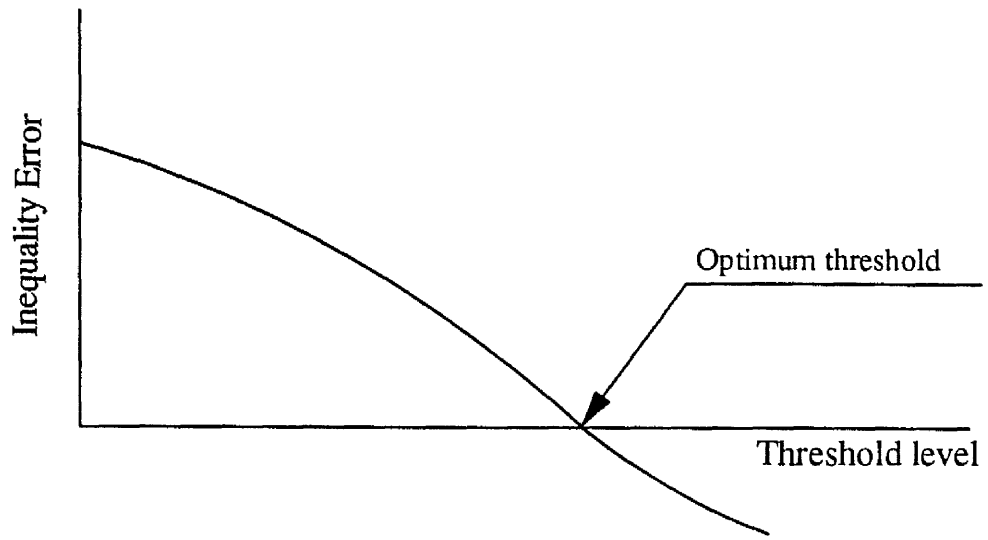

Figure 6.10. Determination of optimum threshold level.

```
C:\COPY E:\XD12\F01625VC.LST C:\AHMED\*.*
C:\AHMED\THROLD4
C:\AHMED\RENAME F01625VC.THR TWO.TWO
C:\AHMED\RLSA
```

Figure 6.11. Example of batch processing file list.

CHAPTER 7

RESULTS AND DISCUSSION

CHAPTER SEVEN
RESULTS AND DISCUSSION

7.1 Bias and Symmetry Checking

As mentioned in Chapter Six, checks on the axial symmetry of the horizontal air jet were carried out prior to commencement of the experimental programme. Apart from comparing the time mean velocity variations across different diameters of the nominally circular jet, the sensitivity of the LDA data to the position of injection of the LDA seeding material (the "smoke") was tested. Firstly, the smoke was injected from one end of the containment box, referred to as position 1 in figures 7.1 to 7.4. Then the smoke was injected from the other end of the box, referred to as position 2. This change in the seeding arrangements apparently produced no significant change in the data, thereby indicating that no bias had occurred because of the distribution of the seeding particles in the flow.

The above figures show the time mean axial velocity component (U) non-dimensionalised with regard to the centre-line mean velocity (U_{cl}). The symbol R represents the radial position and is normalised by $R_{1/2}$, the radial position at which the velocity component has fallen to $U = 0.5U_{cl}$. These figures present the measurements at selected axial locations and serve to confirm the uniformity of the seeding of the jet as well as the surrounding medium. Also, only the two lower Reynolds numbers were considered since it took longer for the uniform steady state to be reached under these conditions than with the higher Reynolds number condition ($1.7x10^5$).

Further checks on the symmetry of the jet flow were also made. Following the procedures established with the hot film measurements (section 4.6), the data were collected across the jet diameter at different azimuthal angles, the z axis being taken as the reference position for which $\theta = 0$, see figure 4.4. Figures 7.5 and 7.6 present the time mean axial velocity distributions measured for angles in the range $\theta = 0°$ to $\theta = 135°$. As before, the data were collected across the full extent of the diameter of the jet and covered all the angles in the same fashion as described in section 4.6. The figures also include data derived from experiments to investigate the influence of concentration of the seeding for $Re = 1.7x10^5$ to ensure that the planned experimental programme could be assumed to be completely free from the velocity bias effects which can occur when the seeding is unevenly distributed through the flow field (Mierisch (1994)).

7.2 Optimum Conditions for the Secondary Jet

Another experimental parameter which needed to be decided upon was the volumetric flow rate of the secondary jet. Two positions on the jet centre-line at the downstream stations $x/D = 2.0$ and $x/D = 4.0$ were chosen to investigate this factor. In particular, the downstream station corresponding to $x/D = 2.0$ was selected and used to determine the optimum conditions for the secondary jet. This plane lies approximately mid-way along the potential core and experience shows that the effect of the excitation in this position is generally less ambiguous when compared with other positions in the potential core i.e. at $x/D = 4.0$. This feature will be seen clearly in the data presented in a later stage of this chapter.

Based on the study by Szajner and Turner (1987), the volumetric flow rate

in the secondary jet was arbitrarily fixed at a constant value of 2% of the prime jet flow rate ($Q_s = 0.02Q_o$). The excited jet was then tested for different Strouhal numbers as shown in figure 7.7. In this figure, the vertical axis represents the ratio of the root mean square value of the axial velocity fluctuation under excitation conditions $(u_{rms})_e$ to that of the natural jet $(u_{rms})_n$. The horizontal axis represents the Strouhal number (St_D), based on the jet velocity at the exit plane (x/D = 0.0) U_j and the nozzle diameter (D).

It can be seen from figure 7.7 that the data for the lowest Reynolds number ($Re = 1.5x10^4$) exhibits only a small response to the excitation whereas that for the other two Reynolds numbers ($Re = 7.0x10^4$) and ($Re = 1.7x10^5$) show a much greater response. Figure 7.7 also reveals that the two highest velocities show the same trend in response to the excitation and that each curve develops two distinctive peaks. The first peak occurs for a Strouhal number of approximately $St_D = 0.33$ and the second one corresponds to a value of approximately $St_D = 0.64$.

The optimum Strouhal number for each case represented in figure 7.7 were then tested against different volumetric flow rates of the secondary jet leading to the results presented in figure 7.8. It is clear that a flow rate for the secondary jet of up to 5% of the primary jet has the major influence on the jet behaviour. This is in good agreement with the findings of Szajner and Turner (1987). On the basis of these results, and noting that the experimental apparatus behaved more reliably at lower rates of flow in the secondary jet, a value of 2% was chosen for the whole of the present experimental programme.

In order to further justify the use of the axial position defined by x/D = 2.0

to fix the optimum conditions for the secondary jet flow, a limited number of measurements at x/D = 4.0 were also carried out. Figures 7.9 and 7.10 show the degree of disturbance caused by the excitation in comparison with the natural jet (i.e. without excitation) at the centre-line of the jet in the plane x/D = 4.0. It can be seen that the influence of the excitation at this station is less obvious than that at x/D = 2.0 and that the fluctuation level $(u_{rms})_e/(u_{rms})_n$ is only half that at x/D = 2.0 over the range of Strouhal number and secondary jet flow rate considered in the experiments.

Having carried out all the above checks, the experimental programme for the present investigation could be started. This chapter presents the results for the various time mean and fluctuating flow parameters which have been measured using the two-dimensional LDA system.

7.3 Time Mean Velocity Distributions

It is traditional in jet flow measurement to put the axial variations of the radial distributions of the axial velocity component at the top of the results agenda. This policy has been followed in the present thesis. Thus, figures 7.11, 7.12 and 7.13 show the time mean distributions of the axial velocity component for the natural jet at different axial locations and reveal that there is a distinct flattening of the jet profile as it travels downstream. It was convenient to show this effect by normalising the velocity at each measuring point across the jet for the different axial stations with regard to the axial velocity component U_j at the exit plane of the nozzle (x/D = 0.0). The radial positions were also normalised with regard to the nozzle radius.

Figure 7.14 and 7.15 present the data for the natural jet in an alternative form. In this case, the values for the time mean axial velocity component have been non-dimensionalised with respect to the velocity level at the centre-line at the appropriate axial station. In addition, the radius has now been scaled with respect to the value for $R_{1/2}$ in the particular axial position x/D. The collapse of the velocity distributions onto a single curve for x/D > 5.0 confirms that the natural jet has attained the expected similarity condition - see also section 2.2.1.8.

Figures 7.16, 7.17 and 7.18 confirm that the excitation has very little effect on the distributions of the time mean axial velocity component at the lowest Reynolds number ($Re = 1.5x10^4$) in comparison to that for the two highest Reynolds numbers - see figures 7.19 to 7.23. In order to show the influence of the excitation more clearly, the mean axial velocity component measured for the four excited cases (St_D = 0.2, 0.4, 0.6, 0.8) was normalised with regard to the centre-line velocity of the natural jet in the corresponding axial position at that particular Reynolds number. It can be assumed from the distributions of the time mean axial velocity presented in figures 7.16, 7.17 and 7.18, that the jet is not very susceptible to the excitation at $Re = 1.5x10^4$, particularly for the flow within the potential core.

Figure 7.19 shows that there is a central region of flow with a constant axial velocity level (i.e. a "top-hat" profile) at x/D = 1.0 for $Re = 1.7x10^5$ in the case of the natural jet. This "top-hat" region is significantly narrower for the cases of excited jet. Thus, a difference arises between the natural jet profile, which is presented in the form of a solid line, and the profiles for the four excited jet conditions within the region from $R/R_{1/2} = 0.625$ to $R/R_{1/2} = 0.85$. This shows that the free shear layer springing from the lip of the nozzle interacts with the pulsed

secondary jet and that this generates strong coherent structures so that the shear layer becomes much wider for the case of the excited jet. These generated coherent structures evidently have a major effect on the behaviour of the excited jet as it travels further downstream. This influence can be seen clearly in figures 7.20 to 7.23.

A theoretical prediction for the development of a natural free jet has been made by Tollmien, based on Prandtl's mixing length hypothesis. This solution is given in tabular form by Abramovich (1963). Goertler obtained an alternative solution, based on Prandtl's eddy-viscosity model, which is tabulated in Rajaratnam (1976). These solutions are compared with the experimental data in figure 7.23. Goertler's solution appears to be slightly superior to Tollmien's solution around the axis of the jet. However, in the outer region of the jet, the Tollmien curve agrees with the present experimental data better than the Goertler curve. This trend has also been observed while analysing the results of other investigators, e.g. Wygnanski and Fiedler (1969) results - see section 2.2.1.1.

Figures 7.24 and 7.25 present the radial distributions of the time mean radial velocity component V. Here, V was normalised with regard to the velocity level of the axial component at the centre-line. Figure 7.24 shows the distribution of V across the jet for different axial position for Re = 1.7×10^5. Figure 7.25 presents the radial distribution of V at x/D = 15.0 for different pulsation frequencies.

7.4 Decay of the Centre-Line Velocity

The potential core region is identified as the region in which the axial velocity component (at the centre-line of the jet) remains constant. Examination of

the measured data shows that the length of this potential core region is approximately 3.5 diameters for the lowest Reynolds numbers ($1.5x10^4$) and 4.5 diameters for the two highest Reynolds numbers - see figure 7.26. In addition, the centre-line value of the axial velocity component decays faster for the case of the lowest Reynolds number in comparison with the other two Reynolds numbers. This is illustrated in figure 7.26 where the curve which represents the decay of the centre-line velocity for the case of $Re = 1.5x10^4$ is seen to be lower than the curves which represent the data for the other two Reynolds numbers ($7.0x10^4$ and $1.7x10^5$).

Results from the investigations performed on a natural jet by Capp (1983), Panchapakesan and Lumley (1993), and Wygnanski and Fiedler (1969) have also been presented along with the data obtained in the present investigation in figure 7.26. It is seen that the LDA data by Capp (1983) and the moving hot wire data presented by Panchapakesan and Lumley (1993) agree with the present data better than that of Wygnanski and Fiedler (1969). This discrepancy is thought to be due to experimental errors in the results given by Wygnanski and Fiedler (1969), consistent with turbulent fluctuation and longitudinal cooling errors which can contaminate the results signals from the hot wire anemometer system at the turbulence intensities encountered in the flow of a free jet.

Figure 7.27 shows the decay of the centre-line velocity of the axial component for the case of the lowest Reynolds number ($1.5x10^4$) for the natural jet as well as for the four jet flows with excitation. There are no obvious differences between the results for the excited jet flows and the natural jet, nor between the four excited jet flow conditions. In fact, all the data represented by the curves collapse fairly well upon each other. Surprisingly, it must be concluded that the jet in this

low Reynolds number condition is insensitive to the aerodynamics excitation provided by the annular jet flow.

In contrast, at the higher velocity level Re = $7.0x10^4$, all the excitation conditions produced a similar variation of the centre-line velocity and there is a clear difference between these variations and the natural jet case. Most importantly, the length of the potential core region shrinks to 3 nozzle diameters, in the case of $St_D = 0.8$ and only 2.5 diameters for $St_D = 0.2$, 0.4, and 0.6, - see figure 7.28.

The effect of the excitation on the behaviour of the jet at a Reynolds number of $1.7x10^5$ can be seen easily in the mean velocity profiles measured for x/D = 1.0, - see figure 7.19. Figure 7.29 compares these effects for both the natural and excited cases. The results generally show that the decay of the excited jet is much faster than for the natural jet and, in the case of $St_D = 0.6$, the decay starts as early as x/D = 2.0. In examining these results, comparison has also been made with the results presented by other investigators for alternative techniques of excitation (see section 2.4.1). This comparison shows that the centre-line velocity levels measured by Crow and Champagne (1971) agree fairly well with the author's data. However, the results of Raman and Cornelius (1994) diverge beyond approximately x/D = 2.0, before returning to the author's curves at approximately x/D = 8.0. Thus, it is obvious that the excitation method used by Raman and Cornelius (1994) had a much stronger effect on the development of the jet than either that used by Crow and Champagne (1971) or the author in the region from x/D = 2.0 to x/D = 8.0.

7.5 Rate of Spread of the Jet

The rate of development of a free jet is often expressed in terms of the

variation of the half-width of the jet with axial distance from the nozzle exit. This half-width defined as the radial position $R_{1/2}$ at which the velocity falls to half the value of the centre-line velocity at each downstream station (i.e. $U = 0.5U_{cl}$). This is a more useful definition than any radial measure based upon locating the edge of the jet and provides a convenient measure of the lateral extent of the jet in any axial position. Figure 7.30 illustrates the variation of the half-width of the natural jet with axial distance. It can be seen that this variation is approximately the same for all Reynolds numbers up to x/D = 4.0. The departure of the natural jet flow data at the lowest Reynolds number ($Re = 1.5x10^4$) from the other two sets of data is obvious and is consistent with the decay of the velocity at the centre-line as shown in figure 7.26.

The solid lines in figure 7.30 represent the best linear fit to the experimental data, obtained by the least squares method when presented in terms of the parameter $R_{1/2}/D$ versus the axial position (x/D). The slopes of these lines ($dR_{1/2}/dx$) are 0.11 for the case of $Re = 1.5x10^4$ and 0.084 for the other two Reynolds number cases ($Re = 7.0x10^4$ and $Re = 1.7x10^5$). The discrepancies between the above values and those reported in Chapter Two (section 2.2.1.6) can possibly be attributed to the axial positions in which the present experiments are carried out. Most of the data reported in section 2.2.1.6 were taken far downstream from the jet nozzle in the self-preserving region (for which $x/D > 15.0$), rather than in the "near field" studied in the present investigation ($x/D \leq 15$). However, better agreement was found with the LDA data from Capp (1983), who investigated the free air jet at $Re = 9.2x10^4$ for x/D in the range 0.0 to 125.0. Figure 7.30 also includes data from the measurements of Wygnanski and Fiedler (1969), who used hot wire anemometry at a Reynolds

number of Re = $1.0x10^5$ - for x/D in the range 0.0 to 97.0. The data due to Wygnanski and Fiedler (1969) are seen to be lower than those from the present investigation, possibly due to inherent differences in accuracy between the HWA and LDA techniques especially in the region where the turbulence intensity levels are high.

Similar methods of analysis can be applied to study the development of the excited jet. As could be expected from the radial distributions of the axial time mean velocity, figures (7.16 to 7.18) and its decay along the centre-line of the jet (figure 7.27), there is no dramatic change in the spreading rate of the excited jet with in the case of Re = $1.5x10^4$, see figure 7.31. However, the excited jet does spread more rapidly for the other two Reynolds numbers, as is shown in figures 7.32 and 7.33. It can also be observed from the data presented in figures 7.32 and 7.33 that excitation at Strouhal numbers close to $St_D = 0.2$ and $St_D = 0.6$ have the greatest influence on the behaviour of the jet.

7.6 Entrainment Rate

An estimate of the entrainment rate has been obtained by numerical integration of the distributions of the time mean axial velocity component (U) across the jet width. This procedure has been explained in section 6.2.1.3 and figures 6.6 and 6.7. Here, it was necessary to make an arbitrary choice of the radial limits of the integration. After due consideration, the integration was limited to the radius at which the velocity level had fallen to a value of $U/U_{cl} = 0.2$. This choice serves two purposes. Firstly, it provides a well-defined basis on which to study the effect of the different excitation frequencies and compare these with the natural case. Secondly,

it enables the effect of the velocity data at the edge of the jet, where the velocity levels are at their lowest and the experimental errors are greatest, to be minimised.

Figure 7.34 presents data for the entrainment rate of the natural jet. It can be seen that the natural jet attains a greater entrainment rate at the lowest Reynolds number ($Re = 1.5x10^4$) in comparison to the other two Reynolds numbers of $Re = 7.0x10^4$ and $1.7x10^5$. This can be attributed to the viscous effects becoming dominant at low velocities and causing coalescence of the large coherent structure, which in turn engulf a larger amount of the surrounding fluid. This effect is reduced at the higher velocities, resulting in fuller velocity profiles at the exit plane of the jet ($x/D = 0.0$). The figure also shows that, in the cases corresponding to Reynolds numbers $Re = 7.0x10^4$ and $Re = 1.7x10^5$, the results are very close to each other. This agrees well with the measurements of Ricou and Spalding (1961) and Hill (1972) who concluded that the effect of Reynolds number is negligible on entrainment rate for Reynolds numbers Re in excess of $4.0x10^4$. The solid lines represent the best least squares linear fit to the measurements, and can be presented in the form of the equations:-

$$\frac{Q_x - Q_o}{Q_o} = 0.290\frac{x}{D} \quad for \quad Re = 1.5\times10^4 \qquad 7.1$$

$$\frac{Q_x - Q_o}{Q_o} = 0.252\frac{x}{D} \quad for \quad Re = 7.0\times10^4 \qquad 7.2$$

$$\frac{Q_x - Q_o}{Q_o} = 0.227\frac{x}{D} \quad for \quad Re = 1.7\times10^5 \qquad 7.3$$

The entrainment rate was also calculated for the natural jet at $Re = 1.7x10^5$.

These calculations were carried out following the analysis by Hinze (1976) of the time mean velocity distribution in the cross-section of a free jet in the region of partial self-preservation where only the time mean axial velocity component exhibits similarity. This analysis showed that the entrainment rate can be described by an expression of the form:-

$$\frac{Q_x - Q_o}{Q_o} = 8\ G^2\ K\ C \qquad 7.4$$

where G, K and C are constants related to the linear growth of the natural jet. Constant G represents the non-dimensional rate of spread of the jet and this can be obtained from figure 7.30 for the case of Re = 1.7×10^5. A value of 0.084 was obtained. Constant K represents the decay rate of the centre-line velocity with axial position and can be calculated from figure 7.26. A value of 5.88 was obtained from the data. Finally, constant C can be calculated from equation 7.5.

$$C = \int_0^{\infty} e^{-c_o \left(\frac{R}{R_{1/2}}\right)^2} \frac{R}{R_{1/2}}\ d\left(\frac{R}{R_{1/2}}\right) \qquad 7.5$$

Before calculating C, constant c_o was evaluated by fitting the experimental data of the radial distribution of the time-mean axial velocity component presented in figure 7.23 into an exponential form - see section 2.2.1.1 and equation 2.1. The value of $c_o = 0.681$ was obtained - then integration of equation 7.5 yielded the value of 0.734 for C. The substitution of constants G, K and C in equation 7.4 yields a value of entrainment rate (Q_x - Q_o/Q_o) = 0.236. This value of the entrainment rate and the calculated value from equation 7.3 fall within the range reported by Baskaya et al

(1995) who used the analysis by Hinze (1976) to estimate the entrainment rate for a jet of saturated/superheated steam jet issuing into air.

Figure 7.35 shows that, in the case of the Reynolds number Re = $1.5x10^4$, the largest entrainment rate occurred at an excitation frequency defined by $St_D = 0.6$. Beyond x/D = 7.0, the average increase of about 21% in the entrainment rate. This is consistent with the findings of Szajner and Turner (1987). However, it is also seen that excitation at $St_D = 0.2$ produces a stronger effect in the case of Re = $7.0x10^4$ and $1.7x10^5$, and that the average increase in entrainment, beyond x/D = 7.0, is then approximately 50%. Refer to figures 7.36 and 7.37 for further details.

Figures 7.38, 7.39 and 7.40 present data relating to the variation of the entrainment rate with Strouhal number for all the axial locations (x/D = 1.0 to x/D = 15.0) explored in the present investigation. Examining the largest axial positions (i.e. x/D = 9.0, 12.0 and 15.0), the influence of excitation is seen to be greatest on the entrainment rate in comparison with the early stage of the jet development up to x/D = 7.0. In the case of the lowest Reynolds number (Re = $1.5x10^4$), the biggest effect occurs at $St_D = 0.6$ whereas, for the other two Reynolds numbers, the biggest effect occurs at $St_D = 0.2$.

7.7 Influence of Excitation on Turbulence Intensity

The turbulent velocity fluctuations were calculated from the time series data provided by the LDA system. The instantaneous fluctuation levels u', v' relative to the time average values U_{cl} could then be reduced to the standard measures of the turbulent structure.

Figures 7.41 to 7.43 show the variation of the root mean square velocity fluctuation u_{rms} across the jet for different downstream stations. Low values of this turbulence level are found in the centre region of the jet, close to the exit plane of the nozzle, since here the flow is essentially potential and is not significantly effected by the mixing shear layers. Similarly, figures 7.44 and 7.45 present non-dimensional values for the root mean square values u_{rms} and v_{rms} , using different combinations of the Reynolds and excitation Strouhal numbers. The particular conditions applying in each case are included on the figures themselves. For all excitation conditions, it may be observed that the root mean square turbulence levels u_{rms} and v_{rms} are considerably higher than for the case of the natural jet. Figure 7.45 is included to stress the almost isotropic nature of the turbulence in the excited jet and to cover the full Reynolds number range over which data were collected.

The axial variations of the turbulence intensity levels at the jet centre-line are plotted in figure 7.46. These profiles are seen to increase monotonically for all Reynolds numbers considered in the present investigation. It can be observed that the maximum intensity value of approximately 0.26 which is reached at x/D = 15.0 is lower than that reported by Capp (1983), Rodi (1972), and Wygnanski and Fiedler (1969) in the self preserving region - see also section 2.2.1.8 of this thesis. However, the monotonic increase in the turbulence intensity within the range of the experiments (x/D • 15.0) indicates that an asymptotic value close to that reported in section 2.2.1.8 could well be reached further downstream in the self-preserving region.

Once again, the excitation does not appear to produce any strong effect at $Re = 1.5x10^4$ as is shown from the axial profiles of the turbulence intensity in figure 7.47. The turbulence intensity for the natural jet, as well as the four excitation cases

at this Reynolds number is seen to increase steadily with axial distance and the results are in close agreement for the different downstream stations. This lack of change could perhaps have been anticipated from the behaviour of the other parameters such as the mean velocity profiles and the decay of the centre-line velocity. However, there are distinct peaks in the axial profiles of the turbulence intensity along the jet centre-line for Reynolds numbers Re = $7.0x10^4$ and $1.7x10^5$. At Re = $7.0x10^4$ - see figure 7.48, the first peak occurs at x/D = 2.0 for a Strouhal number $St_D = 0.6$, and the values increase gradually up to x/D = 12.0. In contrast, the first peak occurs at the same excitation condition $St_D = 0.6$ for Re = $1.7x10^5$, but this time at approximately x/D = 2.8, - see figure 7.49.

The changes in the turbulence intensity distributions of the radial component v_{rms} are less violent than for the axial component u_{rms} and the higher effects are seen to occur at $St_D = 0.6$ for both Re = $7.0x10^4$ and $1.7x10^5$ - see figures 7.50 and 7.51.

No attempt was made to measure the circumferential component w' of the turbulent fluctuations for the following combination of reasons. Firstly, to have done so would have required another channel of LDA equipment which was not readily available to the author. Secondly, there were severe financial and time constraints on the project. Thirdly, the available literature suggest that w_{rms} and v_{rms} are within 5% of each other for most positions within a free jet. See, for example, Smith and Hughes (1977) and Abid (1994).

7.8 Influence of Excitation on Turbulent Shear Stress Levels

Figures 7.52 to 7.55 present the radial distributions of the shear stress normalised with regard to the centre-line velocity of the jet in the corresponding

axial position at that particular experimental condition.

As expected, the lowest Reynolds number ($Re = 1.5x10^4$) shows no great response to excitation. This can be seen in figure 7.52 where there is no substantial difference between the data of the shear stress of the free natural jet and the free excited jet even in the region of higher shear (i.e. mixing region) around $R/R_{12} = 1.0$, at $x/D = 3.0$. In contrast, the difference is quite clear for Reynolds number $Re = 7.0x10^4$ particularly at $x/D = 5.0$ - see figures 7.53 and 7.54, and the highest peak of the shear stress is seen to occur at an excitation frequency specified by $St_D = 0.6$ - refer to table 5.2.

It has been shown through the presentation of the results that the conditions of $Re = 7.0x10^4$ and $Re = 1.7x10^5$ respond similarly to excitation. Figure 7.55 presents the profiles of the shear stress in the plane defined by $x/D = 15.0$ and the highest peak occurs at $St_D = 0.6$. The figure also presents the shear stress profiles measured by Capp (1983) and Rodi (1975) in the self-preserving region along with the present results. The solid curve represents the least squares fit to the natural jet data of the present investigation. The LDA measurements of the shear stress in a free air jet given by Capp (1983) agreed well with the present measurements of the natural jet near the axis and near the outer edge of the jet but were in general higher in the middle. In contrast, the shear stress profile given by Rodi (1975) using HWA agreed well near the axis but was higher in the middle and lower near the outer edge of the jet.

7.9 Flatness and Skewness Factors

The flatness factor $F_u = (\overline{u^4}/(\overline{u^2})^2)$ is a factor which can be used to indicate the

degree of intermittency in a turbulent flow. Near the edge of a free turbulent jet, the motion at a point alternates between slow fluctuation of low intensity and rapid fluctuation of high intensity. This effect of inhomogeneity of turbulent intensity makes the flatness factor of a velocity component exceed its Gaussian value of three. Large flatness factor usually indicates that the distribution of intensity of the quantity is spotty, Townsend (1976).

The distributions of the flatness factor are illustrated in figures 7.56 to 7.58. At an early stage of the jet development (x/D = 3.0), positive peaks occur for the flatness factor ($\overline{u^4}/(\overline{u^2})^2$) profiles at different radial positions corresponding to different excitation frequencies - see figure 7.56. In the case of the natural free jet, the peak in the flatness factor appeared earlier at approximately $R/R_{12} = 0.5$ and attained the highest value of 4.5. In attempting to explain these results physically, it can be assumed that positive spikes in the time series signal correspond to the fast moving rotational zones created by the large eddies which are convected past the measuring volume. Such positive velocity spikes appear to attain lower magnitudes and to occur at a greater radius for all cases of jet excitation when compared to the natural jet. This trend indicates that the nature of the jet is changed by the enforced pulsation of the potential core. Beyond the potential core at x/D = 7.0 for example, the time series signals of the axial velocity become more regular in all the excited cases and the flatness factor assumes a constant value close to 3 from the jet centre to approximately the edge of the jet ($R/R_{12} = 1.75$). This value equals that for a Gaussian distribution of the turbulence fluctuation and is the type of signal which is commonly found to occur at the centre-line of a natural jet - Townsend (1976). Outside the range of $0.0 < R/R_{12} > 1.75$, the flatness factor increases sharply - see

figures 7.57 and 7.58.

The coefficient of skewness $S_u = (\overline{u^3}/(\overline{u^2})^{2/3})$ is commonly used to check the symmetry of the probability distribution function of a particular component of the velocity fluctuations. In the region dominated by the jet, the results show that the skewness is indeed zero at the centre-line, as would be expected for any axisymmetric flow, and increases monotonically towards the edge of the jet. Figure 7.59 presents profiles of the skewness factor for x/D = 3.0 at a Reynolds number Re = 1.7×10^5. Note here that the relatively large scatter in the values of the skewness around the nominally zero value at the centre-line is due to the very large random negative or positive peaks which have been recorded in the velocity time series signal for the excited jet. These large values have a dominating influence on the derived turbulence quantities such as the Skewness Factor and the scatter is noticeable up to x/D = 7.0 for the natural jet and for the excited jet at $St_D = 0.8$ - see figure 7.60. There is excellent agreement between the distributions at the centre-line of the jet at x/D = 15.0, as is shown in figure 7.61.

7.10 Intermittency Results

7.10.1 General Comment

As discussed in Chapter Six, the intermittency of a flow is a characteristic of any real fluid flow and is a measure of the phenomenon in which the flow switches from "turbulent" to "non-turbulent" in a random manner. In fact, the intermittency is a measure of the time fraction of the time during which the flow can be said to be turbulent. This definition depends critically upon the method used to determine the state of the flow - the turbulence detector - and many methods have been described

in the literature.

The aim of this part of the project was to utilise a new method of intermittency measurement, initiated by Jeung (1993). Jeung (1993) calculated the overall average of the global and zonal properties on a numerical basis i.e. the summation of the sample of a flow property divided by the total number of those samples in the time record. Unfortunately, it has now become apparent that these calculations may only be assumed to be valid if the samples of the instantaneous velocity components are separated by equal time intervals, as is the case with the data collected using thermal anemometers (e.g. hot wire or hot film).

Since the LDA system provides data with arrival times which vary in a random fashion, the numerical averages can be expected to differ from the time average of a flow variable, particularly in the determination of the more complicated statistics such as the intermittency, even when the LDA data rate is high. In spite of the considerable time which has been devoted to this problem by the present author, there is still a degree of ambiguity in the approach and more work is needed before the final verdict can be reached. To this end, only the instantaneous time series velocity data obtained from the LDA system at x/D = 12.0, for the natural jet at Re = 1.7×10^5, has been reprocessed. The method used will now be explained.

7.10.2 Distribution of the Inequality Error

The "inequality error" at any stage in the iterative series of calculations used to determine the intermittency is defined as the difference between the Right Hand Side (RHS) and the Left Hand Side (LHS) of equation 6.3. Again, due to time limitation, only one flow variable, that is the normal stress (u'^2), has been considered in the present work - see section 6.2.2.1. As previously stated in section 6.3, the

iterative approach introduced by Jeung (1993) was also followed by the present author to find the optimum threshold level. Here, however, the calculations have been based on the time mean averages of the global and the zonal properties, rather than on numerical averages as used by Jeung.

This optimum threshold level is found by minimising the error between the RHS and LHS of the equation which defines the normal stress - see equation 6.3.

Figures 7.62 and 7.63 illustrate how the inequality error for the normal stress term converged toward zero, for the chosen conditions ($x/D = 12.0$, $Re = 1.7x10^5$) and the natural jet. Note that in these figures, the vertical axis represents the inequality error which has been scaled to match the maximum value for each individual time record of the particular radial position under consideration. These scales have been purposely chosen to allow detailed consideration of the appropriate threshold level and intermittency factor corresponding to the first minimum value of the inequality error. The curves of the inequality error also tend to zero in both cases when the intermittency factor approaches zero or one values.

One of the practical problems which arising with this method is that the iterative procedure converges slowly, making it extremely difficult to determine the most appropriate threshold level and hence the intermittency factor.

7.10.3 Distribution of the Threshold Level and Intermittency Factor for Convergence

The radial distributions of the converged threshold level are plotted in figure 7.64. Here, the vertical axis represents the optimum threshold level, using the instantaneous shear stress level (u'v'(t)) as a detector function. As mentioned in the

previous section, the difficulty of choosing the optimum threshold level necessitated an arbitrary choice, made by choosing the optimum threshold level of each record at a point where the inequality error has just reduced by one digit. For example, the optimum threshold and the corresponding intermittency factor were chosen for the radial position $R/R_{1/2} = 0.07$ - see figure 7.62 where the inequality error ((LHS - RHS)/LHS)x100% drops from the value of 0.0103 to 0.0096. Note that the other axis of figure 7.64 represents the radial position across the jet, and that the jet is assumed to be axisymmetric.

Figure 7.65 shows the radial distribution of the intermittency factor at x/D = 12.0. It will be clear from this figure that the difference in the value of the intermittency factor between the point near the centre-line of the jet (i.e. $R/R_{1/2} = 0.07$) and the point near the edge of the jet (i.e. $R/R_{1/2} = 1.9$) was not as great as expected. In addition, difficulties were experienced in assigning the most appropriate threshold level. Because of these problems the present author is not completely satisfied with this approach and feels that more work will be needed before any final conclusion can be reached on the validity of the method proposed by Jeung (1993).

7.10 Time Series Velocity Data and the Energy Spectrum

An attempt has been made to show the effect of the periodic pulsations of the secondary annular jet on the time records of the instantaneous velocity fluctuations of the axial velocity component. Figure 7.66 illustrates the time series of this instantaneous velocity component for x/D = 3.0, normalised by its mean value at the jet centre-line. Here, the abscissa represents the time normalised by the periodic

time of the secondary pulsation, in this case corresponding to a Strouhal number $St_D = 0.2$ (f = 100 Hz). In the figure, the circles represent the experimental data, which are seen to follow the sine wave reasonably well. This indicates that the periodic pulsation does indeed influence the primary jet all the way across the radius to its centre. Furthermore, the energy spectrum of the velocity fluctuation shown in figure 7.67 confirms that the dominant frequency of the time series is 100 Hz.

The effect of the pulsation becomes less pronounced in moving towards the edge of the jet (say at $R/R_{1/2} = 0.7$). In these outer regions of the jet, background disturbances from the mixing region also become involved. For this reason, the data in figure 7.68 do not follow the sine wave so well as is the case at the centre-line. It is also apparent that the dominant frequency has now shifted to 114 Hz, as shown by the energy spectrum - see figure 7.69.

7.11 General Remarks

In this chapter, results for the development of an axisymmetric air jet with and without aerodynamic excitation have been presented. Detailed measurements of the time mean and turbulent fluctuation velocity components obtained using a two component LDA system are given up to x/D = 15.0. The jet flow parameters related to the linear growth of the jet i.e. the spreading and entrainment rates of the jet have also been presented for the three Reynolds numbers of $Re = 1.5x10^4$, $7.0x10^4$ and $1.7x10^5$ based on the nozzle outlet diameter.

Results for the axisymmetric natural jet have been compared with the data obtained for the four excited jet flow conditions. It is found that the aerodynamic excitation exerts a greater influence on the jet configuration at the two higher

Reynolds numbers in comparison with the lower Reynolds number ($Re = 1.5x10^4$) where virtually no changes in jet development are observed. In particular, it was found that excitation at a Strouhal number $St_D = 0.2$ produced the biggest change in the spreading and entrainment rates of the jet. In contrast, the axial variations of the turbulence intensity at the centre-line and the radial distributions of the shear stress at successive axial stations reveal that the greatest effects occurred under an excitation condition of $St_D = 0.6$. It can therefore be concluded that excitation at a frequency defined by either of these Strouhal numbers ($St_D = 0.2$ and 0.6) had a major effect on the behaviour of the jet and that the change produced at the other Strouhal numbers i.e. $St_D = 0.4$ and $St_D = 0.8$ were relatively less significant.

Some of the results of this investigation have been compared with published experimental data. This comparison shows that the results of the present investigation are in good agreement with those of other investigators for both the natural and the excited jet flow conditions. It has been convenient when presenting the experimental results in this chapter to normalise the data for the excited jet to those of the natural jet, so that the effect of the excitation can be more clearly seen.

The second part of the data reduction has focused upon reporting on an application of the iterative method initiated by Jeung (1993) for intermittency calculations. As a result of this reconsideration of the method, it is now considered that the intermittency analysis carried out by Jeung (1993) may no longer be valid. The principle reason for this belief is that Jeung used numerical approximations to the global and zonal properties (i.e. ensemble averages) rather than basing these averages on the particle arrival times. In the present study, only one set of data has been processed using this corrected iterative approach and intermittency calculations

have been made for the natural jet only. Although some preliminary data are presented, these are not entirely as expected and it is perhaps too early to report on the efficiency of the scheme. More work is needed to reach any firm conclusion.

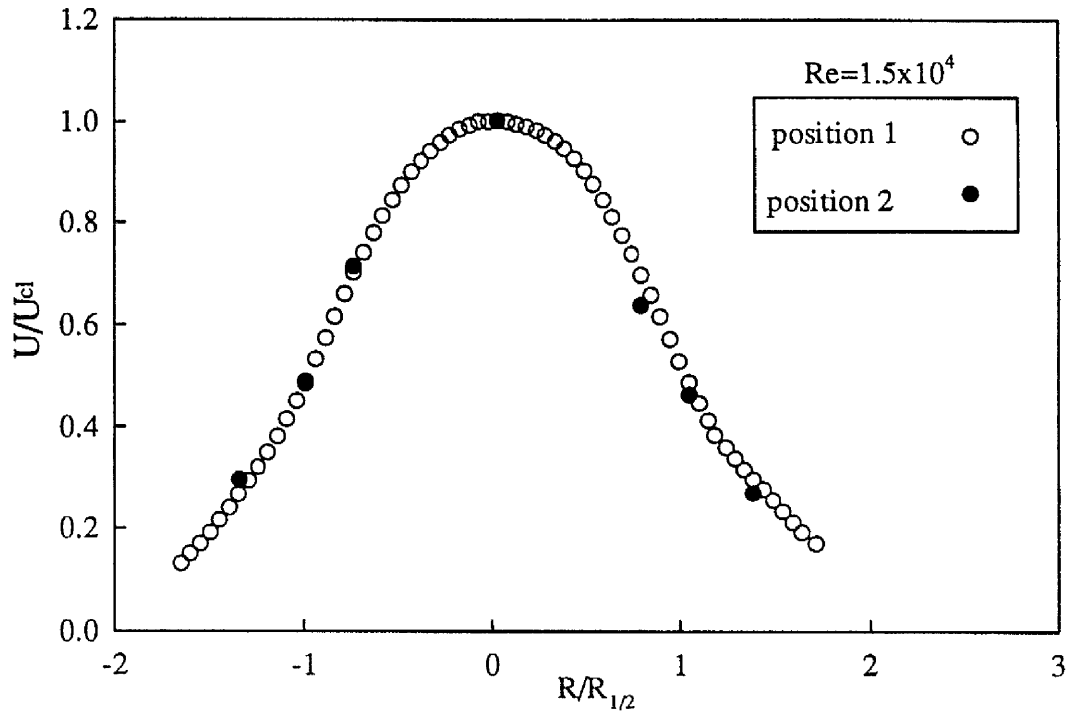

Figure 7.1. Mean velocity profiles at x/D=3.0, for different positions of the smoke generator. Used to test for the existence of seeding density bias on the velocity data.

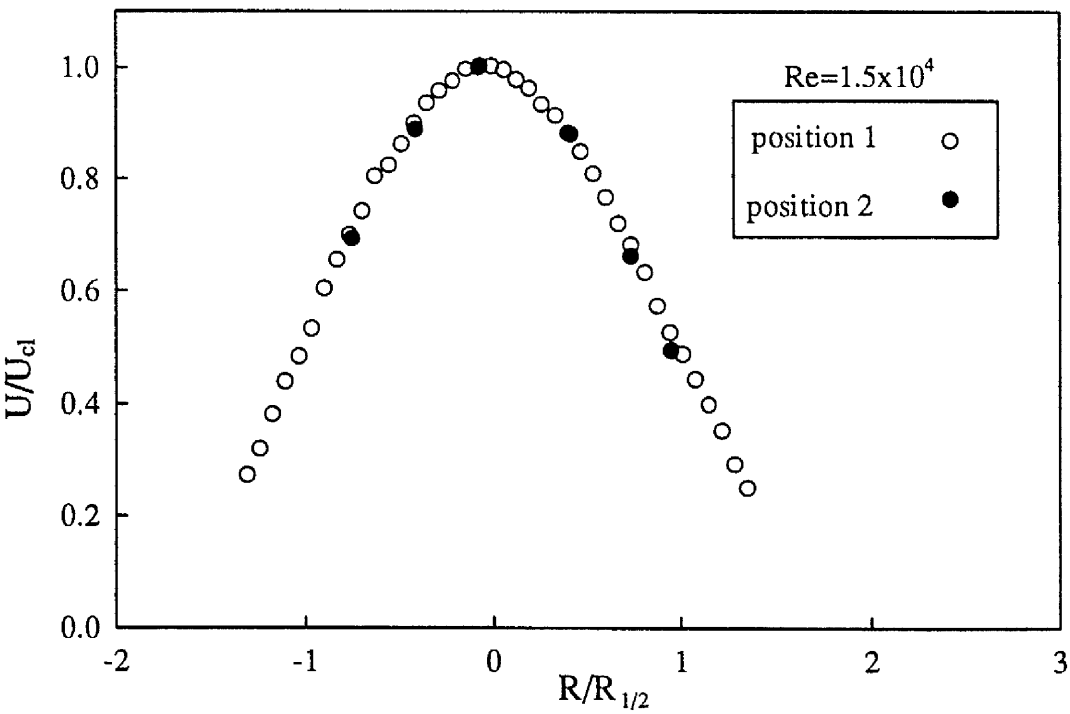

Figure 7.2. Mean velocity profiles at x/D=12.0, for different positions of the smoke generator. Used to test for the existence of seeding density bias on the velocity data.

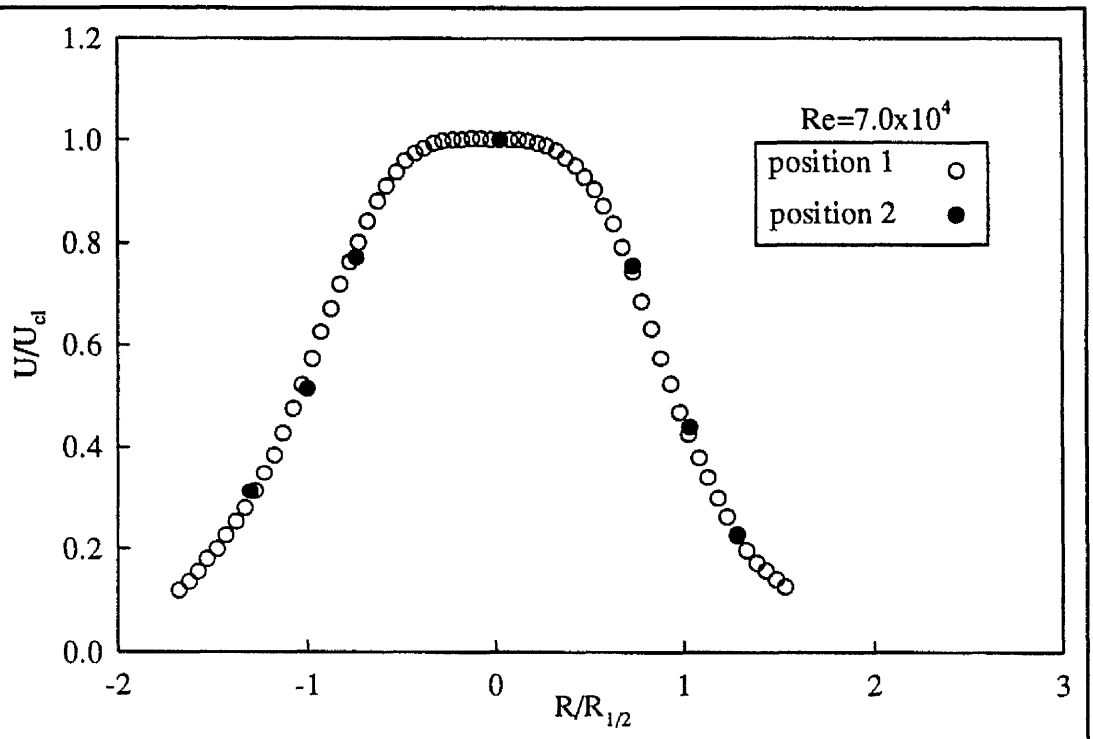

Figure 7.3. Mean velocity profiles at x/D=3.0, for different positions of the smoke generator. Used to test for the existence of seeding density bias on the velocity data.

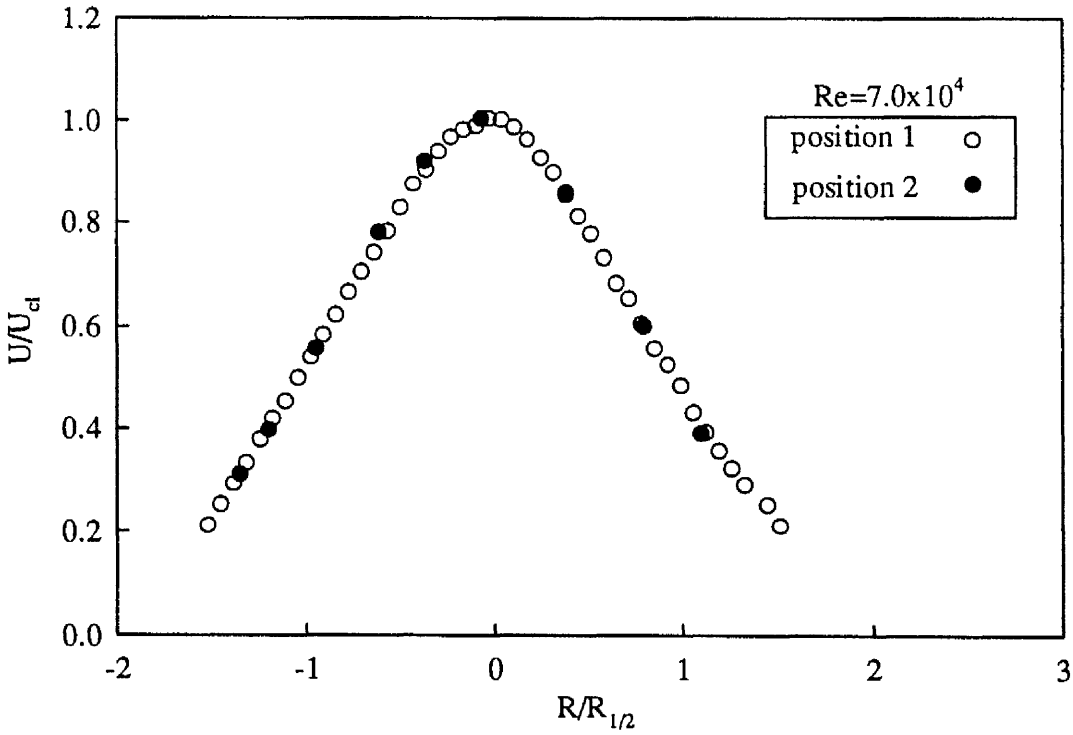

Figure 7.4. Mean velocity profiles at x/D=7.0, for different positions of the smoke generator. Used to test for the existence of seeding density bias on the velocity data.

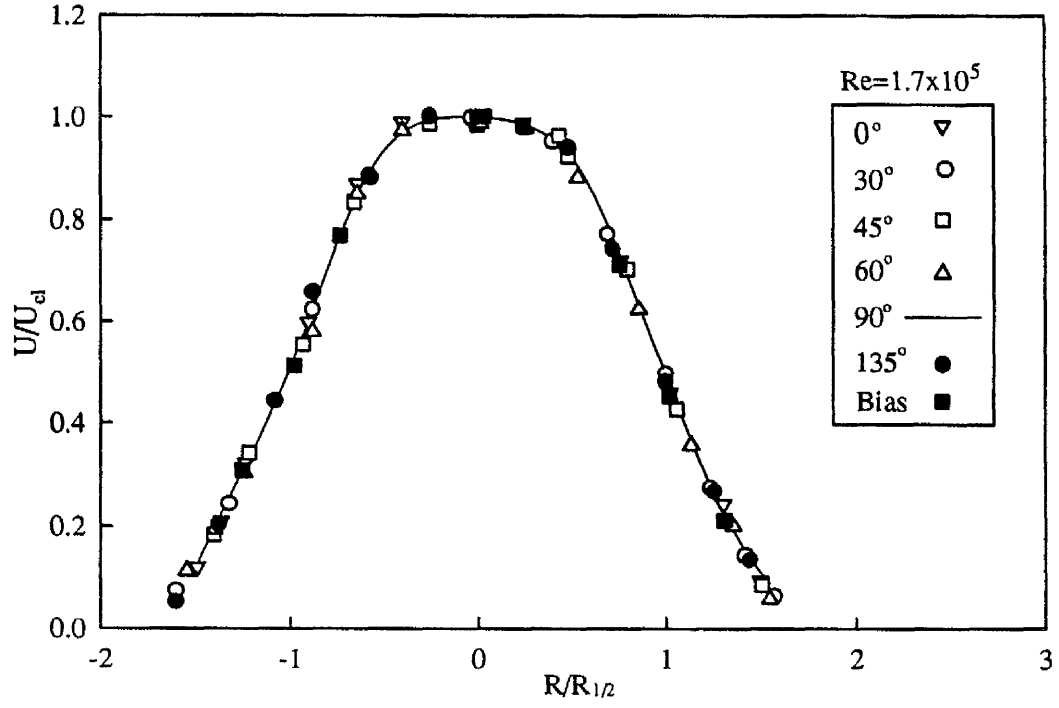

Figure 7.5. Mean velocity profiles at x/D=3.0, for different azimuthal angles to check the symmetry of the jet and to test for the existence of seeding density bias on the velocity data.

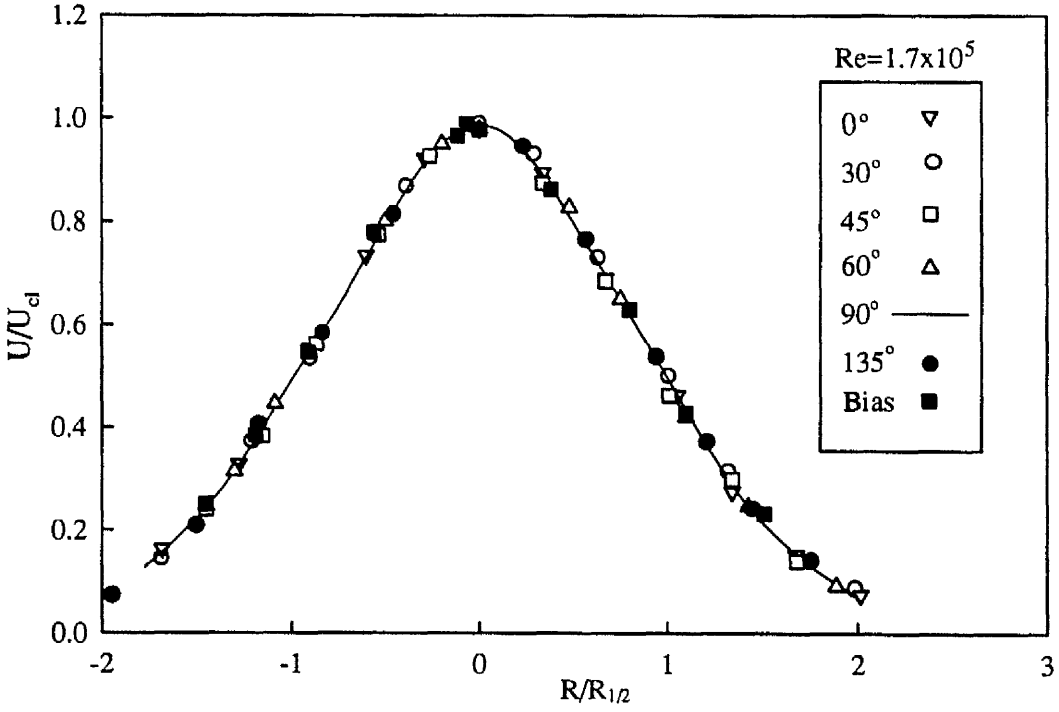

Figure 7.6. Mean velocity profiles at x/D=7.0, for different azimuthal angles to check the symmetry of the jet and to test for the existence of seeding density bias on the velocity data.

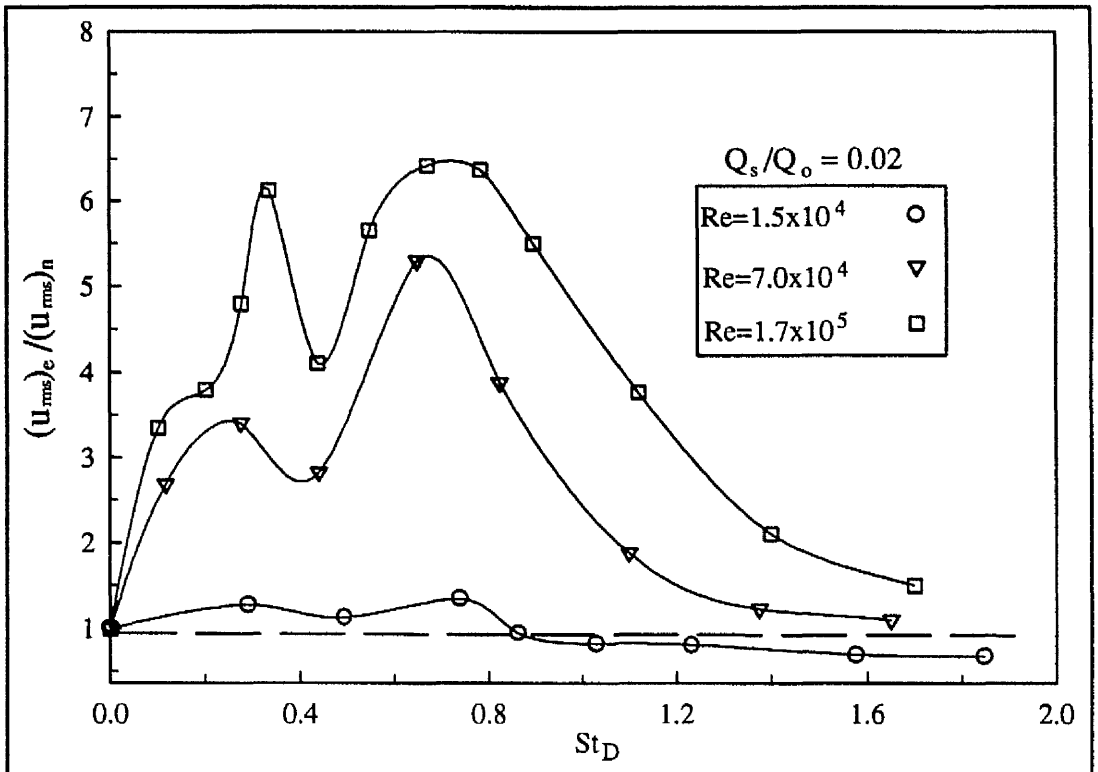

Figure 7.7. Fluctuating conditions on centre-line of excited jet at x/D=2.0.

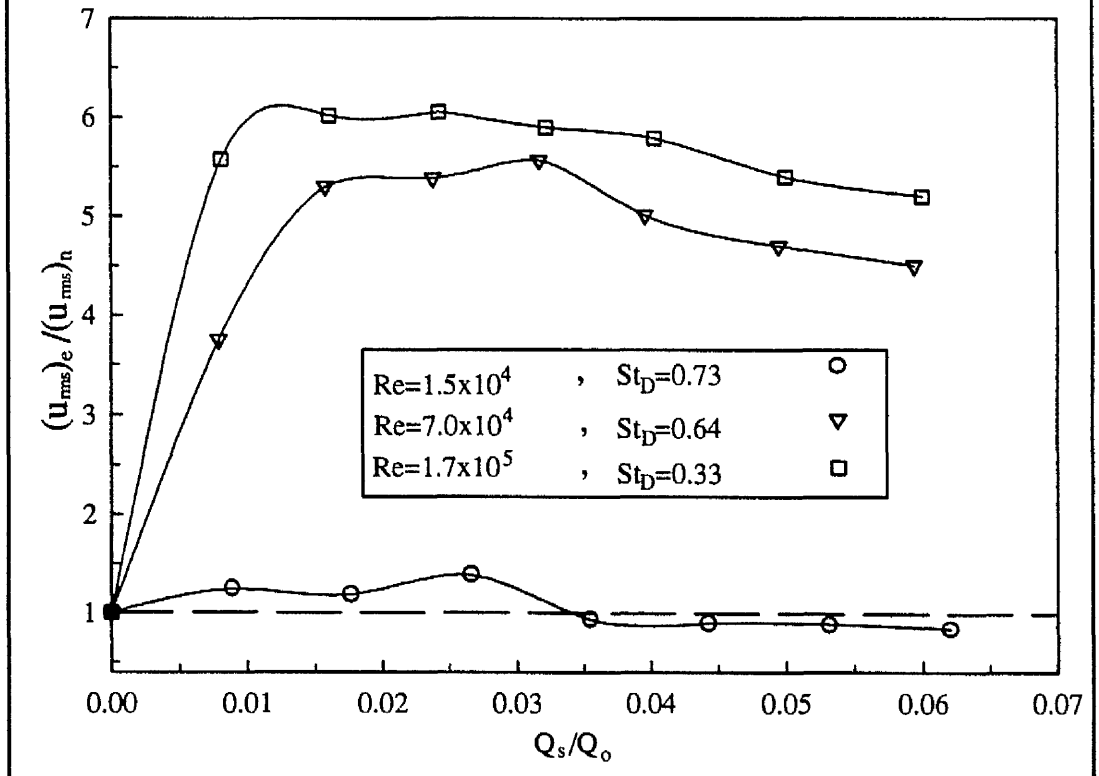

Figure 7.8. Fluctuating conditions on centre-line of excited jet at x/D=2.0.

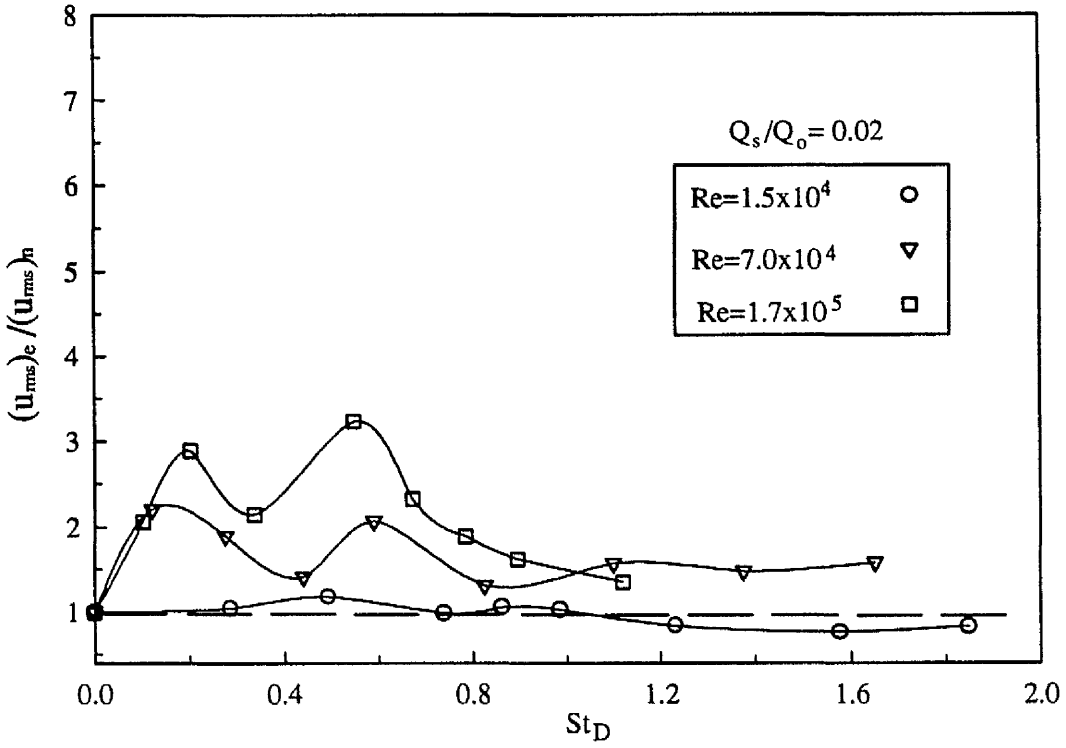

Figure 7.9. Fluctuating conditions on centre-line of excited jet at x/D=4.0.

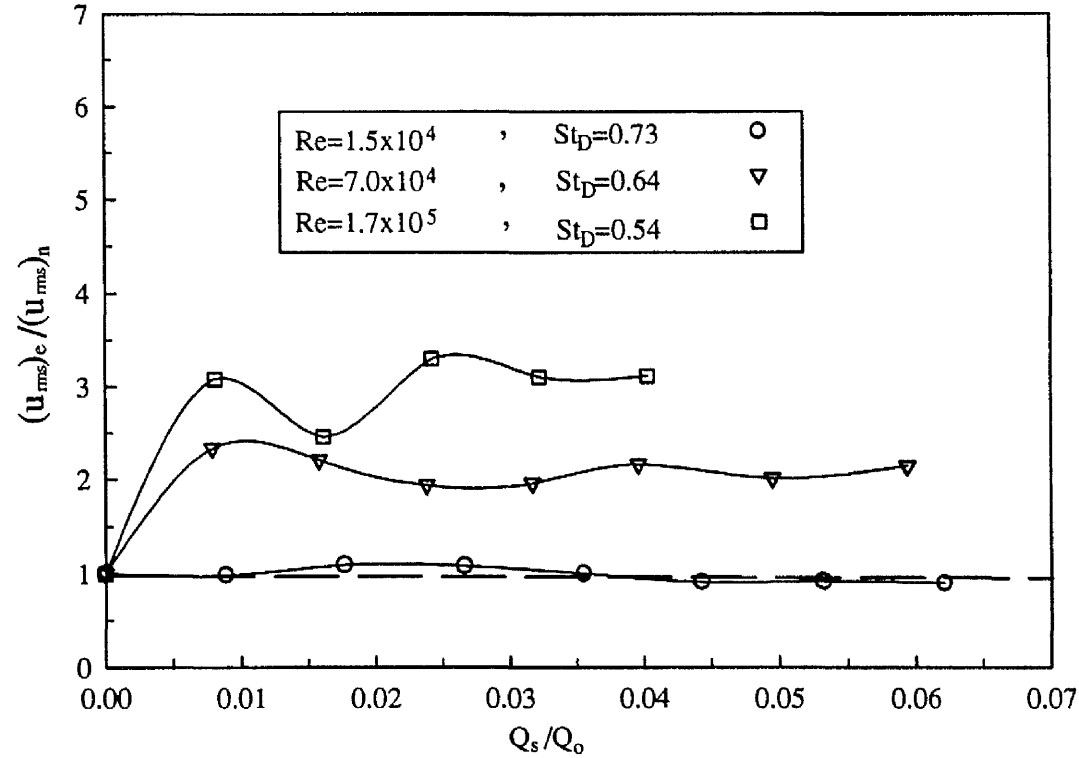

Figure 7.10. Fluctuating conditions on centre-line of excited jet at x/D=4.0.

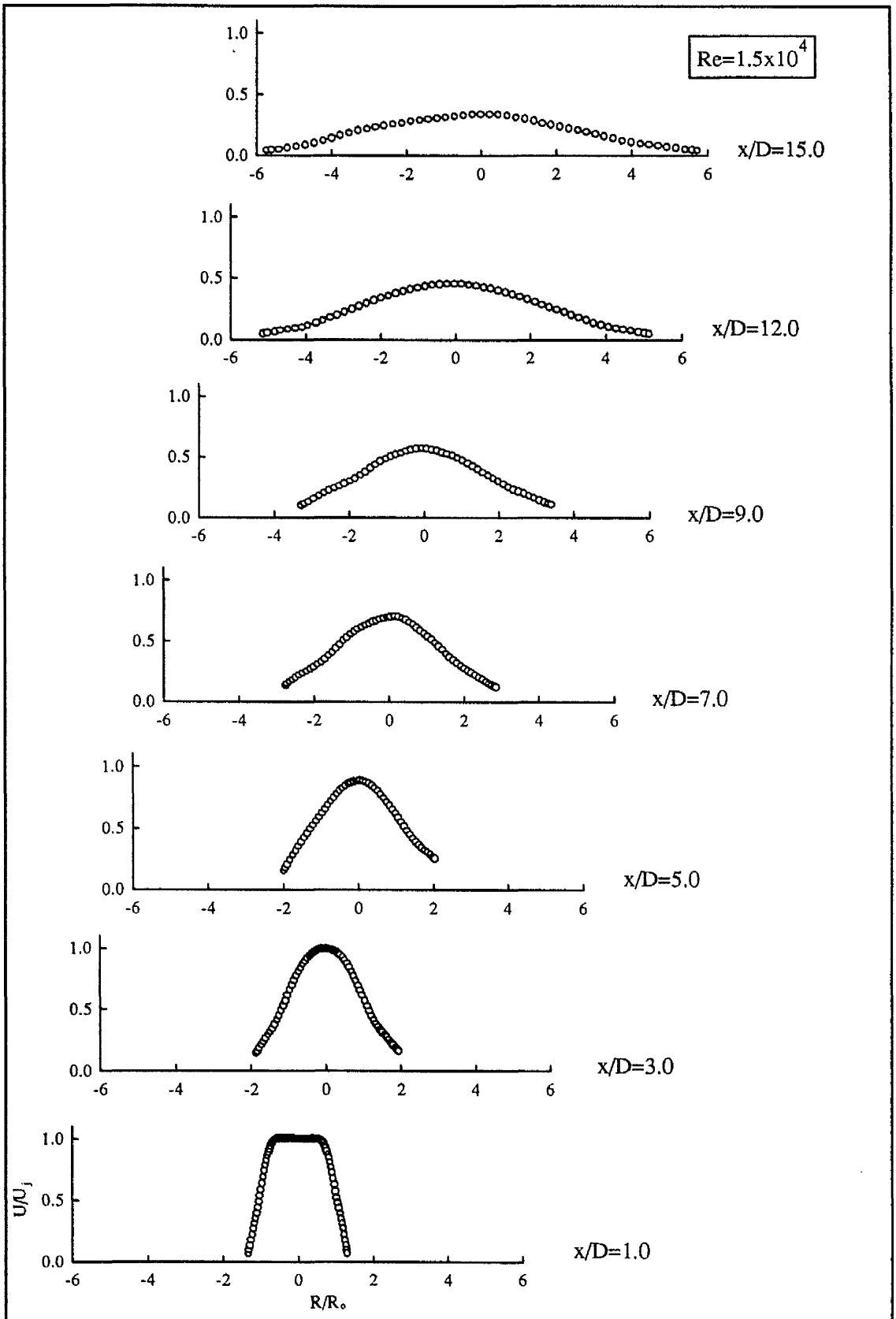

Figure 7.11. Mean velocity profiles for the natural jet at different downstream stations.

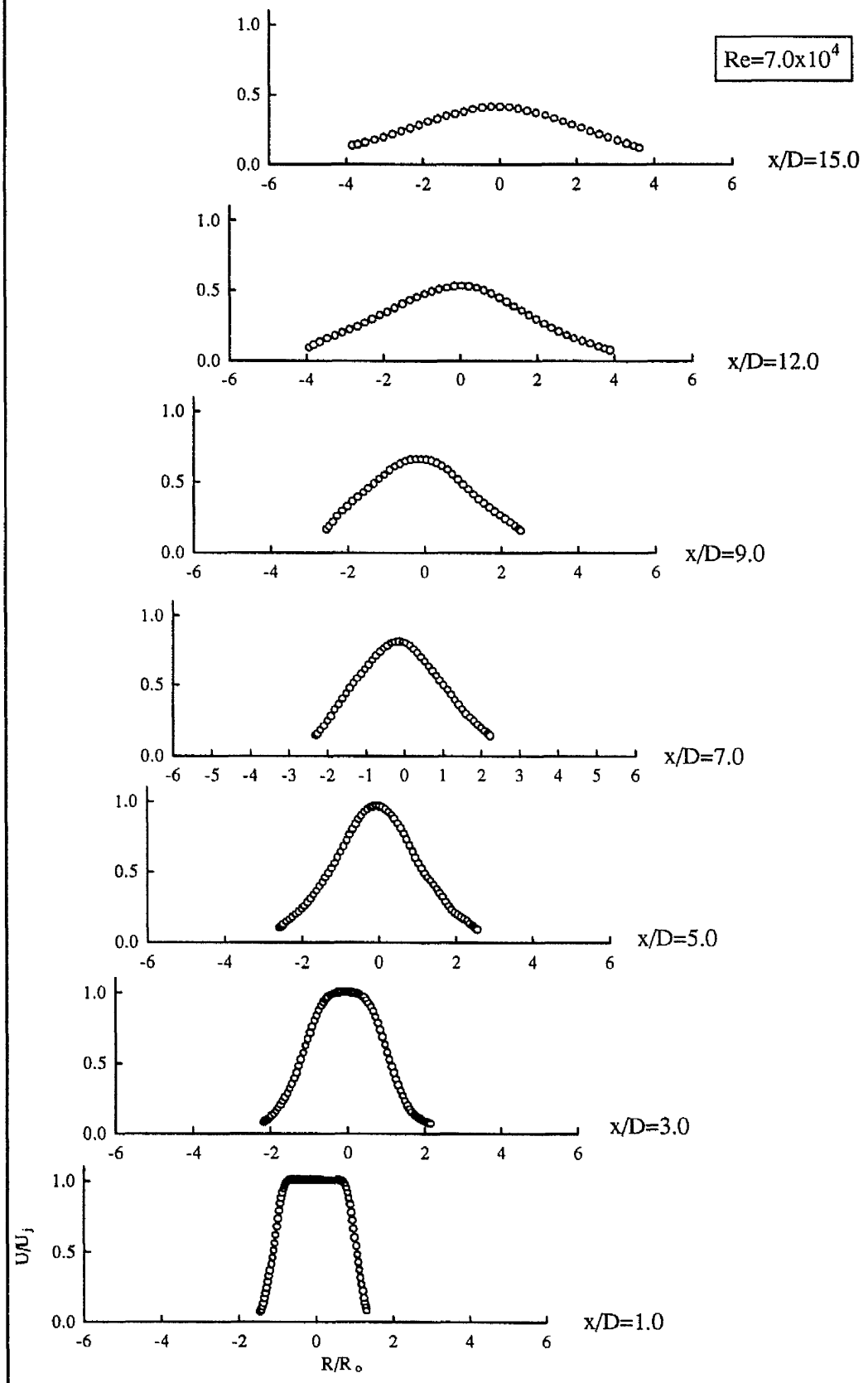

Figure 7.12. Mean velocity profiles for the natural jet at different downstream stations.

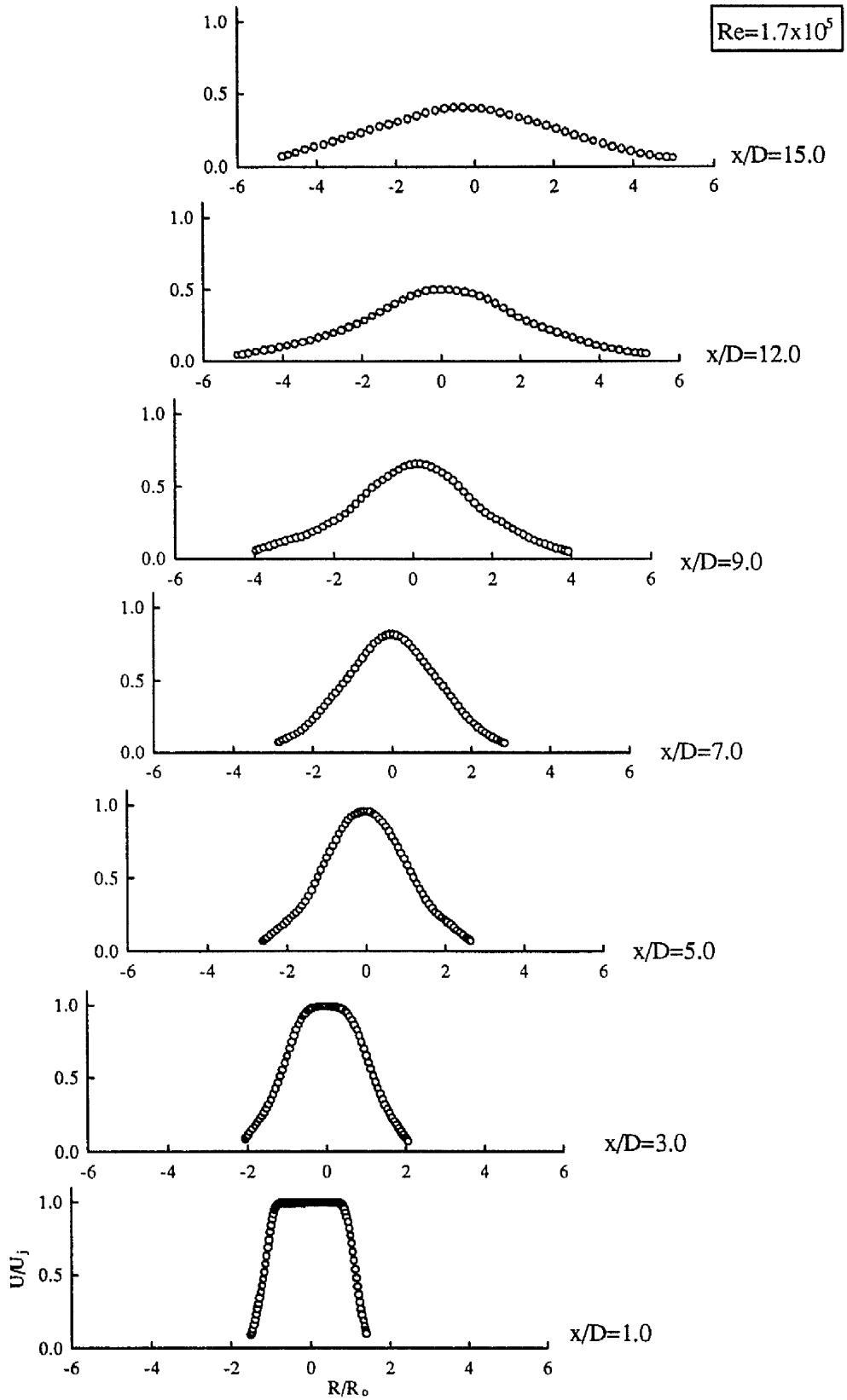

Figure 7.13. Mean velocity profiles for the natural jet at different downstream stations.

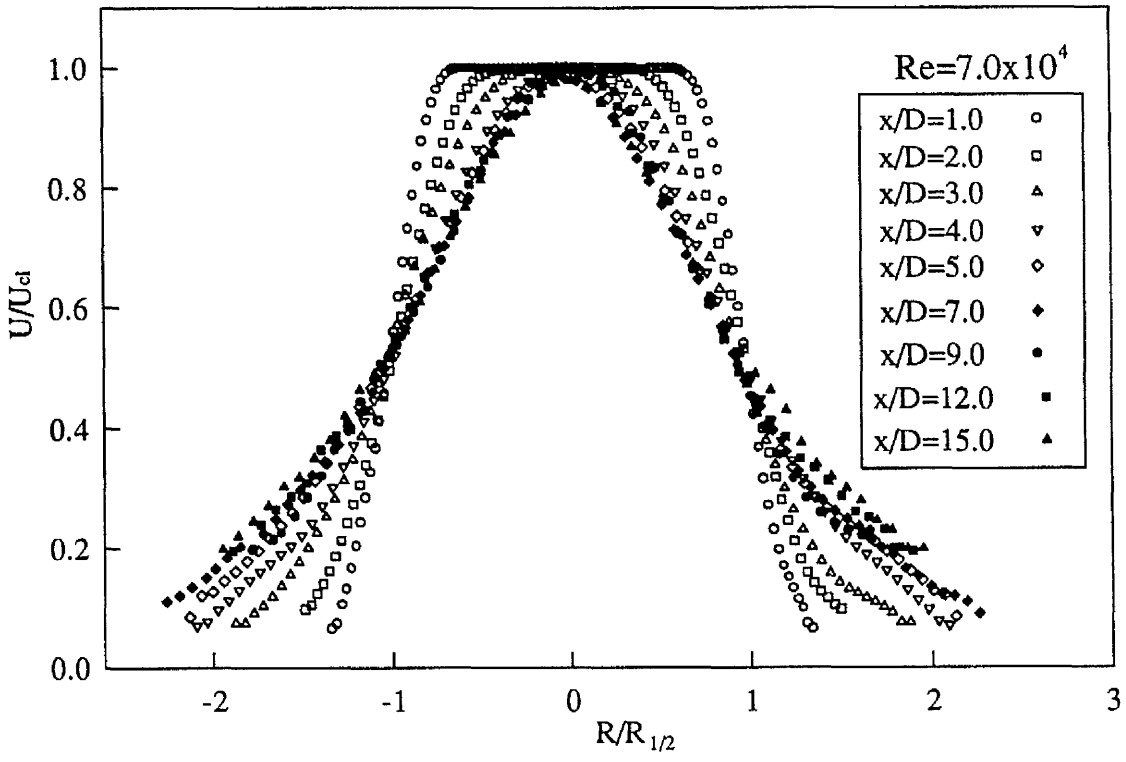

Figure 7.14. Mean velocity profiles for the natural jet at different downstream stations.

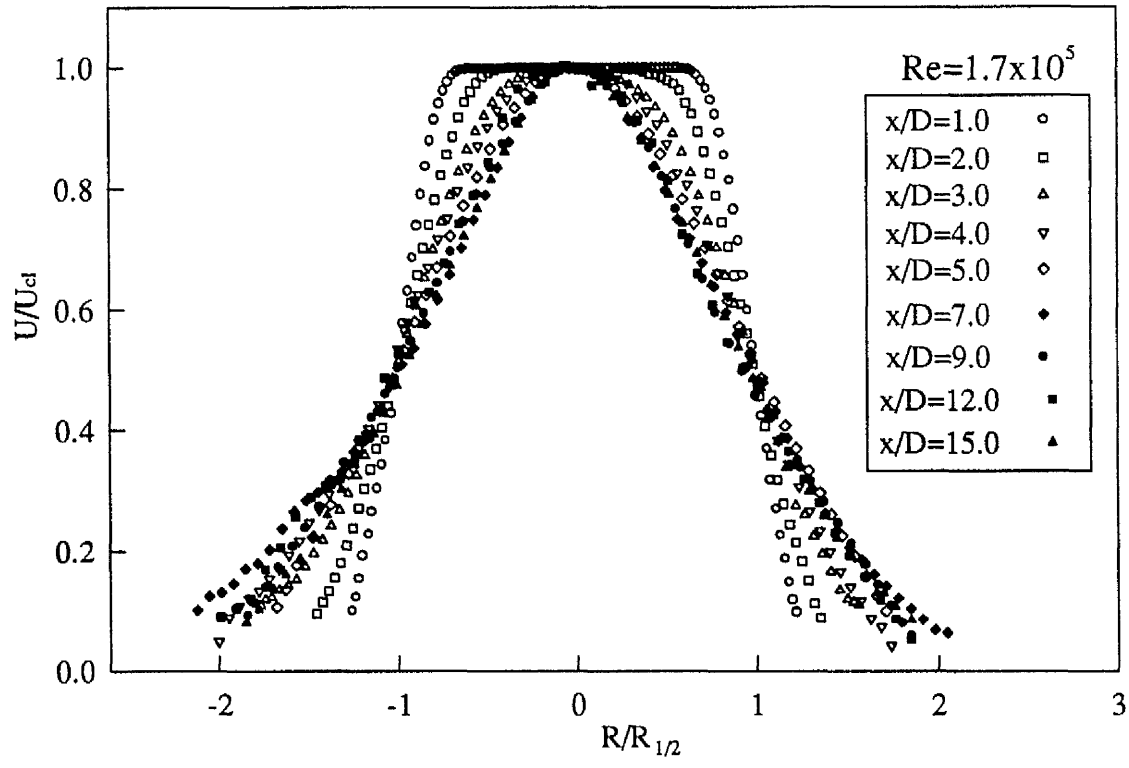

Figure 7.15. Mean velocity profiles for the natural jet at different downstream stations.

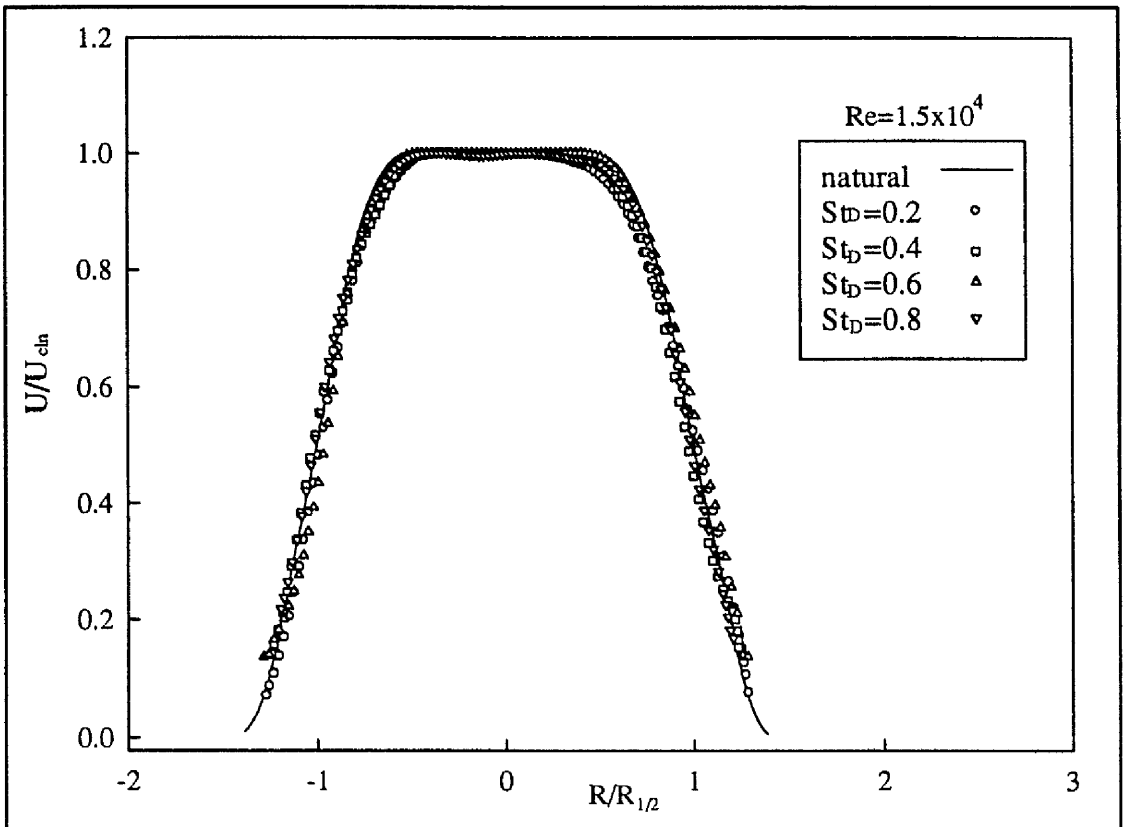

Figure 7.16. Mean velocity profiles at x/D=1.0 for different pulsation frequencies.

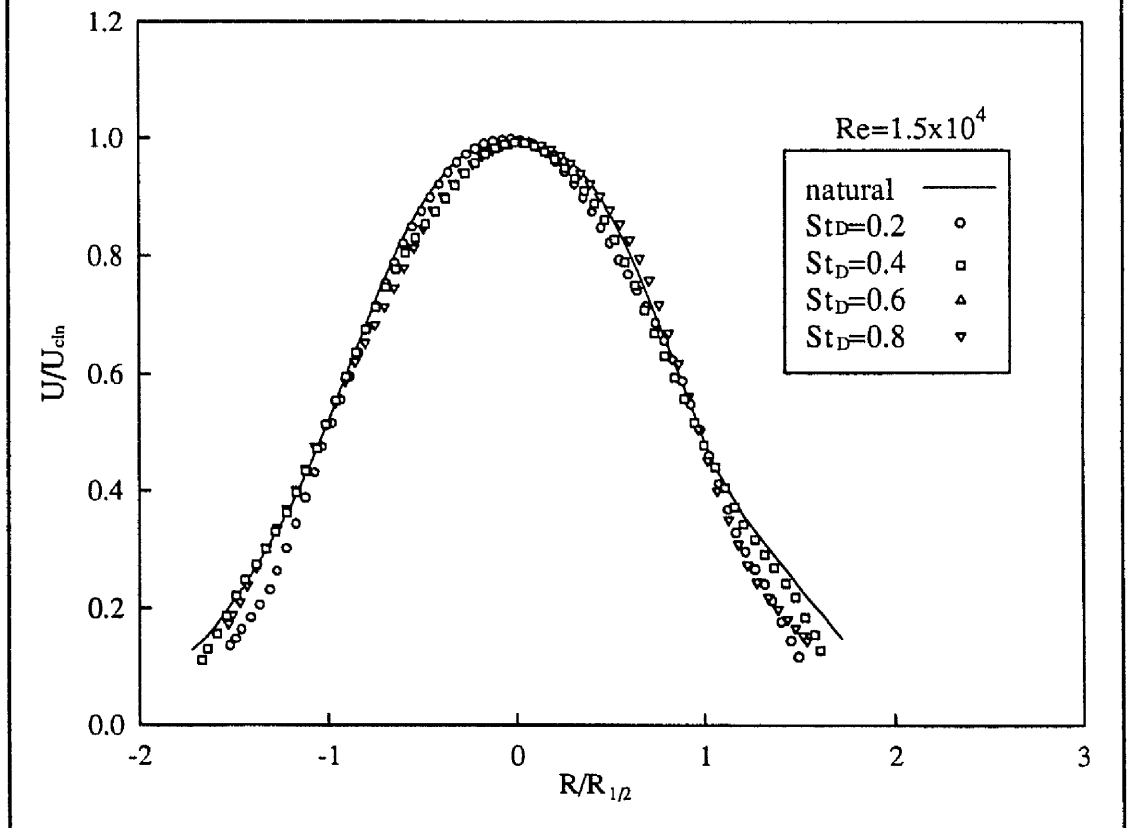

Figure 7.17. Mean velocity profiles at x/D=3.0 for different pulsation frequencies.

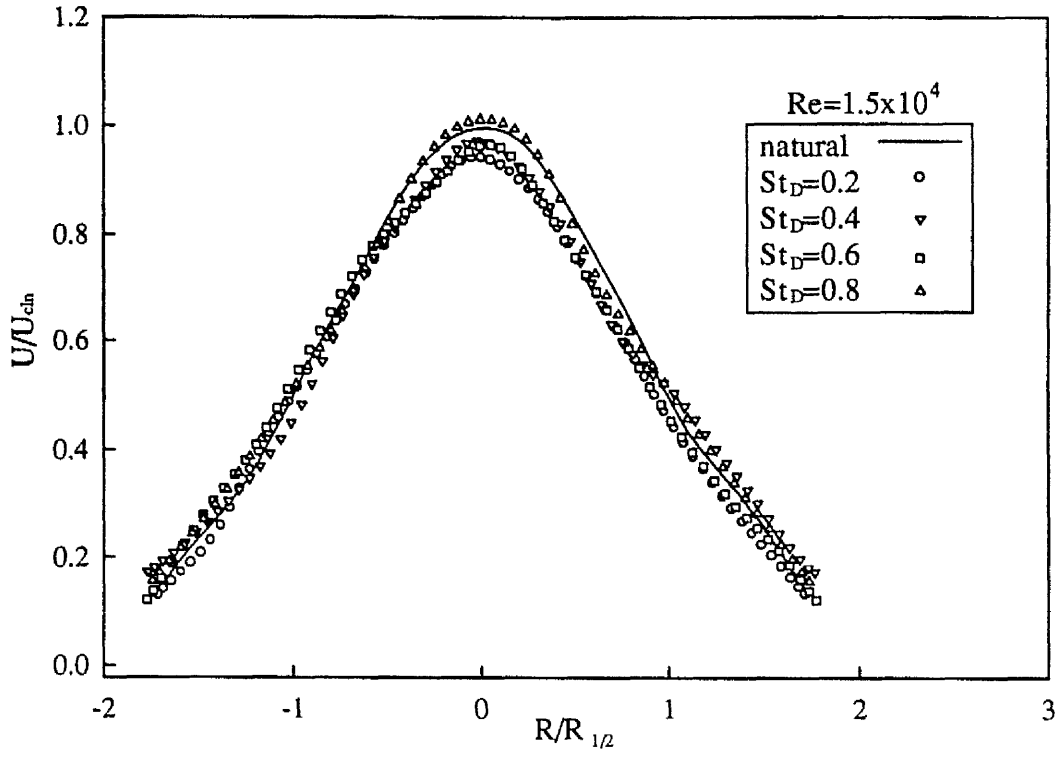

Figure 7.18. Mean velocity profiles at x/D=5.0 for different pulsation frequencies.

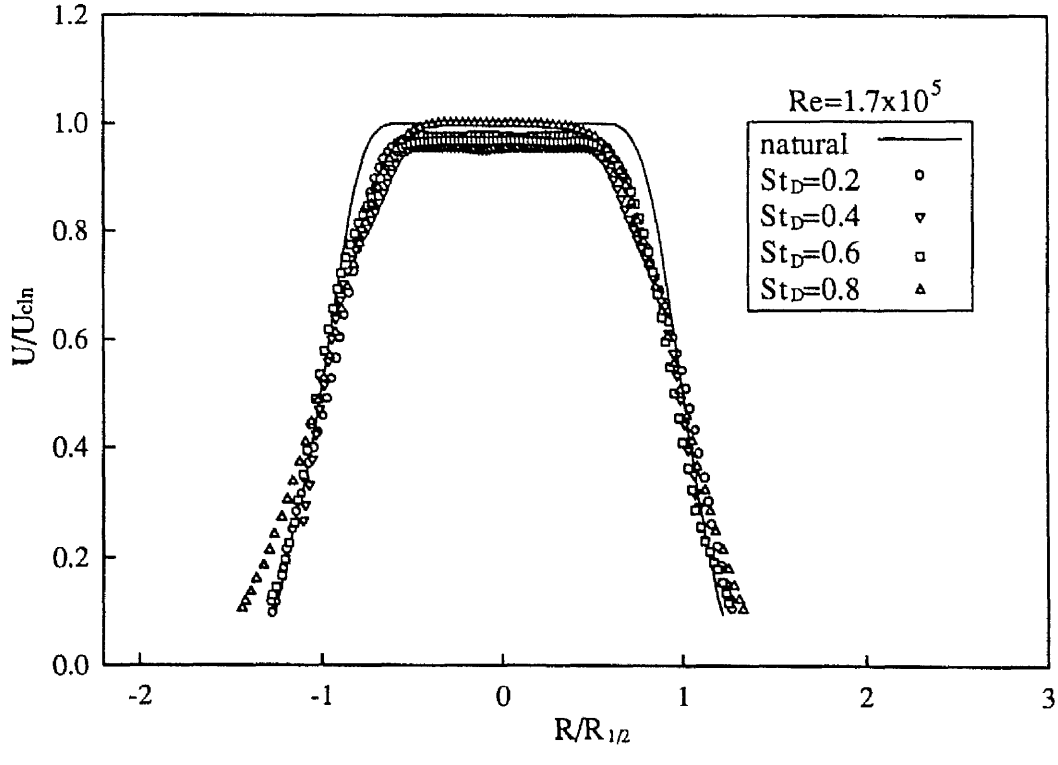

Figure 7.19. Mean velocity profiles at x/D=1.0 for different pulsation frequencies.

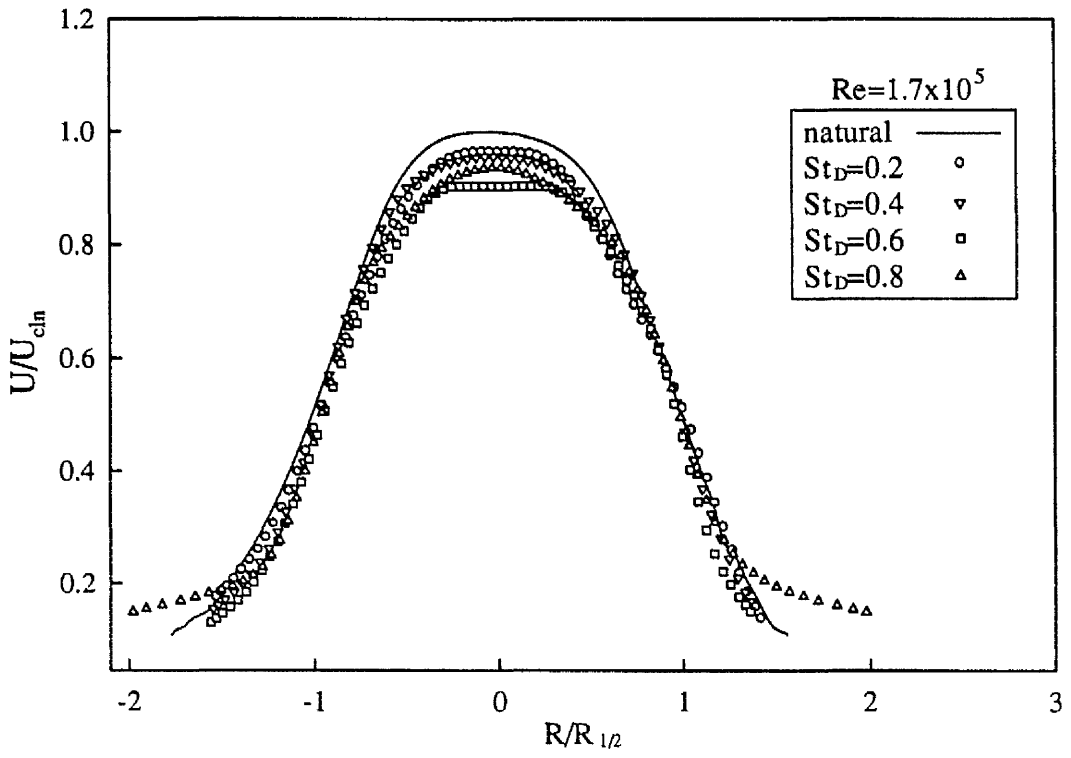

Figure 7.20. Mean velocity profiles at x/D=3.0 for different pulsation frequencies.

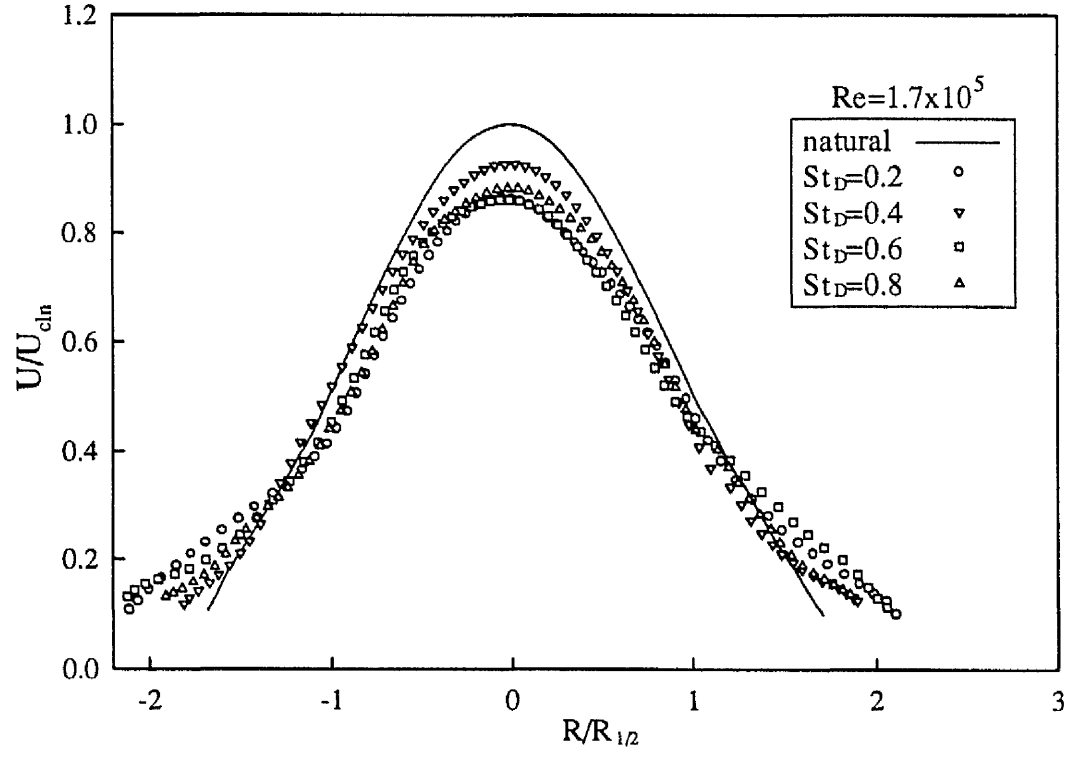

Figure 7.21. Mean velocity profiles at x/D=5.0 for different pulsation frequencies.

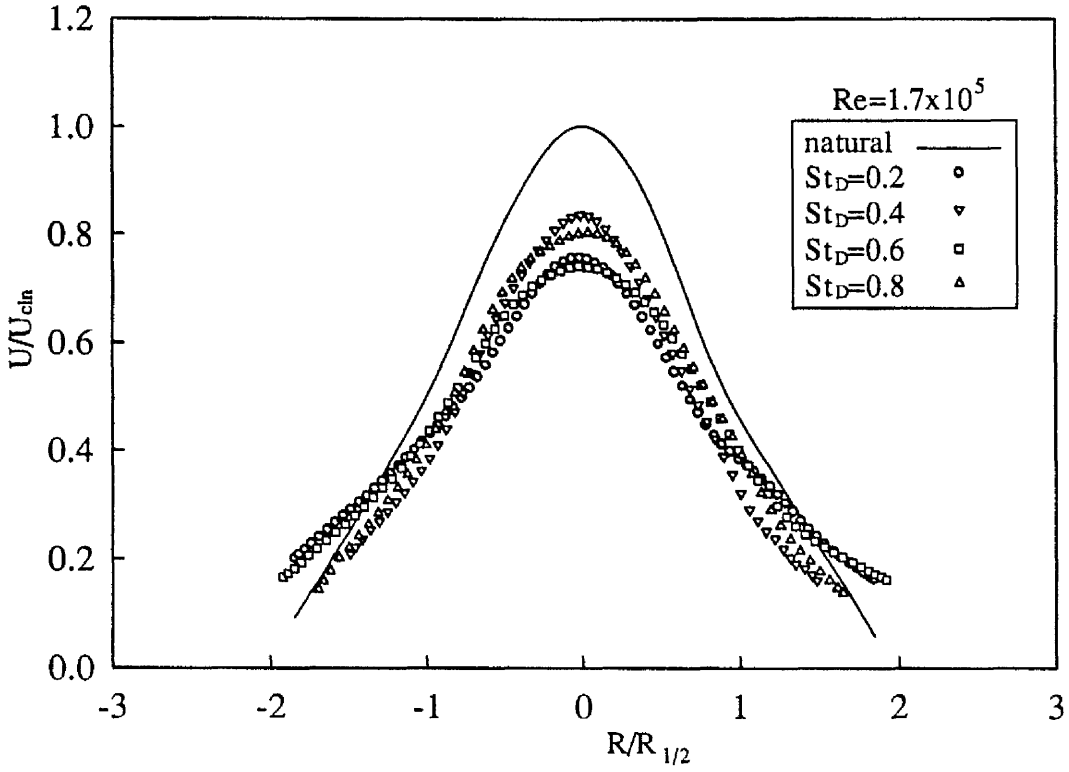

Figure 7.22. Mean velocity profiles at x/D=9.0 for different pulsation frequencies.

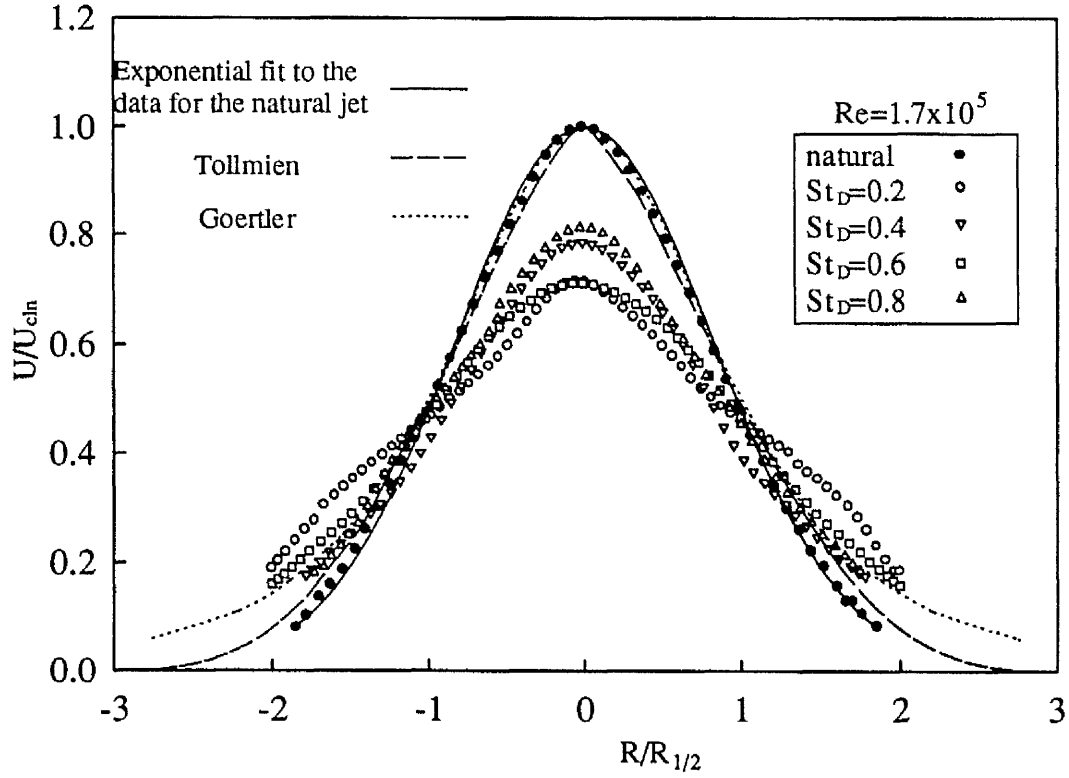

Figure 7.23. Mean velocity profiles at x/D=15.0 for different pulsation frequencies.

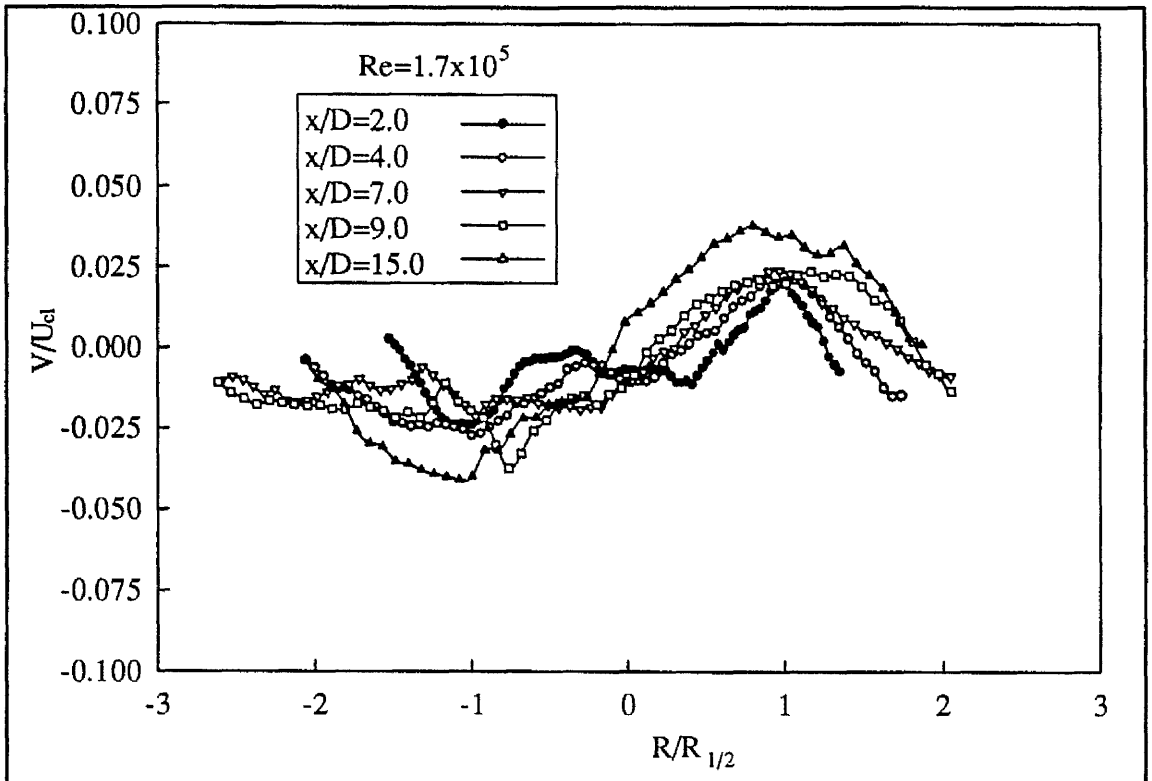

Figure 7.24. Distributions of the time mean radial velocity component of the natural jet at different axial positions.

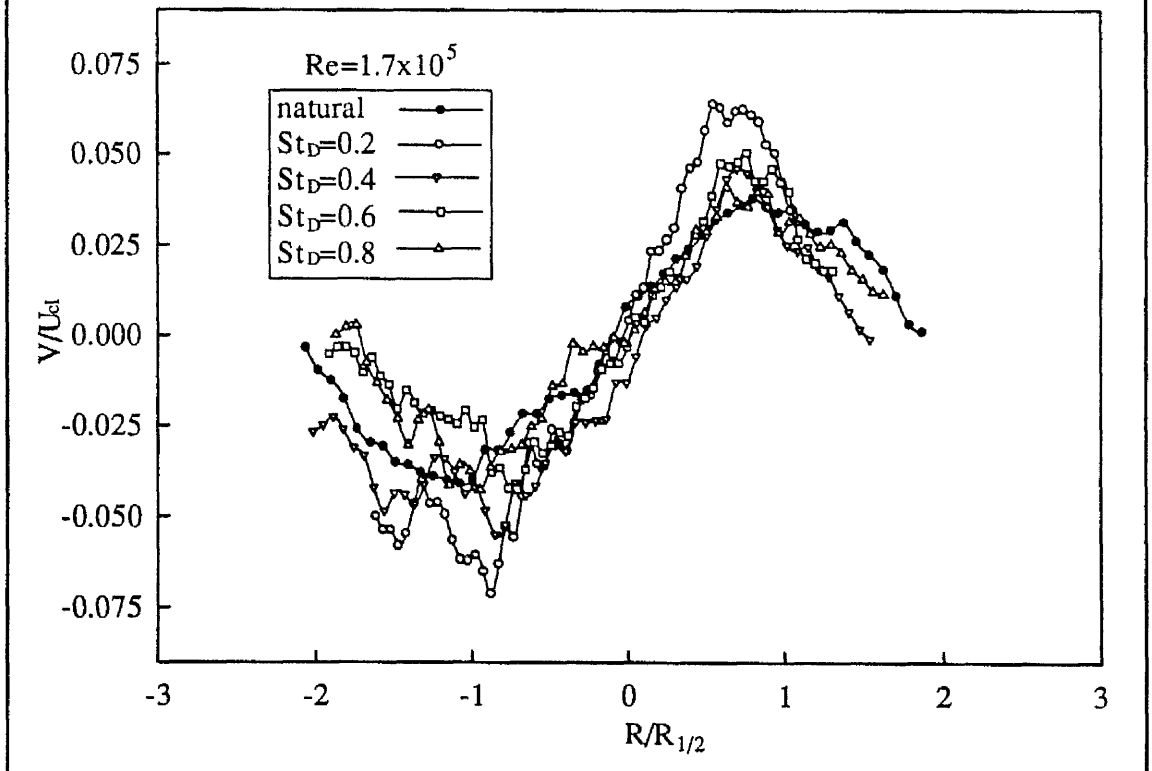

Figure 7.25. Distributions of the time mean radial velocity component at x/D=15.0 for different pulsation frequencies.

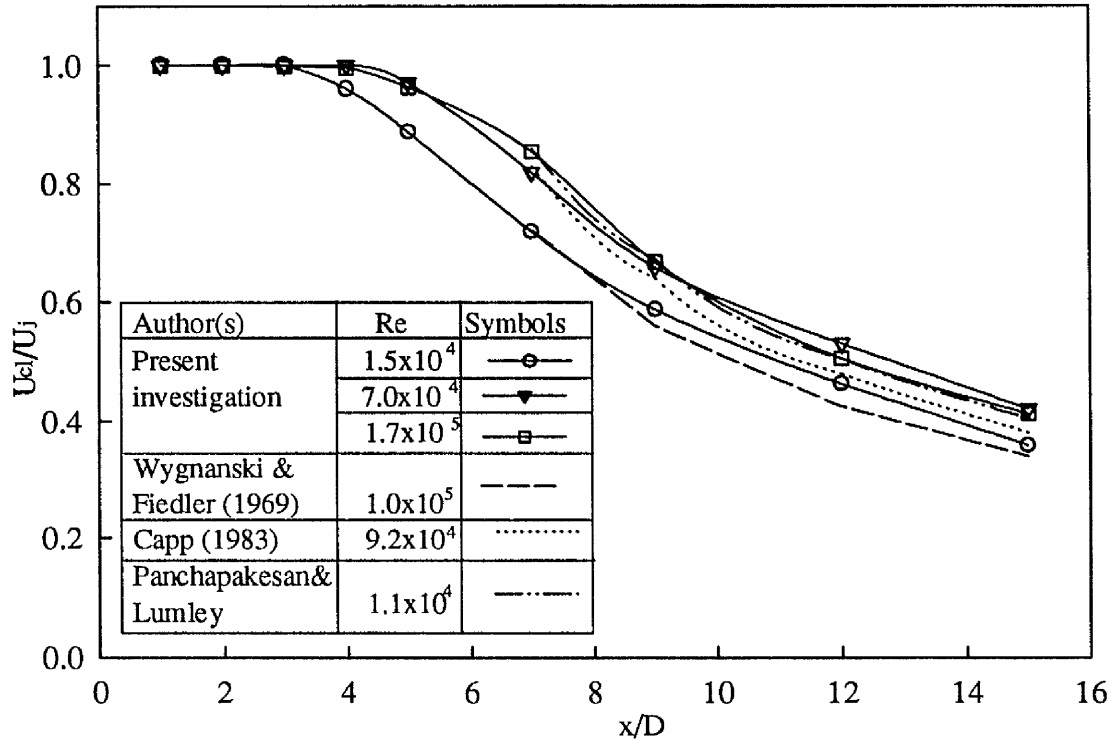

Figure 7.26. Decay of the centre-line velocity of the natural jet for different Reynolds number.

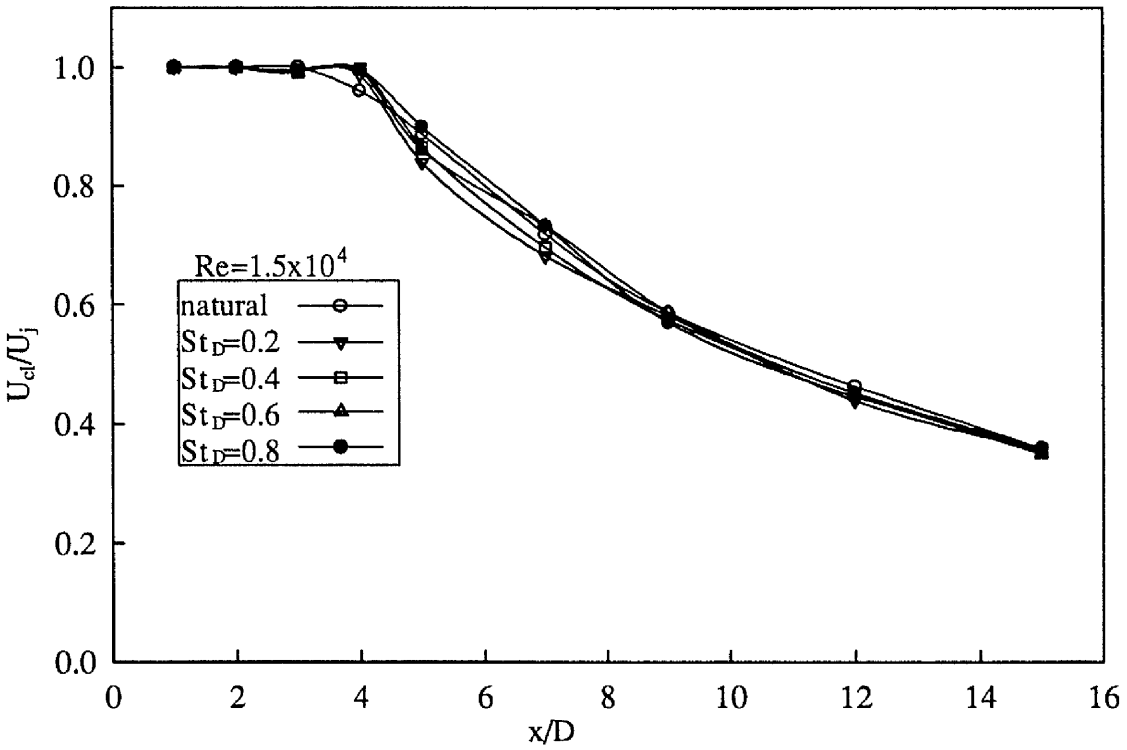

Figure 7.27. Decay of the centre-line velocity for different pulsation frequencies.

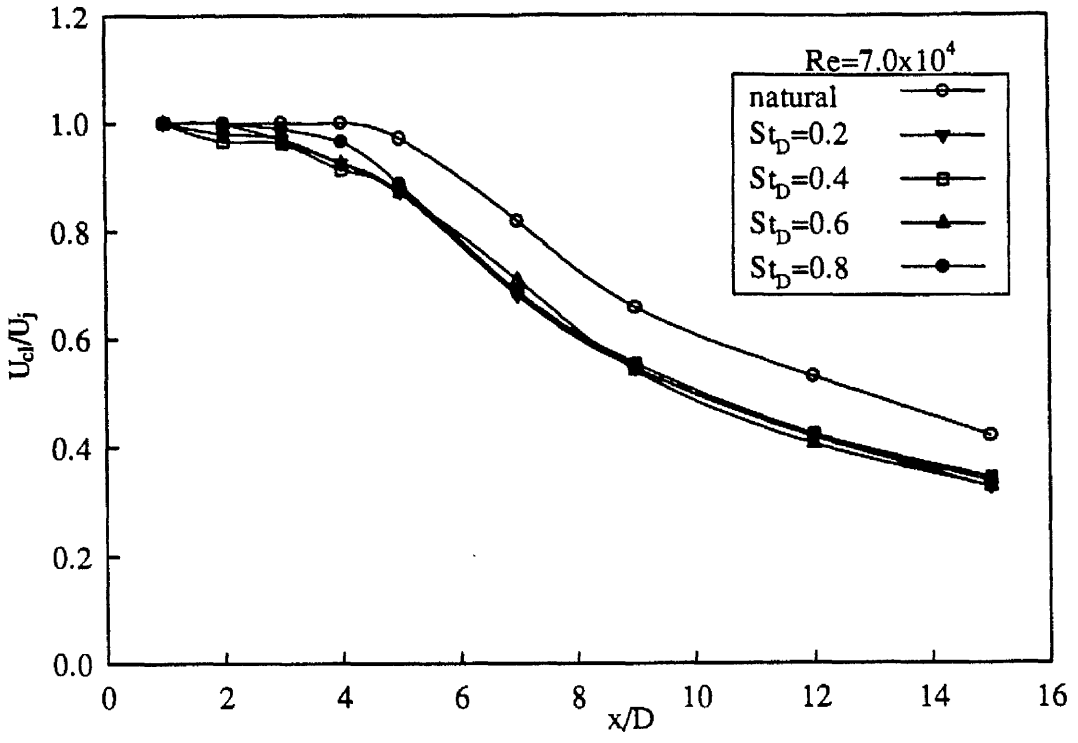

Figure 7.28. Decay of the centre-line velocity for different pulsation frequencies.

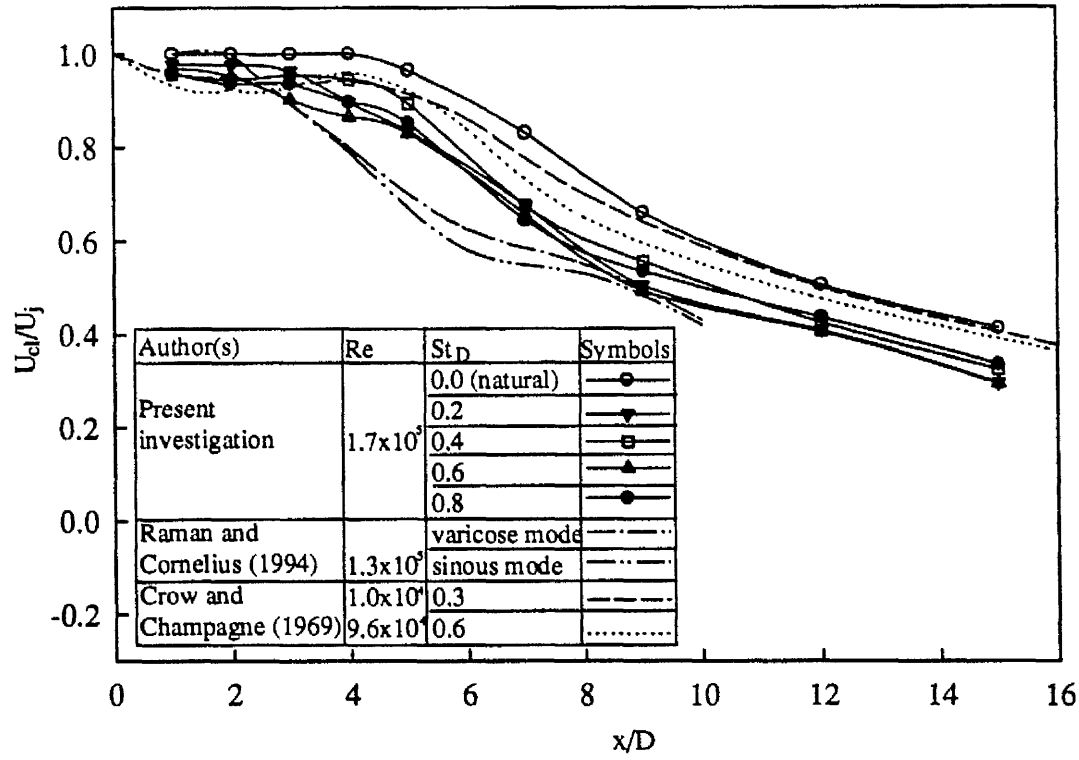

Figure 7.29. Decay of the centre-line velocity for different pulsation frequencies.

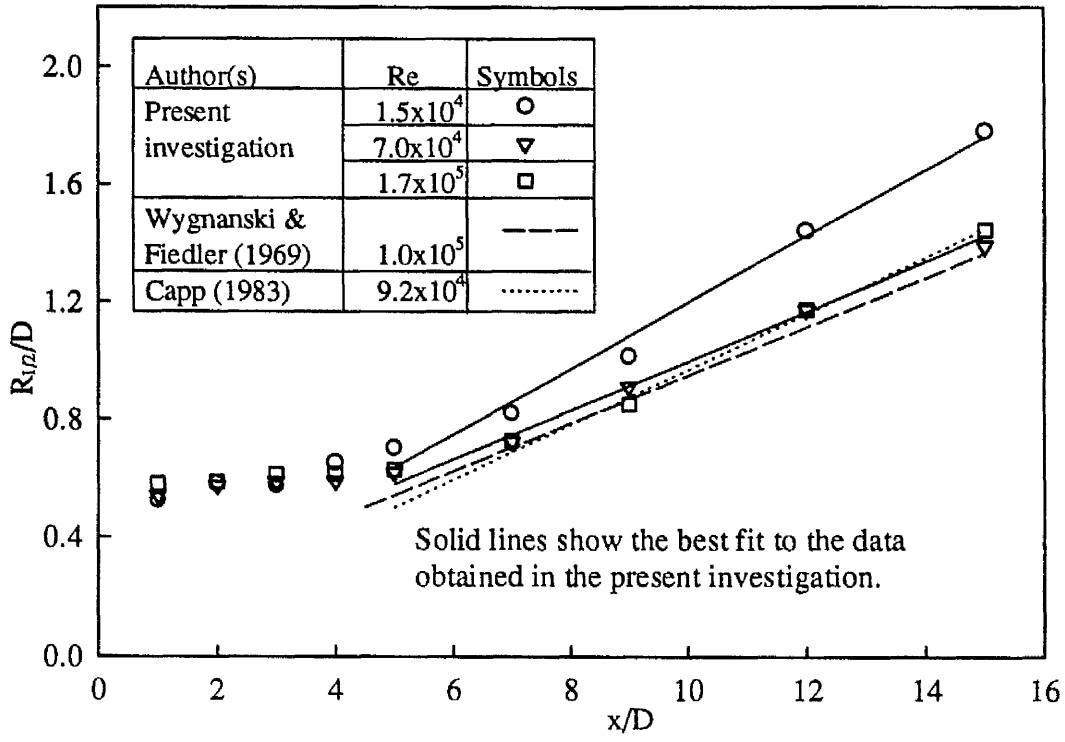

Figure 7.30. Half-width of natural jet as a function of distance.

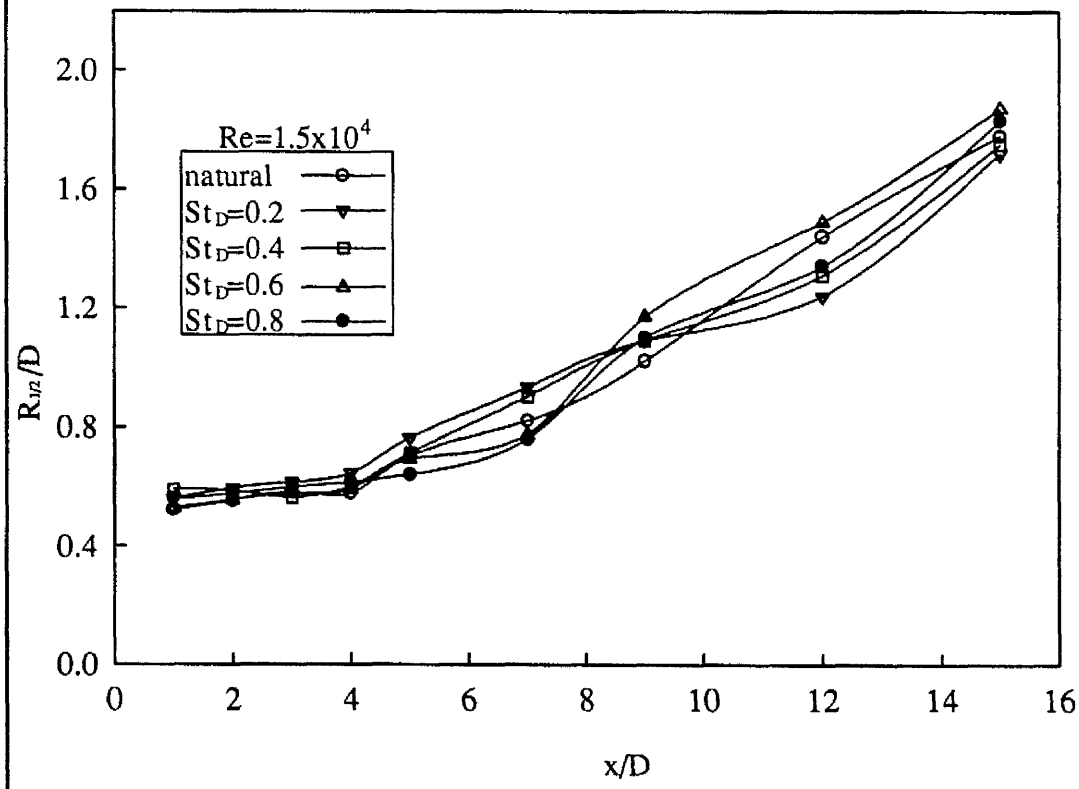

Figure 7.31. Half-width of the jet with and without excitation as a function of distance.

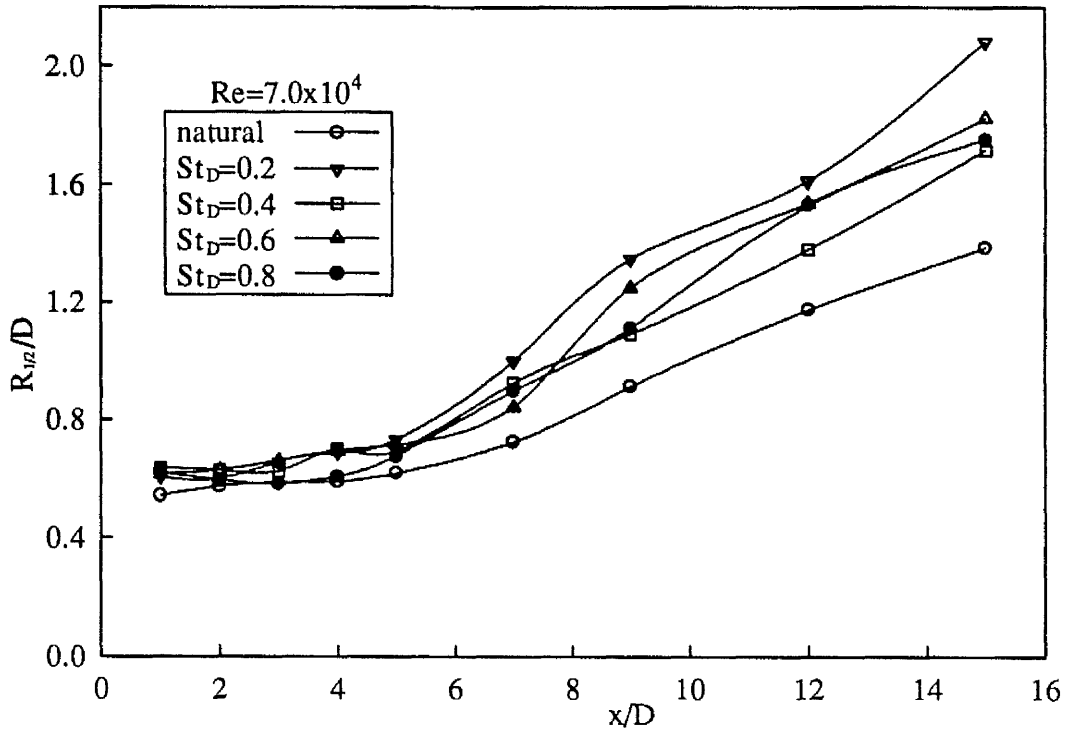

Figure 7.32. Half-width of the jet with and without excitation as a function of distance.

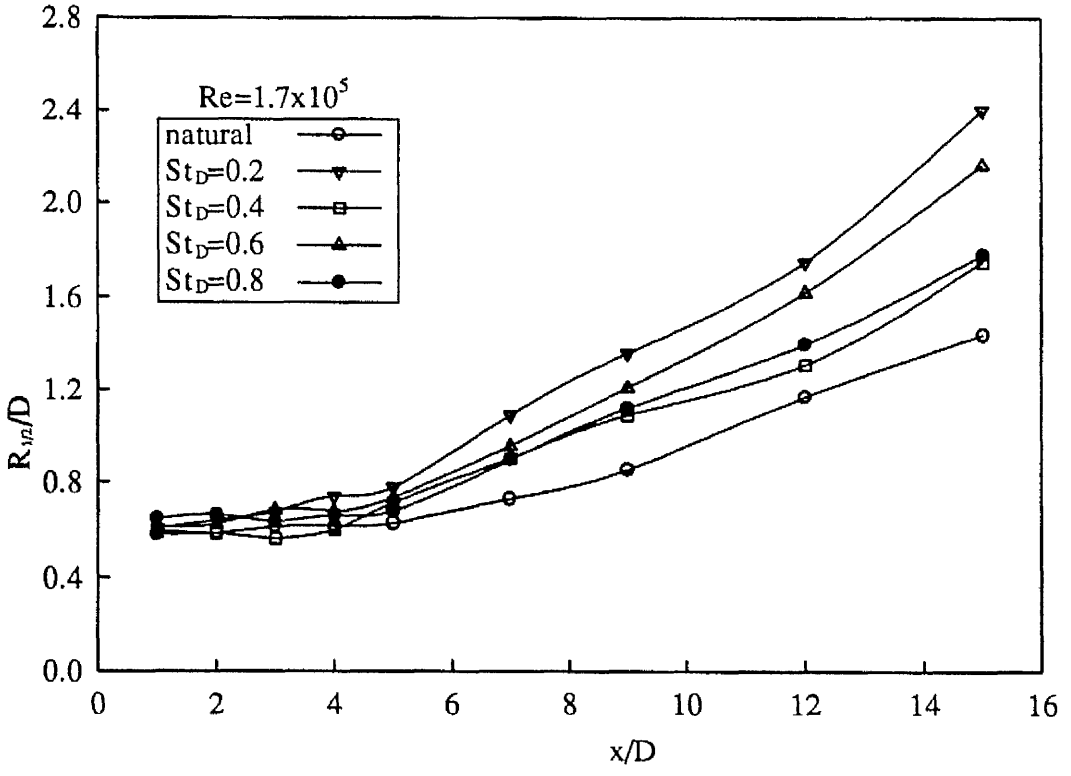

Figure 7.33. Half-width of the jet with and without excitation as a function of distance.

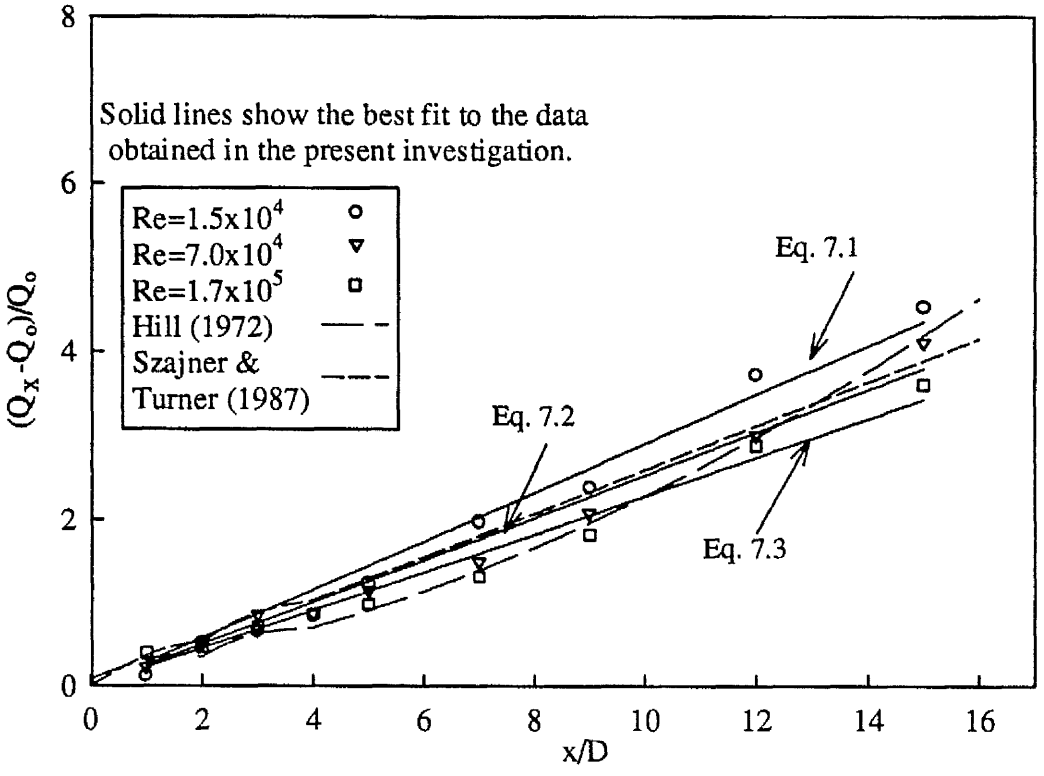

Figure 7.34. Entrainment of the natural jet.

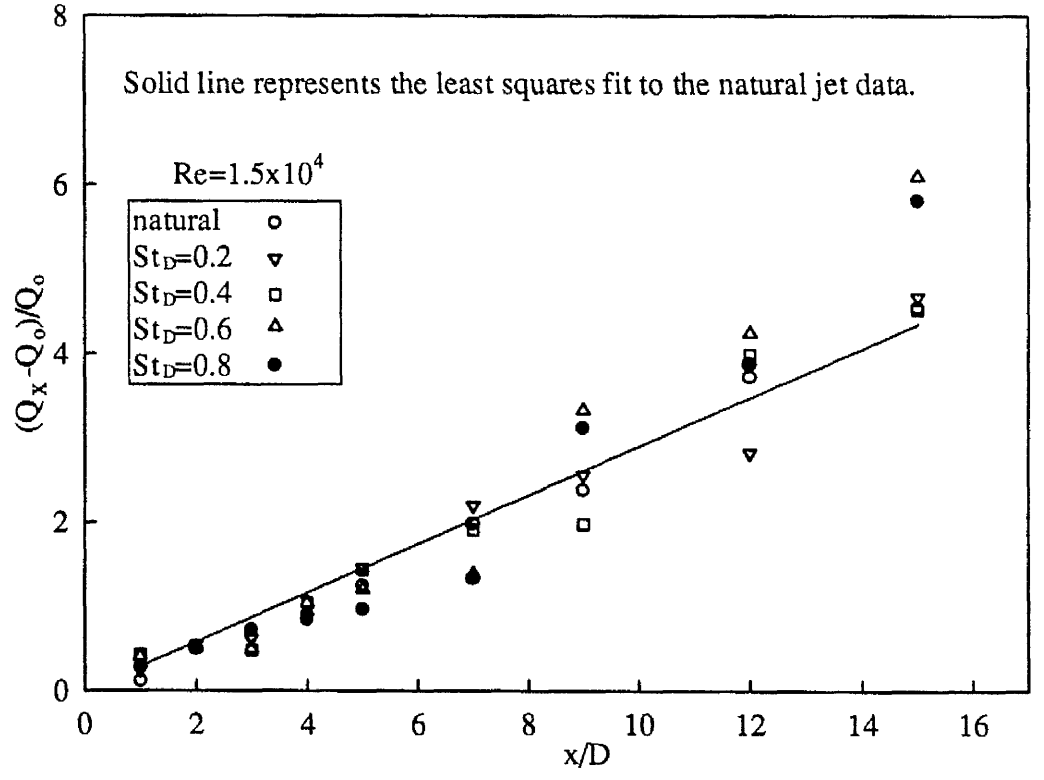

Figure 7.35. Entrainment of the jet with and without excitation.

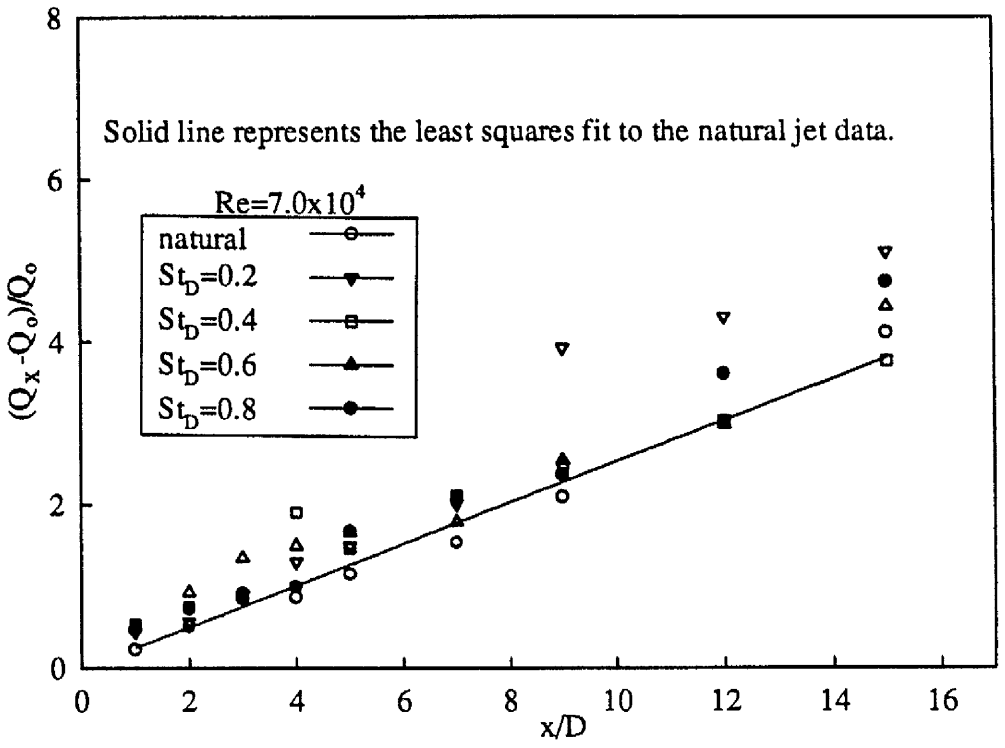

Figure 7.36 Entrainment of the jet with and without excitation.

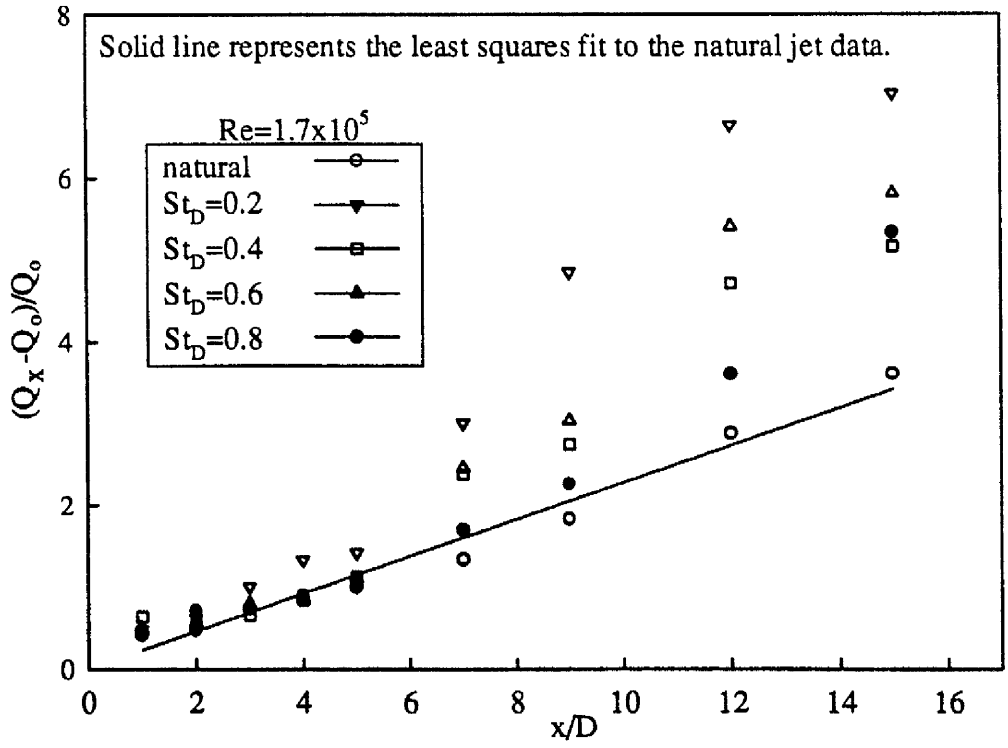

Figure 7.37. Entrainment of the jet with and without excitation.

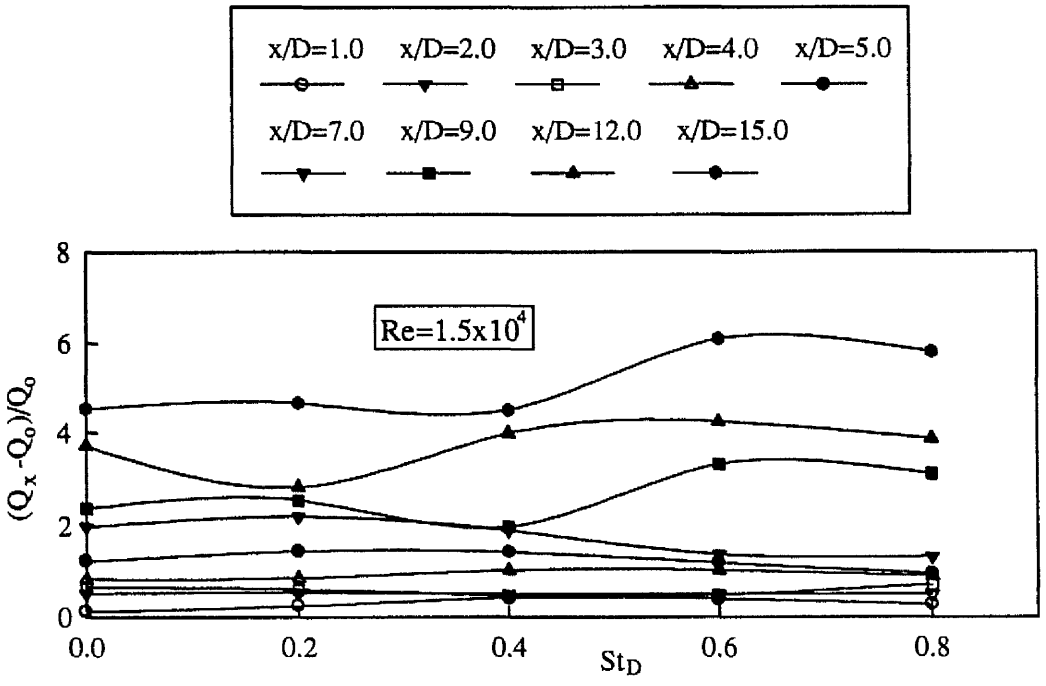

Figure 7.38. Variation of the entrainment rate at different downstream stations.

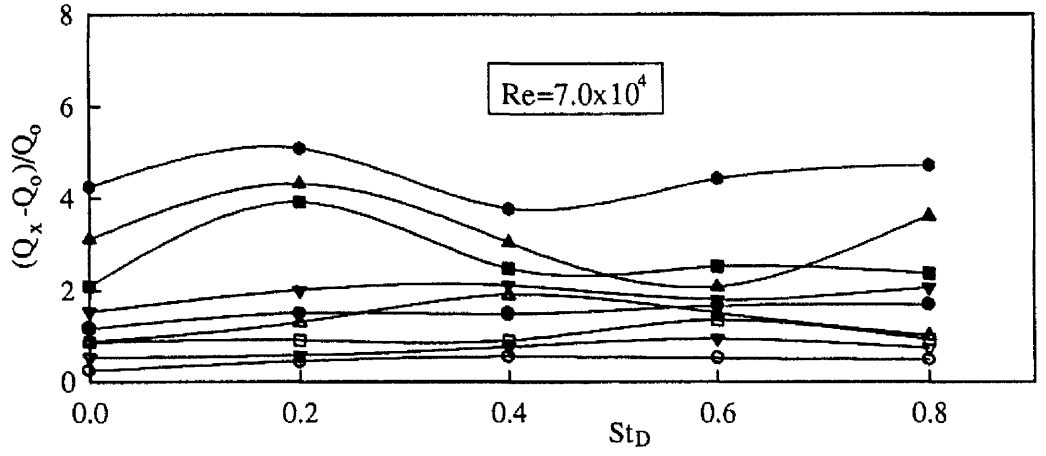

Figure 7.39. Variation of the entrainment rate at different downstream stations.

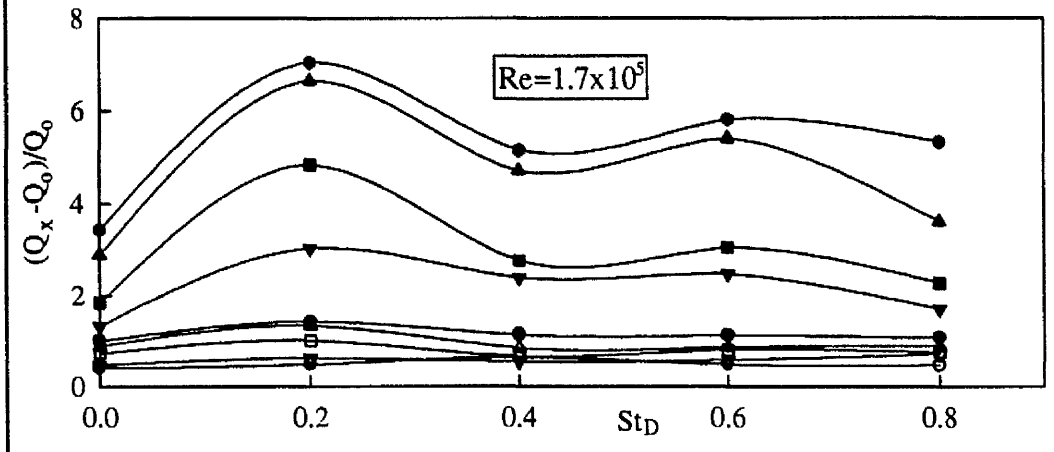

Figure 7.40. Variation of the entrainment rate at different downstream stations.

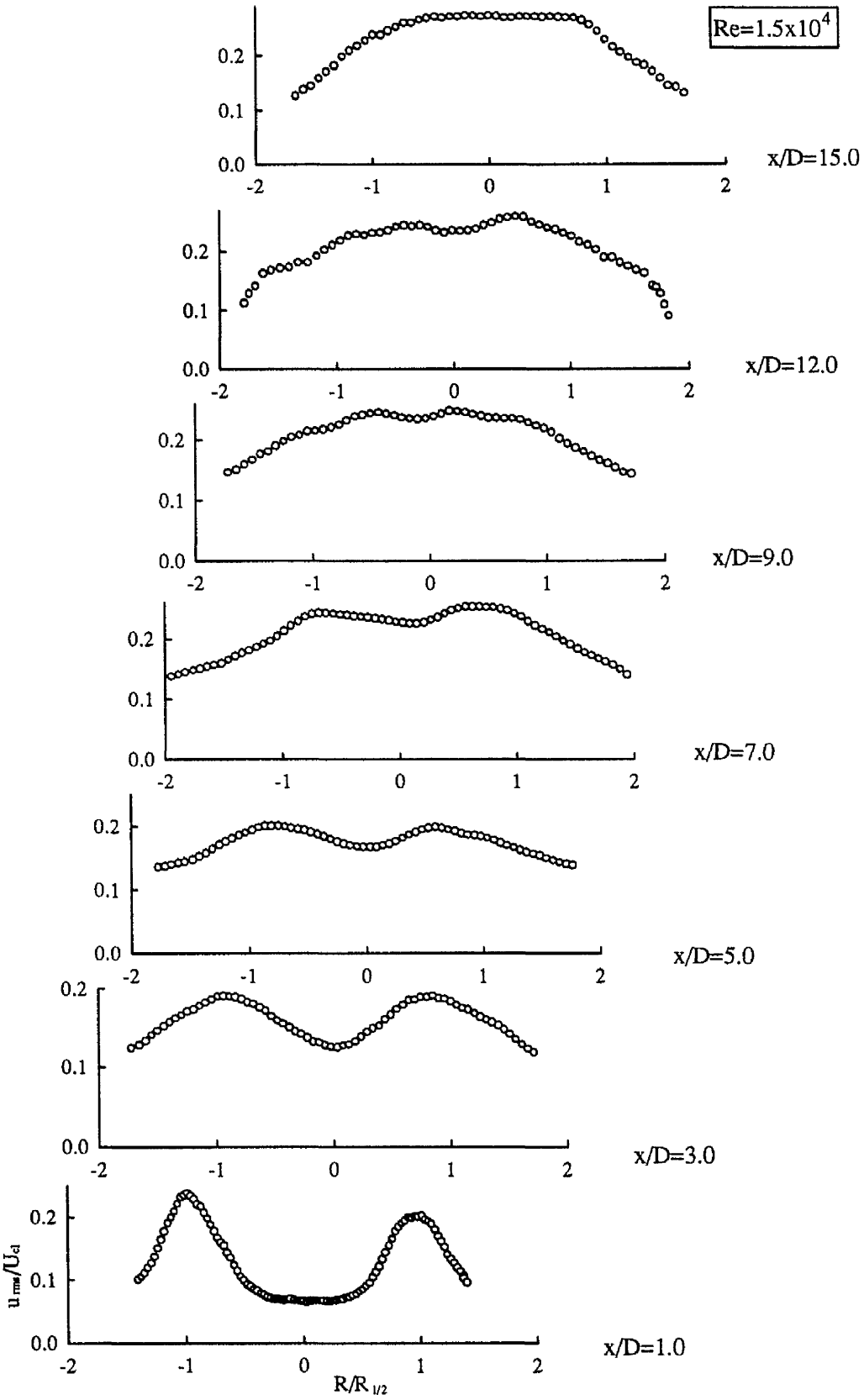

Figure 7.41. Profiles of the rms value of the axial velocity component u_{rms}.

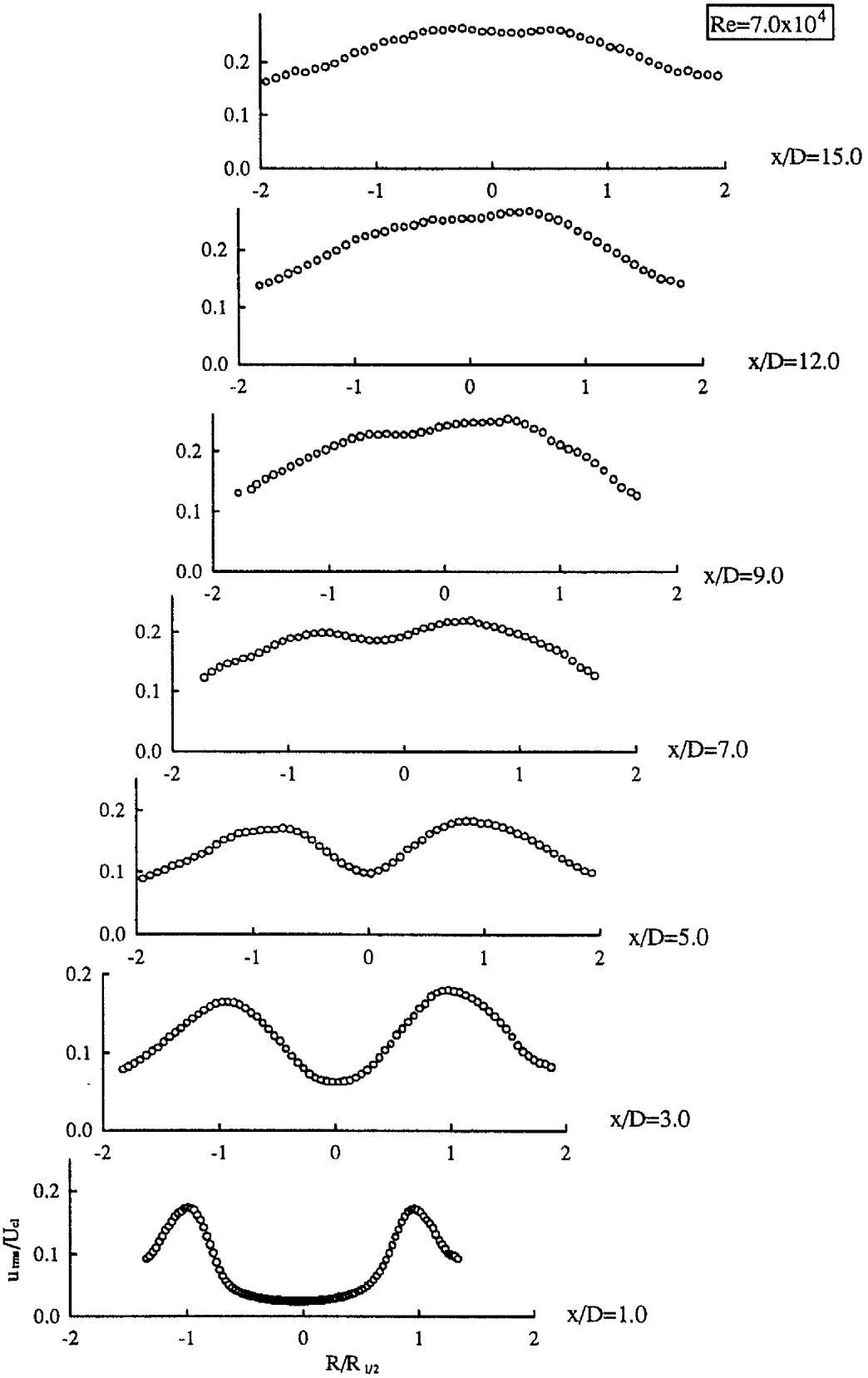

Figure 7.42. Profiles of the rms value of the axial velocity component u_{rms} .

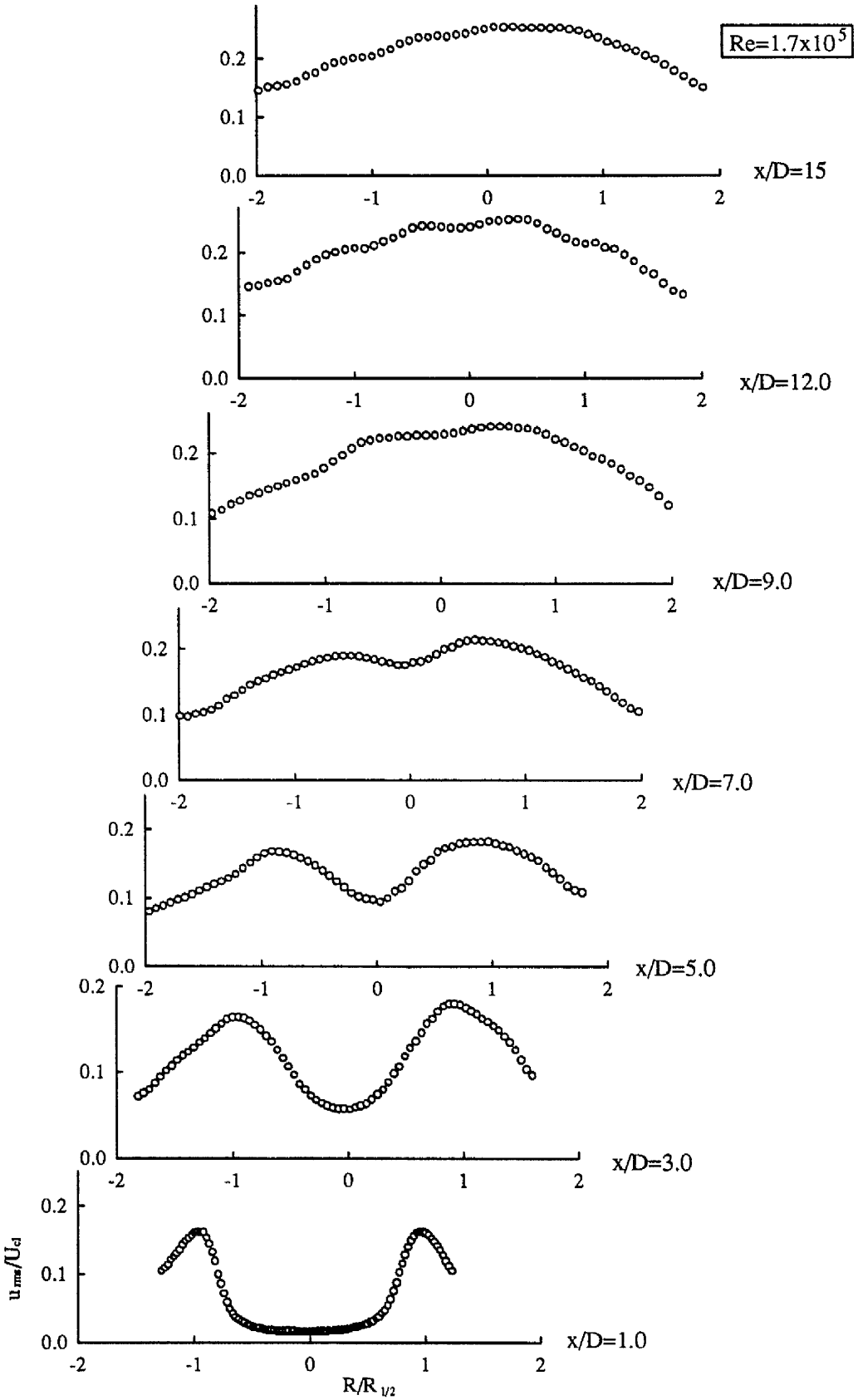

Figure 7.43. Profiles of the rms value of the axial velocity component u_{rms}.

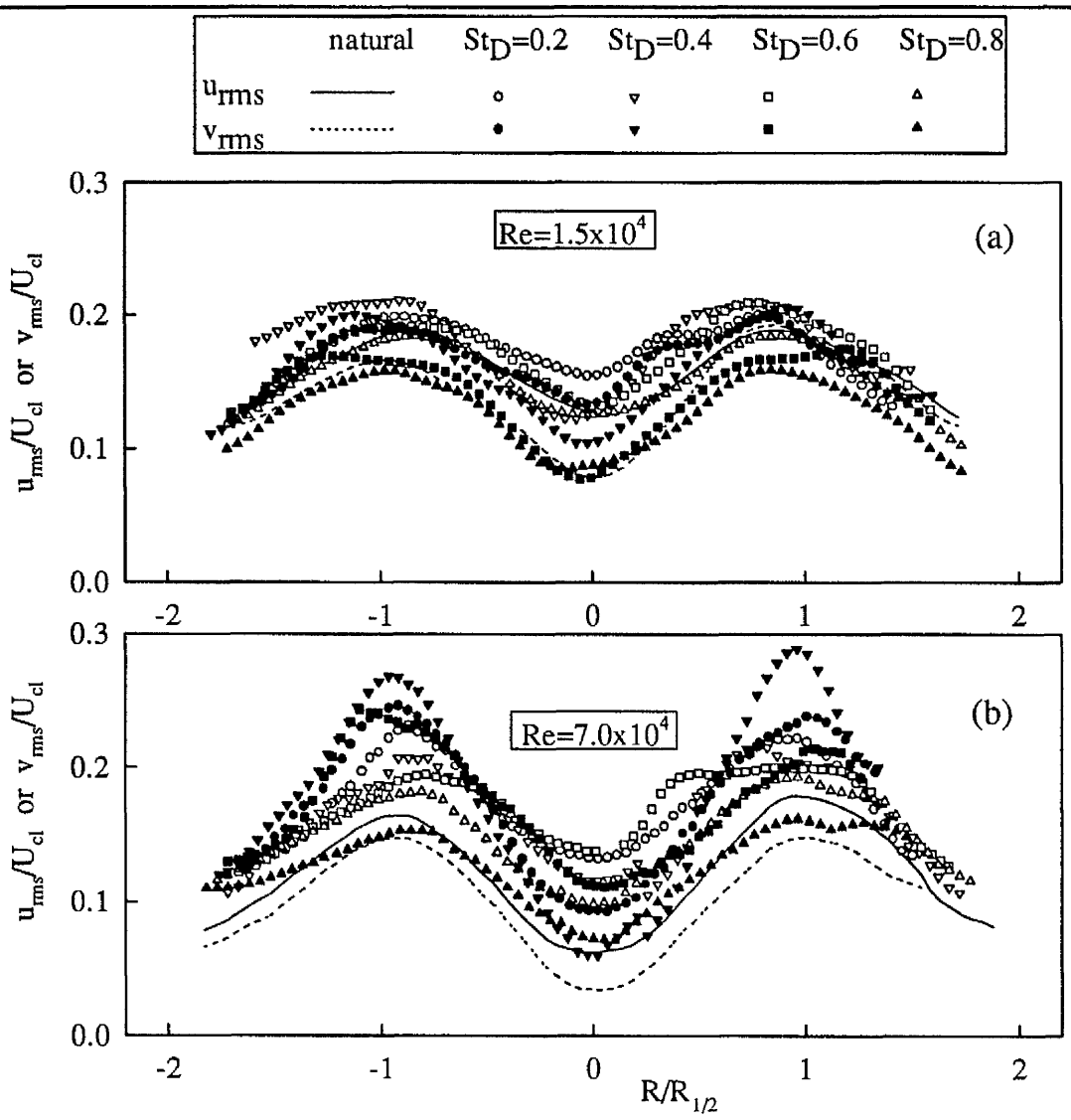

Figure 7.44. Distributions of the u_{rms} and v_{rms} turbulent components at x/D=3.0 for different pulsation frequencies.

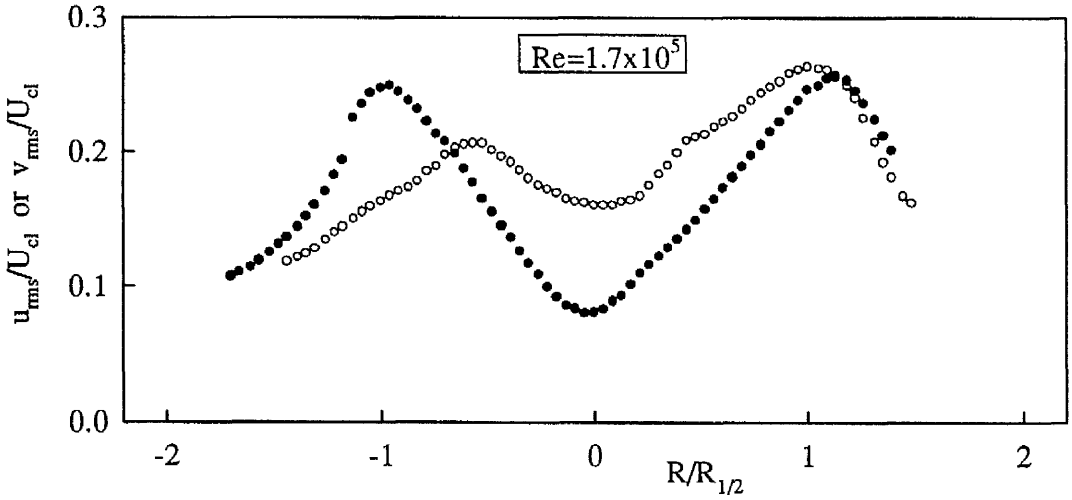

Figure 7.45. Distributions of the u_{rms} and v_{rms} turbulent components at x/D=3.0 for St_D = 0.2.

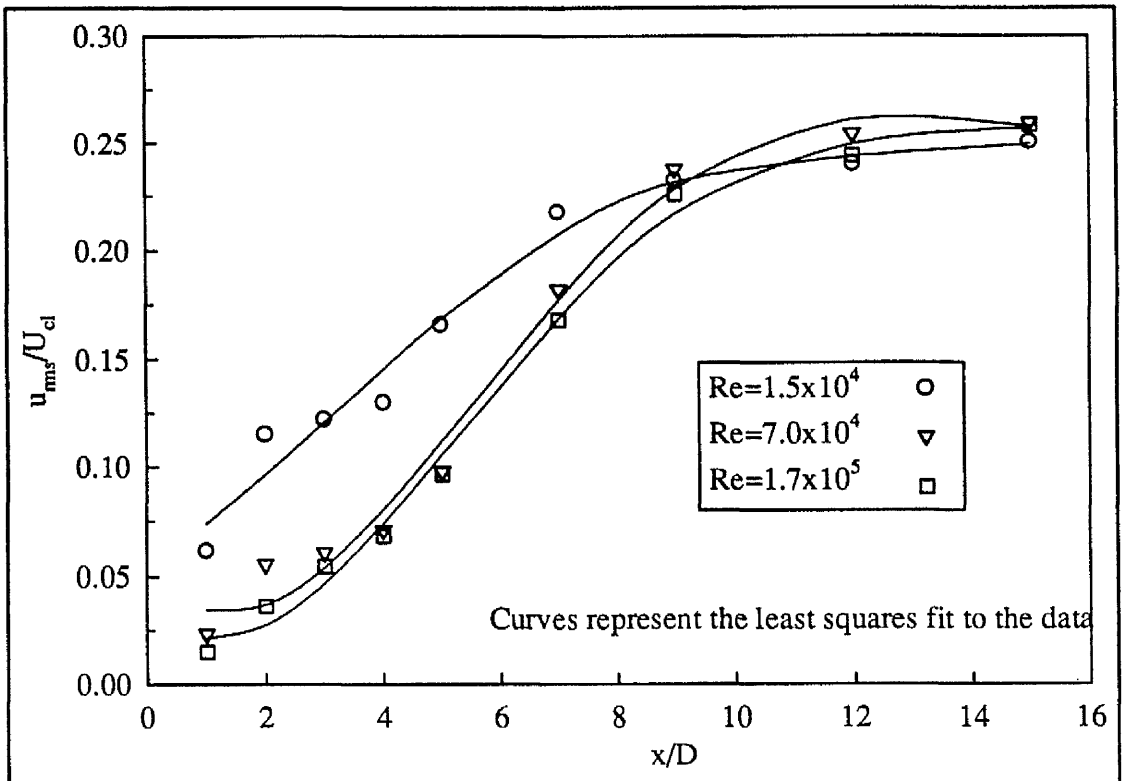

Figure 7.46. Turbulence intensity variations along the jet centre-line.

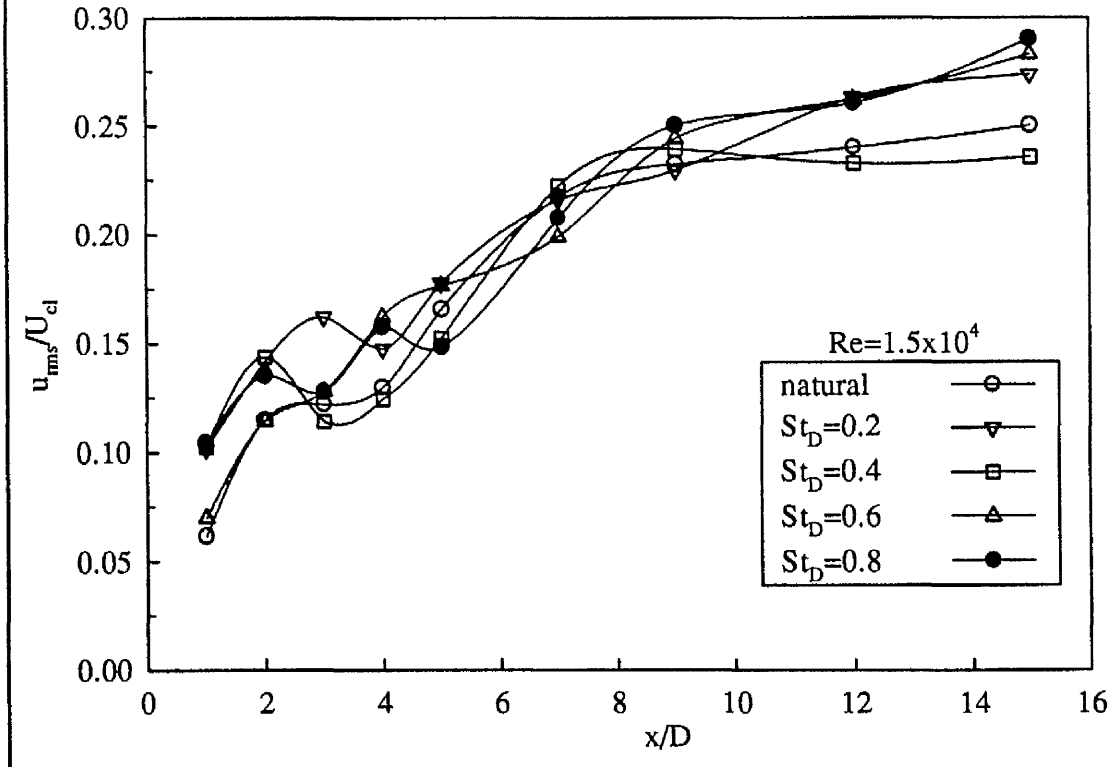

Figure 7.47. Turbulence intensity variations along the jet centre-line for different pulsation frequencies.

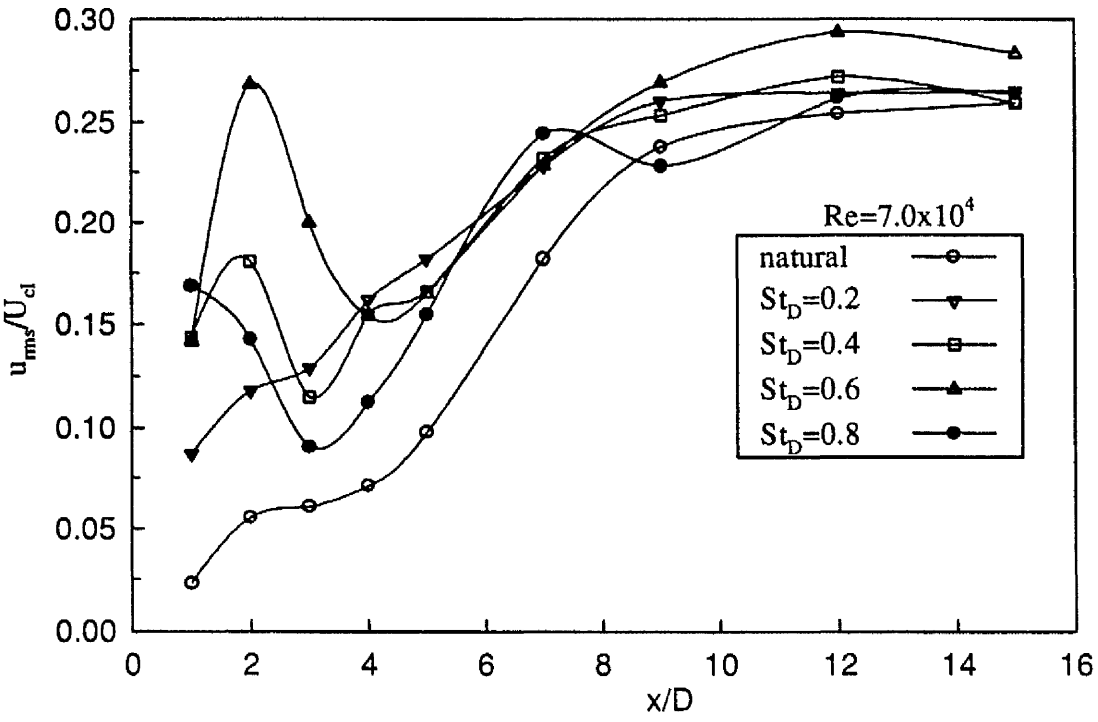

Figure 7.48. Turbulence intensity variations along the jet centre-line for different pulsation frequencies.

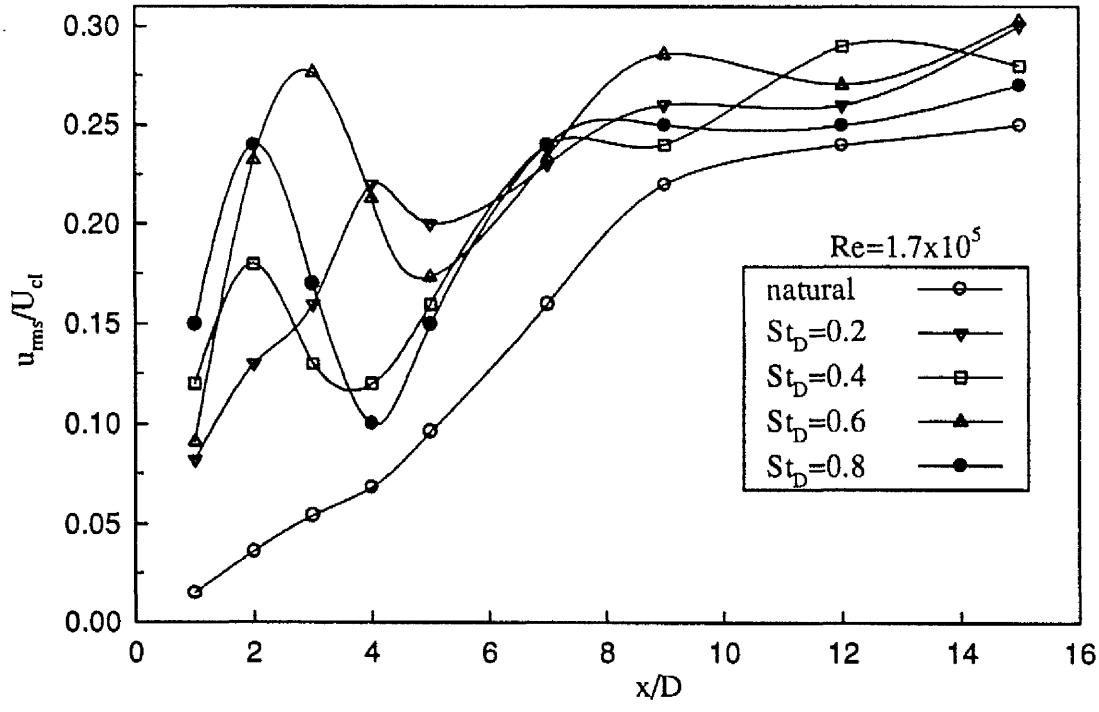

Figure 7.49. Turbulence intensity variations along the jet centre-line for different pulsation frequencies.

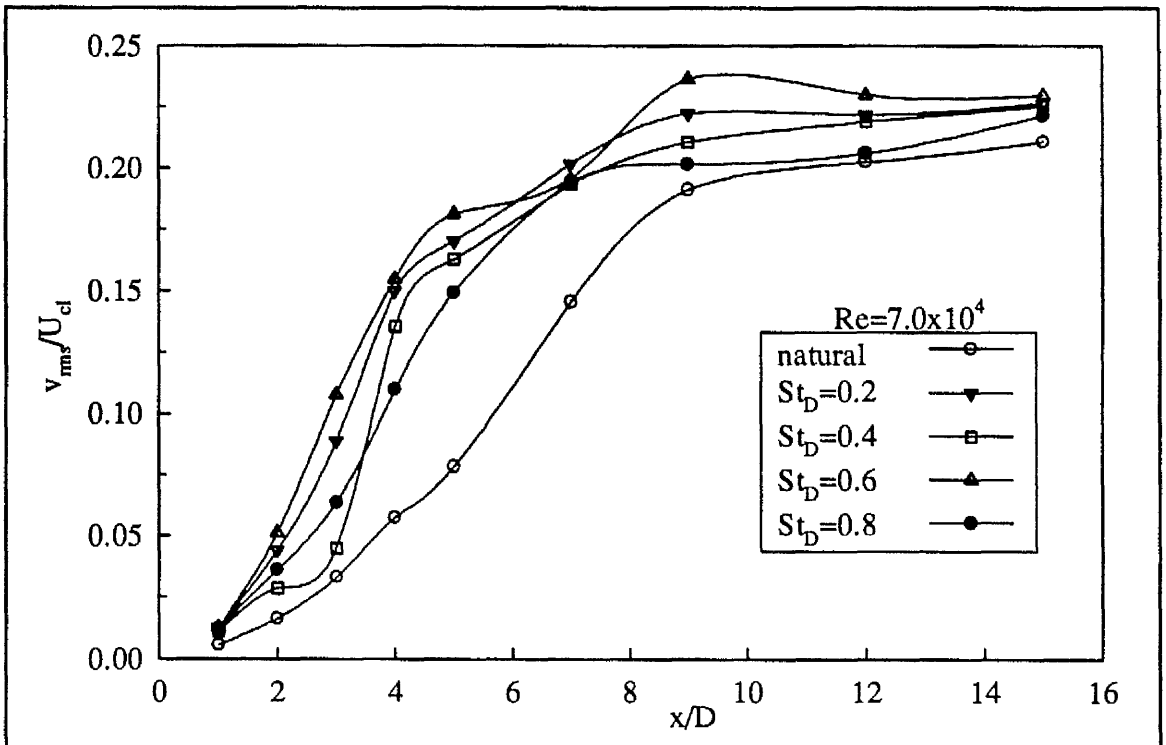

Figure 7.50. Turbulence intensity variation of the radial velocity component along the jet centre-line for different pulsation frequencies.

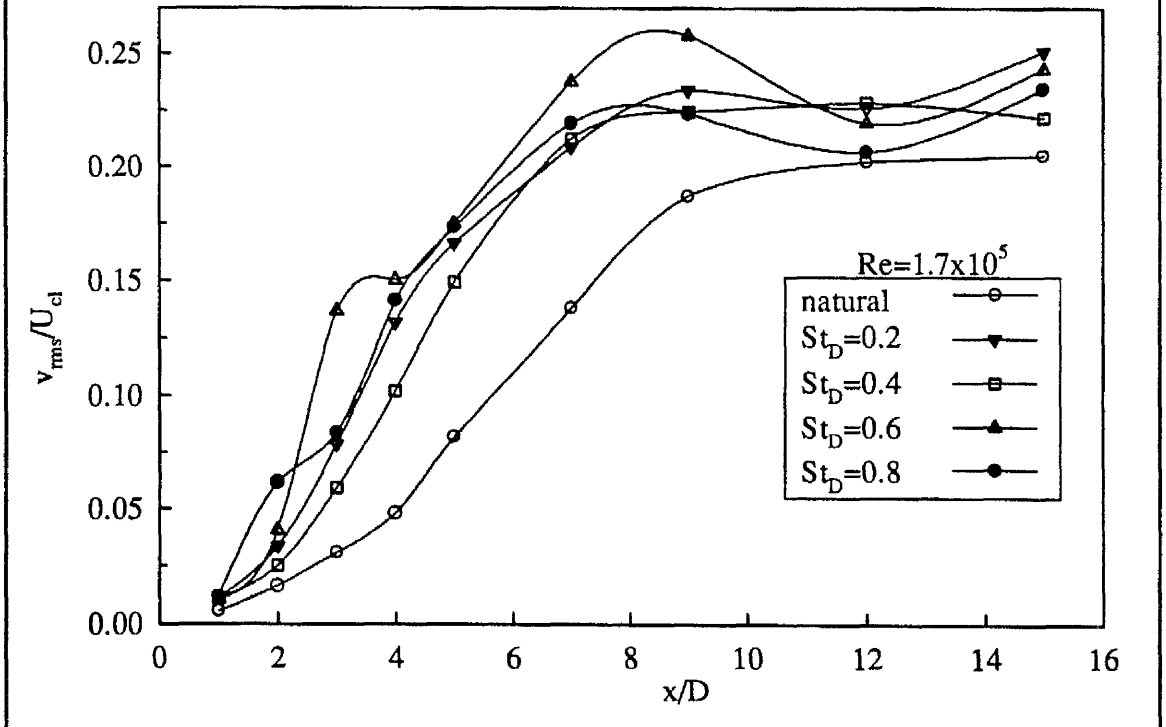

Figure 7.51. Turbulence intensity variation of the radial velocity component along the jet centre-line for different pulsation frequencies.

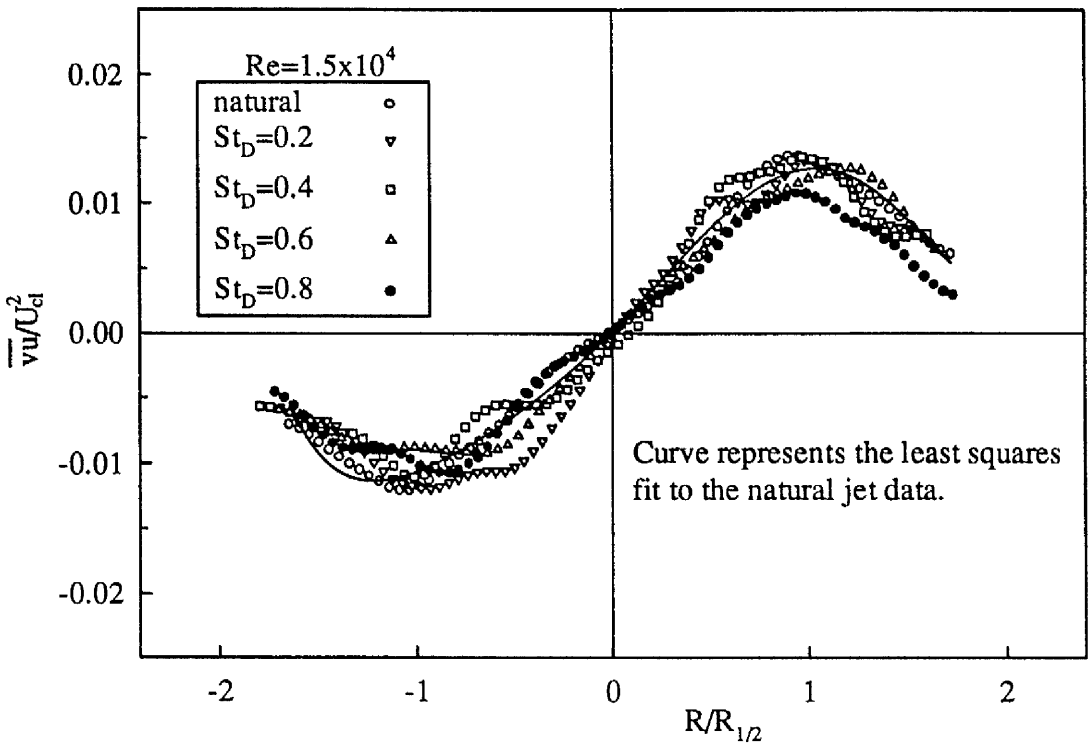

Figure 7.52. Radial distributions of the shear stress at x/D=3.0 for different pulsation frequencies.

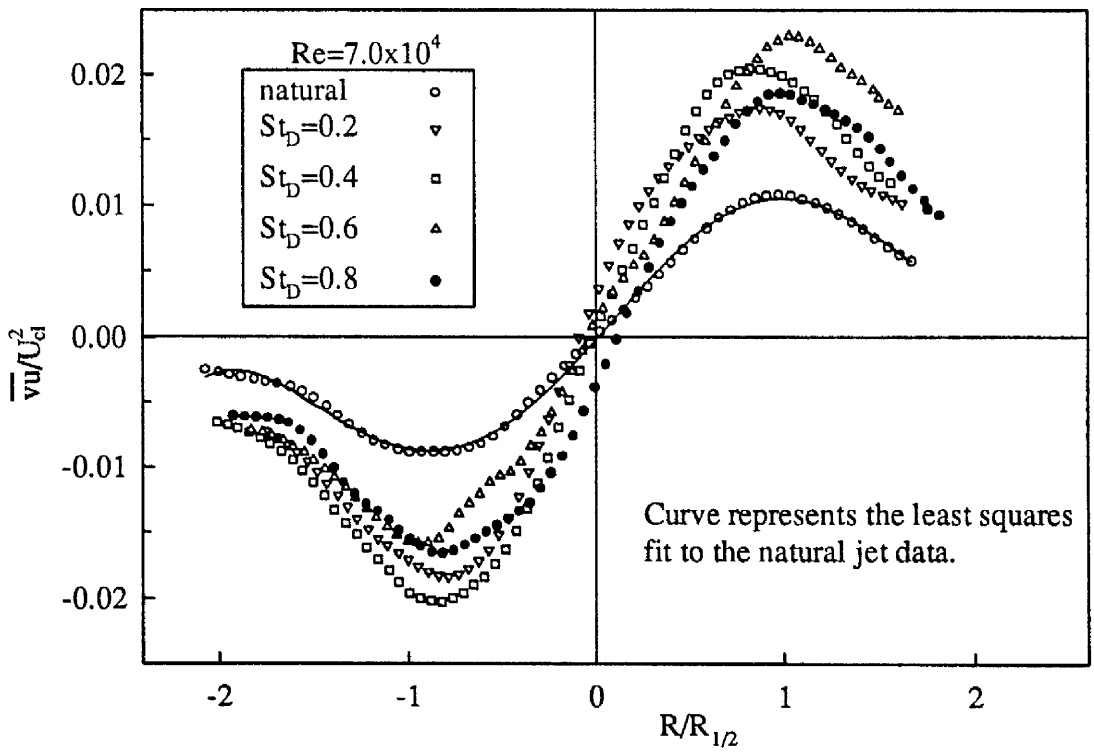

Figure 7.53. Radial distributions of the shear stress at x/D=5.0 for different pulsation frequencies.

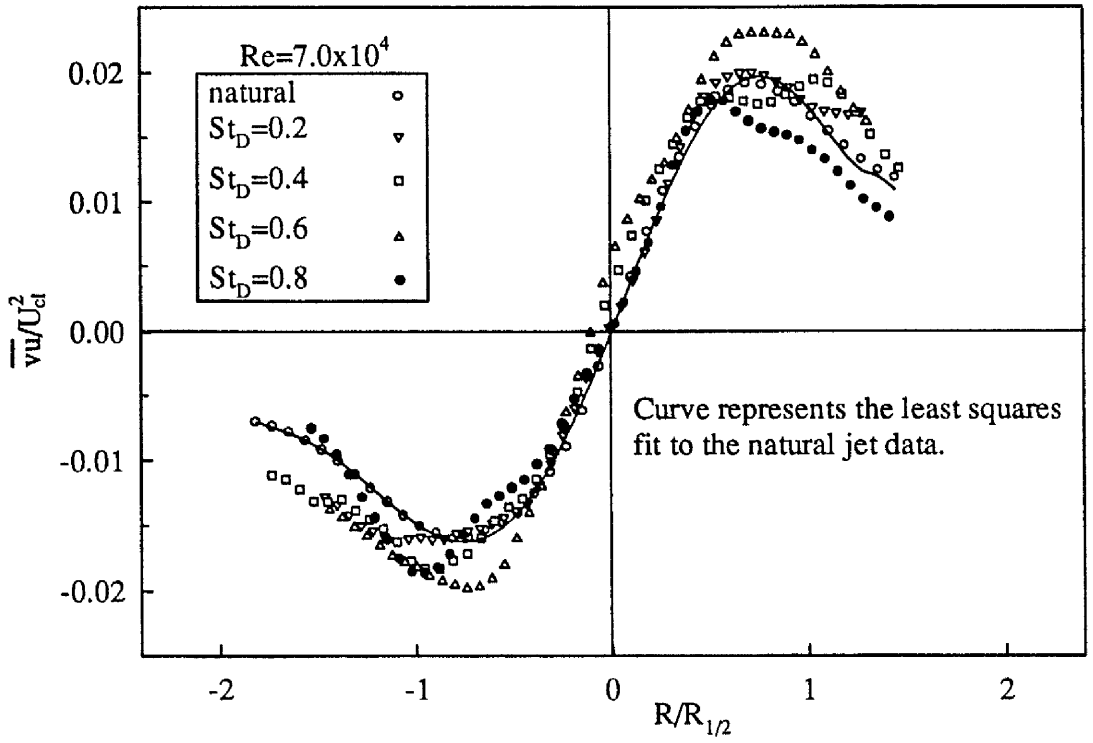

Figure 7.54. Radial distributions of the shear stress at x/D=12.0 for different pulsation frequencies.

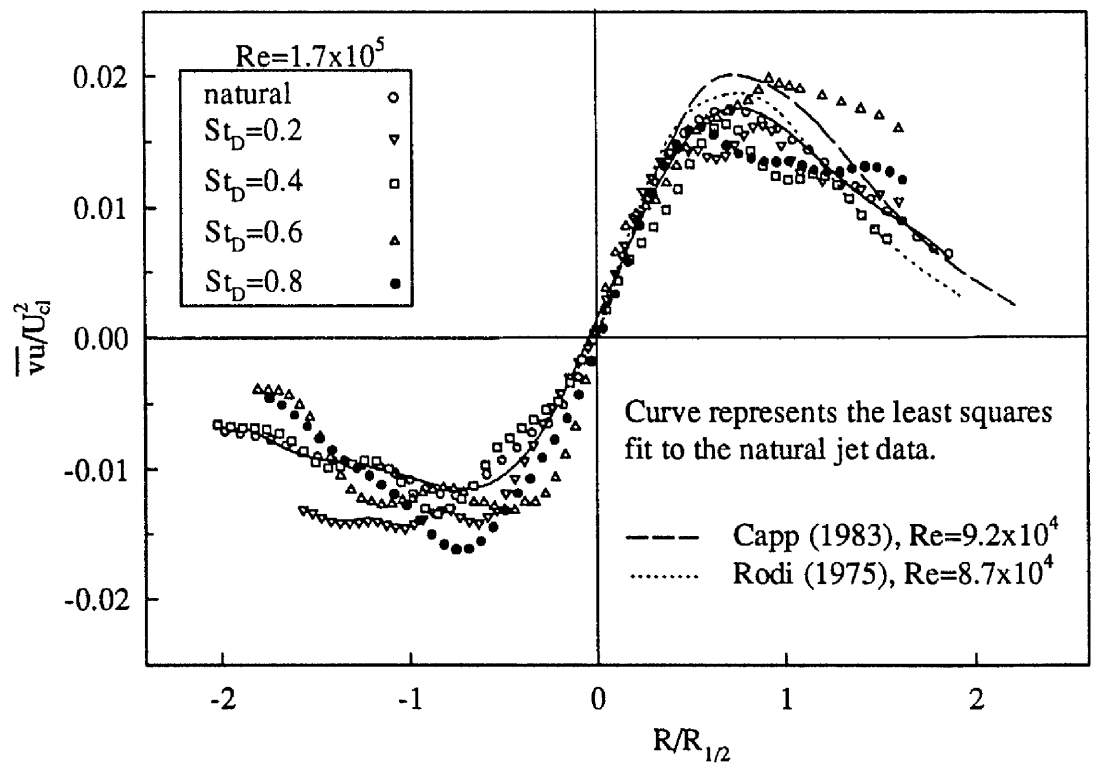

Figure 7.55. Radial distributions of the shear stress at x/D=15.0 for different pulsation frequencies.

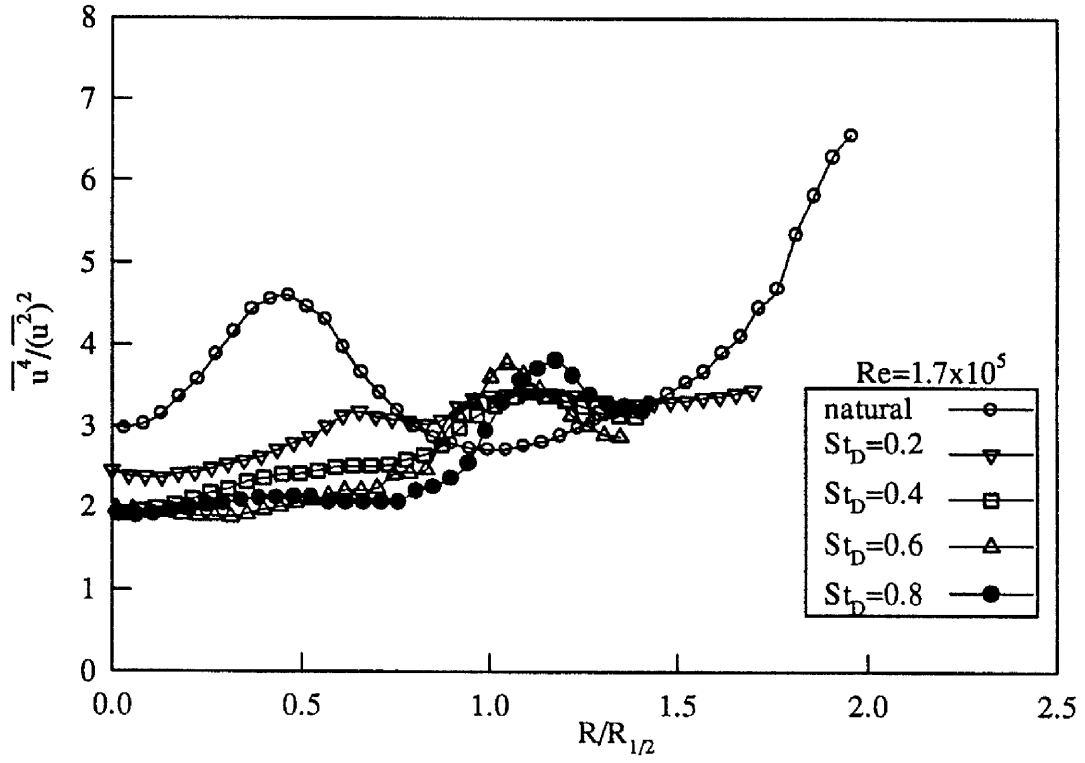

Figure 7.56. Flatness factor profiles at x/D=3.0, for different pulsation frequencies.

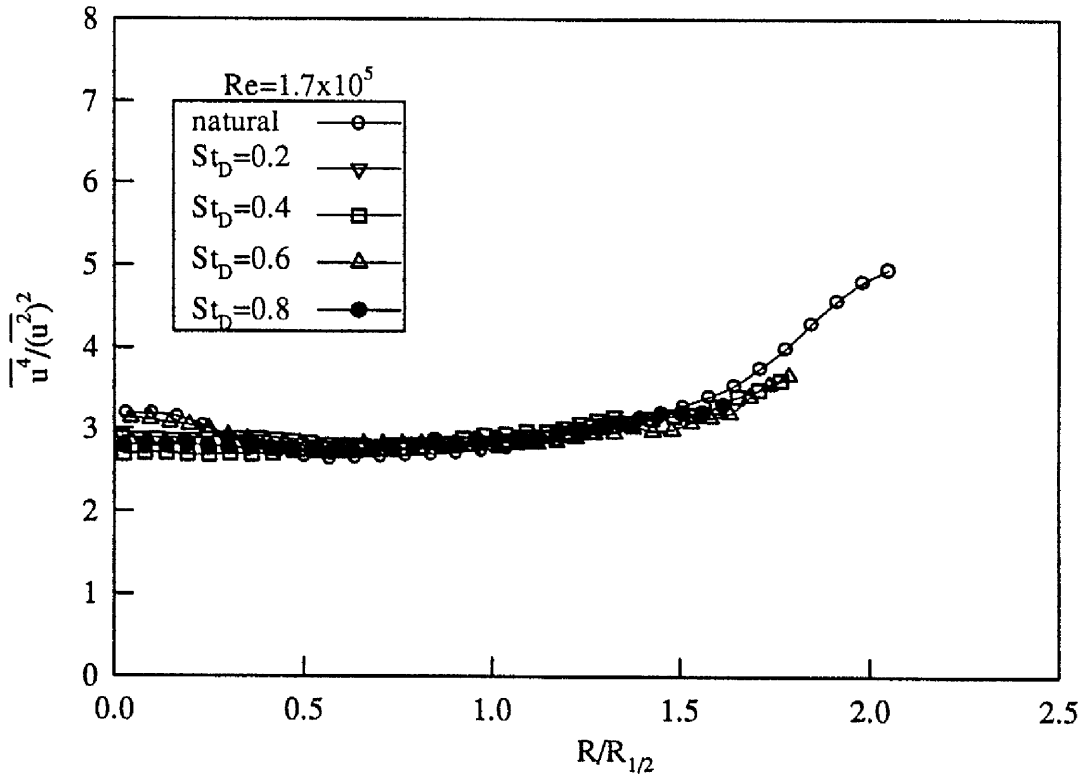

Figure 7.57. Flatness factor profiles at x/D=7.0, for different pulsation frequencies.

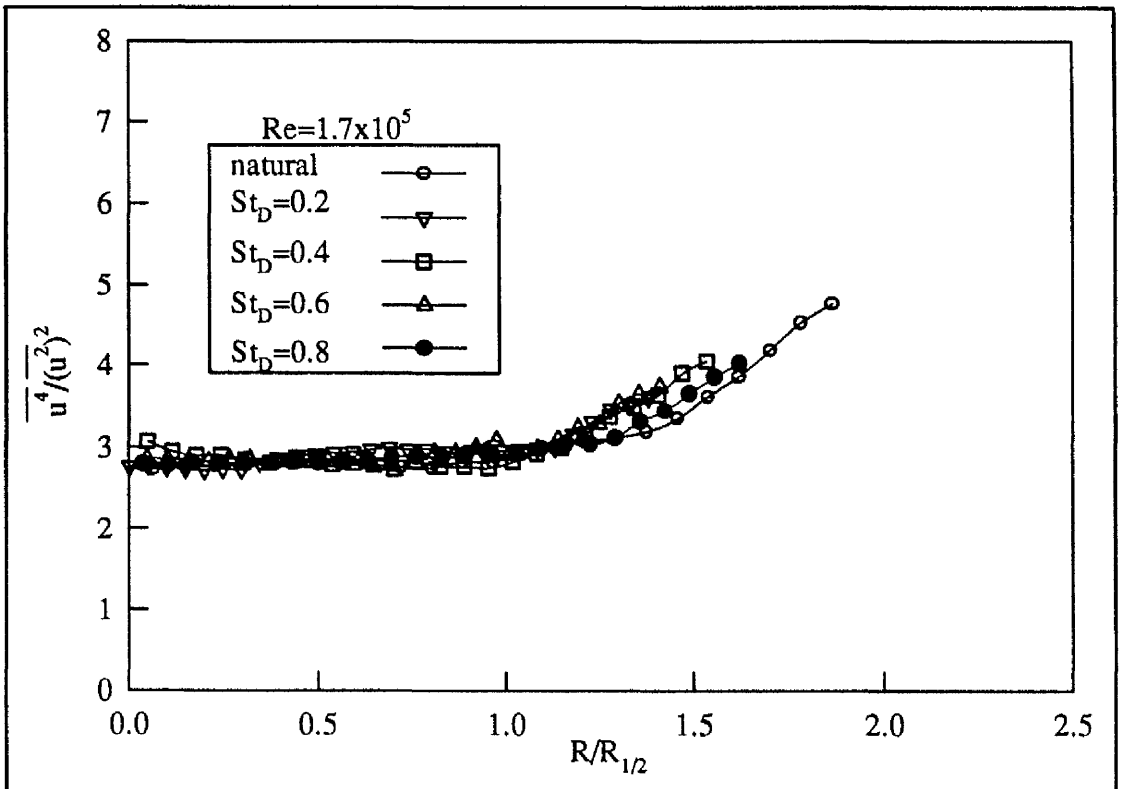

Figure 7.58. Flatness factor profiles at x/D=15.0, for different pulsation frequencies.

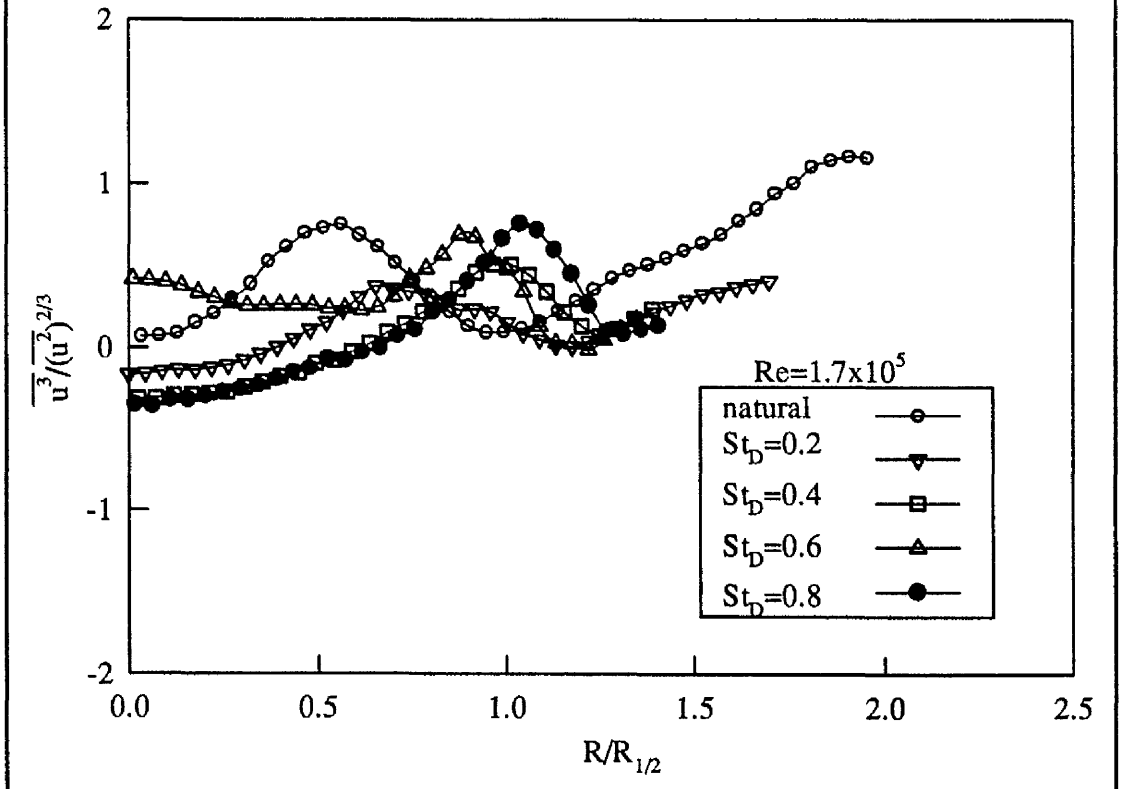

Figure 7.59. Skewness factor profiles at x/D=3.0, for different pulsation frequencies.

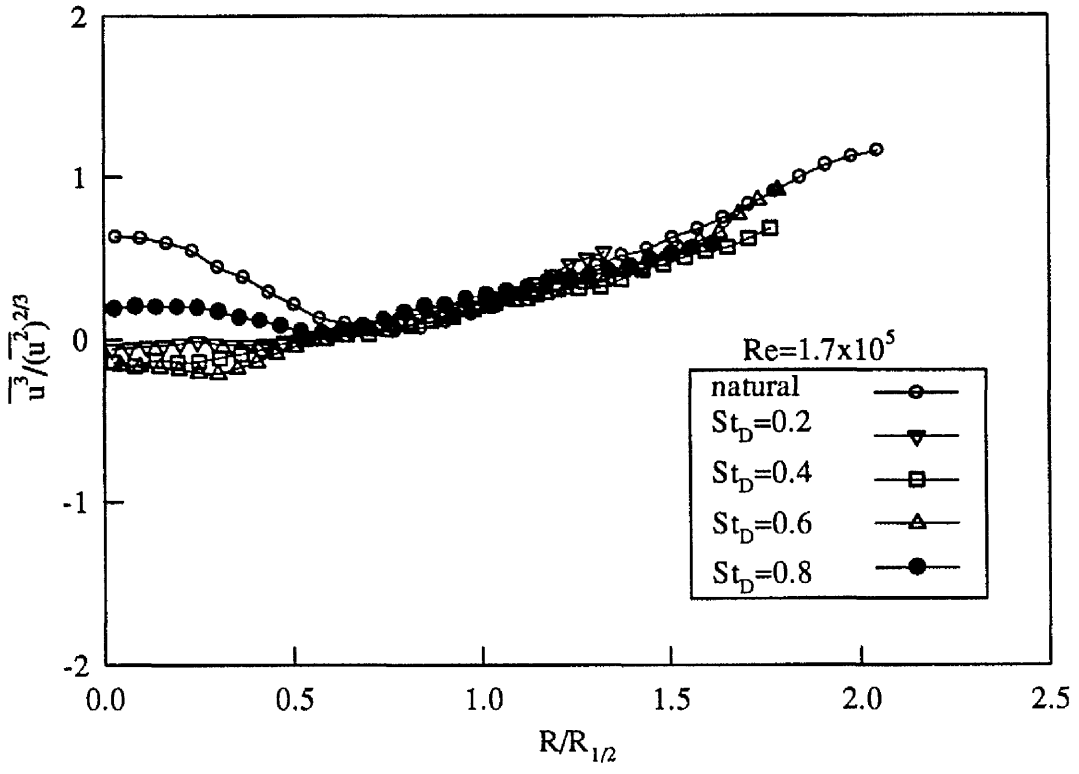

Figure 7.60. Skewness factor profiles at x/D=7.0, for different pulsation frequencies.

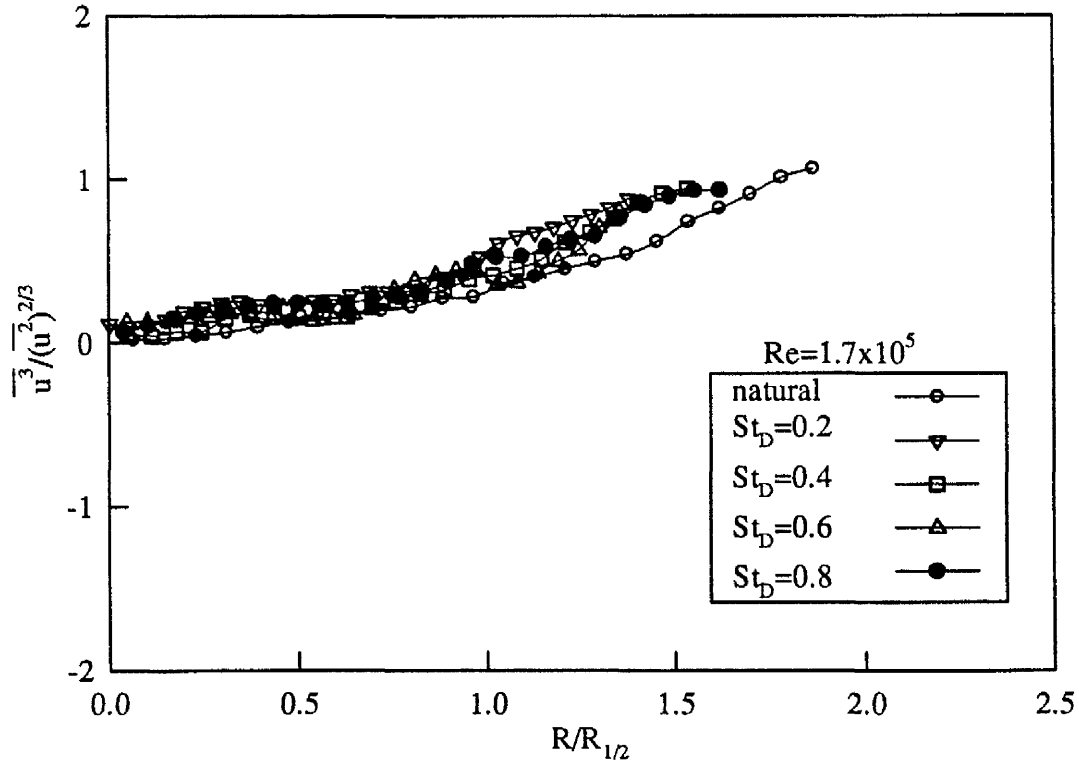

Figure 7.61. Skewness factor profiles at x/D=15.0, for different pulsation frequencies.

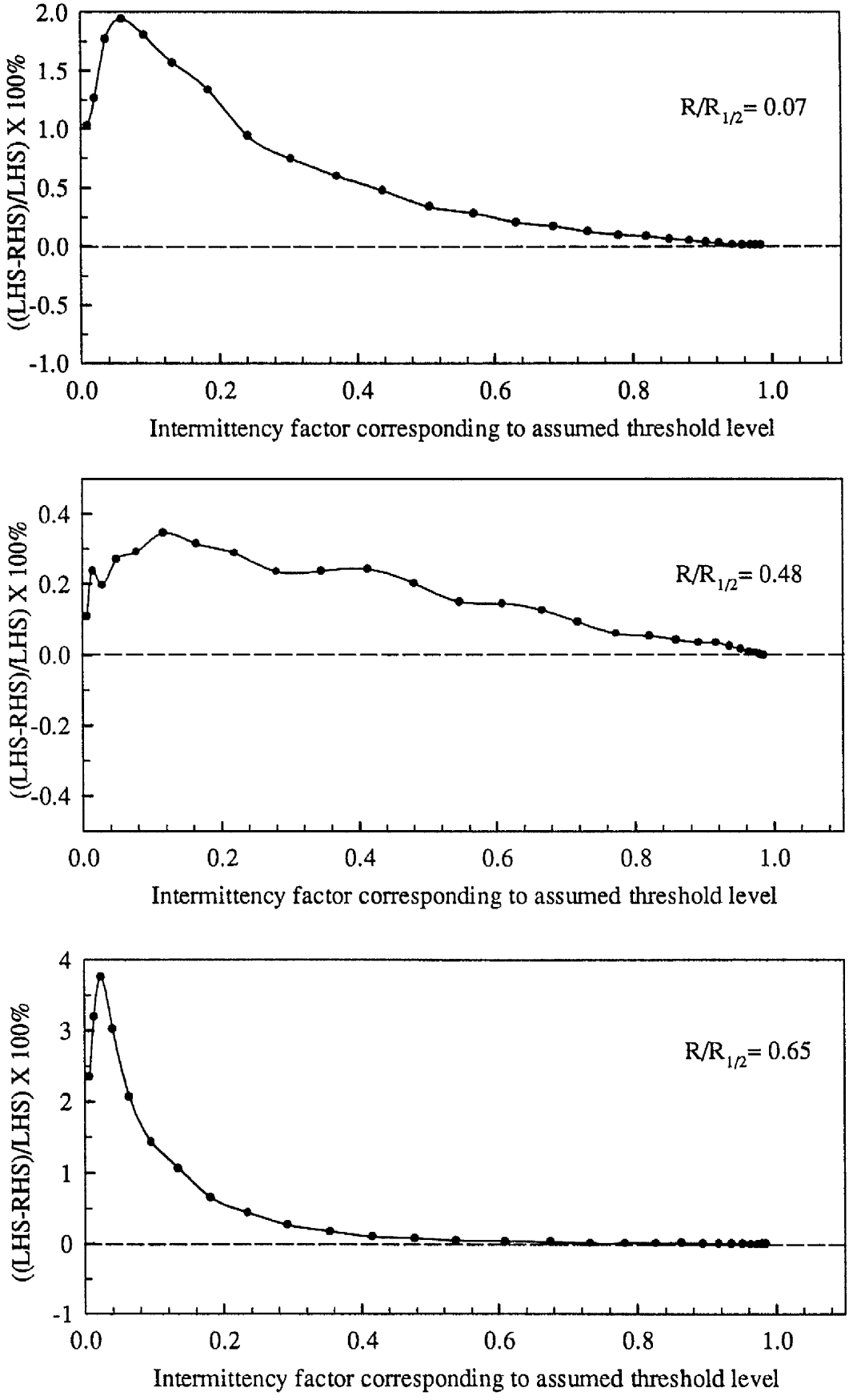

Figure 7.62. Variation of inequality error for natural jet at x/D=12.0, Re = 1.7×10^5.

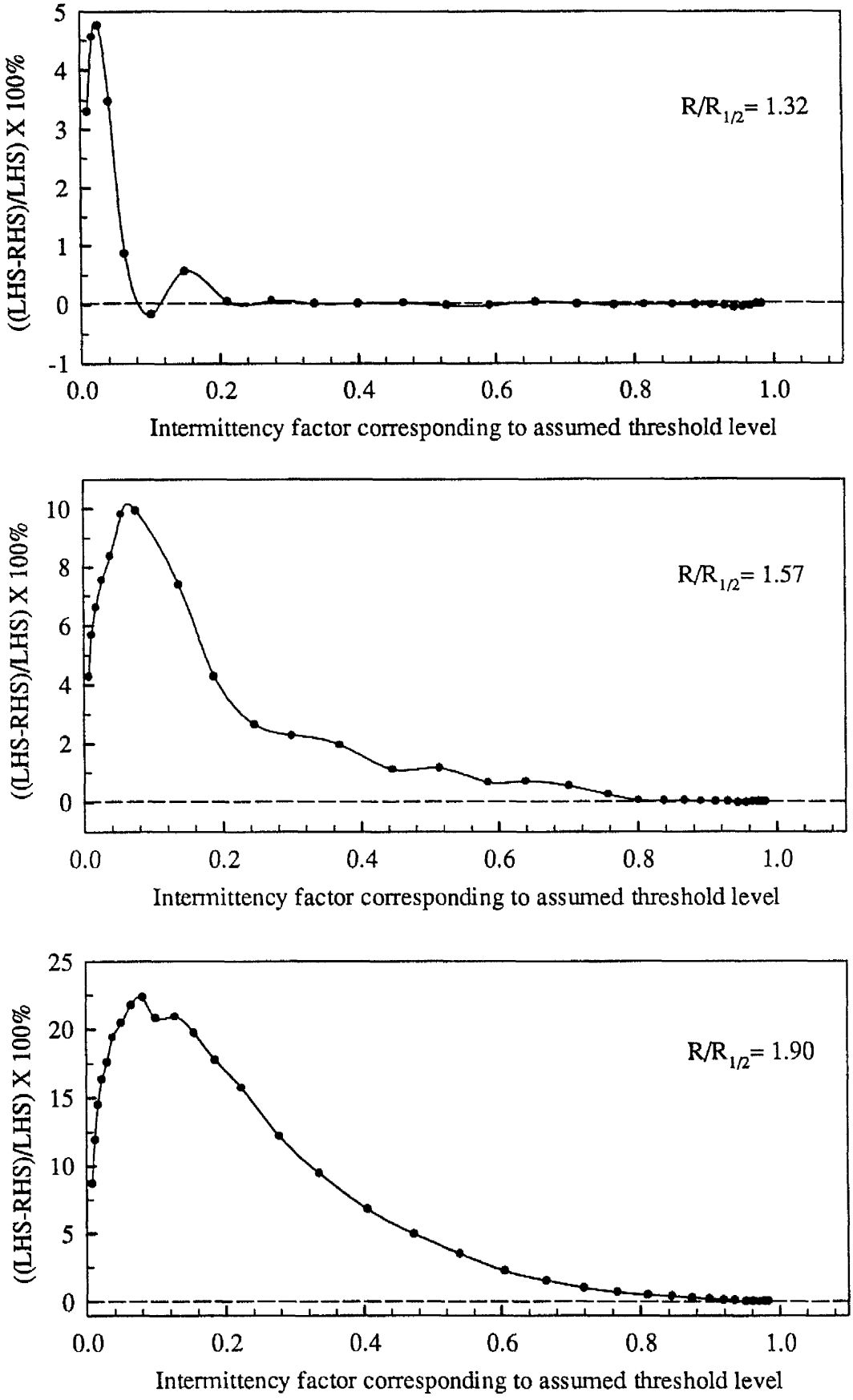

Figure 7.63. Variation of inequality error for natural jet at x/D=12.0, Re = 1.7×10^5.

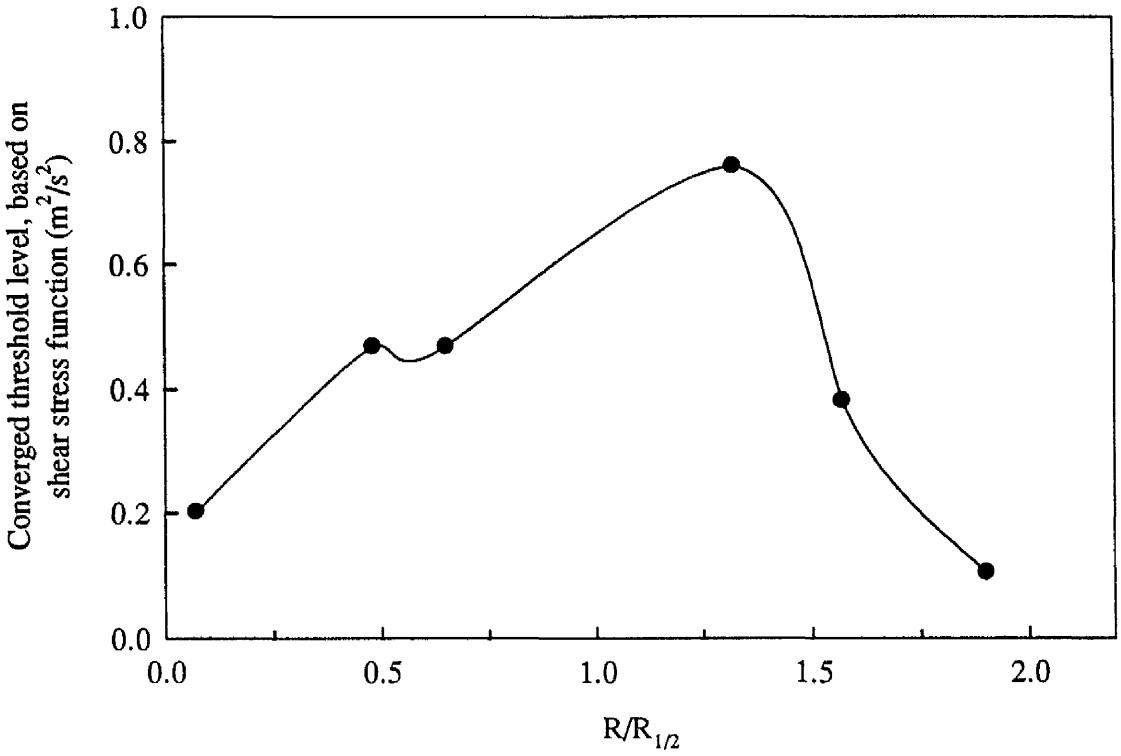

Figure 7.64. Radial distribution of the assumed threshold level required to achieve convergence at x/D=12.0, for natural jet, Re=$1.7x10^5$.

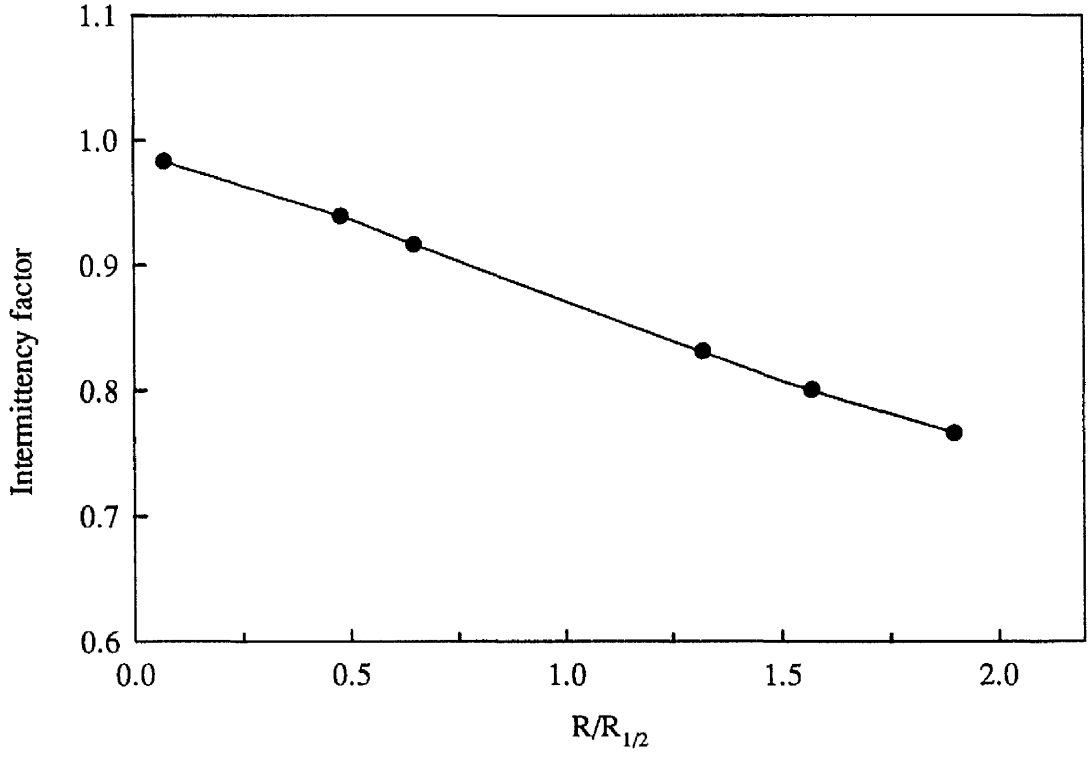

Figure 7.65. Radial distribution of the intermittency factor at x/D=12.0, for natural jet, Re=$1.7x10^5$.

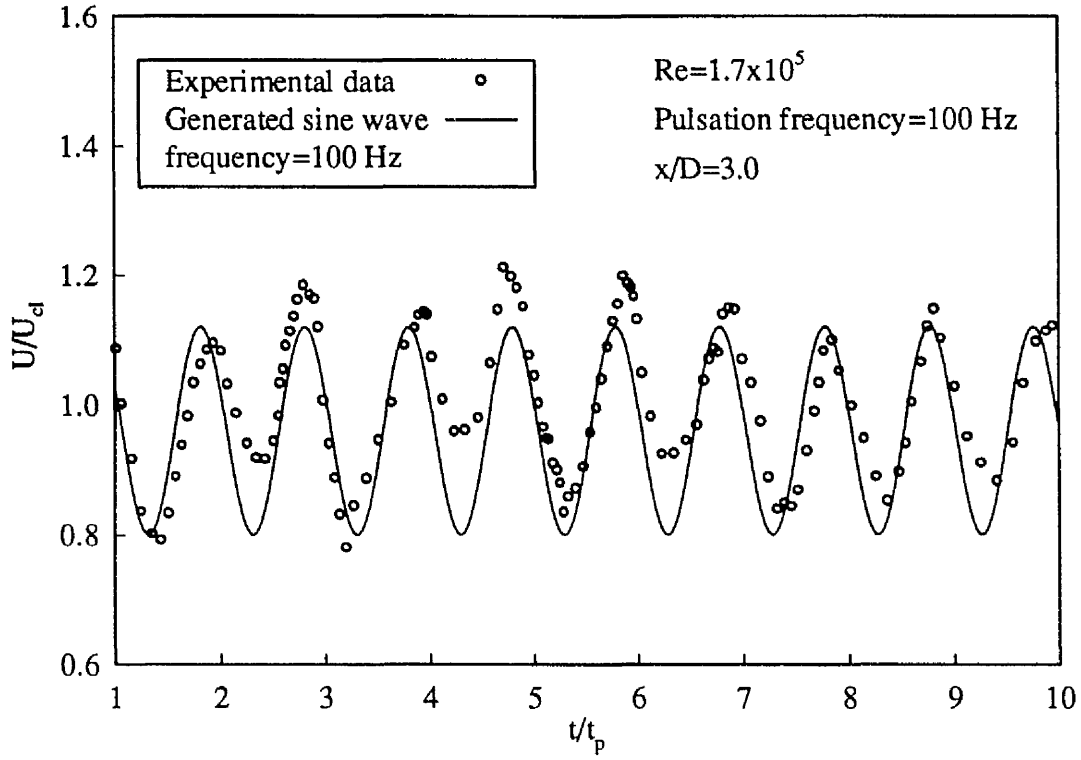

Figure 7.66. Time series to show variation of the instantaneous axial velocity component at the centre-line of the excited jet.

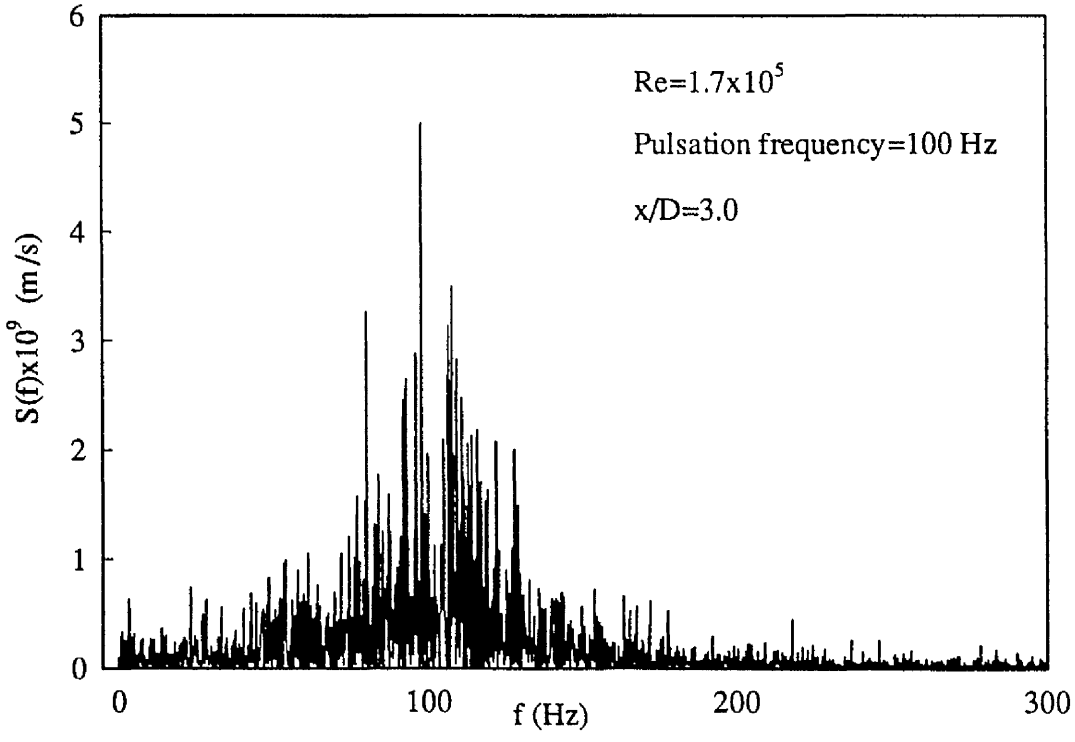

Figure 7.67. Spectrum for the conditions at centre-line of excited jet.

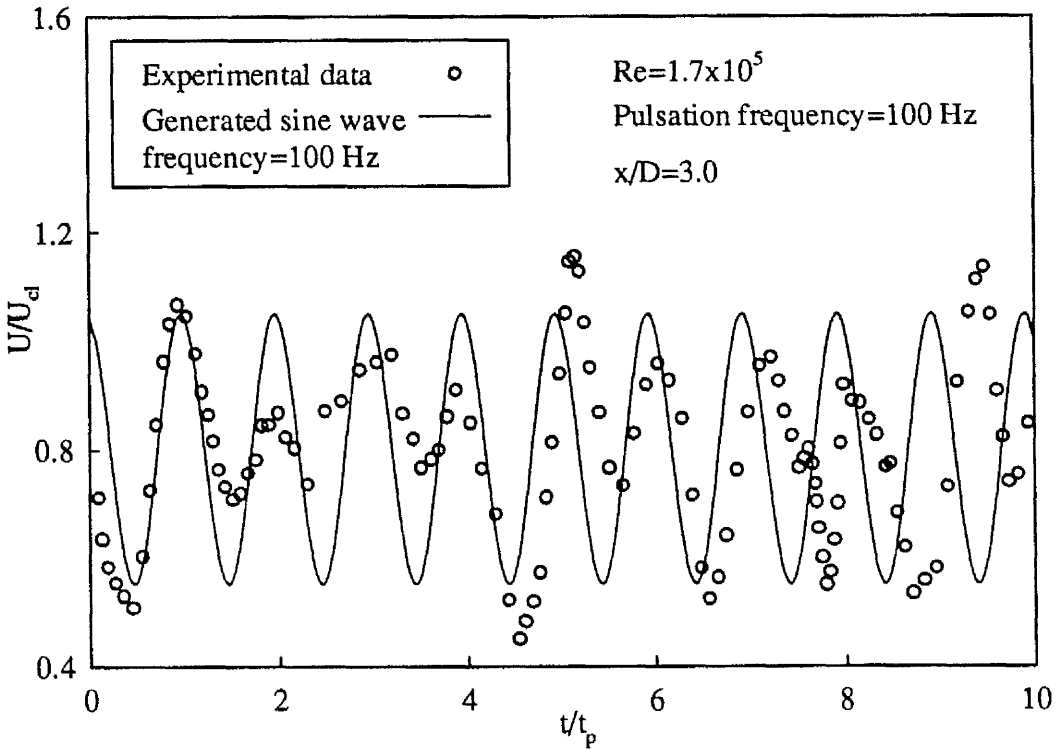

Figure 7.68. Time series to show variation of the instantaneous axial velocity component in the excited jet at $R/R_{1/2}$=0.7.

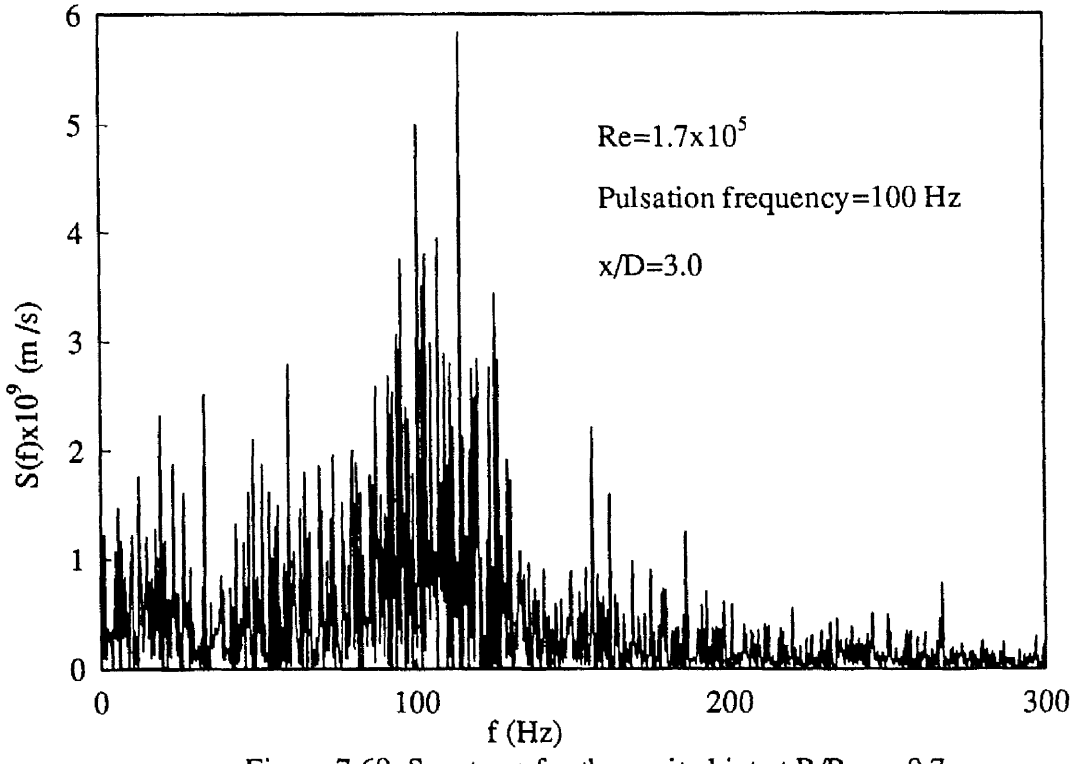

Figure 7.69. Spectrum for the excited jet at $R/R_{1/2}$ =0.7.

CHAPTER 8

FLOW VISUALISATION

CHAPTER EIGHT
FLOW VISUALISATION

Flow Visualisation is a potentially powerful technique for the study of fluid flow problems which enables information to be collected about the flow patterns across a whole plane rather than merely at a point in the flow as with most other methods. It gives information of a different nature from that which can be obtained from point measuring probes such as the hot film anemometer or laser Doppler anemometer. Both of these anemometry techniques provide time records of the local velocity level, while flow visualisation yields the history of the movement of a cloud of marked particles over a significant area of view. Thus, it was desirable that solid evidence in the form of visualised pictures should be obtained in connection with the LDA data to provide physical insight into the more global features of the flow. The flow visualisation, as will be seen at a later stage in this chapter, reveals how the toroidal vortices formed by pulsation and the coherent structures into which these vortices are transformed play a dominant role in the overall development of the shear layer, and are largely responsible for entrainment and mixing.

8.1 Experimental Set-up

The free jet air flow rig previously described in Chapter Three was used for the flow visualisation experiments. The commercial smoke generator described in section 3.4 was used to seed the flow. The smoke was injected through the secondary flow pipe, so that a good contrast could be obtained between the "puffs" of the secondary jet and the primary jet. Also, this method allowed the interface

between the edge of the jet and the surrounding fluid to be marked clearly. This was achieved by making a junction in the air pipe which supplies the secondary jet before it enters the rotating valve of the jet excitation mechanism - see section 3.3 and figure 3.4. Furthermore, the diameter of the pipe was reduced from 30.0mm to 10.0mm just before the junction to create a vacuum region into which the smoke was naturally drawn - see figure 8.1. This technique of introducing the smoke to mark the flow pattern has advantages over the conventional smoke wire technique which has been used in many previous studies, see for example, Szajner and Turner (1986) and Jeung (1993). It does not involve as many electrical connections, therefore it is easier to set-up and does not need high skill to operate. Finally, it provides a continuous stream of dense white smoke which suited the purpose of this investigation extremely well.

For improved contrast, the inside walls of the containment box was covered with black cardboard. Since it proved impossible to eliminate the background light coming from the laboratory windows, all the flow visualisation experiments were carried out after sunset.

A video camera was mounted on a tripod outside the containment box so as to view the flow region through a window in the containment box. The view was usually taken across a plane which formed a 45° angle with the streamwise flow direction. The camera was connected to a television screen, allowing instant monitoring of the visualisation and enabling the motion of flow to be recorded for further processing. Figure 8.1 shows the arrangement of the flow visualisation apparatus.

8.2 Laser Sheet Generator

One of the most critical requirements for flow visualisation photography is to obtain sufficient intensity of light on the subject of interest. Early flow visualisation studies employed several different type of light source depending upon the particular test being conducted. However, the two most widely used light sources were the stroboscope - see for example Mueller (1989) - and high intensity short duration flash lamps. The latter types of light source was used by Szajner and Turner (1986) to obtain still photographs of an aerodynamically excited jet flow. Their light source was synchronized with the shutter of a camera and operated similarly to any camera using an electronic flash.

The most significant developments in the field of smoke visualization in the past two decades have occurred because of the introduction of the laser. Although other light sources have been used for many years to produce a narrow sheet of light, the very small rate of spread of a laser beam, together with the variety of power levels available has had a dramatic effect on flow visualization.

The required sheet of laser light is usually produced by reflecting the laser beam from a segment of cylinder as illustrated in figure 8.2. Two methods are commonly used to create the laser light sheet. Firstly, it can be in the form of a continuous light sheet - see for example Geropp and Leder (1987), Seiler et al (1990), and Haynes and Turner (1992). Secondly, it can be in the form of a short duration pulsed light sheet - see for example Grant and Smith (1987) and Shand and Ereaut (1990).

The laser light sheet used in the present investigation was of the continuous

form. This sheet was produced by a light sheet generator as shown in figures 8.2 and 8.3. Initially, the raw laser beam was brought to the containment box by the fibre link in the same fashion as had been used for the LDA measurements - see figure 5.3 and section 5.6. The laser sheet generator was made of a metal box which has a rectangular slot from one end to allow the launch of the light sheet. The box also has a hole at the other end, enabling the fibre which carries the laser beam to be fitted. A brass disk is fixed inside the metal box which carries a set of four mirrors. These mirrors have different radii of curvature which, when chosen appropriately, enable the production of different dimensions of laser sheet. Now the radius of curvature is inversely proportional to the divergence angle of the laser light sheet. For example, a mirror with a bigger curvature gives a narrower, smaller divergence angle light sheet, which is the case of mirror number 1 as shown in figure 8.3. As the curvature of the mirror is reduced, so the light sheet becomes wider with a bigger divergence angle. The different curvatures of the mirrors, numbered from 1 to 4 can be seen in figure 8.3.

When the laser beam enters the box, it is reflected by a plane mirror to one of the curved mirrors on the brass disk: the particular mirror is selected to suit the arrangement of the flow and the light sheet. For example, mirror number 1 was used to visualise the near field of the flow ($x/D \leq 4$), and mirror number 4 (cylindrical rod) was used to visualise the full range of the working section, as will be discussed further in section 8.4. The light sheet generator is so designed that selection of the mirror can be achieved manually by rotating a knob attached to the brass disk.

The advantages of this generator (built in-house) is that it offers a simple and compact way of producing a light sheet from the laser source. The equipment is

easily transported and can be used to produce a range of light sheets with different angles of divergence. Above all, the intensity losses of the laser light in the generating system are small (about 10%), see Tollerfield and Turner (1991).

8.3 Experimental Programme

The position of the laser sheet relative to the nozzle outlet plane is shown in figure 8.1. The laser light sheet was launched towards the nozzle from the opposite side, in the same streamwise flow plane (y-z plane), hence the laser sheet and the streamwise flow direction share a common axis.

The pictures presented in the succeeding section were initially captured by a video camera, which was connected to a monitor and a video recorder. The video film[1] was then played back and relevant frames were chosen and digitised using a frame grabber which interfaced to a PC 486. From this digitised image, the printer, was used to produce the hard copies which are presented in the following section.

Two planes of jet flow were illuminated at each experiment. The first is the plane normal to the nozzle plane, meaning it passes through the centre-line of the nozzle. The second plane is parallel to the first and cuts through the edge of the jet to show the azimuthal distribution of the toroidal vortices formed by the pulsed secondary jet surrounding the primary jet.

Both the initial region ($x/D \leq 4$) and the full range of the axial distance ($x/D \leq 15$) were filmed. The initial region was illuminated by the laser sheet produced from mirror number 2 and the whole flow region was illuminated using

[1]The full events of the flow visualisation experiments for the experimental program mentioned in section 5.7 can be seen on a video film.

mirror number 4.

8.4 Experimental Results

Figure 8.4 shows the large scale structure of the toroidal vortex formed by the pulsation of the secondary jet at $St_D = 0.2$ (f = 4.5 Hz) for $Re = 1.5x10^4$. This sequence of video frames covers the initial region of the jet up to $x/D \approx 3.0$ and can be seen to capture two "puffs" of the pulsating jet. The first vortex is formed at approximately x/D = 0.6, and its developed version can be seen at $x/D \approx 2.3$. As the toroidal vortex moves downstream from the nozzle, it produces flow rotation about its circular axis which lies in a plane normal to the central axis of the jet. During this rotational motion, the toroidal vortex is seen to draw in the surrounding air and therefore plays a major role in the entrainment of free stream fluid - see also section 7.5. Enhanced mixing also occurs due to the large interfacial areas of the streamwise structures. Thus, the toroidal vortex is seen to undergo a violent transition resulting in the sudden diffusion of the smoke traces. The vortex can not be identified further than $x/D \approx 2.3$ downstream.

A broader view of the events shown in figure 8.4 are presented in figure 8.5. In this photograph, the toroidal vortices are followed further downstream up to $x/D \approx 6.5$. The toroidal vortices are seen to remain as well defined "coherent" structures up to a distance of $x/D \approx 3.0$. The roll-up of the vortices continue until the entire core of the jet flow has been consumed (or entrained by the vortex) at which point only random turbulence is revealed by the smoke trace. Beyond a distance of $x/D \approx 3.2$, the smoke traces become too diffuse to show any orderly structure of the jet flow.

Figure 8.6 presents a picture of the flow for a plane of the flow close to the edge of the jet but lying parallel to the plane shown in figure 8.5. The first batch of cloud represents the first pulse and the second batch represents the second pulse. Focusing on figures 8.4 and 8.6 at the same time, good azimuthally uniform toroidal vortices surrounding the primary jet can be imagined.

The lateral growth of the toroidal vortices shown in figure 8.6 can be seen more clearly in figure 8.7. The experimental conditions corresponding to this photograph were, $Re = 1.5x10^4$ and $St_D = 0.4$, and the view covers the initial jet development region up to $x/D \approx 3.0$ in the same plane as that of figure 8.6. Figure 8.8 shows the flow region of the jet slightly downstream of there, where the smoke is still visible, and extends up to $x/D \approx 7.0$. However, in this case the jet was excited at a higher frequency so that $St_D = 0.6$ but with the same Reynolds number. It can be seen clearly that the toroidal vortices initiated by pulsing the secondary jet at the nozzle exit plane, retain a regular coherent structure up to approximately 3.3 nozzle diameters downstream. For positions beyond $x/D = 5.0$, this regular structure is practically lost. The toroidal vortex just after $x/D = 3.3$ undergoes fusion and a large cloud is observed, inferring that almost the entire core of the jet has disappeared and the mixing region shown in figure 1.2 has penetrated the centre-line of the jet.

Figures 8.9 to 8.12 show that, for increasing Reynolds number, the smoke does not reveal any structure and, for most of the time, the coherent structure of the toroidal vortices is much less clearly observable than the case with lower Reynolds number. For this reason, pictures for the highest Reynolds number condition $Re = 1.7x10^5$ could not be obtained.

Regions of intense entrainment measured by LDA - see for example figure 7.31, in which elements of the surrounding atmosphere are engulfed by the larger scale structures, are revealed by the lateral spread of the smoke. The effect of excitation on the rate of spread of the jet - see for example 7.27 in the axial direction was also observed.

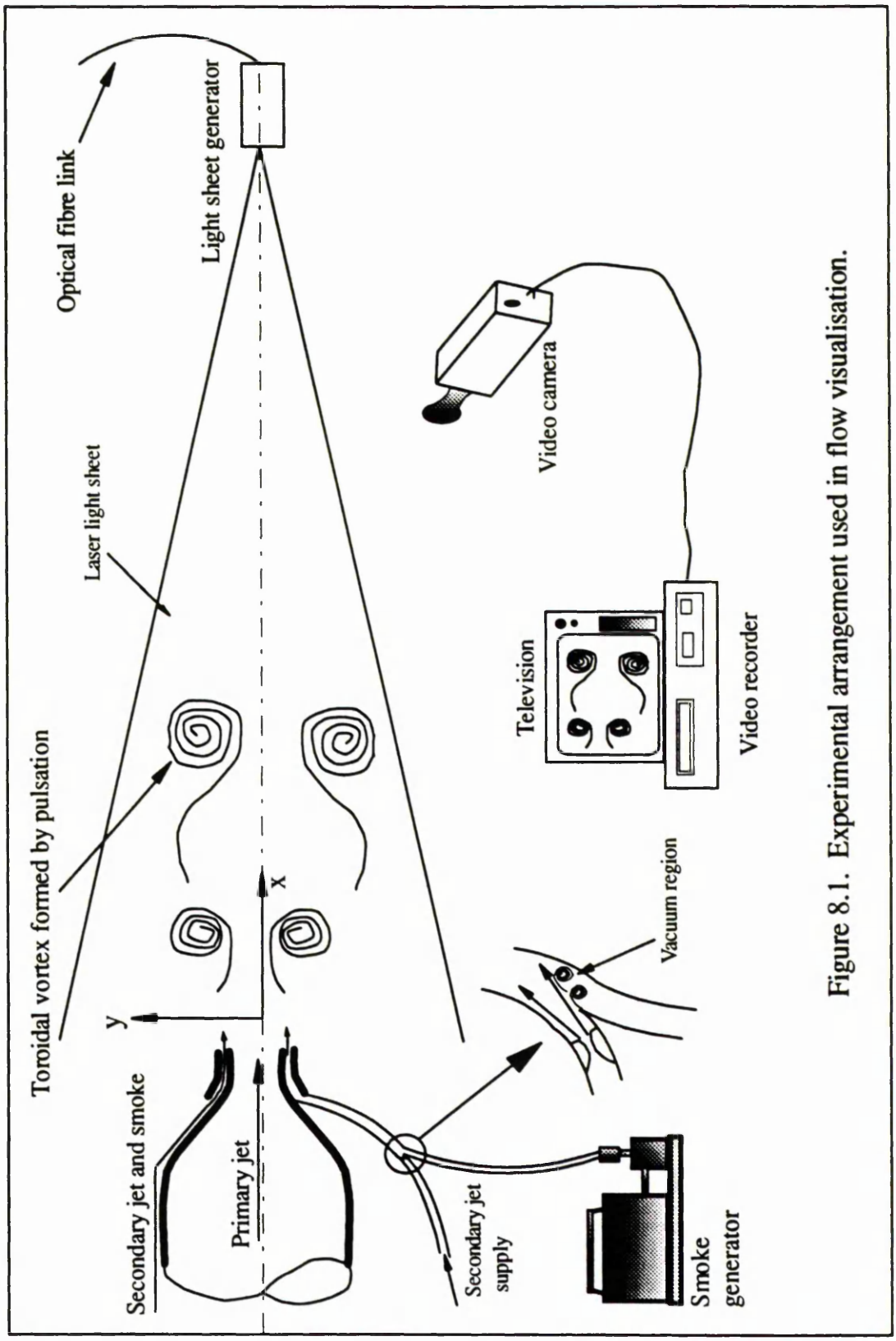

Figure 8.1. Experimental arrangement used in flow visualisation.

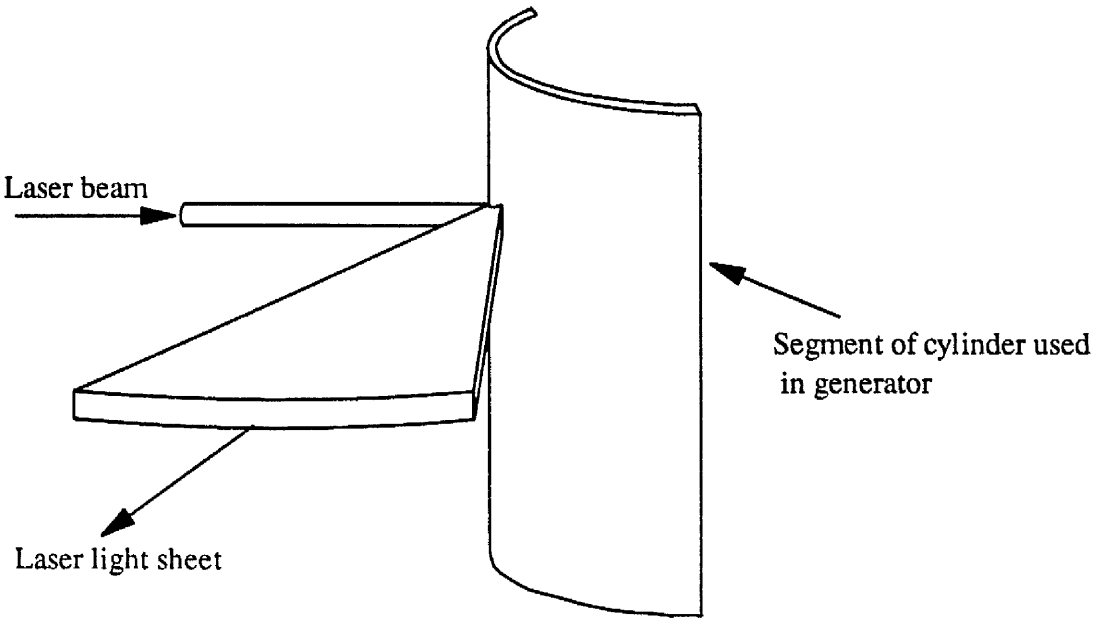

Figure 8.2. Principle of producing a light sheet
using a segment of cylindrical mirror.

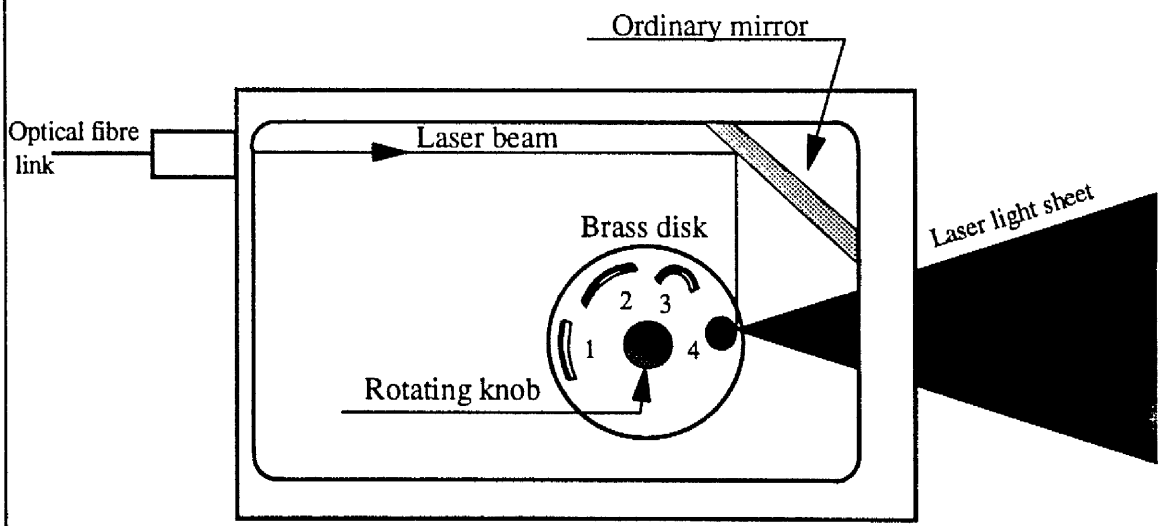

NB. items 1,2,3 are segments of glass tube-surface silvered.
item 4 is a surface silvered glass rod.

Figure 8.3. Side view of the light sheet generator.

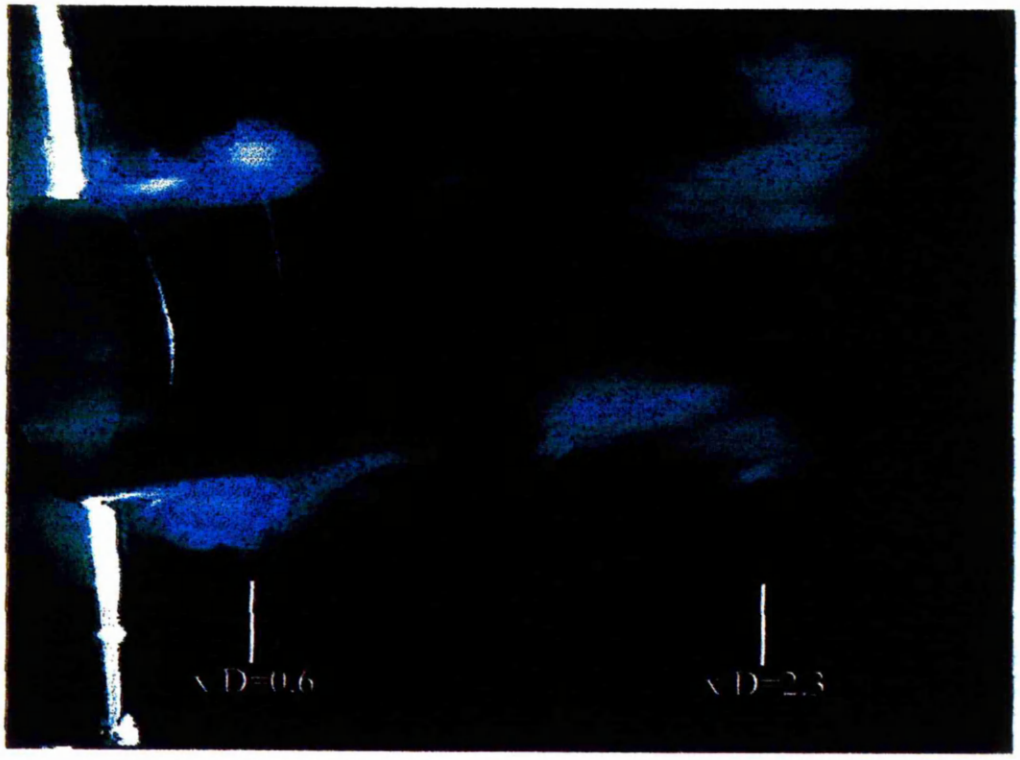

Figure 8.4. Picture of excited jet at $St_D = 0.2$, taken in the initial region at $Re = 1.5 \times 10^4$.

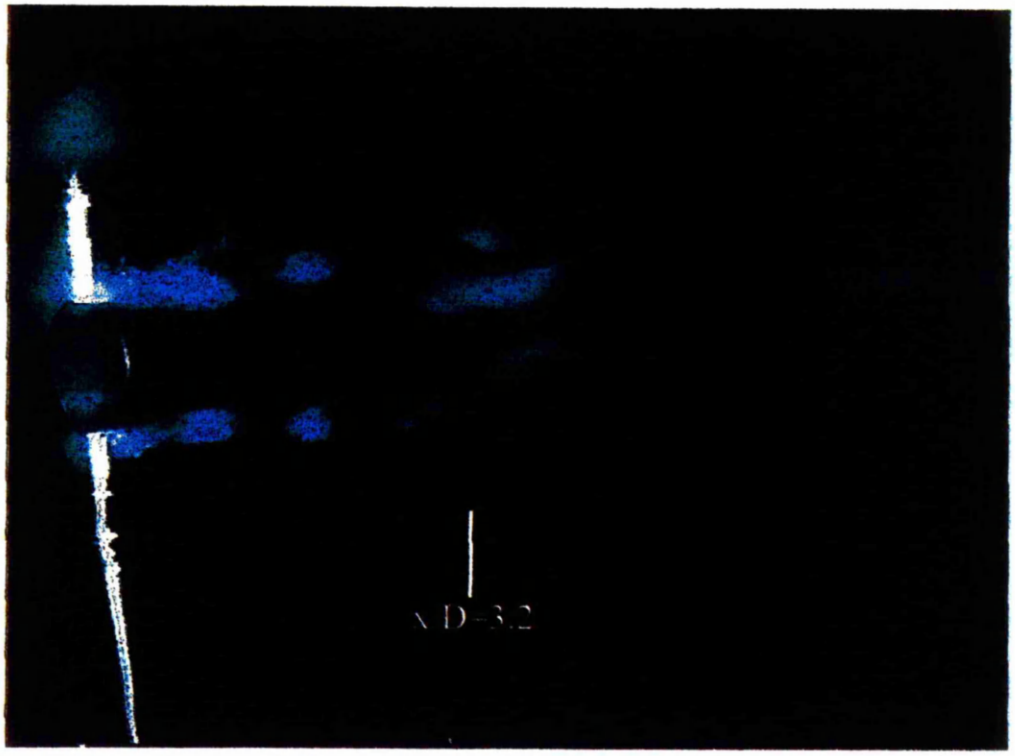

Figure 8.5. Picture of the excited jet at $St_D = 0.2$, $Re = 1.5 \times 10^4$, taken for the flow region 0.0 <x/D>6.5, before the disappearance of the smoke trace.

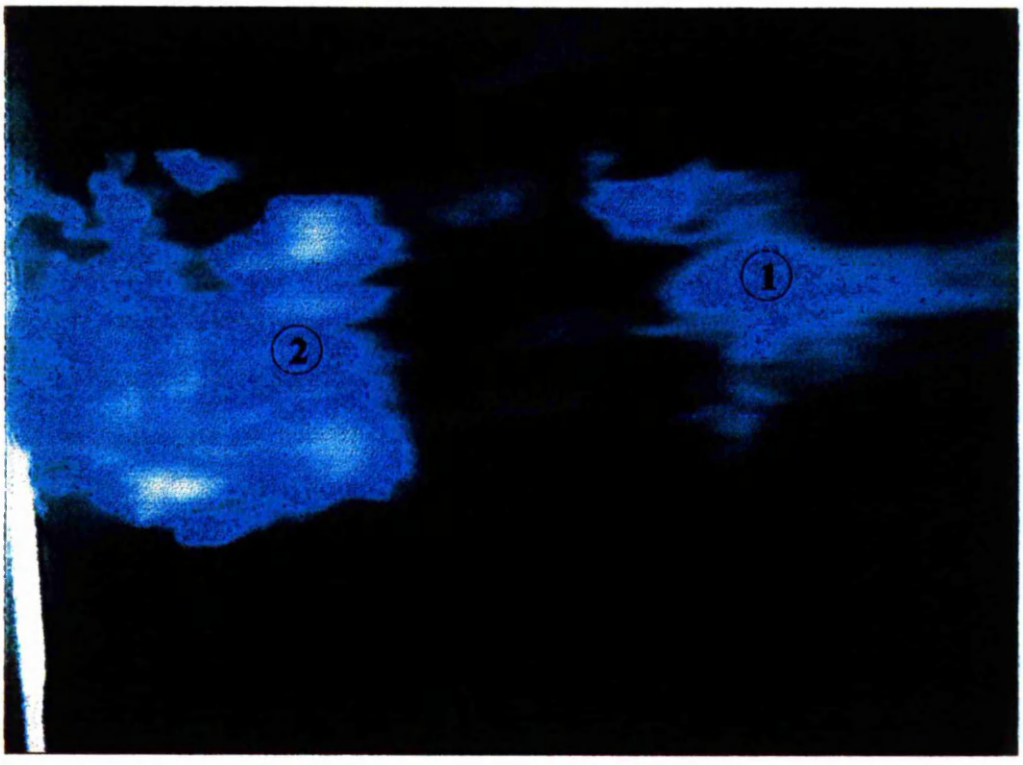

Figure 8.6. Excitation at $St_D = 0.4$, $Re = 1.5 \times 10^4$. The laser sheet is directed at the edge of the primary jet to show the formation of the azimuthal toroidal vortices surrounding primary jet .

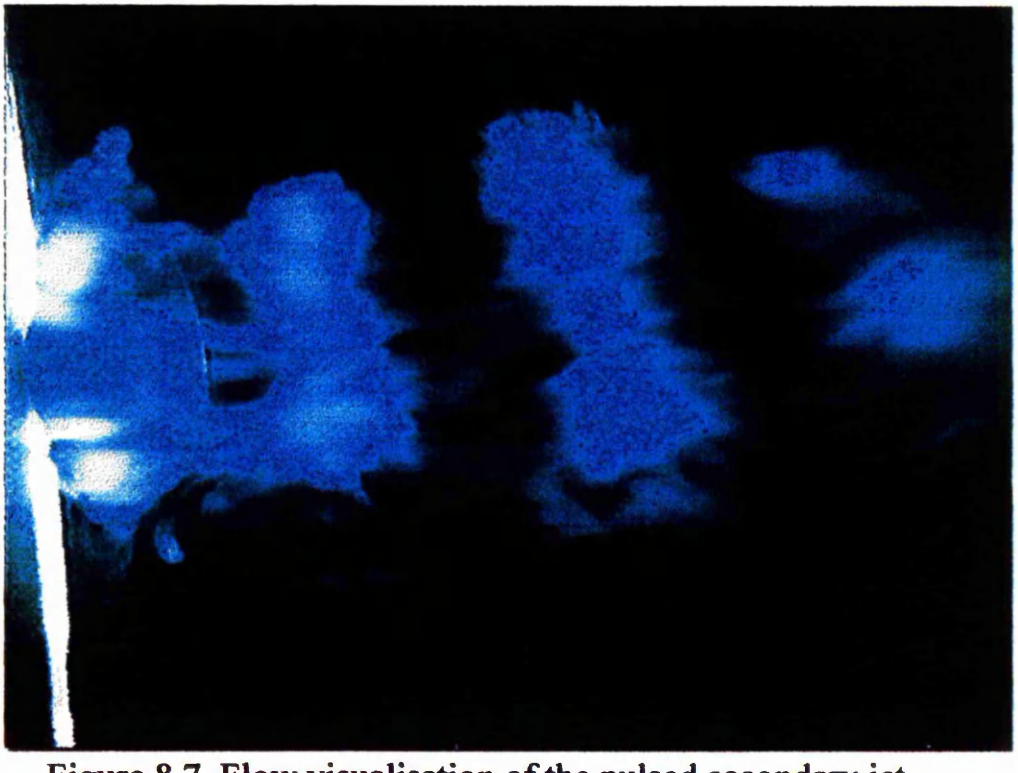

Figure 8.7. Flow visualisation of the pulsed secondary jet at $St_D = 0.4$, $Re=1.5x10^4$.

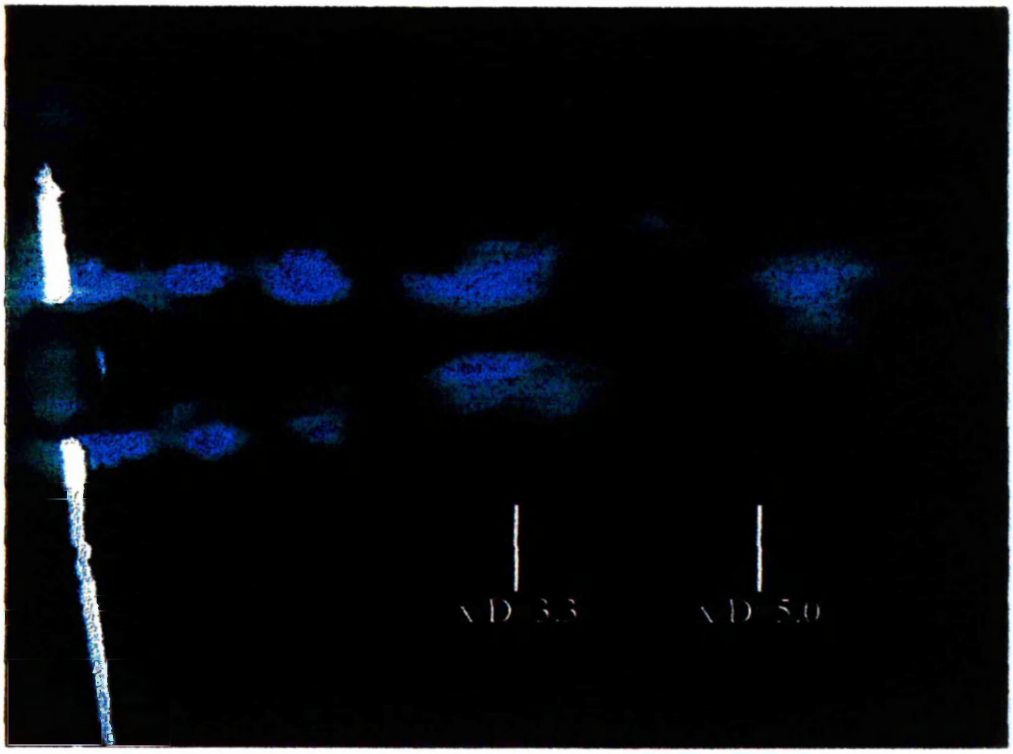

Figure 8.8. Excitation at $St_D = 0.6$, Re = $1.5x10^4$. This picture was taken in the region up to x/D = 7.0, where the smoke was still visible.

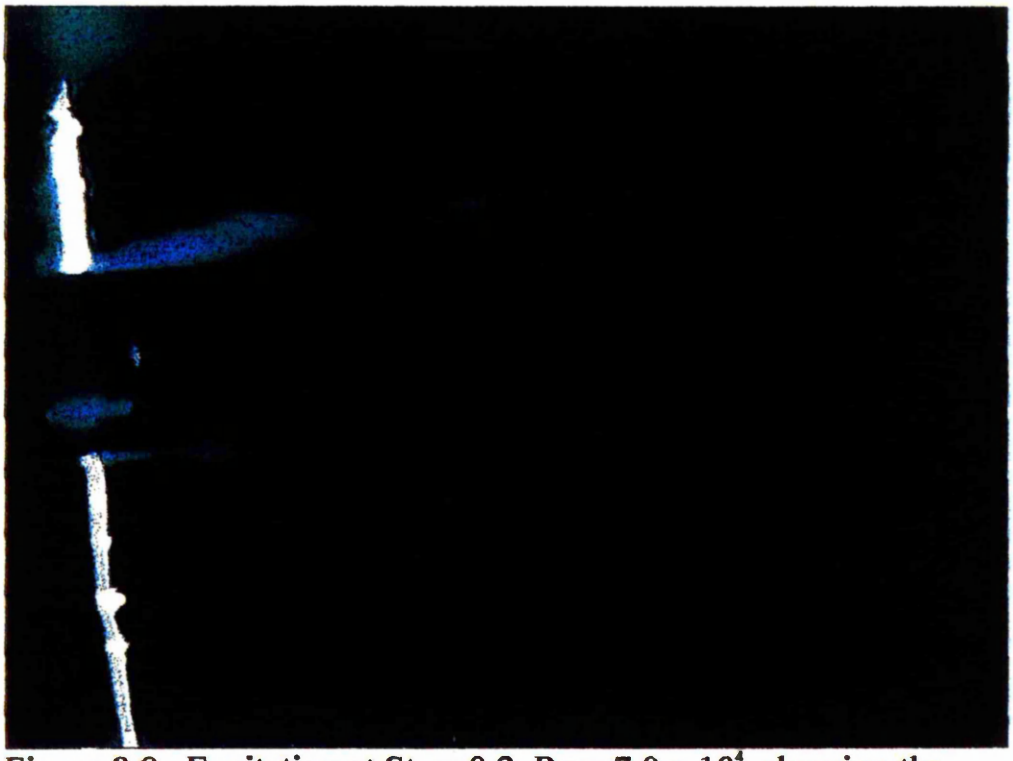

Figure 8.9. Excitation at $St_D = 0.2$, Re = 7.0×10^4, showing the initial development region.

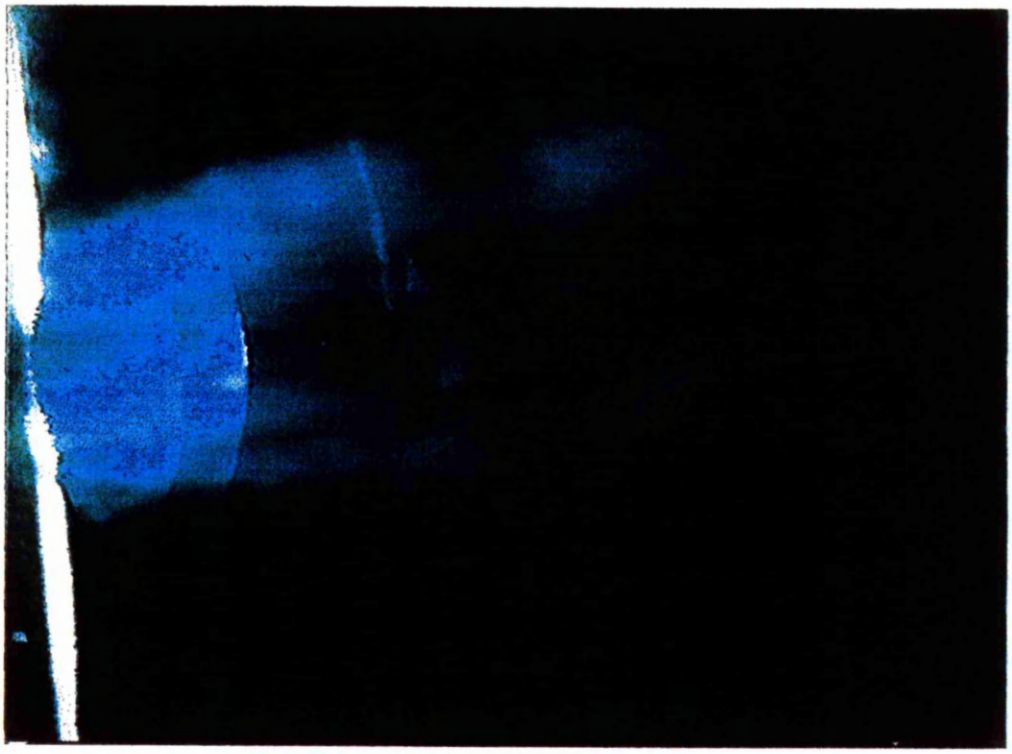

Figure 8.10. Flow visualisation of the secondary jet at $St_D = 0.2$, $Re = 7.0x10^4$.

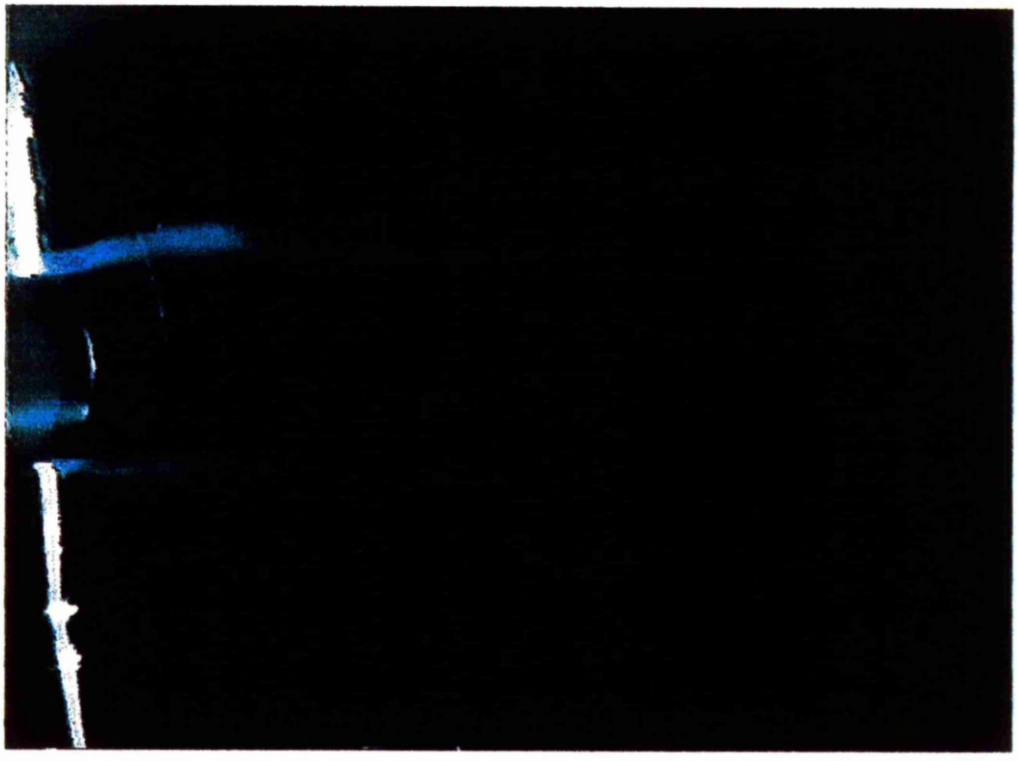

Figure 8.11. Excitation at $St_D = 0.6$, $Re = 7.0x10^4$. Picture of the initial region.

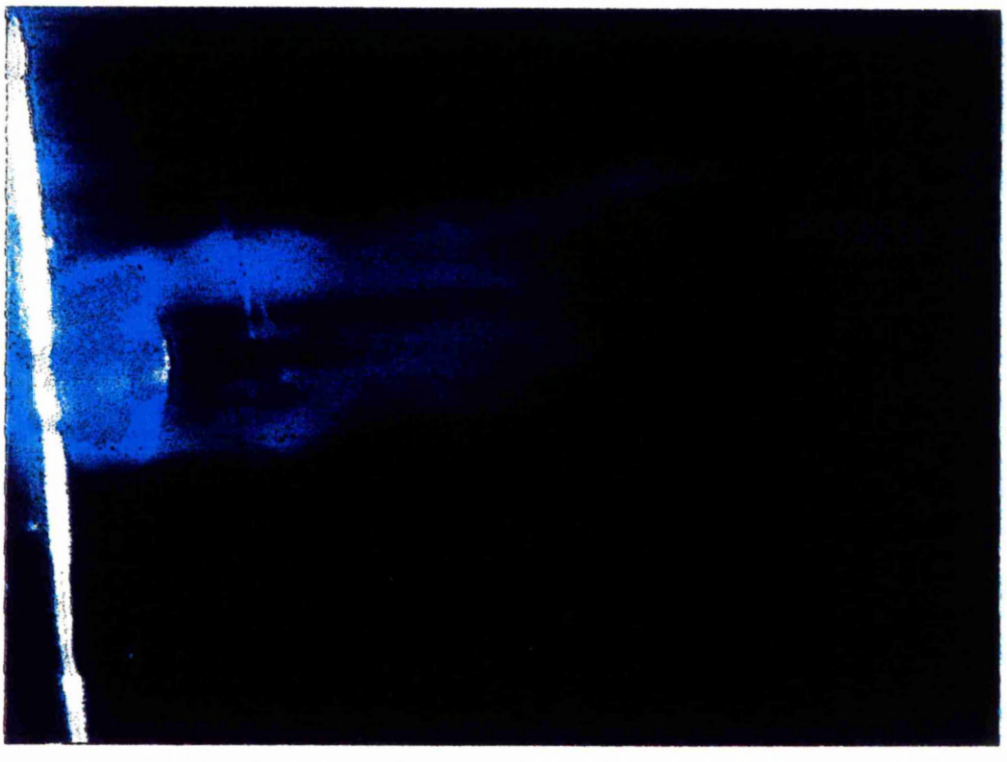

Figure 8.12. Flow visualisation of the secondary jet at $St_D = 0.6$, $Re = 1.7 \times 10^5$. This picture was taken at the edge of the jet.

CHAPTER 9

CONCLUSION AND RECOMMENDATIONS

CHAPTER NINE

CONCLUSIONS AND RECOMMENDATIONS FOR FUTURE WORK

9.1 Influence of Excitation on the Measured Parameters

A free air jet produced by a convergent nozzle of 102.0mm outlet diameter has been investigated with and without aerodynamic excitation. Constant hot film anemometry combined with on-line data acquisition was used in the first part of this investigation to familiarize the author with the nature of the natural free jet and to develop the experimental apparatus and techniques needed for application of the two-component LDA technique. In fact, a simple natural jet (without excitation) was studied during this part of the investigation. Measurements were taken at three axial positions, these being x/D = 3.0, 9.0 and 13.0, mainly to investigate the axial symmetry (and freedom from circumferential variations) of the jet.

Subsequently, the LDA method has been used to obtain the majority of the data presented in this thesis for the natural and excited jet, at Reynolds numbers of $1.5x10^4$, $7.0x10^4$ and $1.7x10^5$. Seeding the jet with the smoke generated by the smoke generator described in section 3.4 provided suitable seeding particles and there was no evidence of any seeding concentration or velocity bias in the LDA data.

The jet was excited aerodynamically by pulsing a secondary annular jet surrounding and co-axial with the primary jet. An axial position of x/D = 2.0 was chosen to determine the optimum conditions of the secondary jet. These initial

experiments showed that the turbulence fluctuation level at the centre-line reached its maximum when the secondary jet flow rate was in the range of 2% to 5% (of the flow rate in the primary jet) for all the Reynolds numbers quoted above. This finding is in a good agreement with the data of Szajner and Turner (1987). Based upon this result, the fixed value of $Q_s/Q_o = 0.02$ was employed in all the subsequent experiments because it was found to be approximately the value of the optimum condition for the two cases of $Re = 7.0x10^4$ and $Re = 1.7x10^5$. A similar response to the aerodynamic excitation for these two Reynolds numbers (i.e. strong excitation effects) can be seen throughout the results for the time mean velocity components and turbulence properties.

Both the axial and radial variations of the different time average flow properties have been measured for the axisymmetric free jet of air under controlled pulsation conditions at four Strouhal numbers, namely $St_D = 0.2$, 0.4, 0.6 and 0.8. This data has been compared with the corresponding results for the natural free jet. It is found that the changes in behaviour brought about by excitation of the jet are not significant for the case of $Re = 1.5x10^4$ since a comparison of the measured parameters of the excited jet with the natural jet show only small differences. In contrast, the excitation produces very significant changes in the development of the jet for $Re = 7.0x10^4$ and $Re = 1.7x10^5$.

In the initial region ($x/D \leq 4.0$), the time mean axial velocity profiles reveal that there are no significant differences between the excited and natural jets. However, further downstream, comparisons between the excited and natural jets show large differences which become particularly marked at $Re = 1.7x10^5$.

In general, aerodynamic excitation increases the rate of decay of the time mean axial velocity component with axial distance. It also increases entrainment of the surrounding fluid into the jet, resulting in a more rapid rate of spread of the jet. At the same time, the potential core is shortened by about 25% compared to the natural case. The average increase in the entrainment rate varies between 20% and 50%, dependent on the actual experimental conditions. The results show that the maximum changes occur at $St_D = 0.2$ and 0.6 which fall within the range reported by Hussain and Zaman (1981) for controlled perturbation of a similar axisymmetric jet.

9.2 The Influence of Excitation on the Intermittency

In the second stage of this investigation, it was intended to concentrate on the intermittency calculations. Thus, the iterative scheme proposed by Jeung (1993) was further developed and adapted by the author in the first stage of this analysis so that intermittency calculations could be made for the turbulent jet flow.

A considerable amount of time was expended in an attempt to show the influence of excitation on the intermittency distributions, using Jeung's (1993) software as the basis. Unfortunately, all the results so produced were illogical. It then occurred to the author that Jeung's software had been written to compute the property averages i.e. the global and zonal averages on a numerical (or ensemble) mean basis instead of the time mean basis on which the true intermittency relationships are defined. This difference is believed to provide a source of error due to the variable arrival times of the bursts in the velocity time record measured using the LDA system. Thus, the software needed to be re-written to calculate the

intermittency properties based upon approximations to the time mean values. One set of data for the natural jet at x/D = 12.0 and Re = $1.7x10^5$ has been processed.

The results obtained using this modified iterative method, presented in Chapter Seven for the jet conditions mentioned above, again do not show the expected variation for the intermittency when plotted across the radius of the jet. This suggests that it would be premature to report on the efficiency of this technique: more work will be needed before any final decision can be made.

Flow visualisation pictures have revealed that pulsation of the secondary jet produces circumferentially uniform toroidal vortices surrounding the primary jet. This has been shown clearly by filming the edge of the jet as well as its central region, particularly in the initial development region up to x/D = 4.0 where the toroidal vortices are most distinct.

An attempt at three-component LDA measurement was also made but, unfortunately, this was not successful due to the difficulty of achieving satisfactory alignment of the three beam systems with the mechanical support system then available. Nevertheless, the experience gained has been recorded in the thesis as a guide for future workers.

9.3 Recommendations for Future Work

The scope for future experimental and computational work with the aerodynamically excited jet arrangement is wide. For example, a three-component LDA system would enable the azimuthal velocity component W to be measured.

Subsequently, the measurements made in the present study could be extended further downstream into the self-preserving region (say up to x/D = 140.0), noting that this is the region which has been examined by most previous workers. The data obtained in this self-preserving region would make it easier to calculate the terms in the momentum equation and thereby enable the effect of excitation on this balance to be studied.

Alternatively, another technique might be employed to evaluate the form and movement of the large scale structures. One possibility here might be to employ the arrangement described by Yule (1978), although with the original constant temperature hot wire anemometer substituted by the LDA system. This would enable any flow reversals to be detected and would exploit the advantages of the LDA technique - see section 5.1.

Use of an entirely different field technique such as Particle Image Velocimetry (PIV), could provide whole-field measurements of the velocity components in the plane of the light sheet. This would permit a better understanding of the behaviour of the jet. Study of the movement of the large scale structures should also yield an improved understanding of the performance of the aerodynamically excited jet.

More work will be necessary to assess the performance of the iterative method for intermittency calculations. To achieve this, the LDA data obtained by the author will need to be re-assessed, possibly extending the analysis to a greater number of axial stations, say from x/D = 1.0 to x/D = 100.0, and more radial positions. However, noting that the inequality method assumes the use of time

averaged values of the global and zonal quantities, it may be sensible to modify the software to cope with the analogue signals produced by a thermal anemometer so that the samples of a time record of a flow property can be separated by equal time intervals. Subsequently, more flow variables will be examined, such as the flatness and skewness factors and the turbulent shear stresses.

The biggest attraction for the present author, however, would be to take the extremely detailed data yielded by this investigation and use it to validate a Computational Fluid Dynamics (CFD) code. For example, the data could be input as initial conditions into the Phoenics computational code and then used to predict the development of the jet further downstream. In this case, the performance of several alternative turbulence models would need to be tested e.g. the k-ϵ, Prandtl mixing-length, Reynolds stress (RMS) models, before making a systematic study of the influence of different excitation conditions.

REFERENCES

REFERENCES

1. **Abid, K. A.**
"Experimental and computational investigation of the effect of initial conditions on the development of a jet in a co-flowing air-stream". Ph.D. thesis, UMIST, (1994).

2. **Abramovich, G. N.**
"The theory of turbulent jets".
MIT Press, Cambridge, (1963).

3. **Albertson M. L., Dai, B. Y., Jensen, R. A., and Rouse, H.**
"Diffusion of submerged jets".
American Society of Civil Engineers, Transactions, (1948).

4. **Al-Sudane, A. H. S.**
"Development of round jets for variation of initial conditions".
M.Sc. dissertation, UMIST, (1990).

5. **Al-Sudane, A. H. S.**
"Software development for flow measurements".
Internal report, The Manchester School of Engineering, University of Manchester, (1996)

6. **Al-Sudane, A. H. S., Jeung, W. R., and Turner, J. T.**
"Aerodynamic excitation and control of an axisymmetric turbulent jet".
Euromech colloquium 328, Berlin, October, (1994).

7. **Al-Sudane, A. H. S., and Turner, J. T.**
"Measurement in a free turbulent jet".
ASME/EALA Laser Anemometry Conference, Hilton Head, South Carolina, (1995).

8. **Al-Sudane, A. H. S., and Turner, J. T.**
"Measurement in an aerodynamically excited free jet using three-dimensional LDA - initial development".
Proceeding of a colloquium held at University of Strathclyde, Glasgow,

U.K., 7th-8th April (1994).

9. Antonia, R. A., and Bilger, R. W.
"An experimental investigation of an axisymmetric jet in a co-flowing air stream".
Journal of Fluid Mechanics, Vol. 61, Part 4, (1973).

10. Antonia, R. A.
"Conditionally sampled measurements near the outer edge of a turbulent boundary layer".
Journal of Fluid Mechanics, Vol. 56, Part 1, (1972).

11. Baltas, C., and Morris, P. J.
"Turbulent characteristics of the noise production region of an excited round jet. Part 1. Time-average flow properties".
AIAA Journal, October, (1984).

12. Baltas, C., and Morris, P. J.
"Turbulent characteristics of the noise production region of an excited round jet. Part 2. Large scale structure characteristics".
AIAA Journal, October, (1984).

13. Baskaya, S., Gilchrist, A., and Fraser, S. M.
"Investigation of axisymmetric turbulent steam jets using laser-Doppler anemometry".
ASME/EALA Laser Anemometry Conference, South Carolina, (1995).

14. Biringen, S.
"An experimental investigation of a turbulent round jet in a co-flowing air stream".
J. Basic Eng., Trans. AMSE, (1986).

15. Boguslawski, L., and Popiel, Cz. O.
"Flow structure of the free round turbulent jet in the initial region".
Journal of Fluid Mechanics, Vol. 90, Part 3, (1979).

16. Boisson, H. C., Chassaing, P., and Minh, H. Ha.
"Conditional analysis of intermittency in the near wake of a circular cylinder".
Phys. Fluids, Vol. 29, March, (1983).

17. Bremhorst, K., and Hollis, P. G.
"Velocity field of an axisymmetric pulsed, subsonic air jet"
AAIA Journal, Vol 28, No. 12, December (1990).

18. Bruun, H. H., Khan, M. A., Al-Kayiem H. H., and Fardad, A. A.
"Velocity calibration relationships for hot-wire anemometry".
J. Phys. E: Sci. Instrum. Vol. 21, (1988).

19. Bruun, H. H.
"Use of computer in hot-wire anemometry".
UMIST, Advanced hot-wire anemometry course, Lecture 7, May, (1986).

20. Bruun, H. H.
"A time-domain analysis of the large-scale flow structures in a circular jet".
Journal of Fluid Mechanics, Vol. 83, Part 4, (1977).

21. Buchhave, P.
"Optical toolkit".
Riso National Laboratory, Denmark, Summer school on optical diagnostics for flow processes, lecture 3, September (1993).

22. Capp, S. P.
"Experimental investigation of the turbulent axisymmetric jet".
Ph.D. dissertation, State University of New York at Buffalo, (1983).

23. Cenedese, A., Doglia, G., Romano, G. P., De Michele, G., and Tanzini, G.
"LDA and PIV velocity measurement in free jets".
Experimental Thermal and Fluid Science, (1994).

24. Charnay, G., Mathieu, J., and Comte-Bellot, G.
"Response of a turbulent boundary layer to random fluctuations in the external stream".
Phys. Fluids, Vol. 19, September, (1976).

25. Collins, D. J., Harch, H. W., and Platzer, M. F.
"Measurement of van-excited jets".
Proc. 2nd int. Symp. on Appl. of laser anemometry to fluid mech., Lisbon, July, (1984).

26. Collis, D. C., and Williams, M. J.
"Two dimensional convection from hot wire at low Reynolds number".
Journal of Fluid Mechanics, Vol. 6, (1959).

27. Comte-Bellot, G., Sabot, J., and Saleh, I.
"Detection of intermittent events maintaining Reynolds stress".
Proceeding of the dynamic flow conference, Marseille, (1978).

28. Crow, S. C., and Champagne, F. H.
"Orderly structure in jet turbulence".
Journal of Fluid Mechanics, Vol. 48, Part 3, (1971).

29. Csanady G. T.
"On the energy balance of a turbulent mixing layer".
Journal of Fluid Mechanics, Vol. 15, Part 4, (1962).

30. Curtet, R., and Ricou, F.
"On the tendency to self-preservation in axisymmetric ducted jets".
Journal of Basic Engineering, December, (1964).

31. Davies, J. T.
"Turbulence phenomena"
Acadamic press, (1972)

32. Dhawan, S., and Narasimha, R.
"Some properties of boundary layer flow during the transition from laminar to turbulent motion".
Journal of Fluid Mechanics, Vol. 3, (1958).

33. Donaldson, C. D., Snedeker, S. R., and Margolis, D. P.
"A study of free jet impingement. Part 2. Free jet turbulent structure and impingement heat transfer".
Journal of Fluid Mechanics, Vol. 45, Part 3, (1971).

34. Drain, L. E.
"The laser Doppler technique".
John Wiley and Sons, (1980).

35. Durst, F., Melling, A., and Whitelaw, J. H.
"Principles and practice of laser Doppler anemometry".
Academic press, (1976).

36. Eaton, J. K., and Wicker, R. B.
"Near field of a coaxial jet with and without axial excitation".
AIAA Journal, Vol. 32, No. 3, March, (1994).

37. Fiedler H. E., and Frenholz, H. H.
"On management and control of turbulent shear flows".
Prog. Aerospace Sci. Vol. 27, (1990).

38. Fiedler H. E., and Mensing, P.
"The plane turbulent shear layer with periodic excitation".
Journal of Fluid Mechanics, Vol. 150, (1985).

39. Fraser, C. J., Graham, D., and Milne, S. J.
"Digital processing of hot wire anemometer signals in intermittency turbulent flow".
Flow Meas. Instrum. Vol. 1, July, (1990).

40. Freymuth, P.
"On transition in a separated laminar boundary layer".
Journal of Fluid Mechanics, Vol. 25, Part 4, (1966).

41. Gutmark, E., and Ho, C. M.
"Preferred modes and the spreading rates of jets".
Phys. Fluids, Vol. 26, October, (1983).

42. Haynes. I. D, and Turner, J. T.
"High speed on-line whole field processing of complex flows".
Sixth international symposium on application of laser techniques to fluid mechanics and workshop on computers in flow measurements. Lisbon, Portugal, (1992).

43. Hedley, T. B., and Keffer, J. F.
"Some turbulent/non-turbulent properties of the outer intermittent region of a boundary layer".
Journal of Fluid Mechanics, Vol. 64, Part 4, (1974).

44. Hedley, T. B., and Keffer, J. F.
"Turbulent/non-turbulent decision in an intermittent flow".
Journal of Fluid Mechanics, Vol. 64, Part 4, (1974).

45. Heyes, A. L.
"Laser anemometry in high speed vertical flow around a lifting delta wing".
Ph.D. thesis, University of Manchester, (1994).

46. Hill, B. J.
"Measurement of local entrainment rate in the initial region of axisymmetric turbulent air jets".
Journal of Fluid Mechanics, Vol. 51, Part 4, (1972).

47. Hinze, J. O.
"Turbulence".
McGraw.Hill, New York, (1975).

48. Husain, H. S., and Hussain, A. K. M. F.
"Controlled excitation of elliptic jets".
Phys. Fluids, Vol. 26, October, (1983).

49. Hussain, A. K., and Zedan, M. F.
"Effect of the initial condition on the axisymmetric free shear layer: Effect of the initial momentum thickness".
Phys. Fluids, Vol. 21, July, (1978).

50. Hussain, A. K., and Zedan, M. F.
"Effect of the initial condition on the axisymmetric free shear layer: Effect of the initial fluctuation level".
Phys. Fluids, Vol. 21, September (1978).

51. Hussain, A. K. M. F., and Husain, Z. D.
"Turbulence structure in the axisymmetric free mixing layer".
AIAA Journal, Vol. 18, (1980).

52. Hussain, A. K. M. F., and Clark, A. R.
"Upstream influence on the near field of a plane turbulent jet".
Phys. Fluids, Vol. 20, September (1977).

53. Hussain, A. K. M. F., and Zaman, K. B. M. Q.
"The preferred mode of the axisymmetric jet".
Journal of Fluid Mechanics, (1981).

54. Hussein, H. J.
"Measurements of turbulent flows with flying hot wire anemometry".
The heuristics of thermal anemometry, Toronto (1990).

55. Hussein, J. H., Capp, S. P., and George, W. K.
"Velocity measurements in a high-Reynolds-number, momentum-conservation, axisymmetric, turbulent jet".
Journal of Fluid Mechanics, Vol. 258, (1994).

56. Hussein, J. H., and George, W. K.
"Measurement of small scale turbulence in an axisymmetric jet using moving hot-wire".
Seventh symposium on turbulent shear flows, Stanford University, (1989).

57. Irhouma, A. A.
"Measurements of flow and droplet diversion in a model pwr bundle with blockage using laser anemometry"
Ph.D. thesis, University of Manchester, (1991).

58. Jeung, W. R.
"Intermittency measurements in a free jet using hot film and laser Doppler anemometry".
Ph.D. thesis, University of Manchester, (1993).

59. Jeung, W. R. and Turner, J. T.
"Intermittency measurements in a turbulent free jet"
Proc. FLUCIME, Toulouse, (1994).

60. Kelemenis, C. I
"Turbulent fluid and heat transfer in a cross-flow tube bundle"
Ph.D. thesis, University of Manchester, (1993).

61. Khan, M. K., MacKenzie, K. A., and Brunn, H. H.
"The effect of blockage correction in hot wire probe calibration facilities".
J. Phys. E: Sci. Instrum. Vol. 20, (1987).

62. Kollmann, W.
"Prediction of the intermittency factor for turbulent shear flows".
AIAA Journal, June, (1983).

63. Kovasznay, L. S. G.
"Turbulence measurements".
Applied Mechanics, Vol. 12, No. 6, (1959).

64. Kovasznay, L. S. G., Kibson, V., and Blackwelder, R. F.
"Large-scale motion in the intermittent region of a turbulent boundary layer".
Journal of Fluid Mechanics, Vol. 41, Part 2, (1970).

65. Kuethe A., M., and Ohio A.
"Investigations of the turbulent mixing regions formed by jets".
Journal of Applied Mechanics, (1935).

66. Kusek, S. M., Corke, T. C., and Reisenthel, P.
"Seeding of helical modes in the initial region of an axisymmetric jet".
Experiments in Fluid, Vol. 10, (1990).

67. Lading, L., Wigley, G., and Buchhave, P.
"Optical diagnostics for flow processes".
Plenum Press, New York, (1994).

68. Latigo, B. O.
"Coherent structure interactions in a two stream plane turbulent mixing layer with impulsive acoustic excitation".
Phys. Fluids, Vol. 10, October (1989).

69. MacGregor, S. A.
"Air entrainment in spray jets".
Int. J. Heat and Fluid Flow, Vol. 12, No. 3, (1991).

70. Morrison, J. F., and Bradshaw, P.
"Bursts and wall shear stress fluctuation in turbulent boundary layer".
Seventh symposium on turbulent shear flows, Stanford University (1989).

71. Muller, T. J.
"The role of smoke visualization and hot-wire anemometry in the study of transition".
Advanced in turbulence, (1989).

72. Murlis, J., Tasai, H. M., and Bradshaw, P.
"The structure of turbulent boundary layer at low Reynolds numbers".
Journal of Fluid Mechanics, Vol. 122, (1982).

73. Obot, N. T, Graska, M. L., and Trabold, T. A.
"The near behaviour of round jets at moderate Reynolds number".
The Canadian Journal of Chemical Engineering, Vol. 62, (1984).

74. Panchapakesan, N. R., and Lumley, J. L.
"Turbulent measurements in axisymmetric jets of air and helium.
Part 1. Air jet".
Journal of Fluid Mechanics, Vol. 246, (1993).

75. Prandtl, L., and Bericht V ber.
"Untersuchungen Zur ausgebildelen turbulenz".
ZAMM, 51, 136, (1925).

76. Quinn, W. R., and Militzer, J.
"Effect of nonparallel exit flow on round turbulent free jets".
Int. J. Heat and Fluid Flow, Vol. 10, No. 2, June (1989).

77. Rajaratnam, N.
"Turbulent jets".
AEPC Press, Amsterdam, (1976).

78. Raman, G., and David, C.
"Jet mixing control using excitation from miniature oscillating jets".
AIAA, Vol. 33, No. 2, (1994).

79. Ribeiro, M. M., and Whitelaw, J. H.
"Coaxial jets with and without swirl".
Journal of Fluid Mechanics, Vol. 96, Part 4, (1980).

80. Ricou, F. P., and Spalding, D. B.
"Measurement of the entrainment by axisymmeterical turbulent jets".
Journal of Fluid Mechanics, Vol. 11, (1961).

81. Rockwell, D. O.
"External excitation of planar jets"
Transactions of the ASME, Journal of Applied Mechanics, (1973).

82. Rockwell, D. O., and Niccolls, W. O.
"Large amplitude axial excitation of planar jet flow".
Transactions of the ASME, Journal of Fluids Engineering (1975).

83. Rodi, W.
"A new method of analysing hot wire signals in highly turbulent flow, and its evaluation in a round jet"
Disa Information no. 17, (1975).

84. Rodi, W.
"The prediction of free boundary by use of two-model of turbulence"
Ph.D. thesis, University of London, (1972).

85. Sabot, J., and Comte-Bellote, G.
"Intermittency of coherent structures in core region of fully developed turbulent pipe flow".
Journal of Fluid Mechanics, Vol. 74, Part 4, (1976).

86. Sato, H.
"The stability and transition of a two-dimensional jet".
Journal of Fluid Mechanics, Vol. 7, Part 1, (1960).

87. Schlichting, H.
"Boundary layer theory".
McGraw-Hill, New York, (1968).

88. Sedat, S., Carmody, T., and Rouse, H.
"Jet diffusion in the region of flow establishment".
Journal of Fluid Mechanics, Vol. 27, Part 2, (1967).

89. Sharpe, G. J.
"Solving problems in fluid dynamics".
Longman scientific and technical, New York (1994).

90. Simmons, J. M., and Lai, J. C. S.
"Jet excitation by an oscillating vane".
AIAA Journal, Vol. 19, No. 6, (1981).

91. Smith, D. J.
"Turbulence measurement in a jet in a co-flowing free stream".
Internal report, University of Manchester (1975).

92. Smith, D. J., and Hughes, T.
"Some measurement in a turbulent circular jet in the presence of a co-flowing free stream".
Aero. Quarterly, Vol. XXVIII (1977).

93. Squire, M. A., and Trouncer, B. A.
"Round jet in a general stream".
R.A.E. Report No. 1904, January (1944).

94. Stevens, M.
"Collation of data on turbulent jet flows".
Technical report, Department of Mechanical Engineering, UMIST, (1992).

95. Swales, C. R, Brake, C. J., and Barrett, R. V.
"Development of a pin hole meter for alignment three dimensional laser Doppler anemometers".
Dantec Information no. 12, (1993).

96. Swaminathan, M. K., Bacic, R., Rankin, G. W., and Sridhar, K.
"Improved calibration of hot-wire anemometers".
J. Phys. E: Sci. Instrum., Vol. 16, (1983).

97. Szajner A., and Turner, J. T.
"Aerodynamic excitation of a turbulent free jet".
Technical report, Department of Mechanical Engineering, University of Manchester, (1987).

98. Szajner A., and Turner, J. T.
"Visualisation of an aerodynamically excited free jet".
Turbulent Shear Flow Conference, Toulouse (1987).

99. Taulbee, D. B.
"The round jet: Experiment and inferences".
Ph.D. dissertation, State University of New York at Buffalo (1987).

100. Townsend, A. A.
"The structure of turbulent shear flow".
University Press, Cambridge, (1976).

101. Townsend, A. A.
"Self-preserving flow inside a turbulent boundary layer"
Journal of Fluid Mechanics, Vol. 22, Part 4, (1965).

102. Trabold, T. A., Esen, E. B., and Obet, N. T.
"Entrainment by turbulent jets issuing from sharp-edged inlet round nozzles".
Transactions of the ASME, Journal of Fluids Engineering (1987)

103. Turner, J. T.
"Some aspects of production and measurement in turbulent shear flows".
Ph.D. thesis, University of Manchester, (1971).

104. Wygnanski, I., and Fiedler, H. E.
"Some measurement in the self-preserving jet".
Journal of Fluid Mechanics, Vol. 38, Part 3, (1969).

105. Wygnanski, I., and Fiedler, H. E.
"The two-dimensional mixing region".
Journal of Fluid Mechanics, Vol. 41, Part 2, (1970).

106. Wygnanski, I. J.
"Coherent motion in excited free shear flows".
AIAA Journal, Vol. 25, February (1987).

107. Yule, A. J.
"Large-scale structure in the mixing layer of a round jet".
Journal of Fluid Mechanics, Vol. 89, Part 3, (1978).

108. Yule, A. J., and Damou, M.
"Investigation of ducted jets".
Internal report, Department of Mechanical Engineering, UMIST (1993).

109. Zaman, B. M. Q., and Hussain, K. M. F.
"Vortex pairing in a circular jet under controlled excitation. Part 1. General jet response".
Journal of Fluid Mechanics, Vol. 101, Part 3, (1980).